METAL COMPLEXES OF THIOSEMICARBAZONES AND HYDRAZONES

Thesis submitted to
the University of Calicut in partial fulfillment of the
requirements for the award of the degree of

DOCTOR OF PHILOSOPHY IN CHEMISTRY

Under the Faculty of Science

NIBILA. T. A

Under the guidance of

Dr. K. K. Aravindakshan
Professor (Retd.)
&
Dr. Pradeepan Periyat
Associate Professor

DEPARTMENT OF CHEMISTRY
UNIVERSITY OF CALICUT
KERALA - 673635

NOVEMBER 2020

Dr. K.K. ARAVINDAKSHAN
Professor (Retd.)
Department of Chemistry
University of Calicut

Calicut University (PO)
Kerala-673635

CERTIFICATE

This is to certify that the thesis entitled, **"Metal Complexes of Thiosemicarbazones and Hydrazones"** is an authentic record of the research work carried out by **Ms. Nibila. T. A,** under our supervision in partial fulfillment of the requirement for the Degree of Doctor of Philosophy in Chemistry, under the Faculty of Science of the University of Calicut. The contents of this thesis, in full or in parts, have not been submitted to any other Institute or University for the award of any other degree. The thesis has undergone plagiarism check using URKUND software at CHMK library, University of Calicut.

Dr. K. K. ARAVINDAKSHAN
(Research Supervisor)

Dr. PRADEEPAN PERIYAT
(Research co-guide)

DECLARATION

I, Nibila T A, hereby declare that this thesis entitled '**Metal complexes of thiosemicarbnazones and hydrazones'** is the report of the original research work done by me for the award of the degree of Doctor of Philosophy in Chemistry, under the supervision of Dr. K. K. Aravindakshan, Professor (Retd.), Department of Chemistry, University of Calicut and Dr. Pradeepan Periyat, Associate Professor (Co-guide), Department of Chemistry, University of Calicut (on leave).

I further declare that this thesis has not formed the basis for the award of any other degree.

C. U. Campus, **Nibila.T.A**
Date:

ACKNOWLEDGMENT

First and foremost, to Almighty God for giving endless blessing during this work as a part of his generous help throughout my life.

I am deeply indebted to my supervisor, ***Dr. K. K. Aravindakshan****, Professor (Retd.), Department of Chemistry, University of Calicut, for his wholehearted support, sincere and valuable guidance and unceasing encouragement extended to me without which the research couldn't have been completed. It is a great honour to me to complete this research under his supervision. I am also grateful to* ***Dr. Pradeepan Periyat****, Associate Professor, Department of Chemistry, University of Calicut (on leave). I sincerely express my gratitude to* ***Yahya A Ismayil****, Head of the Department of Chemistry, University of Calicut, and former heads* ***Dr. P. Raveendran*** *and* ***Dr. K. Muraleedharan*** *for providing me the necessary facilities. I would like to extend my gratitude to all other teachers and non-teaching staff of this department for their valuable help and support. I would like to express my utmost gratitude to all the teachers taught me in my academic life.*

Muhammed M K, *my husband without him this effort would have been worth nothing. I couldn't have completed this research without his constant support and encouragement. I am also grateful to my son* ***Aizen Ayan Muhammed*** *for giving me humble time. I would like to thank* ***Muhammed Koroth,*** *Deputy Secretary To Government of*

Kerala (Retd.) who had been of great help in the successful completion of my research.

I remember the motivation, help and whole-hearted support of my friends and co-researchers for the successful accomplishment of this research work. My grateful thanks are extended to ***Sophisticated Analytical instruments facility (STIC), Cochin*** *for SCXRD analysis and* ***Central Drug Research Institute (CDRI), Lucknow*** *for providing elemental analysis and ESI-MS spectral facility. I am also thankful to* ***Central Sophisticated Instrumental Facility (CSIF), University of Calicut*** *for providing TGA and computational facilities. My thanks are extended to* ***Athmic biotech solutions laboratory, Trivandrum*** *for biological studies. I acknowledge University of Calicut, for the financial support for this work.*

I am adorably thankful to my family for their prayers, love and support throughout my life.

Nibila. T. A

PREFACE

Coordination chemistry is an extensive area of research since late nineteenth century. Compounds with electronegative donor atoms like sulphur, nitrogen or oxygen play significant role in the formation of coordination compounds. Out of many versatile multifunctional ligands, thiosemicarbazones and hydrazones are effective and resourceful in coordination chemistry due to their wide range of applications in analytical-, pharmaceutical- and biological fields.

Previous reports on the synthesis, characterization and antimicrobial studies of some transition metal complexes of thiosemicarbazones are promising and favourable for further research. The metal complexes of substituted thiosemicarbazones and hydrazones have attracted much attention due to their antibacterial-, antifungal- and antioxidant properties. Hence it was considered to be worthwhile and interesting to synthesize N(4)-methyl(phenyl)thiosemicarbazones and isonicotinoylhydrazones of different carbonyl derivatives and their transition metal complexes.

In the present programme of research work, eight different ligands i.e., 2,4-dihydroxybenzaldehyde N(4)-methyl(phenyl)thiosemicarbazone, 4-[N,N-(dimethyl)amino]benzaldehyde N(4)-methyl(phenyl)thiosemi carbazone, 4-benzyloxybenzaldehyde N(4)-methyl(phenyl)thiosemi carbazones, 4-hydroxy-3-methoxyacetophenone N(4)-methyl(phenyl) thiosemicarbazones, Crotonaldehyde isonicotinoylhydrazone, 4-[N,N-(dimethyl)amino]benzaldehyde isonicotinoylhydrazone, 4-hydroxy-3-

methoxyacetophenone isonicotinoylhydrazone and 4-(4-benzyloxy benzalidene)amino-2,3-dimethyl-1-phenyl-3-pyrazolo-5-one, were synthesised and characterized. Their coordinating behaviour towards typical transition metal ions like Co(II), Ni(II), Cu(II), Zn(II) and Cd(II) were studied and the new complexes were prepared. They were characterized using various analytical and spectral techniques and tentative structures were assigned to them. One of the ligands, 4-(4-benzyloxybenzalidene)amino-2,3-dimethyl-1-phenyl-3-pyrazolo-5-one was not used for the synthesis of metal complexes.

The content in this thesis is divided in to two parts consisting of 13 chapters. Chapter I of Part I, '**Synthesis, characterizations and computational studies**', gives a brief description of the history, significance and applications of coordination complexes. A brief review of thiosemicarbazones, hydrazones and their complexes followed by the significance and scope of the present investigation are also included in this chapter.

The materials used, procedures adopted for the synthesis of the ligands and the physico-chemical techniques used for the characterization of the ligands and the complexes are given in Chapter II.

The synthesis and characterization of the ligands, 2,4-dihydroxy benzaldehyde N(4)-methyl(phenyl)thiosemicarbazone, 4-[N,N-(dimethyl)amino]benzaldehyde N(4)-methyl(phenyl)thiosemi carbazone, 4-benzyloxybenzaldehyde N(4)-methyl(phenyl)thiosemi carbazone, 4-hydroxy-3-methoxyacetophenone N(4)-methyl(phenyl) thiosemicarbazone, crotanaldehyde isonicotinoylhydrazone, 4-[N,N-

(dimethyl)amino]benzaldehyde isonicotinoylhydrazone and 4-hydroxy-3-methoxyacetophenone isonicotinoylhydrazone and their transition metal complexes are described in Chapters III, IV, V , VI, VII, VIII and IX, respectively. Single crystal X-ray diffraction analysis together with computational studies of a novel Schiff base, named as 4-(4-benzyloxybenzalidene)amino-2,3-dimethyl-1-phenyl-3-pyrazolo-5-one are presented in chapter X. The reactivity and NLO studies of all the ligands synthesized in the present investigation were done by DFT method. The geometry optimization have been generated at B3LYP/6-311++G(d,p) using the GAUSS-VIEW 5.0.9 program. The details of computational studies are presented in chapter XI. These eleven chapters are included in Part I of the thesis.

In addition to the synthesis and structural studies of the compounds, their antimicrobial- and antioxidant evaluations have been carried out and the results are presented in chapter XII of Part II, '**Biological studies**'. The inhibition effects of 2,4-dihydroxybenzaldehyde N(4)-methyl(phenyl)thiosemicarbazone, 4-[N,N-(dimethyl)amino]benzal dehyde N(4)-methyl(phenyl)thiosemicarbazone, 4-benzyloxybenzal dehyde N(4)-methyl(phenyl)thiosemicarbazone, 4-hydroxy-3-methoxyacetophenone N(4)-methyl(phenyl)thiosemicarbazone and 4-[N,N-(dimethyl)amino]benzaldehyde isonicotinoylhydrazone and their selected complexes on bacterial strains such as *P. aeruginosa E. coli, S. aureus and B. subtilis* and on fungal culture such as *C. albicans and A. niger* are presented here.

The antioxidant activities of 2,4-dihydroxybenzaldehyde N(4)-methyl(phenyl)thiosemicarbazone, 4-benzyloxybenzaldehyde N(4)-

methyl(phenyl)thiosemicarbazone, 4-hydroxy-3-methoxyacetophenone N(4)-methyl(phenyl)thiosemicarbazone and 4-hydroxy-3-methoxyacetophenone isonicotinoylhydrazone and their selected metal complexes were measured using DPPH assay. The results of the analyses are presented in chapter XIII of Part II of the thesis.

The references cited in the text are arranged in a serial order at the end of each chapter.

CONTENTS

PART II
BIOLOGICAL STUDIES

PART I

SYNTHESIS, CHARACTERIZATIONS AND COMPUTATIONAL STUDIES

CHAPTER I

A BRIEF OUTLINE OF THIOSEMICARBAZONES, HYDRAZONES AND THEIR METAL COMPLEXES

1.Introduction

Since late nighteenth century, deliberate efforts were made to prepare and characterize the coordination complexes. Transition metal ions which have partially filled *d* sub-shells, readily combine with different ligands by coordinate bonds to form coordination complexes. French-born Alfred Werner developed the basis for modern coordination chemistry. Werner explained the spatial arrangement of ligands around the metal ions of complexes by suggesting two types of valencies, primary- and secondary valencies. In addition to this, there are many other structural theories on bonding such as Valence Bond Theory (VBT), Crystal Field Theory (CFT), Ligand Field Theory (LFT) and the Molecular Orbital Theory (MOT). More satisfactory explanation for the bonding and the properties of the complexes was given by Crystal Field Theory. Both ionic- and covalent nature of metal-ligand interactions in coordination complexes are considered in MOT.

Transition metal complexes have been of great interest to researchers for many years due to their significant biological applications. The oxidation state and coordination number of the central metal ion determine the geometry and physico-chemical properties of the complex formed. Transition metal ions easily form coordination complexes due to their small size, large charge/size ratio and vacant d-orbitals.

Interaction of transition metal ions with biologically important systems provides extremely bewitching area of coordination chemistry. There are number of coordination compounds that play important roles in

biological process. Our body itself produces and consumes many coordination complexes during the physiological processes such as chlorophyll [magnesium-porphyrin complex, photosynthetic pigment], haemoglobin [iron-porphyrin complex, red pigment in blood], mayoglobin, vitamin–B_{12}, etc. Many enzymes that catalyse physiological process are coordination complexes. Coordination compounds have functions in diverse areas such as medicine, metallurgy, dyes and pigment industries and analytical chemistry. Carboxypeptidase, is a coordination compound catalysing the process of digestion. Coordination compounds have specific colours and find applications in dyes and pigment industries. EDTA is a complex compound used for the determination of hardness of water. The concept of coordination chemistry can be applied in the extraction of metals. Thus, coordination chemistry is the most exigent and indispensable area of modern inorganic chemistry.

The Schiff bases, often called as azomethines [N-subsituted imines] contain carbon-nitrogen double bonds, have been extensively used as a chelating agents in coordination chemistry. Their metal complexes are of great interest due to their biological activities such as anticancer-, antibacterial-, antiviral- and antifungal activities [1-4]. The wide range of biological activities of these compounds are due to the imine groups present in them. Most of the Schiff base compounds have structures quite suitable for chelation with metal ions. They are generally formed by the condensation of primary amines with carbonyl compounds by the reversible reaction in presence of either acid/base catalyst or upon

heating[5]. They are characterized by the presence of an azomethine group, –RC=NR', where R and R' are alkyl, cycloalkyl, aryl or heterocyclic groups. Schiff bases are widely designed by varying the chemical environment about the –C=N- group. The presence of a lone pair of electron in the sp^2hybridized orbital on the imino nitrogen atom makes the azomethine group more significant. In recent years, Schiff bases with N-S-O and N-O-O moieties and their transition metal complexes have massive interest due to their desirable chemical- and physical properties and diverse applications in different fields. They show variable bonding and stereo-chemical possibilities depending on the nature of metal ions, structure of the ligands and metal-ligand interactions.

1.1. Structure and bonding of thiosemicarbazones (TSCs) and their complexes

Thiosemicarbazones are basically Schiff bases that belong to a group of thiourea derivatives and have emerged as an important class of sulphur donor ligands. They are chelating agents with C=N-NH-CS-NH moiety and form complexes with metal ions by bonding through thionate sulphur (=S) and azomethine (=N–) groups, although in some cases they behave as monodentate ligands where they bind through thionate sulphur (=S) alone. The presence of nitrogen and sulphur in chelating agents causes a decrease in solubility of the complexes and allows the complex to be isolated from the solution. TSCs show wide applications due to the electron donating property of sulphur. They exhibit a variety of biological activities, such as antitumor-[6],

antifungal-[7], antibacterial-[8], and antiviral- [9] activities. The remarkable biological activities observed for these compounds are due to their complexing ability.

Complexes of thiosemicarbazones with transition metals have received much attention during last two decades. An all-inclusive review by Campell on the coordination chemistry of thiosemicarbazones deduced that the nature of sulphur donor atoms is the most important single factor affecting the behaviours of thiosemicarbazones as ligands[10]. Various applications of thiosemicarbazones and their metal complexes are the driving forces behind the present study of the synthesis of new N(4)-disubstituted thiosemicarbazones and their metal complexes. Modified thiosemicarbazones can be easily prepared by varying the parent aldehyde or ketone used for the synthesis, particularly with compounds having additional donor sites or by using thiosemicarbazides with substituents on the terminal nitrogen atom. Structure-activity relationship studies revealed that the presence of bulky groups on the terminal nitrogen of the thiosemicarbazone moiety strongly enhances the pharmacological activities of these compounds [11]. Thus, substituted thiosemicarbazones and their complexes were studied exclusively due to their important biological activities [12-19].

Thiosemicarbazones of the type R^1 R^2 C^2 = N^3-N^2H-C^1(=S)-N^1 R^3 R^4 constitute an important class of N,S-donor ligands. They generally bind to the metals through N^2, S or N^3, S donor atoms forming four- or five membered rings, respectively (Fig.1).

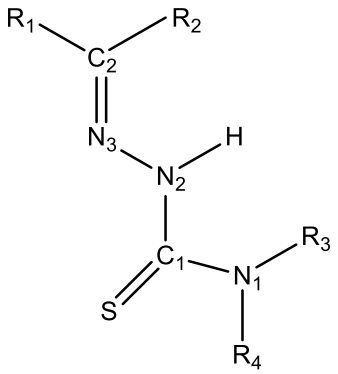

Fig.1. General structure of thiosemicarbazone

The existence of keto-enol tautomerism in equilibrium is an interesting attribute of thiosemicarbazones. In the solid state, they predominantly exist in the keto [thioamido] form, whereas due to the interaction with the solvent molecules they can exhibit keto-enol [thiol] tautomerism in solution (Fig 2). The enol form which predominates in the solution, can effectively coordinate to a metal ion (Fig.2).

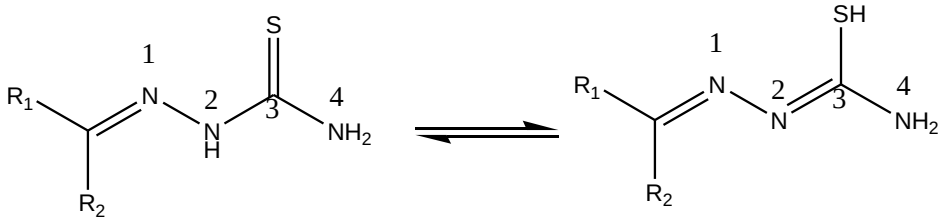

Fig.2. Keto-enol tautomer's of thiosemicarbazone

In most of the metal complexes, thiosemicarbazone exists in keto form. Depending upon the conditions of preparation, the complexes may be cationic, neutral or anionic. It acts as neutral bidentate ligand in the keto form. In enol form it can deprotonate and acts as anionic bidentate

ligand. Thiosemicarbazone molecule itself exists in almost planar structure, with the sulphur atom in *trans*-configuration to azomethine nitrogen atom. The presence of azomethine group makes thiosemicarbazone to exist as E and Z stereoisomers [Fig.3]. Considering the thermodynamic stability, E isomer predominates more in the mixture[20].

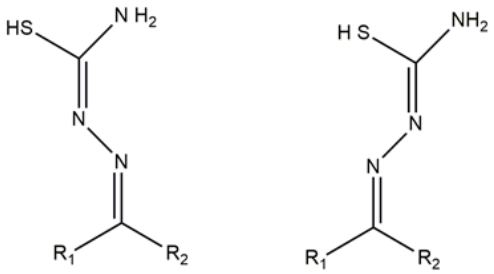

E (*Trans*- form) Z (*Cis*- form)

Fig.3. E and Z stereoiosmers

Detailed research have revealed that the steric effects of various substituents on the thiosemicarbazone moiety decide the spatial arrangements of the ligand. During complexation, the compound will be in the *cis*- form because of the extra stability associated with electron delocalization in chelated complex with the bonding through thione/thiol sulphur and hydrazine nitrogen in a bidentate manner as shown in Fig.4.

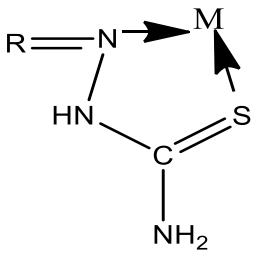

Fig.4. Metal chelation of bidentate thiosemicarbazone moiety

When an additional coordination functionality is present in the nearby position of the donating atoms, thiosemicarbazones coordinate in a tridentate manner as shown in Fig.5.

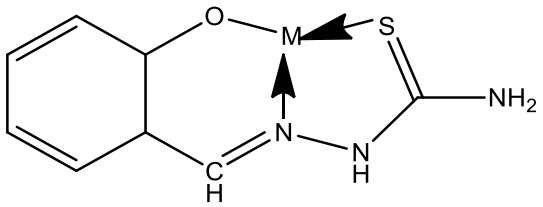

Fig.5. Metal chelation of tridentate thiosemicarbazone moiety

1.2. Metal complexes of thiosemicarbazones

Transition metal complexes of N, S donor ligands have received much attention during last few years. Among N, S donor ligands, thiosemicarbazones have been explored greatly. The transition metal complexes of thiosemicarbazones attracted many researches due to their structural heterogeneity, variable modes of bonding, versatile pharmacological activities and ion sensing potential[13, 21, 22]. Synthesis and characterization of their metal complexes, single crystal structural analysis, biological and pharmaceutical applications were

reviewed in details since 1974. The synthesis and biological applications of complexes of thiosemicarbazones continue to attract the attention of chemists since Domagk first reported on their anticancer activity[23-25]. Structural characterization of thiosemicarbazone complexes that emerged during that period entrenched thiosemicarbazones as an important class of ligand for a variety of reasons[10, 20, 26, 27]. Jayakumar *et al*[28] reported six copper complexes of 2-benzoylpyridine-N^4,N^4-dimethyl-3-thiosemicarbazone (HL). These complexes were characterized by elemental analysis, magnetic susceptibility- and conductivity measurements, FT-IR, UV–Vis and EPR studies. It was found that the thiosemicarbazone coordinated through one of the pyridyl nitrogen, azomethine nitrogen and thioiminolate sulphur atoms. From EPR studies, the binuclear nature of some of the complexes was confirmed. Syntheasis and characterization of four Ru(III) complexes with 4-methyl-3-thiosemicarbazone ligands, (E)-2-(2-chlorobenzylidene)-N-methylhydrazinecarbothioamide (HL^1) and (E)-2-(2-nitrobenzylidene)-N-methylhydrazinecarbothioamide (HL^2), were reported by Sampath *et al*[29]. The complexes were tentatively assigned an octahedral geometry. All the complexes had been examined for DNA binding, DNA cleavage, antioxidant and cytotoxic activities under *in vitro* experimental conditions. The DNA binding abilities of the ligands and complexes were studied and found that the complexes bind to DNA *via* an intercalative mode. Further, *in vitro* antioxidant-, anticancer- and cytotoxic studies done on the ligands and Ru(II) complexes showed that all the Ru(II) complexes served as potential antioxidants and good

cytotoxic agents than the ligands. The conclusion of this study was that the thiosemicarbazone complexes containing triphenylphosphine as co-ligand, led to an improved interaction with DNA, free radical and tumour cell line than the other complexes.

Vibrational-, NMR- and UV-Visible spectroscopic investigation and NLO studies on benzaldehyde thiosemicarbazone using computational calculations were done by Moorthy *et al*[30]. The vibrational, electronic, NBO, optical and frontier molecular interaction studies have been carried out by HF and B3LYP methods with 6-311++G(d,p) basis set. The XRD results revealed that the stabilized molecular systems were confined in orthorhombic unit cell system. The energy gap of HOMO and LUMO was found as 3.87 eV. This was only an intermediate energy gap which indicated the enriched electronic activity of the compound. Synthesis, spectral characterization and biological activities of Mn(II) and Co(II) complexes of benzyloxybenzaldehyde-4-phenyl-3-thiosemicarbazone were reported by Prathima *et al*[31]. The EPR and electronic spectral studies of both the complexes indicated octahedral site symmetry for the metal ions. The ligand had no antibacterial activity but both of the complexes showed considerable antibacterial activities. Soroush Sardari *et al*[32] reported a new series of 31 thiosemicarbazones synthesised by the reactions of various aldehydes and ketones with 4-phenylthiosemicarbazide or thiosemicarbazide at room temperature. All of them showed high activity toward *Mycobacterium Bovis*. Sreenath Reddy *et al*[33] synthesized Ni(II) and Cu(II) complexes of

2-butyl-4-chloro-5-formylimidazole thiosemicarbazone (L) and characterized them by elemental analysis, FT-IR, mass spectra, electronic and EPR spectra. A distorted octahedral geometry was assigned for the complexes from the electronic spectra and EPR calculations. Both the complexes showed only moderate antimicrobial activities against the human pathogens when compared to the standard, Amoxiclav. The Ni(II) and Cu(II)complexes of this ligand were tested for the activity against cancer cell lines, (MDA-MB 231 cell lines) using the MTT assay method. Among the compounds studied, Cu(II) complex showed better activity at 80 μg/ml and the Ni(II) complex at 100 μg/ml. The synthesis, characterization, crystal structures, biological activities and fluorescence studies of the complexes of Cu(II), Zn(II) and Ni(II) with 3-carbaldehyde chromonethiosemicarbazone were reported by Li *et al*[34]. Interactions of the ligand and the complexes with DNA were studied and found that the compounds bind to DNA in an intercalative mode, especially, the Zn(II) complex bind to DNA very strongly than the free ligand, Ni(II)- and Cu(II) complexes. *In vitro* antioxidant activities of the compounds were investigated and found that they have significant activity against superoxide- and hydroxyl radicals. The scavenging property of Cu(II) complex was better than the ligand, Zn(II) and Ni(II) complexes and some standard antioxidants. Biological properties of 4-Benzyloxybenzaldehyde-4-methyl-3-thiosemicarbazone [BBMTSC] and its Cd(II) complex was reported by Suvarapu Lakshmi Narayana *et al*[35]. The results showed that the BBMTSC can act as a strong antioxidant. In addition to antioxidant activity, BBMTSC can act as a

better antibacterial agent against *Staphylococcus aureus* and *Pseudomonas aeruginosa* while its Cd(II) complex showed better activity against *Bacillus subtilis* and *Escherichia coli*. Regarding antifungal activity, the Cd(II)-BBMTSC acted as a better antifungal agent than free BBMTSC.

The synthesis, characterization, antibacterial-, antifungal-, antioxidant- and DNA interaction studies of mononuclear Co(II), Ni(II), Cu(II), Zn(II), Pt(II) and Pd(II) complexes of N,N,-bis-p-methoxyacetophenone thiosemicarbazone were reported by Richa Kothari and Brajraj Sharma [36]. The complexes were characterized by elemental analysis, conductivity measurements, FTIR, ^{1}H NMR-, mass- and electronic spectra. Metal complexes showed better antibacterial-, antifungal- and antioxidant properties than the free ligand. Selvamurugan *et al*[37] reported a new series of Ni(II) complexes of 4-chromone-N(4)-substituted thiosemicarbazones. Characterization of the complexes were carried out by using FT-IR, electronic, ^{1}H, ^{13}C, ^{31}P NMR and ESI-Mass spectra. The ligands were found to act as tridentate. Drug-like properties of the complexes were analysed by DNA/protein interaction studies and *in vitro* cytotoxic studies against human breast cancer cell line (MCF-7). The DNA binding studies showed that the complexes bind to DNA *via* intercalative mode. The complexes with the phenyl substituent on the ligand moiety showed good DNA and protein binding interaction and had a good anticancer activity against human breast cancer cell line (MCF-7), due to the electron withdrawing nature of the phenyl group

on the terminal nitrogen atom of the thiosemicarbazone**.** K. K. Aravindakshan and C G R Nair [38] reported the complexes of vanillin thiosemiearbazone (3-methoxy-4-hydroxybenzaldehyde thiosemicarbazone), (VTSCH) with Co(ll), Ni(ll), Cu(ll), Zn(ll), Cd(ll) and Hg(ll) ions. Structures were assigned to these complexes based on electrical conductivity, magnetic susceptibility and spectroscopic measurements. Spectrophotometric determination of gold(III) using 2-hydroxy-3-methoxybenzaldehyde thiosemicarbazone [HMBATSC] as a chromophoric reagent was reported by Prem Kumar *et al*[39]. Gold(III) ion formed a blue - coloured complex with HMBATSC in an aqueous-DMF solution at pH 6.0. The gold complex showed the absorption maximum at 385 nm, and Beer's law was obeyed in the concentration range, 0.49–8.37 μg/mL. The complex had 1 1: 1 stoichiometry with a stability constant of 1.32 × 106. This method was used for the determination of gold(III) in environmental water samples. Adsorption and inhibition actions of 4-(N,N-Dimethylamino) benzaldehyde thiosemicarbazone [DMABT] on 6061 Al/SiC composite and its base alloy in sulfuric acid medium were reported by Geetha *et al*[40]. The results revealed that DMABT was an effective inhibitor, showing an inhibition efficiency of 70% in 0.5M sulfuric acid. DMABT behaved as cathodic type inhibitor. It obeyed Langmuir's model of adsorption, and the adsorption was predominantly through physisorption. The adsorption process was spontaneous and exothermic process accompanied by an increase of entropy. Inhibition efficiency of DMABT on aluminium composite and its base alloy increased with the increase in concentration of sulfuric

acid and decreased with increase in temperature from 30^0 to 50^0C. K.G. Sangeetha and K.K. Aravindakshan [41] prepared Cd(II) complex of 1-phenyl-3-methyl-4-benzoyl-5-pyrazolone N(4)-methyl-N(4)-phenyl thiosemicarbazone. The ligand crystallized in triclinic system with a space group P-1. Cadmium(II) complex crystallized as a monoclinic crystal system with a space group P21/c. Cadmium was found to be coordinated through oxygen, azomethine nitrogen and thione sulphur. A rapid extractive spectrophotometric determination of copper(II) in environmental samples, alloys, complexes and pharmaceutical samples using 4-[*N*,*N*(dimethyl)amino]benzaldehyde thiosemicarbazone was reported by Karthikeyan *et al*[42]. The investigation showed that yellow Cu(II) complex formed in the pH range, 4.4–5.4 was 1:2. It obeyed Beer's law up to a concentration of 4.7 μg/mL and the optimum concentration range for the determination was 1.2–3.8 μg/mL.

Harness *et al*[43] prepared Cu(II), Zn(II), Cd(II) and Hg(II) complexes of *p*-dimethylaminobenzaldehyde thiosemicarbazone [dmabTSC]. The ligand and complexes were strongly fluorescent in DMSO but their luminesce almost entirely quenched in dichloromethane. Elemental analyses and molar conductivity data suggested a bimetallic copper complex while each of the other complex contained a single metal center as expected from the reaction stoichiometry. In all the complexes, dmabTSC coordinated as a neutral bidentate ligand binding through the azomethine nitrogen and thiocarbonyl sulphur. Synthesis, structural characterization, and biological application of p-[N,N-bis(2-

chloroethyl)aminobenzaldehyde thiosemicarbazone and its nickel(II) complex were reported by Anitha *et al*[44]. These compounds were characterized by elemental analyses, IR, electronic- and ^{1}H NMR spectroscopy. The compound, p-[N,N-bis(2-chloroethyl)aminobenzaldehyde thiosemicarbazone crystallised in a triclinic crystal system with a space group, P-1. In 1:2 complex, thiosemicarbazone coordinated to nickel in SNNS mode. The complex was tested for its antibacterial activity against various pathogenic bacteria. Synthesis, characterization and biological activity of a Schiff base derived from 3,4-dihydroxybenzaldehyde and thiosemicarbazide and its with iron(II) and nickel(II) complexes were reported by Xinde Zhu *et al*[23]. The complexes were characterized by elemental analyses, molar conductance, IR, UV/Vis, ^{1}H- NMR and ESI-MS spectra. Mossbauer spectrum was used to identify the electronic state of iron(II) in the ferrous complex. Biological activity tests revealed that the complexes exhibited strong super oxygen dismutase activity and inhibitory actions towards *Escherichia coli*, *Bacillus subtilis*, *Staphylococcus aureus and Cryptococcus neoforms.* A series of complexes of Ni(II) and Cu(II) with benzil bis(thiosemicarbazone) were prepared by Sulekh Chandra *et al*[45]. They were characterized by elemental analyses, mass spectra, molar conductance and magnetic susceptibility measurements and spectral (electronic-, IR and EPR) studies. The involvement of sulphur and azomethine nitrogen in coordination to the central metal ion was confirmed from IR spectral data. Spectral studies suggested an octahedral geometry for the Ni(II) complex and tetragonal geometry for the Cu(II) complex. The free

ligand and its metal complexes were tested *in vitro* against the gram-positive bacteria (*Bacillus macerans*) and gram-negative bacteria (*Pseudomonas striata*). Fungicidal screening tests were conducted for Ni(II) and Cu(II) complexes against phytopathogenic fungi, *Rhizoctonia bataticola, Alternaria alternata,* and *Fusarium odum.* The results showed that the complexes were more active than the free ligand.

The antiviral activities of [bis-(citronellalthiosemi carbazonato)nickel(II)] and [aqua(pyridoxalthiosemicarba zonato)copper(II)] chloride monohydrate were reported by Giorgio Pelosi *et al*[46]. They showed activity against the retroviruses HIV-1 and HTLV-1/-2. The copper complex was anti-HIV active. A series of complexes of Co(III), Ni(II), Cu(II) and Zn(II) with (*E*)-1-(1-hydroxypropan-2-ylidene)thiosemicarbazide(LH) were synthesized by Priya *et al*[47]. These compounds were successfully characterized using various spectro-analytical techniques. The molecular structures of the ligand, (LH) and the Ni(II) and Cu(II) complexes were determined by single crystal X-ray diffraction studies. LH acted as a tridentate ligand and coordinated to Co(III) centre in thiolate form and Ni(II) centre in thione form. The Ligand, (LH) and all the complexes were screened against pathogenic bacterial and fungal strains. Synthesis, characterization, electrochemical studies and *in vitro* antibacterial activity of a novel thiosemicarbazone and its Cu(II), Ni(II), and Co(II) complexes were reported by Salman A. Khan *et al*[48]. These compounds were characterized by FT-IR, NMR studies

and mass spectral analysis. Thiosemicarbazone coordinated to metal through the thionic sulphur and the azomethine nitrogen. *In vitro* antibacterial activities of these compounds were tested by the disc diffusion micro dilution assay against two Gram-positive and Gram-negative bacteria. The results showed that the complex of $CuCl_2$ was better antibacterial agent as compared to chloramphenicol. Five thiosemicarbazone derivatives of benzophenone were synthesized by Bienvenu Glinma *et al*[49]. They were characterized by various spectrometrical methods. These compounds were screened *in vitro* for their antiparasitic activity and toxicity on *Trypanosoma brucei brucei* and *Artemia salina leach*.

1.3. Hydrazone, structure and bonding of the complexes

Schiff bases are a class of compounds consisting of imine (–C=N–) functional groups and are considered to be a versatile pharmacophore for the development of various bioactive compounds. Schiff bases with N, O donor atoms can encapsulate metal ions and appear to be particularly attractive owing to the stability that they can grant to their complexes by chelation. Hydrazones are a promising group of compounds in the Schiff base family. The hydrazones offer a number of attractive features such as the degree of rigidity, conjugated π-system and a NH unit that readily participates in hydrogen bonding or may be a site of protonation-deprotonation. Hydrazones have been reported to demonstrate a broad spectra of biological activities including antimicrobial-, antituberculosis-, anti-inflammatory-, anticancer-, anticonvulsant- and analgesic activities [50, 51]. These

ligands obtained by condensation of hydrazines or hydrazides with aldehydes or ketones are shown in Fig. 6.

Besides their growing interest in coordination chemistry, aroylhydrazones R–CO–NH–N=CH–R', exhibit a variety of biological properties based on the formation of bioactive metal chelates[52]. They can coordinate with transition metal ions through the N atom of azomethine group and O atom of carbonyl group. Therefore, they can coordinate *in vivo* with metal ions as shown in Fig.7. The presence of –C=O group increases the electron delocalization and denticity of the aroylhydrazone ligands[53].

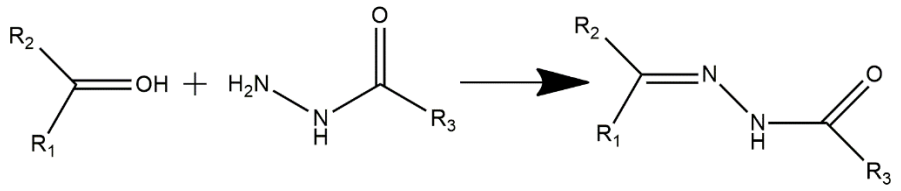

Fig.6. Synthesis of hydrazone

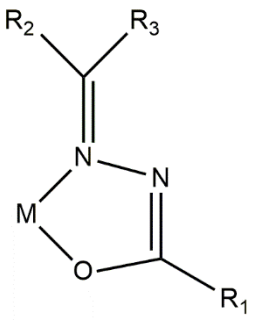

Fig.7. General mode of coordination of aroylhydrazone

The architectural structure of aroylhydrazone unveiles that due to the presence of nucleophilic azomethine [imine] nitrogen and amino nitrogen, azomethine carbon can act as both electrophile and nucleophile and can show configurational isomerism [54] as shown in Fig.8.

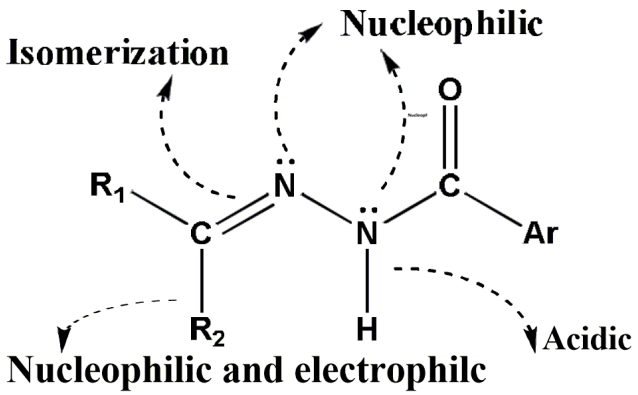

Fig.8. Architectural structure of aroylhydrazone

In the solid state, they generally exist in the amido form, whereas they predominatly exist as an equilibrium mixture of amido and iminol forms in solution (Fig.9). The amido-iminol equilibrium depends on the nature of the substituents on the hydrazide skeleton, pH of the medium, etc.[55]. Hydrazones coordinate to metal center in the neutral amido or anionic iminolate forms. Due to their facile characteristics, they show interesting coordination modes and stereo-chemical probabilities depending on the nature of metal ions, substituents on the ligands and metal-ligand interactions.

Isonicotinic acid hydrazide (isoniazid, INH), is a widely used antituberculosis drug. Isonicotinicotinoylhydrazones have wide range of applications in organic synthesis, analytical chemistry and in medical biotechnology[56]. They show a variety of coordination modes depending on the reaction conditions, type of substituents and stability of the metal complex formed. Their coordination behaviour also depends upon the pH of the medium [57]. They are generally bi-, tri- or poly-dentate ligands capable of forming very stable complexes with transition metal ions.

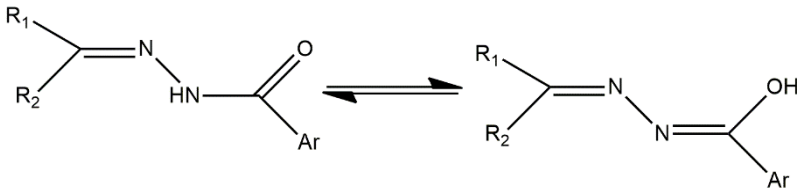

Fig.9. Tautomerism in aroylhydrazone

1.4. Metal complexes of hydrazone

Amrita Parl and Gurmeet Singh [58] reported biologically active isonicotinicotinoylhydrazones of substituted benzaldehydes. These were characterized by AT-IR and ^{1}H NMR spectral analyses. The *in vivo* antibacterial screening showed that N-(benzenesulfonyl)-N'-[(5-chloro-2-hydroxyphenyl)methylidene]pyridine-4-carbohydrazide(GM-I) substituted isonicotinoyl hydrazones exhibit good activity. Ahmed *et al*[59] reported the synthesis and characterization of Mn(II), Co(II), Ni(II) and Cd(II) complexes of salicyldehyde isonicotinoylhydrazone and 2-hydroxynaphthaldehyde isonicotinoylhydrazone. The complexes

were characterized using solubility, melting point, UV measurement and infrared spectroscopy. The coordination of the metal ions to the ligands was through the oxygen of carbonyl group, the nitrogen of the imine group and the oxygen of the hydroxyl group. Moksharagni *et al*[60] prepared isonicotinoyl- and nicotinoyl hydrazones of 2-formyl pyridine, 2-acetyl pyridine and 2-benzoyl pyridine. All of them were characterized by IR, ^{1}H NMR and mass spectral data. They were screened for their antibacterial activities against *Staphylococcus aureus, Bacillus subtilis, Escherichia coli* and *Salmonella typhi*. Isonicotinoylhydrazones showed more antibacterial activity than the corresponding nicotinoylhydrazones.

Co(II), Ni(II) and Cu(II) complexes of isonicotinic acid 2-(9-anthrylmethylene)-hydrazide were prepared by Dianu *et al*[61]. These complexes were characterized by analytical and physico–chemical techniques, such as elemental- and thermal analyses, magnetic susceptibility- and conductivity measurements, electronic-, EPR- and IR spectral studies. The infrared spectral studies suggested the bidentate or monodentate nature of the ligands in the complexes. The pyridine nitrogen did not involve in the coordination. A tetrahedral geometry was suggested for the nitrate complexes and an octahedral geometry for the others. Malhotra *et al*[62] synthesized a series of (E)-N'-(substituted benzylidene)isonicotinohydrazide derivatives. The structure of all the compounds were confirmed by using various spectral techniques like IR-, ^{1}H NMR-, ^{13}C NMR- and mass spectra. All the compounds were tested for their antimicrobial activities in

terms of zone of inhibition, minimum inhibitory concentration, minimum bactericidal concentration and minimum fungicidal concentration in comparison with standard drugs. The results suggested that all the compounds possessed mild biological activities. Among the synthesized derivatives, (E)-N'-(3,4-dimethoxybenzylidene)isonicotinohydrazide**,** (E)-N'-(3,4,5-trimethoxybenzylidene)isonicotinohydrazide and (E)-N'-(4-hydroxy-3-methoxybenzylidene)isonicotinohydrazide showed considerable antimicrobial activities. Ram K. Agarwal *et al*[63] prepared a new series of complexes of cobalt(II) and nickel(II) with N-isonicotinamido-2′,4′-dichlorobenzalaldimine (INH-DCB) with a general composition, $MX_2 \cdot n$(INH-DCB). The complexes were characterized by elemental analyses, IR- and electronic spectra, magnetic susceptibility- and conductivity measurements. An octahedral geometry was suggested for all the complexes. The metal complexes were tested for their antifungal- and antibacterial activities on different species of pathogenic fungi and bacteria and their biopotency was also discussed. Vidya Desai and Rachana Shinde [64] developed a new, simple and convenient environmentally benign synthesis of nicotinoylhydrazones in good yield using lemon juice as natural catalyst. A variety of hydrazones have been synthesized by this green methodology, proving its versatility. These hydrazones were screened for antimicrobial activity and revealed that they exhibited good activity against *E-Coli* than *S. Aureus*. Most of these compounds showed better antitubercular action than that of the standard drugs,

pyrazinamide, streptomycin and ciprofloxacin. These may be potential candidates for the development of new drug substrates in future.

Cobalt(II), nickel(II) and copper(II) complexes of (*E*)-N'-(2-hydroxy-5-nitrobenzylidene)isonicotinohydrazide were reported by Fasina *et al*[51]. These complexes were characterized based on elemental analyses, conductivity measurements, IR- and electronic absorption spectroscopy. The data suggested 1:2 [M:L] stoichiometry for the copper and cobalt complexes and a 1:1 [M:L] for the nickel complex. The electronic absorption spectral data supported octahedral geometry for cobalt(II) and copper(II) complexes and square planar for nickel(II) complex. *In vitro* antimicrobial properties of the compounds were screened against five pathogenic bacteria using the agar-well diffusion method and showed that the activity was in the order Ni>Co>Cu complexes. They can be used as entities for the development of new antimicrobial agents. A new series of quinoline hydrazone derivatives and their metal complexes were synthesized by Mandewale *et al*[65]. The biological properties of these compounds were evaluated against *Mycobacterium tuberculosis* (H37 RV strain). Most of them showed 100% inhibitory activity at a concentration of 6.25–25 μg/mL, against *Mycobacterium tuberculosis*. Complexation with Cu(II)and Zn(II) effectively enhanced the conformational rigidity of the hydrazones and were found to be good materials for photochemical applications. Fluorescence properties of all these compounds were also investigated. Surendra Prasad and Ram K. Agarwal [66] reported that nickel(II) complexes of a novel ligand, N-isonicotinamido-furfuraldimine. The

hydrazone behaved as a neutral bidentate N and O donor ligand. The complexes were characterized by elemental analyses, molecular weight determinations, magnetic susceptibility measurements, thermo gravimetric, electrochemical and spectroscopic studies. The complexes had octahedral geometry. The antimicrobial studies of the complexes showed that they were moderate antibacterial and antifungal agents. Khlood S. Abou-Melha[67] synthesized Mn(II), Fe(III) Co(II), Ni(II), Cu(II) and UO_2(II) complexes of isonicotinic acid (2-hydroxybenzylidene)hydrazide, (HL). The ligand and its metal complexes were characterized by using elemental- and thermal analysis, IR-, electronic-, mass- and ^{1}H NMR spectra, as well as magnetic moment- and conductance measurements. All complexes, except those of Cu(II) and UO_2 displayed octahedral configuration. The Cu(II) complex had a square planar geometry distorted towards tetrahedral. The UO_2(II) complex had a hepta-coordination. The ligand and its metal complexes were tested against a gram +ve bacterium (*Staphylococcus aureus*), a gram −ve bacterium *(Escherichia coli*)and Fungus (*Candida albicans*). The tested compounds showed good antibacterial activities. Synthesis and characterization of lanthanide(III) perchlorato complexes of N-isonicotinamido-p-dimethylaminobenzalaldimine (INH-PDAB) and N-isonicotinamido-3-methoxy-4-hydroxybenzalaldimine were reported by Ram K. Agarwal and Rajendra K. Sarin [68]. The complexes were characterized by using analytical-, magnetic and IR- and UV-Vis spectral methods. The thermal stabilities of compounds were also studied. Kelode *et al*[69] synthesized and characterized a Schiff base derived from 2,4-

dihydroxy benzophenone and isonicotinoyl hydrazid and its complexes with Cr(III), Mn(III), Fe(III), Co(II), Ni(II), Cu(II), Zn(II), VO(IV) and Zr(IV) ions. As per IR spectral data, the hydrazone acted as a monobasic bidentate ligand, coordinating through O^- of the deprotonated phenolic group and the nitrogen atom of imine group. The magnetic susceptibility measurements and electronic spectral data suggested square planar geometry for the Ni(II) and Cu(II) complexes, square pyramidal geometry for the Mn(III) and VO(IV) complexes and octahedral geometry for the other complexes. EL-Bahnasawy *et al*[70] have reported the synthesis of cobalt, nickel, copper and zinc complexes of the isonicotinoyl hydrazones derived from benzoylacetone (Bz), salicyaldehyde (Sal) and 2-hydroxynaphthaldehyde (Naph). The compounds were subjected to thermal analysis. Their electrical conductivities were measured at different temperatures. Agarwal *et al*[71] reported the synthesis, spectral and thermal studies of oxovanadium(IV) complexes of N-isonicotinamido-3',4',5'-trimethoxybenzalaldimine (INH-TMB) and N-isonicotinamido-2'-furanaldimine (INH-FUR). They were characterized on the basis of analytical-, conductance-, molecular weight-, and magnetic moments-, IR- and electronic spectral data. The infrared data of the complexes suggested the bidendate nature of the ligands, coordinating through carbonyl-oxygen- and azomethinic-nitrogen atoms. Thermal stabilities of the complexes were investigated by thermo gravimetric analysis. Kriza *et al* [72] prepared Co(II), Ni(II), Cu(II), Zn(II), Cd(II) and Hg(II) complexes of glyoxal bis-isonicotinoyl hydrazone (isoniazid, H_2L) and their structures were

confirmed by using elemental analyses, magnetic susceptibility and thermo gravimetric studies. IR-, electronic, ^{1}H-NMR and EPR spectral studies were also carried out. The stoichiometric formulae were$[M(H_2L)(H_2O)_2](NO_3)_2 \cdot xH_2O$, where M=Co(II), Ni(II) or Cu(II) and $[M(H_2L)](NO_3)_2$, where M=Zn(II), Cd(II) or Hg(II) and H_2L= glyoxal bis-isonicotinoyl hydrazone. Ligand acted as a neutral tetradentate one coordinating through carbonyl oxygen- and azomethine nitrogen atoms. The hydrazone and it's complexes were tested for activities against a number of bacteria by well–diffusion technique in DMF.

2. Conclusions

It is evident from our brief literature survey that nitrogen-sulphur donor ligands systems play important role in coordination chemistry. The studies of complexes of this type of ligands have considerable attention in the light of tautomerism present in them. Transition metal complexes of N, S, O donor ligands have great interest due to their chemical- and structural peculiarities and also due to their analytical and biological applications. There are only a few reports on the synthesis, characterization and applications of metal complexes of substituted thiosemicarbazones and isonicotinoylhydrazones of 4-hydroxy-3-methoxyacetophenone, 4-[N,N(dimethyl)amino]benzaldehyde and crotonaldehyde. Therefore, in the present course of research, we have decided to synthesis and characterize the metal complexes of these ligands.

3. Scope and significance of the present investigation

Thiosemicarbazones and hydrazones are prominent ligands. The study of thiosemicarbazone- and hydrazone metal complexes showed that they have distinct solubility, better stability and promising biological activities. Our literature survey revealed that reports on systematic investigation on the coordination behaviour of N(4)-disubstituted thiosemicarbazones of substituted aldehydes and ketones are very less. It also revealed that di-substitution on N(4) of thiosemicarbazide moiety enhances their biological activities. Aroylhydrazones are multidentate ligands which form a variety of bioactive metal chelates with various metal ions by coordinating through oxygen and nitrogen atoms. By virtue of the presence of active thiosemicarbazone and hydrazone skeleton, we hope that these compounds and their complexes will be conceivably useful chemotherapeutic agents.

In the present investigation, we have synthesized transition metal complexes of different N(4)-methyl(phenyl)thiosemicarbazones and isonicotinoylhydrazones ligands. The main ligands that we have prepared during this investigations and their abbreviations are given below:

1. 2,4-Dihydroxybenzaldehyde N(4)-methyl(phenyl)thiosemicarbazones (HL) (DBMPTSC)

2. 4-[N,N-(Dimethyl)amino]benzaldehyde N(4)-methyl(phenyl)thiosemicarbazone (HL) (PDBMPTSC)

3. 4-Benzyloxybenzaldehyde N(4)-methyl(phenyl)thiosemicarbazones (HL) (BBMPTSC)

4. 4-Hydroxy-3-methoxyacetophenone N(4)-methyl(phenyl)thiosemicarbazones (HL) (AMPTSC)

5. Crotanaldehyde isonicotinoylhydrazone (HL) (CINH)

6. 4-[N,N-(Dimethyl)amino]benzaldehyde isonicotinoylhydrazone (HL) (PDBINH)

7. 4-Hydroxy-3-methoxyacetophenone isonicotinoylhydrazone (HL) (AINH)

8. 4-(4-Benzyloxybenzalidene) amino-2,3-dimethyl-1-phenyl-3-pyrazolo-5-one (L)

We have prepared the complexes of the first seven of these ligands with Co(II), Ni(II), Cu(II), Zn(II) and Cd(II) ions. These metal complexes were characterized by various physic-chemical methods like elemental analyses, magnetic susceptibility measurements and IR-, UV-Vis and ^{1}H NMR spectral techniques. Tentative structures of the compounds have been suggested. These studies are described in chapters three to nine. One of the ligands, 4-(4-benzyloxybenzalidene) amino-2,3-dimethyl-1-phenyl-3-pyrazolo-5-one was not used for the synthesis of metal complexes. Its single crystal X-ray diffraction analysis together with computational studies are presented in Chapter X. The reactivity and NLO studies of all ligands were done by DFT method. The geometry optimization have been generated at B3LYP/6-

311++G(d,p) using the GAUSS-VIEW 5.0.9 program. The details of computational studies are presented in Chapter XI. These eleven chapters are included in Part I of the thesis.

Besides the structural studies of the complexes, we have conducted their antimicrobial- and antioxidant evaluation and the results are presented in Part II. The inhibition effects of 2,4-dihydroxybenzaldehyde N(4)-methyl(phenyl)thiosemicarbazone, 4-[N,N-(dimethyl)amino]benzaldehyde N(4)-methyl(phenyl)thiosemi carbazone, 4-benzyloxybenzaldehyde N(4)-methyl(phenyl)thiosemi carbazone, 4-hydroxy-3-methoxyacetophenone N(4)-methyl(phenyl) thiosemicarbazone and 4-[N,N-(dimethyl)amino]benzaldehyde isonicotinoylhydrazone on bacterial strains such as *P. aeruginosa E. coli*, *S. aureus* and *B. subtilis* are of this part and on fungal cultures such as *C. albicans* and *A. niger* are included in Chapter XII.

The antioxidant activity of 2,4-dihydroxybenzaldehyde N(4)-methyl(phenyl)thiosemicarbazone, 4-benzyloxybenzaldehyde N(4)-methyl(phenyl)thiosemicarbazone, 4-hydroxy-3-methoxyacetophenone N(4)-methyl(phenyl)thiosemicarbazone and 4-hydroxy-3-methoxyacetophenone isonicotinoylhydrazoneand their metal complexes were evaluated using DPPH assay. The results of the analysis are presented in Chapter XIII of Part II of thesis.

The references cited in the text are arranged in a serial order at the end of each chapter.

References

[1] D. Barton, W. Ollis, Comprehensive Organic Chemistry, Vol. 2, Chap. 9.10. 3, Pergamon Press, Oxford, 1979.

[2] T. Hitoshi, N. Tamao, A. Hideyuki, F. Manabu, M. Takayuki, Preparation and characterization of novel cyclic tetranuclear manganese (III) complexes: MnIII 4 (X-salmphen) 6 (X-salmphenH2= N, N′-di-substituted-salicylidene-1, 3-diaminobenzene (X= H, 5-Br), Polyhedron 16(21) (1997) 3787-3794.

[3] M.E. Hossain, M. Alam, J. Begum, M.A. Ali, M. Nazimuddin, F. Smith, R. Hynes, The preparation, characterization, crystal structure and biological activities of some copper (II) complexes of the 2-benzoylpyridine Schiff bases of S-methyl-and S-benzyldithiocarbazate, Inorganica Chimica Acta 249(2) (1996) 207-213.

[4] C. Leelavathy, S.A. Antony, Synthesis, spectral characterization and biological activity of metal (II) complexes with 4-aminoantipyrine derivatives, Spectrochimica Acta Part A: Molecular and Biomolecular Spectroscopy 113 (2013) 346-355.

[5] S. Sonar, S. Vaidya, M. Bagal, T. Chondhekar, Potentiometric study of binary complexes of transition metal ion Cu^{+2} with scihff base ligands, Heterocyclic Letters 8(1) (2018) 185-189.

[6] W.-x. Hu, W. Zhou, C.-n. Xia, X. Wen, Synthesis and anticancer activity of thiosemicarbazones, Bioorganic & medicinal chemistry letters 16 (2006) 2213-8.

[7] R. Paiva, L. Kneipp, C. Goular, M. Albuquerque, A. Echevarria, Antifungal activities of thiosemicarbazones and semicarbazones against mycotoxigenic fungi, Ciencia e Agrotecnologia 38 (2014) 531-537.

[8] K.S.A. Melha, In-vitro antibacterial, antifungal activity of some transition metal complexes of thiosemicarbazone Schiff base (HL) derived from N4-(7′-chloroquinolin-4′-ylamino) thiosemicarbazide, Journal of Enzyme Inhibition and Medicinal Chemistry 23(4) (2008) 493-503.

[9] C. Shipman, SH Smith, JC Drachand D, L. Klaymann, Antimicrol. Agents Chemother 19 (1981) 682.

[10] M.J. Campbell, Transition metal complexes of thiosemicarbazide and thiosemicarbazones, Coordination Chemistry Reviews 15(2-3) (1975) 279-319.

[11] A.E. Graminha, A.A. Batista, J. Ellena, E.E. Castellano, L.R. Teixeira, I.C. Mendes, H. Beraldo, Ruthenium (II) complexes containing N (4)-tolyl-2-acetylpyridine thiosemicarbazones and phosphine ligands: NMR and electrochemical studies of cis–trans isomerization, Journal of Molecular Structure 875(1-3) (2008) 219-225.

[12] D.X. West, S.B. Padhye, P.B. Sonawane, Structural and physical correlations in the biological properties of transition metal heterocyclic thiosemicarbazone and S-alkyldithiocarbazate complexes, Complex Chemistry, Springer1991, pp. 1-50.

[13] J. Casas, M. Garcıa-Tasende, J. Sordo, Main group metal complexes of semicarbazones and thiosemicarbazones. A structural review, Coordination Chemistry Reviews 209(1) (2000) 197-261.

[14] T.S. Lobana, R. Sharma, G. Bawa, S. Khanna, Bonding and structure trends of thiosemicarbazone derivatives of metals—an overview, Coordination Chemistry Reviews 253(7-8) (2009) 977-1055.

[15] D.R. Richardson, P.C. Sharpe, D.B. Lovejoy, D. Senaratne, D.S. Kalinowski, M. Islam, P.V. Bernhardt, Dipyridyl thiosemicarbazone chelators with potent and selective antitumor activity form iron complexes with redox activity, Journal of medicinal chemistry 49(22) (2006) 6510-6521.

[16] D. Kovala-Demertzi, P.N. Yadav, J. Wiecek, S. Skoulika, T. Varadinova, M.A. Demertzis, Zinc (II) complexes derived from pyridine-2-carbaldehyde thiosemicarbazone and (1E)-1-pyridin-2-ylethan-1-one thiosemicarbazone. Synthesis, crystal structures and antiproliferative activity of zinc (II) complexes, Journal of Inorganic Biochemistry 100(9) (2006) 1558-1567.

[17] M. Karatepe, F. Karatas, Antioxidant, pro-oxidant effect of the thiosemicarbazone derivative Schiff base (4-(1-phenylmethylcyclobutane-3-yl)-2-(2-hydroxybenzylidenehydrazino) thiazole) and its metal complexes on rats, Cell Biochemistry

and Function: Cellular biochemistry and its modulation by active agents or disease 24(6) (2006) 547-554.

[18] Z. Afrasiabi, E. Sinn, W. Lin, Y. Ma, C. Campana, S. Padhye, Nickel (II) complexes of naphthaquinone thiosemicarbazone and semicarbazone: Synthesis, structure, spectroscopy, and biological activity, Journal of Inorganic Biochemistry 99(7) (2005) 1526-1531.

[19] M. Belicchi-Ferrari, F. Bisceglie, C. Casoli, S. Durot, I. Morgenstern-Badarau, G. Pelosi, E. Pilotti, S. Pinelli, P. Tarasconi, Copper (II) and cobalt (III) pyridoxal thiosemicarbazone complexes with nitroprusside as counterion: syntheses, electronic properties, and antileukemic activity, Journal of medicinal chemistry 48(5) (2005) 1671-1675.

[20] D.X. West, A.E. Liberta, S.B. Padhye, R.C. Chikate, P.B. Sonawane, A.S. Kumbhar, R.G. Yerande, Thiosemicarbazone complexes of copper (II): structural and biological studies, Coordination Chemistry Reviews 123(1-2) (1993) 49-71.

[21] N. Raja, R. Ramesh, Mononuclear ruthenium (III) complexes containing chelating thiosemicarbazones: Synthesis, characterization and catalytic property, Spectrochimica Acta Part A: Molecular and Biomolecular Spectroscopy 75(2) (2010) 713-718.

[22] İ. Kızılcıklı, B. Ülküseven, Y. Daşdemir, B. Akkurt, Zn (II) and Pd (II) Complexes of Thiosemicarbazone-S-alkyl Esters Derived from 2/3-Formylpyridine, Synthesis and Reactivity in Inorganic and Metal-Organic Chemistry 34(4) (2004) 653-665.

[23] X. Zhu, C. Wang, Z. Lu, Y. Dang, Synthesis, characterization and biological activity of the Schiff base derived from 3, 4-dihydroxybenzaldehyde and thiosemicarbazid, and its complexes with nickel (II) and iron (II), Transition Metal Chemistry 22(1) (1997) 9-13.

[24] X. Zhong, J. Yi, J. Sun, H.-L. Wei, W.-S. Liu, K.-B. Yu, Synthesis and crystal structure of some transition metal complexes with a novel bis-Schiff base ligand and their antitumor activities, European journal of medicinal chemistry 41(9) (2006) 1090-1092.

[25] M.S. Refat, I.M. El-Deen, Z.M. Anwer, S. El-Ghol, Bivalent transition metal complexes of coumarin-3-yl thiosemicarbazone derivatives: Spectroscopic, antibacterial activity and

thermogravimetric studies, Journal of Molecular Structure 920(1-3) (2009) 149-162.

[26] M.A. Ali, S. Livingstone, Metal complexes of sulphur-nitrogen chelating agents, Coordination Chemistry Reviews 13(2-3) (1974) 101-132.

[27] S. Padhye, G.B. Kauffman, Transition metal complexes of semicarbazones and thiosemicarbazones, Coordination Chemistry Reviews 63 (1985) 127-160.

[28] K. Jayakumar, M. Sithambaresan, A.A. Aravindakshan, M.P. Kurup, Synthesis and spectral characterization of copper (II) complexes derived from 2-benzoylpyridine-N4, N4-dimethyl-3-thiosemicarbazone: Crystal structure of a binuclear complex, Polyhedron 75 (2014) 50-56.

[29] K. Sampath, S. Sathiyaraj, G. Raja, C. Jayabalakrishnan, Mixed ligand ruthenium(III) complexes of benzaldehyde 4-methyl-3-thiosemicarbazones with triphenylphosphine/triphenylarsine co-ligands: Synthesis, DNA binding, DNA cleavage, antioxidative and cytotoxic activity, Journal of Molecular Structure 1046 (2013) 82–91.

[30] N. Moorthy, P.J. Prabakar, S. Ramalingam, G. Pandian, P. Anbusrinivasan, Vibrational, NMR and UV–visible spectroscopic investigation and NLO studies on benzaldehyde thiosemicarbazone using computational calculations, Journal of Physics and Chemistry of Solids 91 (2016) 55-68.

[31] B. Prathima, Y.S. Rao, G. Ramesh, M. Jagadeesh, Y. Reddy, P. Chalapathi, A.V. Reddy, Synthesis, spectral characterization and biological activities of Mn (II) and Co (II) complexes with benzyloxybenzaldehyde-4-phenyl-3-thiosemicarbazone, Spectrochimica Acta Part A: Molecular and Biomolecular Spectroscopy 79(1) (2011) 39-44.

[32] S. Sardari, S. Feizi, A.H. Rezayan, P. Azerang, S. mohammad Shahcheragh, G. Ghavami, A. Habibi, Synthesis and biological evaluation of thiosemicarbazide derivatives endowed with high activity toward Mycobacterium bovis, Iranian Journal of Pharmaceutical Research: IJPR 16(3) (2017) 1128.

[33] A.S. Reddya, L.S. Krishnaa, H. Rashmib, P.U.M. Devib, Y. Saralac, A.V. Reddya, Synthesis, spectroscopic characterization and

biological applications of Cu (II) and Ni (II) complexes with 2-butyl-4-chloro-5-formylimidazole thiosemicarbazone, Journal of Applied Pharmaceutical Science 6(10) (2016) 107-112.

[34] Y. Li, Z.-Y. Yang, J.-C. Wu, Synthesis, crystal structures, biological activities and fluorescence studies of transition metal complexes with 3-carbaldehyde chromone thiosemicarbazone, European journal of medicinal chemistry 45(12) (2010) 5692-5701.

[35] S.L. Narayana, B. Sung-Ok, T. Vijaya, N. Venkateswarlu, Biological Properties of 4-Benzyloxybenzaldehyde-4-Methyl-3-Thiosemicarbazone and its Cd (II) Complex, Research Journal of Biotechnology Vol 11 (2016) 12.

[36] R. Kothari, B. Sharma, Synthesis, characterization, antibacterial, antifungal, antioxidant and dna interaction studies of thiosemicarbazone transition metal complexes, World J. Pharm. Pharm. Sci 3(7) (2014) 1067-1080.

[37] S. Selvamurugan, R. Ramachandran, P. Vijayan, R. Manikandan, G. Prakash, P. Viswanathamurthi, K. Velmurugan, R. Nandhakumar, A. Endo, Synthesis, crystal structure and biological evaluation of Ni (II) complexes containing 4-chromone-N (4)-substituted thiosemicarbazone ligands, Polyhedron 107 (2016) 57-67.

[38] K.K. Aravindakshan, C.G.R. Nair, Preparation and characterization of vanillin thiosemicarbazone complexes with Co(II), Ni(II), Cu(II), Zn(II), Cd(II) and Hg(II), Proceedings of the Indian Academy of Sciences - Chemical Sciences 93(2) (1984) 111-115.

[39] D.P. Kumar, A.P. Kumar, T.V. Reddy, P.R. Reddy, Spectrophotometric Determination of Gold (III) Using 2-Hydroxy-3-Methoxy Benzaldehyde Thiosemicarbazone as a Chromophoric Reagent, ISRN Analytical Chemistry 2012 (2012).

[40] G.M. Pinto, J. Nayak, A.N. Shetty, Adsorption and inhibitor action of 4-(N, N-dimethylamino) benzaldehyde thiosemicarbazone on 6061 Al/SiC composite and its base alloy in sulfuric acid medium, Synthesis and Reactivity in Inorganic, Metal-Organic, and Nano-Metal Chemistry 41(2) (2011) 127-140.

[41] K. Sangeetha, K. Aravindakshan, Synthesis, structural and spectroscopic studies of 1-phenyl-3-methyl-4-benzoyl-5-pyrazolone

N (4)-methyl-N (4)-phenyl thiosemicarbazone and its cadmium (II) complex, Inorganica Chimica Acta 469 (2018) 25-31.

[42] J. Karthikeyan, P.P. Naik, A.N. Shetty, A rapid extractive spectrophotometric determination of copper (II) in environmental samples, alloys, complexes and pharmaceutical samples using 4-N, N (dimethyl) amino] benzaldehyde thiosemicarbazone, Environmental monitoring and assessment 176(1-4) (2011) 419-426.

[43] R. Harness, C. Robertson, F. Beckford, Thiosemicarbazone complexes of group 12 elements. An investigation of the thiosemicarbazone from p-dimethylaminobenzaldehyde, Journal of Undergraduate Chemistry Research 7(3) (2008) 92-97.

[44] A. Sankaraperumal, A. Nityananda Shetty, J. Karthikeyan, Synthesis, structural characterization, and biological application of p-[N, N-bis (2-chloroethyl) aminobenzaldehyde thiosemicarbazone and its nickel (II) complex, Synthesis and Reactivity in Inorganic, Metal-Organic, and Nano-Metal Chemistry 45(9) (2015) 1318-1326.

[45] S. Chandra, S. Raizada, M. Tyagi, A. Gautam, Synthesis, spectroscopic, and antimicrobial studies on bivalent nickel and copper complexes of bis (thiosemicrbazone), Bioinorganic Chemistry and Applications 2007 (2007).

[46] G. Pelosi, F. Bisceglie, F. Bignami, P. Ronzi, P. Schiavone, M.C. Re, C. Casoli, E. Pilotti, Antiretroviral activity of thiosemicarbazone metal complexes, Journal of medicinal chemistry 53(24) (2010) 8765-8769.

[47] P.P. Netalkar, S.P. Netalkar, V.K. Revankar, Transition metal complexes of thiosemicarbazone: Synthesis, structures and invitro antimicrobial studies, Polyhedron 100 (2015) 215-222.

[48] S.A. Khan, A.M. Asiri, K. Al-Amry, M.A. Malik, Synthesis, characterization, electrochemical studies, and in vitro antibacterial activity of novel thiosemicarbazone and its Cu (II), Ni (II), and Co (II) complexes, The Scientific World Journal 2014 (2014).

[49] B. Glinma, K. Salomé, F. Gbaguidi, C. Kapanda, J. Bero, J. Quetin-Leclercq, M. Moudachirou, J. Poupaert, G. Accrombessi, E. Gachomo, L. Baba-Moussa, S. Kotchoni, Trypanocidal and cytotoxic evaluation of synthesized thiosemicarbazones as potential drug leads against sleeping sickness, Molecular biology reports 41 (2014).

[50] L. Wang, D.-G. Guo, Y.-Y. Wang, C.-Z. Zheng, 4-Hydroxy-3-methoxy-benzaldehyde series aroyl hydrazones: synthesis, thermostability and antimicrobial activities, RSC Advances 4(102) (2014) 58895-58901.

[51] T.M. Fasina, C.U. Dueke-Eze, F.N. Idika, Synthesis, Spectroscopic and Antimicrobial properties of Co (II), Ni (II) and Cu (II) complexes of (E)-N'-(2-hydroxy-5-nitrobenzylidene) isonicotinohydrazide, Journal of Applied Sciences and Environmental Management 21(1) (2017) 120-125.

[52] A.A. El-Sherif, Synthesis, spectroscopic characterization and biological activity on newly synthesized copper (II) and nickel (II) complexes incorporating bidentate oxygen–nitrogen hydrazone ligands, Inorganica Chimica Acta 362(14) (2009) 4991-5000.

[53] N.K. Singh, N. Singh, A. Sodhi, A. Shrivastava, G.C. Prasad, Synthesis, characterization and antitumour studies on N-salicyl-N′-thiobenzohydrazide and its copper (II) complex, Transition Metal Chemistry 21(6) (1996) 556-559.

[54] X. Su, I. Aprahamian, Hydrazone-based switches, metallo-assemblies and sensors, Chemical Society Reviews 43(6) (2014) 1963-1981.

[55] M. Sutradhar, M.V. Kirillova, M.F.C.G. da Silva, C.-M. Liu, A.J. Pombeiro, Tautomeric effect of hydrazone Schiff bases in tetranuclear Cu (II) complexes: Magnetism and catalytic activity towards mild hydrocarboxylation of alkanes, Dalton Transactions 42(47) (2013) 16578-16587.

[56] G. Vasilikiotis, Analytical applications of isonicotinoyl hydrazones: I. A new selective reagent for mercury, Microchemical Journal 13(4) (1968) 526-528.

[57] G. Vatsa, O. Pandey, S. Sengupta, Synthesis, spectroscopic and toxicity studies of titanocene chelates of isatin-3-thiosemicarbazones, Bioinorganic chemistry and applications 3 (2005).

[58] G.S. Amrita Parle, Synthesis, Characterization and Biological Evaluation of Novel Isonicotinic Acid HydrazideDerivatives, European Journal of Biotechnology and Bioscience 5(3) (2017) 21-27.

[59] A. Ahmed, M. Dalia, H. Fatmaa, Preparation and Spectral Characterization of Isonazide Ligand with Some Transition Metal Complexes, Australian Journal of Basic and Applied Sciences 9(31) (2015) 42-46.

[60] B. Moksharagni, S. Chandrasekhar, R.K. Hussain, K. Kumar, SYnthesis, spectral characterization and evaluation of invitro antibacterial activity of isonicotinoyl hydrazones bearing pyridine moiety, International Journal of Pharma and Bio Sciences 6(3) (2015) 11-18.

[61] M.L. Dianu, A. Kriza, N. Stanica, A.M. Musuc, Transition metal M (II) complexes with isonicotinic acid 2-(9-anthrylmethylene)-hydrazide, J. Serb. Chem. Soc 75(11) (2010) 1515-1531.

[62] M. Malhotra, G. Sharma, A. Deep, Synthesis and characterization of (E)-N'-(substituted benzylidene)isonicotinohydrazide derivatives as potent antimicrobial and hydrogen peroxide scavenging agents, Acta poloniae pharmaceutica 69(4) (2012) 637-44.

[63] R.K. Agarwal, D. Sharma, L. Singh, H. Agarwal, Synthesis, biological, spectral, and thermal investigations of cobalt (II) and nickel (II) complexes of N-isonicotinamido-2′, 4′-dichlorobenzalaldimine, Bioinorganic Chemistry and Applications (2006)29234.

[64] V. Desai, R. Shinde, Green synthesis of nicotinic acid hydrazide schiff bases and its biological evaluation, Int J Pharm 5 (2015) 930-935.

[65] M.C. Mandewale, B. Thorat, D. Shelke, R. Yamgar, Synthesis and Biological Evaluation of New Hydrazone Derivatives of Quinoline and Their Cu(II) and Zn(II) Complexes against Mycobacterium tuberculosis, Bioinorganic chemistry and applications (2015) 153015.

[66] S. Prasad, R.K. Agarwal, Nickel (II) complexes of hydrazone of isoniazid and their magneto-spectral, electrochemical, thermal and antimicrobial investigations, International Journal of Inorganic Chemistry (2008) 350921.

[67] K.S. Abou-Melha, Transition metal complexes of isonicotinic acid (2-hydroxybenzylidene) hydrazide, Spectrochimica Acta Part A: Molecular and Biomolecular Spectroscopy 70(1) (2008) 162-170.

[68] R.K. Agarwal, R.K. Sarin, Synthesis and characterization of some lanthanide (III) perchlorato complexes of hydrazones of isonicotinic acid hydrazide, Polyhedron 12(19) (1993) 2411-2415.

[69] S.R. Kelode, T.R. Kale, P.R. Mandlik, Synthesis, characterization and thermal studies of Schiff base complexes of Co(II),Ni(II),Cu(II),Zn(II),Cr(III), Fe(III),Mn(III),Vo(IV) and Zr(IV), International Journal of ChemTech Research 5 (2013) 362-366.

[70] R. El-Bahnasawy, E. El-Shereafy, Y. Issa, S. El-Meleigy, Thermal-conductimetric studies on some isonicotinoyl hydrazone derivatives and their metal complexes, Thermochimica acta 173 (1990) 9-16.

[71] R.K. Agarwal, L. Singh, D.K. Sharma, R. Singh, Synthesis, spectral and thermal investigations of some oxovanadium (IV) complexes of hydrazones of isonicotinic acid hydrazide, Turkish Journal of Chemistry 29(3) (2005) 309-316.

[72] A. Kriza, M.L. Dianu, N. Stanica, C. Draghici, M. Popoiu, Synthesis and characterization of some tranzition metals complexes with glyoxal bis-isonicotinoyl hydrazone, Rev Chim 60 (2009) 555-60.

CHAPTER II

MATERIALS AND METHODS

A brief account of the materials used and methods employed for the synthesis of the ligands and the complexes are given in this chapter. The details of various instruments used for the characterization of the ligands and the complexes are also discussed here. However, all specific synthetic procedures and experimental set up are explained in the relevant chapters.

1. Metal salts

For the synthesis of Co(II), Ni(II), Cu(II), Zn(II) and Cd(II) complexes, corresponding metal chlorides were used. They were Sigma Aldrich/ Qualigens , AnalaR or equivalent grade.

2. Solvents

The solvents such as methanol, ethanol, diethyl ether, petroleum ether, chloroform, dimethylformamide and DMSO were used for the synthesis, extraction and recrystallization of the ligands and the complexes. Commercially available solvents like ethanol and methanol were purified according to the standard procedures [1]. Others were E. Merck reagents and used as such. The solvents used for the spectral studies were of spectroscopic grade.

3. Other reagents

Other main reagents used in this work were N-methylaniline, carbon disulphide, sodium chloroacetate, hydrazine hydrate, sodium hydroxide pellets, hydrochloric acid, sulphuric acid, glacial acetic acid, etc. Precursors of ligands such as 4-benzyloxybenzaldehyde, 4-

hydroxy-3-methoxyacetophenone, 2,4-dihydroxybenzaldehyde and crotonaldehyde were purchased from Sigma Aldrich or Alfa Aesar. They were used as such without further purification.

4. Synthesis of ligands

4.1. Synthesis of N(4)-methyl(phenyl)thiosemicarbazide (MPTSC)

N(4)-Methyl(phenyl) thiosemicarbazide was synthesized following a reported procedure [2]. It involves two steps:

4.1.1. Preparation of carboxymethyl N(4)-methyl(phenyl)dithiocarbamate

To a mixture consisting 12 ml (15.2 g, 0.20 mol) of carbon disulphide and 21.6 mL (21.2 g, 0.20 mol) of N-methylaniline, an aqueous solution of 8.4 g (0.21mol in 250 mL) of sodium hydroxide pellets was added. This solution was stirred at room temperature for about 4 hr till the organic layer disappeared. At this point, the resulting pale orange coloured solution was treated with about 23.2 g (0.20mol) of sodium chloroacetate, added in small portions with stirring. The stirring was continued for 1 hr. The solution was then allowed to stand overnight (for about 17 h). The resulting pale yellow solution was acidified with 25 mL of conc. HCl and the buff coloured solid separated was collected and dried. (Yield 80%, M.P 197-198^{0}C).

4.1.2 Preparation of N(4)-methyl(phenyl)thiosemicarbazide

A solution of 17.7g (0.0733mol) of carboxymethyl N(4)-methyl(phenyl)dithiocarbamate in 20 mL of 98% hydrazine

hydrate and 10 mL of water was heated on a water bath for about 10 minutes, when colourless crystals began to appear. Heating was continued for another 5 minutes. The cooled mixture was filtered, washed with water and dried under lamp. The crude product was recrystallized from a mixture of ethanol and water. The colourless, triclinic crystals formed were filtered and dried. (Yield 80%, M.P 122^0C). Mechanism of reaction pathway of N(4)-methyl (phenyl)thiosemicarbazide can be represented as in Scheme 1.

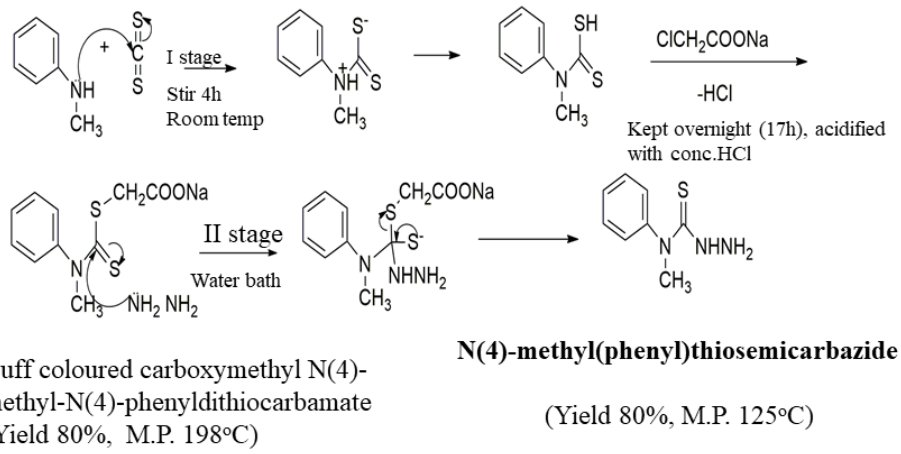

Scheme 1. Mechanism of formation of N(4)-methyl (phenyl)thiosemicarbazide

4.1.3. Preparation of thiosemicarbazones and hydrazones

Thiosemicarbazones and hydrazones (listed below) were prepared by refluxing the precursors in stoichiometric ratio. The details of preparation of each ligand and its complexes are given in the respective chapter. The ligands synthesized and used in this investigation are:

- 2,4-Dihydroxybenzaldehyde N(4)-methyl(phenyl)thiosemicarbazone (HL) (DBMPTSC)
- 4-[N,N(Dimethyl)amino]benzaldehyde N(4)-methyl(phenyl)thiosemicarbazone (HL) (PDBMPTSC)
- 4-Benzyloxybenzaldehyde N(4)-methyl(phenyl)thiosemicarbazone (HL) (BBMPTSC)
- 4-Hydroxy-3-methoxyacetophenone N(4)-methyl(phenyl)thiosemicarbazone (HL) (AMPTSC)
- Crotonaldehyde isonicotinicotinoylydrazone (HL) (CINH)
- 4-[N,N(Dimethyl)amino]benzaldehyde isonicotinicotinoylhydrazone (HL) (PDBINH)
- 4-Hydroxy-3-methoxyacetophenone isonicotinicotinoylydrazone (HL) (AINH)
- 4-(4-Benzyloxybenzalidene)amino-2,3-dimethyl-1-phenyl-3-pyrazolo-5-one (L)

5. Analytical methods

Semi-microanalyses were conducted by standard methods to check the purity of the compounds. Carbon, hydrogen, and nitrogen estimations were carried out by microanalyses using EUROVECTOR EA 3000 at Sophisticated Analytical Instrument Facility, CSIR- Central Drug Research Institute, Lucknow. The percentages of metals present in the

complexes were determined by reported methods [3]. For the estimation of metal, a known amount of the complex was decomposed by digesting with a mixture of concentrated nitric acid and perchloric acid. The decomposition process was repeated twice or thrice by the addition of fresh concentrated nitric acid and finally with concentrated hydrochloric acid to confirm the completion of decomposition process. After cooling, it was extracted with distilled water and the solution was used for the estimation of the metal. Cobalt, zinc and cadmium were estimated by EDTA titrimetric method. Copper was estimated iodometrically using standard sodium thiosulphate solution [4]. Nickel was estimated gravimetrically. Estimation of chloride was done gravimetrically as silver chloride. Sulphur was estimated gravimetrically as barium sulphate.

6. Physico-chemical methods

The physico-chemical studies of the ligands and the complexes were carried out by using spectro-analytical techniques such as IR-, ^{1}H-NMR, ESI-MS, magnetic succesptibility measurements, single crystal X-ray crystallography, thermo garvimetric analysis, electron paramagnetic resonance- and electronic spectral studies. Detailed information concerning NLO-, antimicrobial- and antioxidant studies using the ligands are described in the respective chapters of the thesis.

6.1. Infrared spectra

The FT-IR spectra of the ligands and the complexes were recorded in KBr medium, on a Jasco FTIR 4100 spectrometer (4000-400 cm^{-1}).

6.2. Electronic spectra

UV-Visible spectra of the compounds were recorded on JASCO V-750 Spectrophotometer with a scanning range of 200-900 nm. Depending on the solubilities of complexes, their electronic spectra were recorded either in solution (10^{-3} M) or in the solid state.

6.3. ^{1}H NMR spectra

^{1}H NMR spectra of the ligands and Zn(II) and Cd(II) complexes were recorded in DMSO-*d6* by using Bruker Avance III, 400MHz with 9.4 Tesla super-conducting magnet spectrometer.

6.4. Mass spectra

Mass spectral analysis of the ligands were done at Sophisticated Analytical Instrument Facility, CSIR- Central Drug Research Institute , Lucknow using Waters UPLC-TQD Mass spectrometer with a mass range of 100-2000 Da , Provide [M+1]+ ion or adduct ions.

6.5. Electron Spin Resonance spectra

EPR spectra were recorded on a Varian E-112X-band and JEOL JES-FA200 ESR Spectrometer with X and Q band using tetracyanoethylene (TCNE) as a standard at Sophisticated Analytical Instrument Facility (SAIF), IITB, Bombay. The EPR spectra in solution at 77 K were recorded, using the 100 kHz field modulation; g factors were quoted relative to the standard marker, TCNE (g = 2.00277).

6.6. Magnetic susceptibility measurements

The magnetic susceptibility measurements of the complexes were done at room temperature on a Gouy-type magnetic balance (Sherwood Scientific magnetic susceptibility balance). $Hg[Co(NCS)_4]$ was used as calibrant . Diamagnetic corrections, using Pascal's constants, were applied by adding the diamagnetic contributions of various atoms and structural units [5]. The net magnetic moments of the complexes were calculated in Bohr Magneton (B.M) from the corrected molar susceptibilities.

6.7. Single crystal X-ray crystallography

Crystallographic analysis of the compounds were perfomed on Bruker Kappa APEXII (Mo Kα) diffractometer, at Sophisticated Test and Instrumentation Centre, Kochi. Direct methods were used to solve the structures and refined by full-matrix least-squares method using SHELXL-97/ SHELXL-2014/7 [6, 7]. The crystallographic tools, PLATON [8], ORTEP [9], DIAMOND [10] and MERCURY [11] were used for structure analysis and presentation of the results.

6.8. Thermo gravimetric analysis

Thermo gravimetric analysis of the complexes were done using a Perkin Elmer Simultaneous Thermal Analyser (STA 8000), at Central Sophisticated Instrumentation Facility (CSIF), University of Calicut.

References

[1] O. Solvents, A. Weissberger, ES Proskauer, JA Riddick, EE Toops, Organic Solvents, Interscience, New York (1955).

[2] J.P. Scovill, D.L. Klayman, C.F. Franchino, 2-Acetylpyridine thiosemicarbazones. 4. Complexes with transition metals as antimalarial and antileukemic agents, Journal of Medicinal Chemistry 25(10) (1982) 1261-1264.

[3] A.I. Vogel, J. Bassett, J. Bassett, Vogel's textbook of quantitative inorganic analysis: including elementary instrumental analysis, Longman London1978.

[4] B.S. Furniss, Vogel's textbook of practical organic chemistry, Pearson Education India1989.

[5] A. Earnshaw, Introduction to magnetochemistry, Elsevier2013.

[6] G.M. Sheldrick, Program for the solution of crystal structures, SHELXL-97. (1997).

[7] G. Sheldrick, SHELXL-2014/7: program for the solution of crystal structures, University of Göttingen, Göttingen, Germany (2014).

[8] A. Spek, Single-crystal structure validation with the program PLATON, Journal of applied crystallography 36(1) (2003) 7-13.

[9] L.J. Farrugia, WinGX and ORTEP for Windows: an update, Journal of Applied Crystallography 45(4) (2012) 849-854.

[10] C. Impact, DIAMOND-Crystal and Molecular Structure Visualization (Version 4), (2009).

[11] C.F. Macrae, P.R. Edgington, P. McCabe, E. Pidcock, G.P. Shields, R. Taylor, M. Towler, J. Streek, Mercury: visualization and analysis of crystal structures, Journal of Applied Crystallography 39(3) (2006) 453-457.

CHAPTER III

SYNTHESIS AND CHARACTERIZATION OF TRANSITION METAL COMPLEXES OF 2,4-DIHYDROXYBENZALDEHYDE N(4)-METHYL(PHENYL)THIOSEMICARBAZONE

1. Introduction

Thiosemicarbazones are an important class of multidentate ligands with potential S and N donor sites. They have gained much importance because of the pharmacological activities associated with them. They show antitumor, antiviral and antibacterial activities[1]. They are also used as fungicides and pesticides[2]. Transition metal complexes of thiosemicarbazone have attracted special attention[3]. Thiosemicarbazones with OH group at the ortho position to the azomethine group are of much interest mainly due to the presence of hydrogen bonds of either O-H. . .N or O. . . .H-N type and tautomerism between enol-imine and keto-amine forms. A detailed literature survey revealed that such thiosemicarbazones and their first row transition metal complexes show good antibacterial-, antiviral- and super oxygen dismutase activities[4-6]. Several thiosemicarbazones show good corrosion inhibition activities in acidic medium. Their inhibition capacity against mild steel corrosion is found to enhance with the introduction of groups with delocalized *pi* electron density on the thiosemicarbazone moiety[7].

Quite contrary to these observations, most of the work reported are on unsubstituted thiosemicarbazones. It is found that much less work has been reported on that N(4) di-substituted thiosemicarbazone. Therefore, our attention was drawn to 2,4-dihydroxybenzaldehyde N(4)-methyl(phenyl)thiosemicarbazone (HL) and in this chapter the synthesis and characterization of this new ligand, (Fig.1) and its Co(II), Ni(II), Cu(II), Zn(II), and Cd(II) complexes are discussed.

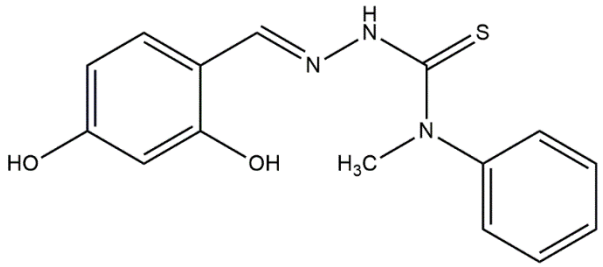

Fig.1. 2,4-Dihydroxybenzaldehyde N(4)-methyl(phenyl) thiosemicarbazone (HL)

*IUPAC Name: (*E*)-2-(2,4-dihydroxybenzylidene)-*N*-methyl-phenylhydrazinecarbothioamide.

2. Experimental

2.1. Materials and methods

Details regarding the chemicals used and the methods adopted for the characterization of the compounds are described in Chapter II.

2.2. Preparation of the ligand (HL)

A mixture of N(4)-methyl(phenyl)thiosemicarbazide (0.005mol) in ethanol (30 ml), 2,4-dihydroxybenzaldehyde (0.005mol) and catalytic amount of glacial acetic acid was refluxed for 4hr on a water bath. Slow evaporation of the solvent yielded yellow coloured single crystals and the product was recrystallized. The synthetic procedure of the ligand, 2,4-dihydroxybenzaldehyde N(4)-methyl(phenyl) thiosemicarbazone (HL) is shown below in the Scheme 1.

2.3. Preparation of the complexes

An ethanolic solution of metal chloride (0.025mol in 30 ml) was added drop wise to an ethanolic solution of HL (0.05mol in 30 ml) and refluxed for 4hr. The product was kept aside for slow evaporation. The precipitate was filtered, washed with ethanol for several times and dried over anhydrous calcium chloride.

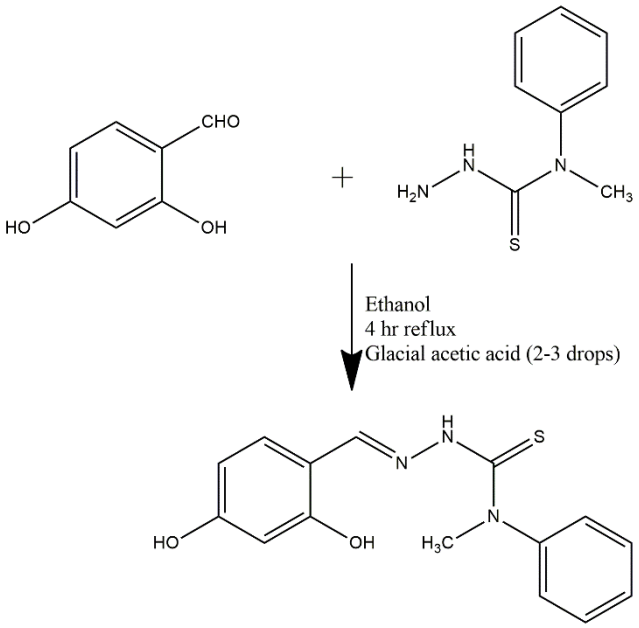

Scheme 1. Synthetic pathway of 2,4-dihydroxybenzaldehyde N(4)-methyl(phenyl)thiosemicarbazone (HL)

3. Results and discussion

The data obtained from the analytical- and physico-chemical studies have been used to assign the structures and geometries of the compounds.

3.1. Characterization of the ligand (HL)

The ligand was characterized by single crystal X-ray analysis, IR, UV-Vis and ^{1}H NMR spectral techniques.

3.1.1. Micro analytical data

The CHNS percentages of the ligand, 2,4-dihydroxybenzaldehyde N(4)-methyl(phenyl)thiosemicarbazone (HL) was in good agreement with the suggested formula, $C_{15}H_{15}N_3O_2S$ (Table 1). It was non-hygroscopic and stable at normal atmospheric conditions. It melted at 179°C and was soluble in DMSO, DMF, chloroform, etc.

Table 1. Physico-chemical and analytical data of HL

Compound (Empirical Formula)	**Yield (%)**	**Melting Point (^{0}C)**	**Colour**	**CHNS Analysis Found % (Calculated)%**			
				C	**H**	**N**	**S**
$C_{15}H_{15}N_3O_2S$	65	179^{0}C	Yellow	59.32 (59.72)	4.91 (4.97)	13.18 (13.93)	9.96 (10.61)

3.1.2. Single crystal X-ray crystallography

Single crystals of HL suitable for X-ray analysis were obtained from its solution in ethanol. A crystal with the dimensions, 0.60 x 0.30 x 0.20 mm was selected for collecting the data. It crystallized with one molecule per asymmetric unit into monoclinic crystal system with a space group of P 21/c. X-ray crystallographic data were collected at 296(2) K on a Bruker Model Kappa Apex II diffractometer by

employing graphite monochromated Mo $K\alpha$ (λ = 0.71073 Å) radiation. Direct methods were used to solve the structure and was refined by least square method on F^2 using SHELXL-97[8]. The crystallographic tools, PLATON[9], ORTEP[10], DIAMOND3.2d[11] and MERCURY3.5.1[12] for windows were used for structure analysis and presentation of the results. All non-hydrogen atoms were refined anisotropically. The details of the X-ray data collection and structure refinements are given in Table 2. Bond distances and angles are listed in Table 3. The PLATON diagram of HL with the atom numbering scheme is shown in Fig.2. The packing pattern of HL is shown in Fig.3. Hydrogen bonding interaction parameters of HL are shown in Fig.4. Crystallographic data of the compound have been deposited with the Cambridge Crystallographic Data Centre as supplementary publication No.1941848.

A torsion angle value of -3.1(2) corresponding to S(1)-C(8)-N(2)-N(3) moiety confirms the *syn-periplanar* configuration of the S(1) atom with respect to azomethine nitrogen atom, N(3). A torsion angle of -5.7(3) corresponding to N(2)-C(8)-N(1)-C(6) moiety indicates a little distortion from the *periplanar* configuration of the phenyl ring of the thioemicarbazone part from azomethine and aromatic aldehyde part. The terminal nitrogen atoms, N(1) and N(3) of the thiosemicarbazide fragment are in an anti-periplanar conformation with respect to the C(8)–N(2) with a torsion angle of [N(1)-C(8)-N(2)-N(3)] 176.98(16)°. Similarly, the nitrogen atoms, N(1) and N(3) of the thiosemicarbazide fragment are in an anti-periplanar conformation

with respect to C(8)–N(2), with a torsion angle −179.16(18)^0. The bond angles of C(10)–C(9)–N(3), C(8)–N(2)–N(3) and C(9)–N(3)–N(2) are 121.10(15), 120.02(15) and 116.70(14)^0, respectively. It is an evidence for the deviation of the co-planarity of thiosemicarbazide- and aldehyde moieties. The bond distances, C(8)–N(1), C(8)–N(2) , C(9)–N(3) and N(2)–N(3) are1.337(2), 1.347(2), 1.274(2) and 1.367(2) Å, respectively. They are found to be intermediate between the analogous single [C–N, 1.47 and N–N, 1.45 Å] and double [C=N, 1.28 and N=N, 1.25 Å] bond distances[13]. Similarly, C(11)-O(2) has a bond distance of 1.3573(18) A^0 which is also consistent with the C-O single bond. The bond distance of C(8)-S(1) is 1.6798(17) A^0, which is intermediate between single- and double bonds. The bond angle of N(1)-C(8)-N(2) is 115.54(15)^0. It is narrower when compared with the bond angle of N(1)-C(8)-S(1) [123.71(12)^0]. This may be due to the intra-molecular hydrogen bonding between the free hydroxyl group and the imine nitrogen. The crystal structures are stabilized by intra-molecular- and inter-molecular hydrogen bonding interactions[14].

Table 2. Crystal data and structure refinement parameters for compound, HL

Identification code	shelx		
Empirical formula	$C_{15}H_{15}N_3O_2S$	Theta range for data collection	2.754 - 28.453 deg
Formula weight	301.36	R indices (all data)	R1 = 0.0682, wR2 = 0.126
Temperature	296(2) K	Goodness-of-fit on F^2	0.961
Refinement method	Full-matrix least-squares on F^2	Limiting indices	-7<=h<=9, -16<=k<=19, -18<=l<=18
Wavelength	0.71073 A	Extinction coefficient	n/a
Crystal size	0.60x0.30 x 0.20 mm	Completeness to theta	25.242 100.0 %
Crystal system, space group	Monoclinic, P 21/c	Reflections collected	11898
Unit cell dimensions		Independent reflections	3745 [R(int) = 0.0322]
a (A^0)	7.5056(5)	Max. and min. transmission	0.957 and 0.878
b (A^0)	14.3457(15)	Data / restraints / parameters	3745 / 0 / 197
c (A^0)	14.1312(14)	Absorption coefficient	0.223 mm^{-1}
α(°)	90 deg	F(000)	632
β(°)	99.802(4) deg	Z	4, 1.335 Mg/m^3
γ(°)	90 deg.	Volume	1499.3(2) A^3

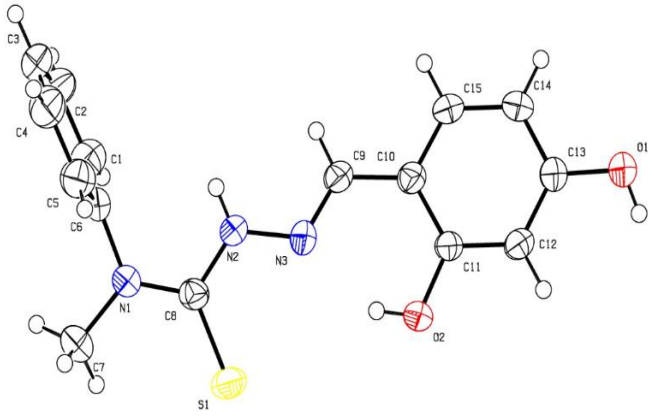

Fig.2. The PLATON diagram of HL with atom numbering scheme

Table 3. Selected structure parameters of HL

Bond Length (Å)		**Bond Angle (°)**		**Torsion Angles (°)**	
C(1)-C(6)	1.376(3)	C(6)-C(1)-C(2)	119.7(2)	N(3)-C(9)-C(10)-C(15)	-175.15(17)
C(1)-C(2)	1.383(3)	N(1)-C(8)-N(2)	115.54(15)	N(3)-C(9)-C(10)-C(11)	5.9(3)
C(1)-H(2)	0.9300	N(1)-C(8)-S(1)	123.71(12)	C(9)-C(10)-C(11)-O(2)	-0.7(3)
C(3)-C(4)	1.367(4)	C(15)-C(10)-C(9)	119.66(15)	O(2)-C(11)-C(12)-C(13)	-179.81(17)
C(4)-C(5)	1.380(3)	O(2)-C(11)-C(12)	117.34(14)	C(11)-C(12)-C(13)-O(1)	179.83(17)
C(5)-C(6)	1.369(3)	C(12)C(11)C(10)	120.39(15)	C(11)-C(12)-C(13)-O(1)	179.83(17)
C(6)-N(1)	1.441(2)	O(1)-C(13)-C(14)	117.39(15)	N(2)-C(8)-N(1)-C(6)	-5.7(3)
C(7)-N(1)	1.462(2)	C(8)-N(1)-C(6)	122.49(13)	S(1)-C(8)-N(1)-C(6)	174.39(14)
C(7)-H(7A)	0.9600	C(8)-N(1)-C(7)	122.12(15)	S(1)-C(8)-N(1)-C(7)	-4.8(2)
C(8)-N(1)	1.337(2)	C(9)-N(3)-N(2)	116.70(14)	N(1)-C(8)-N(2)-N(3)	176.98(16)
C(8)-N(2)	1.347(2)	N(2)-C(8)-S(1)	120.75(13)	S(1)-C(8)-N(2)-N(3)	-3.1(2)
C(8)-S(1)	1.6798(1)	C(11)-C(10)-C(9)	122.70(15)	C(10)-C(9)-N(3)-N(2)	178.31(16)
C(9)-N(3)	1.274(2)	N(3)-C(9)-C(10)	121.10(15)	C(8)-N(2)-N(3)-C(9)	167.96(17)

C(9)-C(10)	1.435(2)	C(8)-N(2)-N(3)	120.02(15)	N(2)-C(8)-N(1)-C(7)	175.13(17)
C(10)-C(15)	1.394(2)	C(6)-N(1)-C(7)	115.39(14)		
C(10)-C(11)	1.401(2)				
C(11)-O(2)	1.3573(18)				
C(11)-C(12)	1.375(2)				
C(12)-C(13)	1.383(2)				
C(13)-O(1)	1.355(2)				
C(13)-C(14)	1.384(2)				
C(14)-C(15)	1.364(3)				
N(2)-N(3)	1.367(2)				
N(2)-H(2N)	0.82(2)				
O(1)-H(1A)	0.8200				
O(2)-H(2A)	0.8200				

3.1.3. Spectroscopic analysis

a) Electronic spectrum

The electronic spectrum of the ligand showed an intense band at 285 nm due to $\pi \rightarrow \pi^*$ transition of the azomethine chromophore and the benzene ring (intra-ligand charge-transfer transition). The band at 333 nm in the spectrum may be attributed to $n \rightarrow \pi^*$ transition. The data are given in Table 4.

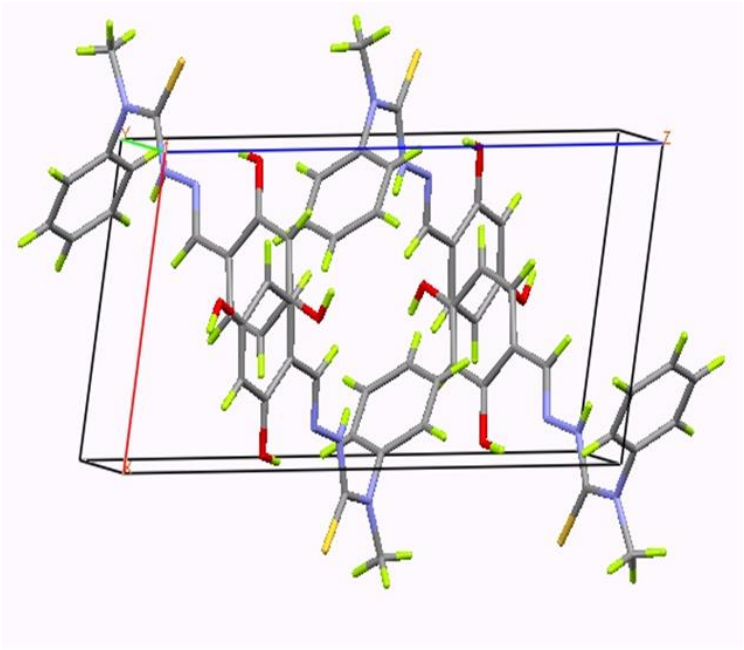

Fig.3. Packing pattern of HL

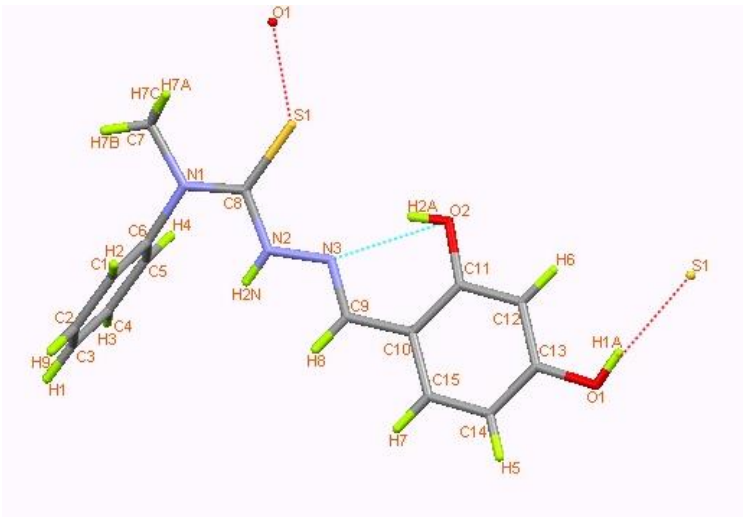

Fig.4. H-bond interactions (shown as *dashed lines*) of HL

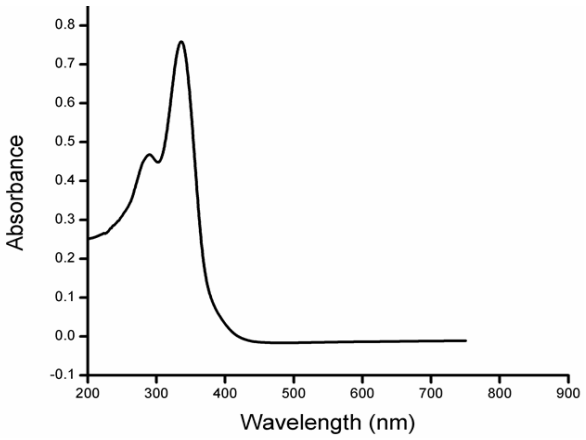

Fig.5. Electronic spectrum of HL

Table 4. Electronic spectral bands of HL

Spectral bands (nm)	**Assignments**
285	$\pi \rightarrow \pi^*$ transition
333	$n \rightarrow \pi^*$ transition

b) Infrared spectrum

The important vibrational bands of the ligand with the tentative assignments are given in the Table 5 and Fig.6. Thioamide (NH–C=S–) group in the ligand indicated the possibility of thione-thiol tautomers[15]. A band of medium intensity at 3290 cm^{-1} due to asymmetric stretching of the secondary –NH group of the thioamide part ruled out the existence of the ligand as a thiol tautomer[16]. The presence of a band at 836 cm^{-1} due to υ(C=S) and the absence of a band ~ 2500 cm^{-1}, characteristic of υ(S-H) confirmed the existence of

the ligand in thione form [17]. The band at 3055 cm^{-1} may be attributed to the stretching vibration of the aromatic C-H group. The presence of an intense band at 1626 cm^{-1} was characteristic of an azomethine (>C=N) group. The medium intensity band at 1040 cm^{-1} in the spectrum can be assigned to δ(N-N) vibration.

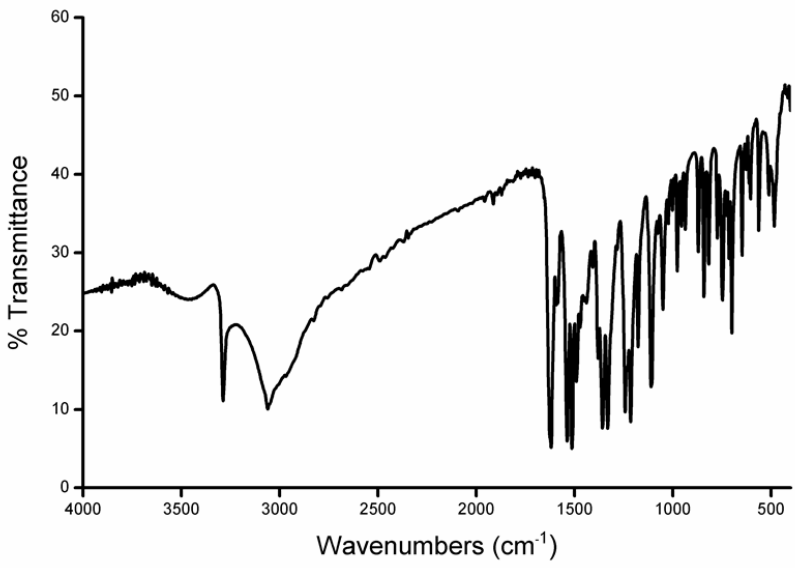

Fig.6. IR spectrum of HL

Table 5. Significant IR spectral bands (in cm^{-1}) of HL

Bands (cm^{-1})	**Assignments**
3290	υ(N-H)
3055	υ(C-H) (aromatic)
1626	υ(C=N)
1040	δ (N-N)
836	υ(C=S)

c) ^{1}H NMR spectrum

The ^{1}H NMR spectrum of the ligand was recorded in DMSO-d_6. There was a sharp singlet peak at 11.54 ppm due to N-H proton attached to azomethine group (Table 6). A sharp signal at 3.58 ppm was assignable to CH_3 protons on the terminal N-atom. The phenolic proton (*O*–OH) showed a singlet at 10.84 ppm and a signal at 8.25 ppm represented the phenolic proton (*p*–OH). The proton attached to azomethine moiety resonated at 9.87 ppm. The multiplet signals appeared in the range of 7.49–6.26 ppm were attributed to eight aromatic protons. A solvent peak observed near to 2.5 ppm.

Table 6. ^{1}H NMR assignments of HL

δ (ppm)	**Assignments**
11.54	N-H proton
10.84	Ar-OH group (*ortho*)
9.87	Azomethine hydrogen
8.25	Ar-OH group (*para*)
7.49 - 6.26 (m)	Aromatic protons
3.584	-CH_3 group on terminal nitrogen atom

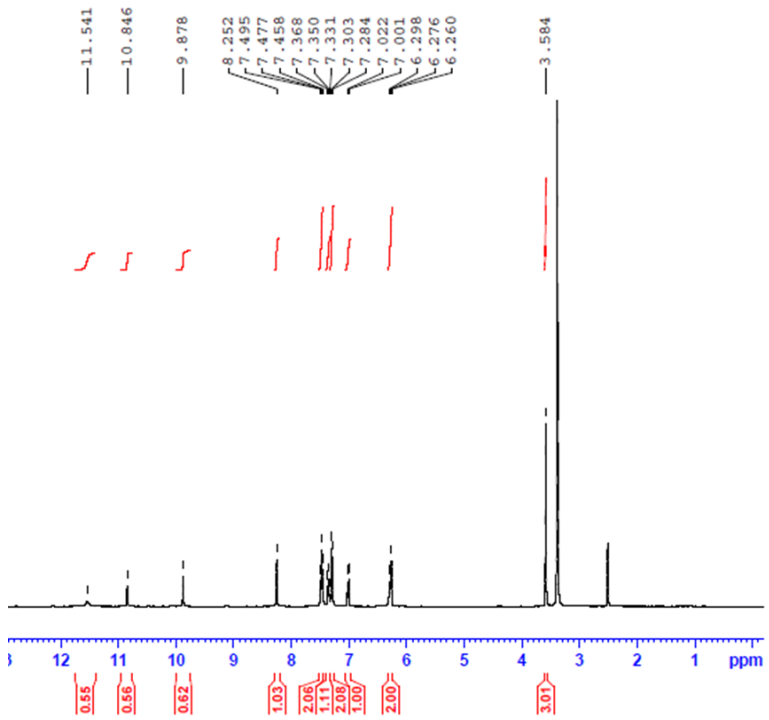

Fig.7. ^{1}H NMR spectrum of HL

3.2. Characterization of the complexes

2,4-dihydroxybenzaldehyde N(4)-methyl(phenyl)thiosemicarbazone (HL) formed stable complexes with Co(II), Ni(II), Cu(II), Zn(II) and Cd(II) ions. These complexes were soluble in chloroform, DMSO, DMF, etc. They were characterized as follows;

3.2.1. Analytical data of metal complexes

The analytical data and physical properties of all the complexes are listed in Table 7. The ligand on interaction with Co(II), Ni(II), Cu(II), Zn(II) and Cd(II) formed complexes with moderate yields. All the

complexes were found to be non-hygroscopic and stable at normal atmospheric conditions. They all had sharp melting points which indicated their purity. The purity was also checked by TLC method. Elemental analytical data of all the complexes were in good agreement with the suggested molecular formulae. The general formula of the complexes was found to be $[M(HL)_2Cl_2].H_2O$, where M = Ni(II) or Cu(II). The Co(II) complex was found to be $[M(HL)_2]Cl_2.H_2O$. The Zn(II) and Cd(II) complexes were of the type, $[Zn(HL)Cl_2]$ and $[CdL_2]$, respectively.

Table 7. Physico-chemical and analytical data of the complexes

Compound	**Colour**	**Yield (%)**	**M.P (^{0}C)**	**Elemental Analysis (%) found (calculated)**				
				C	**H**	**N**	**S**	**Metal**
$[Co(HL)_2]Cl_2.H_2O$	Black	60	192	47.21 (47.96)	4.01 (4.26)	11.01 (11.19)	7.98 (8.52)	7.41 (7.85)
$[Ni(HL)_2Cl_2].H_2O$	Reddish orange	63	197	47.21 (47.98)	4.00 (4.26)	11.02 (11.19)	8.23 (8.53)	7.29 (7.82)
$[Cu(HL)_2Cl_2].H_2O$	Dark green	61	189	47.03 (47.67)	4.01 (4.24)	11.10 (11.12)	8.19 (8.47)	7.89 (8.41)
$[Zn(HL)Cl_2]$	Yellow	60	186	41.01 (41.16)	3.99 (3.43)	9.60 (9.61)	7.30 (7.32)	14.98 (14.94)
$[CdL_2]$	White	68	191	50.03 (50.34)	4.35 (4.12)	11.24 (11.74)	8.92 (8.95)	15.20 (15.72)

3.2.2. Electronic spectra and magnetic moments

The electronic spectra of the metal complexes mostly comprised of d-d transition bands of metal ions and charge-transfer bands involving electronic transitions between metal ions and ligands i.e., LMCT or

MLCT [18]. It mainly gives idea about the geometry around the metal ion in the complex. The weak intensity of the peaks can be attributed to forbidden transitions [19]. The effective magnetic moments of the complexes were calculated in Bohr Magneton (B.M) from the corrected molar susceptibility values that were obtained after applying the diamagnetic corrections to them. These corrections were done for the atoms and structural units using Pascal's constants. Generally, The transition metal complexes give spin-only magnetic moment values depending upon the number of unpaired electrons in them. But in a few cases, they show aberrations from these spin-only values which can be assigned to spin-orbit coupling or orbital contributions. Hence, the magnetic moment values of a metal complex not only contribute information about the number of unpaired electrons and the orbitals in which they are present, but also help us to assign the oxidation state of the metal and thus, to predict the possible structure and geometry of the complex.

The electronic spectra of the ligand and its complexes (Fig.8) were recorded in solid state. The absorption band position and band assignments of the complexes are given in the Table 8. Generally, Co(II) complexes have octahedral, square planar or tetrahedral structures. Octahedral Co(II) has $^4T_{1g}$ the ground state term with three spin-allowed transitions,

$$^4T_{1g}(F) \rightarrow {}^4T_{1g}(P),$$

$$^4T_{1g}(F) \rightarrow {}^4A_{2g}(F) \text{ and}$$

$$^4T_{1g}(F) \rightarrow {}^4T_{2g}(F).$$

Coordination geometry of Co(II) complexes are can be predicted from the observed magnetic moment values. Even though octahedral and tetrahedral Co(II) complexes have same number of unpaired electrons, they can be distinguished by the extent of deviation of the effective magnetic moment values (μ_{eff}) from the spin-only value. High-spin octahedral Co(II) complexes with $^4T_{1g}$ as the ground state term have significant orbital contribution and show magnetic moment values between 4.70 and 5.20 B.M at room temperature. This value is higher than the predicted spin-only value of 3.87 B.M for three unpaired electrons [20]. This could be due to the effect of spin-orbit coupling. Low-spin octahedral Co(II) complexes with ^2E_g ground term have no orbital contribution. The reported magnetic moments of such complexes are in the range of 1.80-1.90 B.M, i.e., close to 1.72 B.M, the spin-only value for one unpaired electron [21]. Square planar complexes of Co(II) are always low-spin(S=1/2) and show magnetic moments in the range of 2.20-2.70 B.M which is rather higher than the expected spin-only value for one unpaired electron (1.73 B.M). This could be due to spin-orbit coupling [20]. Tetrahedral Co(II) complexes with $^4A_2$ ground term have no orbital contribution. The expected magnetic moment value is 3.87-4.7 B.M, which is close to the spin-only value for three unpaired electrons.

Due to spin-orbit coupling, usually the spectrum of Co(II) complex has poor resolution and hence it is complicated. Among the transitions, $^4T_{1g}(F) \rightarrow {}^4T_{1g}(P)$ refers to highest energy transition (lower wavelength). In octahedral complexes, the spin allowed transition,

$^4T_{1g}(F) \rightarrow {}^4T_{2g}(F)$ generally occurs in the near infrared region. The Co(II) complex showed three absorption bands at 277, 490 and 688 nm. In the case of Co(II) complexes, dark colour together with weak and broad bands in the spectra in the range 1000-1200 nm are characteristic of square-planar geometry. They may be due to $^2A_1 \rightarrow {}^2E$ at higher energy and $^2A_1 \rightarrow {}^2B_1$ at lower energy region. In this study, the Co(II) showed a broad band at 688 nm which can be assigned to $^2A_1 \rightarrow {}^2E$ transition. The bands at 490 and 277 nm can be assigned to intra-ligand charge-transfer transitions, $n \rightarrow \pi^*$ and $\pi \rightarrow \pi^*$, respectively. The magnetic moment value of this complex, 2.14 BM, confirmed the square planar environment around the metal ion.

The electronic spectra of octahedral Ni(II)complexes show the following characteristic spin- allowed transitions:

$^3A_{2g}(F) \rightarrow {}^3T_{2g}(F)$

$^3A_{2g}(F) \rightarrow {}^3T_{1g}(F)$

$^3A_{2g}(F) \rightarrow {}^1E_g(D)$

$^3A_{2g}(F) \rightarrow {}^1A_{1g}(G)$ and

$^3A_{2g}(F) \rightarrow {}^3T_{1g}(P)$.

The transition, $^3A_{2g}(F) \rightarrow {}^3T_{2g}(F)$ is usually found in the infrared region. A close pair of bands corresponding to the transitions, $^3A_{2g}(F) \rightarrow {}^3T_{1g}(F)$ and $^3A_{2g}(F) \rightarrow {}^1E_g(D)$, followed by a weaker transition, $^3A_{2g}(F) \rightarrow {}^1A_{1g}(G)$ and a stronger one due to $^3A_{2g}(F) \rightarrow {}^3T_{1g}(P)$ transitions are found in the blue end of the electronic

spectrum. Six-coordinate octahedral Ni(II) complexes have $^3A_{2g}$ ground term in both high-spin and low-spin states.

Octahedral bivalent nickel complexes show the magnetic moment values in the range, 2.90-3.30 B.M. They are slightly higher than the spin-only value for two unpaired electrons. As the ground term is $^3A_{2g}$ there can be no orbital contributions. However, a little higher values of the magnetic moment are due to the spin-orbit coupling or higher state mixing with the ground state term. For tetrahedral Ni(II) complexes, the experimental values of magnetic moments fall in the range of 3.60-4.10 B.M[22]. The observed higher values of the moment than the spin-only value for the two unpaired electrons are owing to the orbital contribution of the spin-triplet ($^3T_1$) ground term. If the distortions in the field of coordinated ligands are large, the magnetic moments with small orbital contributions may result and give rise to an observed moment value as low as 3.20 B.M [23]. Four-coordinate square-planar Ni(II) complexes have spin-singlet ground term and are diamagnetic.

In the present case, Ni(II) complex showed three spin-allowed transitions, $^3A_{2g}(F) \rightarrow {}^3T_{1g}(P)$, $^3A_{2g}(F) \rightarrow {}^3T_{1g}(F)$ and $^3A_{2g}(F) \rightarrow {}^3T_{2g}(F)$ with bands at 311, 573 and 865 nm respectively, indicating its octahedral geometry. A magnetic moment value of 2.76 B.M for the present Ni(II) complex confirmed its octahedral geometry.

The spectroscopic ground state term of copper(II) is ^2D. When the symmetry of copper(II) complex lowers from octahedral to D_{4h} or C_{4v}, the energy levels again split and give more transitions [16]. As a result, the electronic spectrum of a Cu(II) complex becomes more

complicated. As per literature, copper(II) complexes have bands in the range 307 and 304 nm, which may be assigned to $\pi \rightarrow \pi^*$ transitionsof phenyl rings. LMCT transitions (due to the combination of S→Cu and N→Cu) are observed in the range, 423-409 nm [24]. In the case of octahedral Cu(II) complexes which are usually dark blue or green coloured due to the absorption bands present in 200-900 nm region, which is corresponding to $^2E_g \rightarrow {}^2T_{2g}$ transition [25]. The band produced thereby will be a broad one due to Jahn-Teller effect [26]. A regular octahedral Cu(II) complex with a ground term $^2T_{2g,}$ has an observed magnetic moment value in the range, 1.80-2.10 B.M. This is somewhat higher than the spin–only value of 1.73 B.M, corresponding to one unpaired electron. The slightly higher value may be due to spin-orbit coupling. For a tetrahedral Cu(II) complex, the predicted magnetic moment value is around 2.20 B.M. The observed value of magnetic moment fall in the range, 1.95-2.00 B.M [27]. Most of the square planar Cu(II) complexes exhibit a single broad asymmetric d–d band in the region, 625–1388 nm [28] and the broadness of the band is due to the combination of the three spin–allowed transitions, $^2B_{1g} \rightarrow {}^2A_{1g}$, $^2B_{1g} \rightarrow {}^2B_{2g}$, and $^2B_{1g} \rightarrow {}^2E_g$.

In the electronic spectrum of $[CuL_2Cl_2].H_2O$, a broad band observed at 639 nm, may be due to the electronic transition, $^2E_g \rightarrow {}^2T_{2g}$. This observation is consistent with octahedral geometry of the complex. The Cu(II) complex of HL registered a magnetic moment of 1.92 B.M, supporting its octahedral structure. The complexes of Zn(II) and Cd(II) were found to be diamagnetic.

3.2.3. IR spectra and mode of bonding

The IR spectral investigation is used to assign structures and geometries of the compounds by identifying the bands corresponding to the important functional groups. Generally, coordination of a ligand to a metal ion results in an appreciable shift in absorprtion bands of ligand with respect to the metal complexes formed. The significant IR spectral bands of the ligand and the complexes (Fig.9) together with their possible assignments are given in the Table 9.

Table 8. Electronic spectral bands of the complexes.

Compound	**Spectral bands** λ_{max}**(nm)**	**Assignments**
$[Co(HL)_2]Cl_2.H_2O$	277	$\pi \rightarrow \pi^*$
	490	$n \rightarrow \pi^*$
	688	$^2A_1 \rightarrow {}^2E$
$[Ni(HL)_2Cl_2].H_2O$	311	$^3A_{2g}(F) \rightarrow {}^3T_{1g}(P)$
	573br	$^3A_{2g}(F) \rightarrow {}^3T_{1g}(F)$
	865	$^3A_{2g}(F) \rightarrow {}^3T_{2g}(F)$
$[Cu(HL)_2Cl_2].H_2O$	639br	$^2E_g \rightarrow {}^2T_{2g}$

br= broad

The probable assignments of the bands were made in comparison with the spectra of similar type of compounds. The IR spectra of all the compounds showed broad bands in the region, 3200–3600 cm^{-1}, assignable to intra-molecular hydrogen bonded –OH groups. The appearance of bands in this region in the spectra of all the complexes pointed out that the –OH groups have not involved in coordination.

Here, strong and broad absorption in the region 3224-3413 cm^{-1} of all the complexes except that of Co(II) also provided evidence for the presence N-H group or lattice water molecules in them. A strong IR band at 1626 cm^{-1} may be assigned to azomethine group present in the ligand.

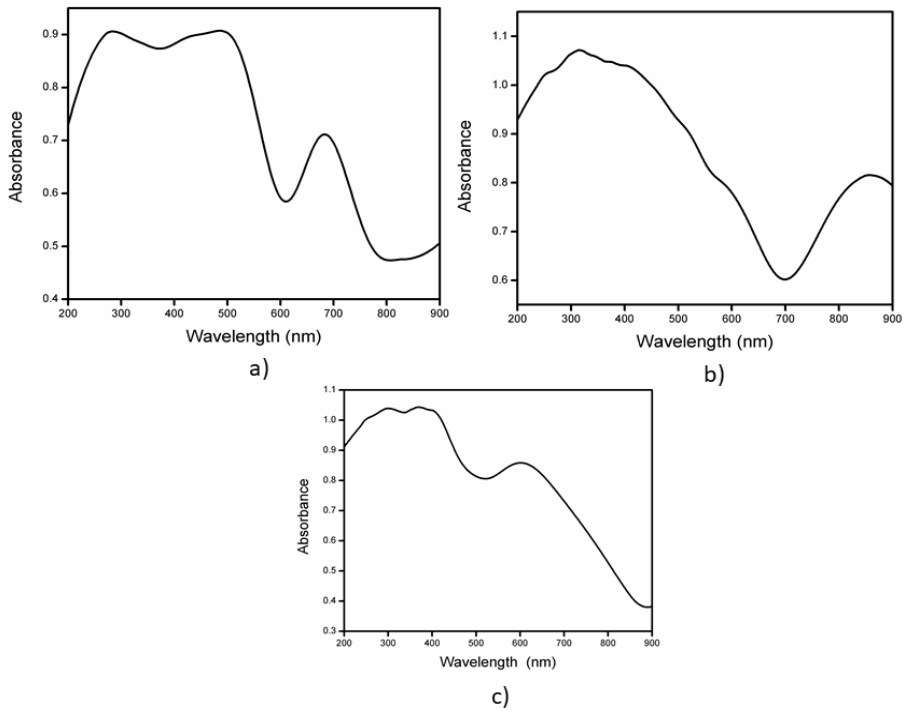

Fig.8. Electronic spectra of a)$[Co(HL)_2]Cl_2.H_2O$ b)$[Ni(HL)_2Cl_2].H_2O$ and c)$[Cu(HL)_2Cl_2].H_2O$

On coordination of the ligand, this band underwent a shift to lower frequencies (1599-1618cm^{-1}) indicating the coordination of the nitrogen of azomethine (C=N) group. Coordination of azomethine

nitrogen weakens the bond order between the carbon and nitrogen, shifting the band due to its vibration to lower frequencies[29]. A medium intensity band at 836 cm^{-1} in the ligand spectrum can be assigned to pure υ(C=S) mode[30]. The shift of this band to lower frequency region (around 800 cm^{-1}) in the spectra of all the complexes, except that of Cd(II) supports the participation of the thiocarbonyl sulphur (C=S) in coordination to the central metal ions [31]. However, in the spectrum of Cd(II) complex, this band suffers a large lowering (approximately 120 cm^{-1}). The position of a new band at 715 cm^{-1} in the spectrum of this complex suggests the presence of C-S-M, formed by the enolisation of –NH-C=S group in the ligand to –N=C-SH and coordinations to the Cd(II) through S^- after deprotonation [32]. This is further supported by the appearance of weak new bonds around 550 cm^{-1} in the spectra of the complexes due to υ(M-N).

Table 9. IR spectral assignments of ligand and metal complexes

Compound	$C_{15}H_{15}N_3O_2S$	$[Co(HL)_2]Cl_2.H_2O$	$[Ni(HL)_2Cl_2].H_2O$	$[Cu(HL)_2Cl_2].H_2O$	$[Zn(HL)Cl_2]$	$[CdL_2]$
υ(NH)/ υ(OH)	3290	3345	3413	3331	3234	3446
υ CH(Ar)	3055	3197	3195	3022	2912	3050
υ (C=N)	1626	1599	1613	1611	1620	1616
υ(C=S)+ υ(C=N)+υ(C- N)	1335	1492	1324	1394	1353	1345
δ(N-N)	1040	1129	1169	1129	1056	1102
υ(C=S)	836	820	831	775	827	820
υ(M-N)	-	566	532	539	548	551

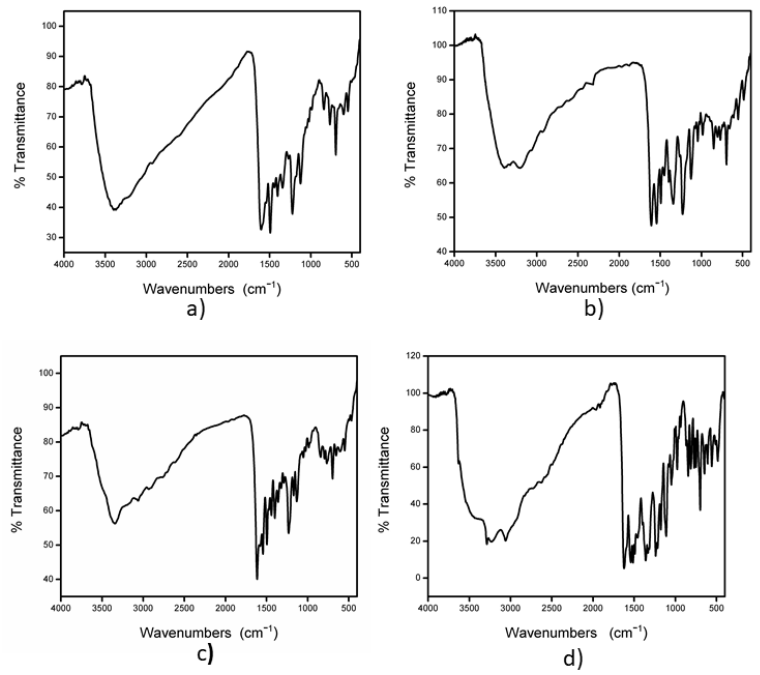

Fig.9. IR spectra of a)$[Co(HL)_2Cl_2].H_2O$ b)$[Ni(HL)_2Cl_2].H_2O$ c)$[Cu(HL)_2Cl_2].H_2O$ d) $[CdL_2]$

3.2.4. Electron paramagnetic resonance (EPR) spectrum

The spectrum of the Cu(II) complex in DMSO solution at liquid nitrogen temperature (77K) at X-band frequency in the region 8.75-9.65 GHz with 100 kHz field modulation was recorded. It provides information which is useful to understand the stereochemistry around the metal ion. The Cu(II) ion with a spin angular momentum, ms = ±1/2 and an effective spin of S = 3/2, gives a doubly degenerate spin state in the absence of the magnetic field. The degeneracy between these states is disturbed in the presence of magnetic field and the energy difference between them is given by, $E = h\nu = g\beta B$, where h is the Planck's constant, ν is the frequency, g is the Lande's splitting

factor (equals to 2.0023 for a free electron), β is the Bohr Magneton and *B* is the magnetic field strength.

The solution spectrum shows four hyperfine spectral lines characteristic of a monomeric Cu(II) complex. The *g-tensor* value can be used to derive the ground state. For this complex, the observed value of $g\|$ was 2.35 and $g^{\perp}$ was 2.03. The trend, $g\| > g^{\perp} > 2.0023$ observed for the complexes indicates that the unpaired electron is localised in $d_{x^2-y^2}$ orbital of Cu(II) ion. In octahedral geometry, the unpaired electron lies in $d_{x^2-y^2}$ orbital. If the trend is $g^{\perp} > g\| > 2$, the unpaired electron lies in the d_z^2 orbital giving $^2A_{1g}$ as the ground state. The $g\|$ value is an important function for indicating covalent character of M-L bond [33]. According to Neiman and Kivelson [34], $g\|$ less than2.3 indicates covalent character while greater than 2.3 indicates ionic character of the metal-ligand bond in complexes. Here, ESR spectrum showed the $g\|$ value of complex as slightly greater than 2.3, indicating a small amount of ionic character of the copper-ligand bond. The exchange interaction between the copper centers in polycrystalline sample is explained by Hathaway expression $G= (g\|-2)/(g\perp-2)$. According to Hathaway and Tomlinson [35], if the value of G is greater than 4, the exchange interaction between copper(II) centers is negligible, whereas when it is less than 4, a considerable exchange interaction exists. Here, a value of G>4.0, indicated negligible exchange coupling in complex (G= 11.83). No signal at half field was observed in the spectrum, ruling out the possibility of a dimeric form [36].

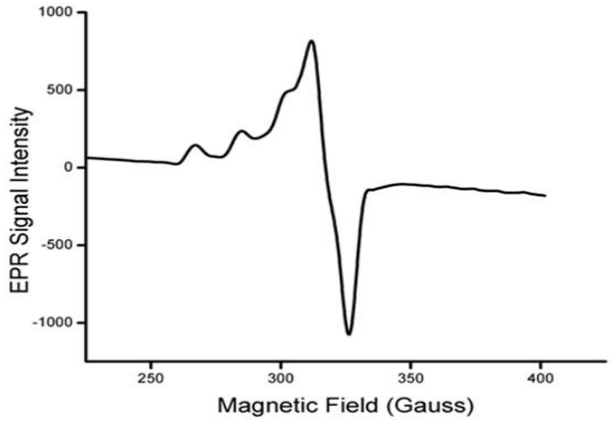

Fig.10. X-Band ESR spectrum of $[Cu(HL)_2Cl_2].H_2O$ complex at LNT in DMSO

3.2.5. ^{1}H NMR spectrum of $[Zn(HL)Cl_2]$

The ^{1}H NMR spectrum of the Zn(II) complex was recorded in DMSO at room temperature(Fig.11). A singlet at 11.55 ppm can be assigned to N–H proton. Another singlet observed at 9.85 ppm can be assigned to azomethine proton. Aromatic protons showed a multiplet peaks in the region, 7.49–6.25 ppm. ^{4}N–CH_3 protons absorbed at 3.38 ppm. The two singlets at 10.87 and 8.25 ppm are assigned to *ortho* and *para* hydroxyl protons, respectively. This ruled out the possibility of coordination of hydroxyl group to Zn(II) ion.

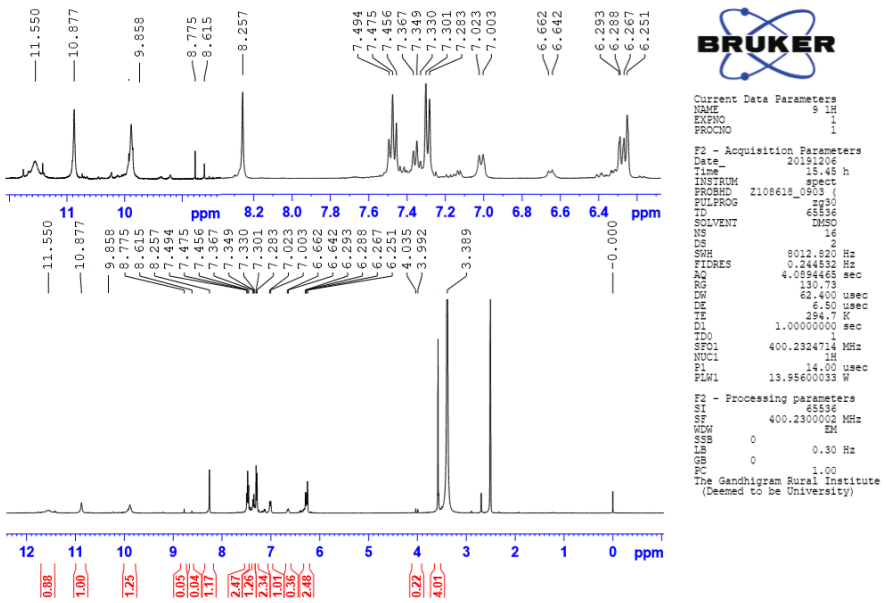

Fig.11. ^{1}H NMR spectrum of $Zn(HL)Cl_2$

3.2.6. Thermo gravimetric analysis

Thermo gravimetric analysis of the metal complexes provides idea about their thermal stabilities. It is also useful to confirm whether the water molecules (if present) are coordinated or not to the central metal ion**.** The complex, $[Co(HL)_2]Cl_2.H_2O$, showed two stages of decomposition at 67°C and between 229-368°C. The first stage of decomposition was at 67^0C with weight loss of 2.01% (calcd. 2.39%) which may be due to the loss of one molecule of lattice water. The second stage of decomposition was in between 229 and 368°C with a weight loss of 19.42% which may be due to the successive degradation of the ligand. The residual mass left behind at 486°C was 7.57% which may be due to the formation of CoO (calcd. 9.98%).

In $[Ni(HL)_2Cl_2].H_2O$, three decomposition stages were observed. Initial mass loss of 1.44% (2.3%) at 92^0C corresponded to the loss of one lattice water molecule. The second stage was at 190–391°C and demonstrated a mass loss of 28.72%. A residual mass of 12.88% (calcd. 12.09%) was left which may be due to the formation of a nickel sulphide.

$[Cu(HL)_2Cl_2].H_2O$ registered the first stage of decomposition at 75.5°C with a weight loss of 1.32% (calcd. 2.3%) which may be due to the elimination of one water molecule in the lattice. The next stage of decomposition occurred in the temperature range, 173–230°C with a mass loss 10.09% due to the decomposition of the ligand moiety. A residual mass of 11.56% may be due to the formation of CuS (calcd. 12.66%).

The Cd(II) complex showed two stages of decomposition. The first decomposition stage occurred at 91^0C with weight loss of 1.44% (calcd. 2.45%) which may be due to moisture. The decomposition stage in the range of 178-486^0C may due to the decomposition of the ligand moiety.

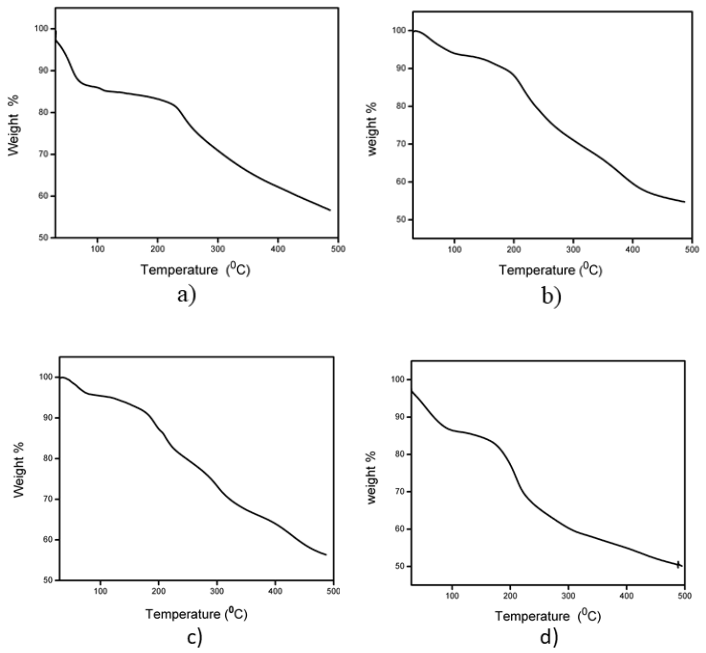

Fig.12. TG curves of a) $[Co(HL)_2]Cl_2.H_2O$ b)$[Ni(HL)_2Cl_2].H_2O$ c)$[Cu(HL)_2Cl_2].H_2O$ and d)$[CdL_2]$

4. Conclusions

We were able to obtain single crystals of 2,4-dihydroxybenzaldehyde N(4)-methyl(phenyl)thiosemicarbazone (HL). The synthesis and characterisation of its Co(II), Ni(II), Cu(II), Zn(II) and Cd(II) complexes are also discussed. The Co(II) complex was assigned square planar geometry. The Ni(II) and Cu(II) complexes were assigned octahedral geometries based on spectroscopic- and magnetic studies. Based on the elemental analyses, IR and NMR spectral data, Zn(II) and Cd(II) complexes were assigned tetrahedral geometry. According to IR and ^1H NMR spectral data, HL was found to function as neutral bidentate ligand in all the complexes, except that of Cd(II), where it

was acted as monoanionic bidentate one. The structures of complexes are presented in Fig.13-16.

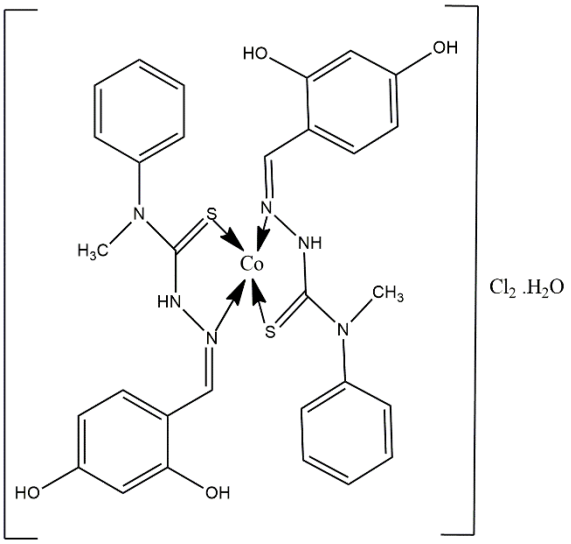

Fig.13. Proposed structure of the Co(II) complex, $[Co(HL)_2]Cl_2.H_2O$

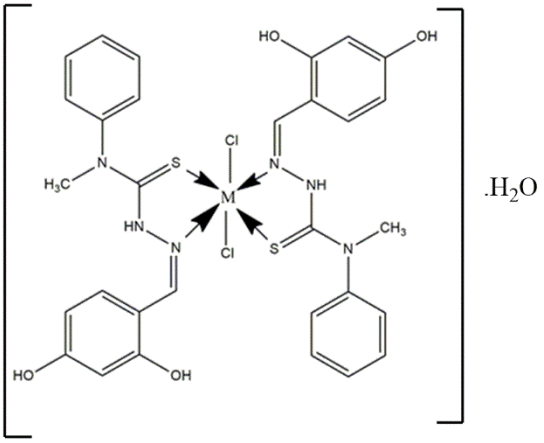

Fig.14. Proposed structure of the complexes, $[M(HL)_2Cl_2].H_2O$ M= Ni(II) or Cu(II).

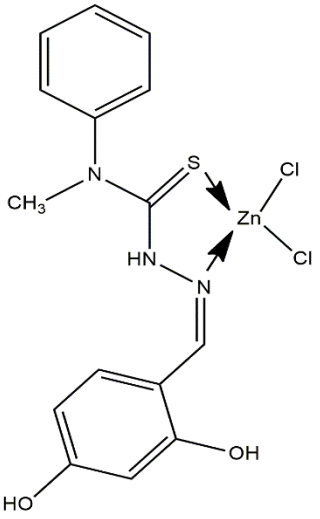

Fig.15. Proposed structure of the Zn(II) complex, $[Zn(HL)Cl_2]$

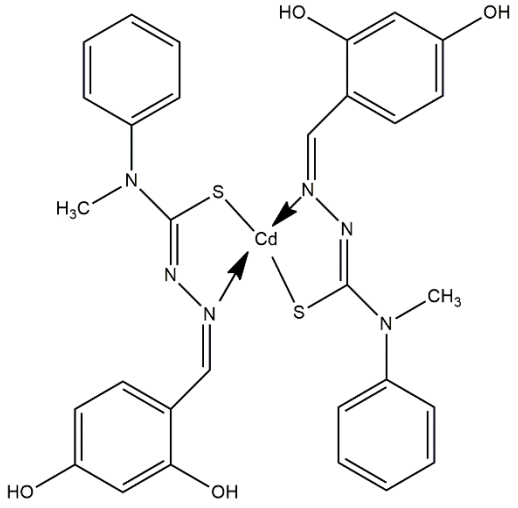

Fig.16. Proposed structure of the Cd(II) complex, $[CdL_2]$

References

[1] N.E. Eltayeb, F. Şen, J. Lasri, M.A. Hussien, S.E. Elsilk, B.A. Babgi, H. Gökce, Y. Sert, Hirshfeld Surface analysis, spectroscopic, biological studies and molecular docking of (4E)-4-((naphthalen-2-yl) methyleneamino)-1, 2-dihydro-2, 3-dimethyl-1-phenylpyrazol-5-one, Journal of Molecular Structure 1202 (2020) 127315.

[2] W. Antholine, J. Knight, H. Whelan, D.H. Petering, Studies of the reaction of 2-formylpyridine thiosemicarbazone and its iron and copper complexes with biological systems, Molecular Pharmacology 13(1) (1977) 89-98.

[3] M.A.M. Alho, N.B. D'Accorso, Behavior of free sugar thiosemicarbazones toward heterocyclization reactions, Carbohydrate Research 328(4) (2000) 481-488.

[4] X. Zhu, C. Wang, Z. Lu, Y. Dang, Synthesis, characterization and biological activity of the Schiff base derived from 3,4-dihydroxybenzaldehyde and thiosemicarbazid, and its complexes with nickel(II) and iron(II), Transition Metal Chemistry 22(1) (1997) 9-13.

[5] Z. Xinde, W. Chenggang, L. Zhifeng, M. Shangyun, Y. Zhenhuan, W. Zishen, Synthesis, characterization and scavenger effect on of copper (II) and zinc (II) complexes derived from thiosemicarbazide, Synthesis and Reactivity in Inorganic, Metal-Organic, and Nano-Metal Chemistry 21(9) (1991) 1365-1373.

[6] Z. Xinde, W. Chenggang, L. Zhiping, L. Zhifeng, W. Zishen, Synthesis and Biological Activity of the Schiff Base N, N′-bis (Salicylidene) thiourea and Its Complexes of Copper (II), Nickel (II) and Zinc (II), Synthesis and Reactivity in Inorganic and Metal-Organic Chemistry 26(6) (1996) 955-966.

[7] K. Khaled, O. Elhabib, A. El-Mghraby, O. Ibrahim, M.A. Ibrahim, Inhibitive effect of thiosemicarbazone derivative on corrosion of mild steel in hydrochloric acid solution, J. Mater. Environ. Sci 1(3) (2010) 139-150.

[8] G. Sheldrick, SHELXL-97, Program for crystal-structure refinement (1997).

[9] A. Spek, P.A.M.C. Tool, University of Utrecht, The Netherlands (1999).

[10] L.J. Farrugia, WinGX and ORTEP for Windows: an update, Journal of Applied Crystallography 45(4) (2012) 849-854.

[11] C. Impact, DIAMOND-Crystal and Molecular Structure Visualization (Version 4), (2009).

[12] C.F. Macrae, I.J. Bruno, J.A. Chisholm, P.R. Edgington, P. McCabe, E. Pidcock, L. Rodriguez-Monge, R. Taylor, J. Streek, P.A. Wood, Mercury CSD 2.0–new features for the visualization and investigation of crystal structures, Journal of Applied Crystallography 41(2) (2008) 466-470.

[13] G.J. Palenik, D. Rendle, W. Carter, The crystal and molecular structures of thiosemicarbazones; an antitumor agent 5-hydroxy-2-formylpyridine thiosemicarbazone sesquihydrate and the inactive acetone thiosemicarbazone, Acta Crystallographica Section B: Structural Crystallography and Crystal Chemistry 30(10) (1974) 2390-2395.

[14] M. Yıldız, H. Ünver, D. Erdener, A. Kiraz, N.O. İskeleli, Synthesis, spectroscopic studies and crystal structure of (E)-2-(2, 4-dihydroxybenzylidene) thiosemicarbazone and (E)-2-[(1H-indol-3-yl) methylene] thiosemicarbazone, Journal of Molecular Structure 919(1-3) (2009) 227-234.

[15] Y.-p. Tian, C.-y. Duan, C.-y. Zhao, X.-z. You, T.C. Mak, Z.-y. Zhang, Synthesis, crystal structure, and second-order optical nonlinearity of Bis (2-chlorobenzaldehyde thiosemicarbazone) cadmium halides (CdL2X2; X= Br, I), Inorganic chemistry 36(6) (1997) 1247-1252.

[16] H.H. Perkampus, LJ Bellamy: The Infrared Spectra of Complex Molecules, Vol. 1, 3. Auflage, Chapman and Hall Ltd., London 1975, 433 Seiten, 32 Abb., 22 Tabellen, Preis:£ 8.—, Berichte der Bunsengesellschaft für physikalische Chemie 80(1) (1976) 99-100.

[17] R.H. Borges, A. Abras, H. Beraldo, Synthesis, characterization and Mössbauer studies of Fe (II) and Fe (III) complexes of 2-acetylpyridine thiosemicarbazone, Journal of the Brazilian Chemical Society 8(1) (1997) 33-38.

[18] J.E. Huheey, E.A. Keiter, R.L. Keiter, O.K. Medhi, Inorganic chemistry: principles of structure and reactivity, Pearson Education India2006.

[19] R.L. Dutta, A. Syamal, Elements of magnetochemistry, Affiliated East-West Press1993.

[20] B.N. Figgis, R.S. Nyholm, 61. Magnetochemistry. Part II. The temperature-dependence of the magnetic susceptibility of bivalent cobalt compounds, Journal of the Chemical Society (1959) 338-345.

[21] A. Sacco, F. Cotton, Magnetic and Spectral Studies of the Structures of Some Methyl Isonitrile Complexes of Cobalt (II), Journal of the American Chemical Society 84(11) (1962) 2043-2047.

[22] N.S. Gill, R.S. Nyholm, 802. Complex halides of the transition metals. Part I. Tetrahedral nickel complexes, Journal of the Chemical Society (Resumed) (0) (1959) 3997-4007.

[23] G. Bullock, F.W. Hartstock, L.K. Thompson, Mononuclear and binuclear copper (II) complexes of some polyfunctional pyridyl phthalazines, Canadian Journal of Chemistry 61(1) (1983) 57-62.

[24] P.M. Krishna, B. Shankara, N.S. Reddy, Synthesis, Characterization, and Biological Studies of Binuclear Copper(II) Complexes of (2E)-2-(2-Hydroxy-3-Methoxybenzylidene)-4N-Substituted Hydrazinecarbothioamides, International Journal of Inorganic Chemistry 2013 (2013).

[25] J. Waters, T. Waters, 477. The colour isomerism and structure of some copper co-ordination compounds. Part VI. The visible absorption spectra of copper complexes, Journal of the Chemical Society (Resumed) (1964) 2489-2492.

[26] D . Sutton, Electronic spectra of transition metal complexes: an introductory text, McGraw-Hill1968.

[27] A. Earnshaw, J. Lewis, 71. Polynuclear compounds. Part I. Magnetic properties of some binuclear complexes, Journal of the Chemical Society (Resumed) (1961) 396-404.

[28] M. Joseph, M. Kuriakose, M.P. Kurup, E. Suresh, A. Kishore, S.G. Bhat, Structural, antimicrobial and spectral studies of copper(II) complexes of 2-benzoylpyridine N (4)-phenyl thiosemicarbazone, Polyhedron 25(1) (2006) 61-70.

[29] Y.K. Bhoon, Magnetic and EPR properties of Mn(II), Fe(III), Ni(II) and Cu(II) complexes of thiosemicarbazone of α-hydroxy-β-napthaldehyde, Polyhedron 2(5) (1983) 365-368.

[30] M.J. Campbell, Transition metal complexes of thiosemicarbazide and thiosemicarbazones, Coordination Chemistry Reviews 15(2-3) (1975) 279-319.

[31] N. Saha, N. Mukherjee, Synthesis, characterisation and coordinating properties of a new pyrazole-derived thiosemicarbazone, a potential antiviral agent: Co(III), Ni(II) and Cu(II) complexes of neutral and deprotonated 5 (3)-methylpyrazole-3 (5)-aldehydothiosemicarbazone, Polyhedron 3(9-10) (1984) 1135-1140.

[32] M. Patil, J. Shah, Structural studies on Cu(II), Ni(II), Co(II), Fe(III), Cr(III) and VO(II) chelates of some methyl-substituted 2-hydroxyacetophenonethiosemicarbazones, Journal of the Indian Chemical Society 58(10) (1981) 944-947.

[33] A. Abou-Hussen, N. El-Metwally, E. Saad, A. El-Asmy, Spectral, magnetic, thermal and electrochemical studies on phthaloyl bis (thiosemicarbazide) complexes, Journal of Coordination Chemistry 58(18) (2005) 1735-1749.

[34] D. Kivelson, R. Neiman, ESR studies on the bonding in copper complexes, The Journal of Chemical Physics 35(1) (1961) 149-155.

[35] A. Tomlinson, B. Hathaway, The electronic properties and stereochemistry of the copper (II) ion. Part II. The monoamine adducts of bisethylenediaminecopper (II) complexes, Journal of the Chemical Society A: Inorganic, Physical, Theoretical (1968) 1685-1688.

[36] N. Raman, R. Jeyamurugan, M. Subbulakshmi, R. Boominathan, C.R. Yuvarajan, Synthesis, DNA binding, and antimicrobial studies of novel metal complexes containing a pyrazolone derivative Schiff base, Chemical Papers 64(3) (2010) 318-328.

CHAPTER IV

SYNTHESIS AND CHARACTERIZATION OF TRANSITION METAL COMPLEXES OF 4-[N,N-(DIMETHYL)AMINO]BENZALDEHYDE N(4)-METHYL(PHENYL)THIOSEMICARBAZONE

1. Introduction

Thiosemicarbazones of substituted carbonyl compounds show marked differences in their donor properties compared to those of unsubstituted ones. Moreover, the biological activities of thiosemicarbazones are found to be considerably enhanced by the presence of certain substituents on the carbonyl compounds [1]. It is also observed that substitution on terminal nitrogen atom of the thiosemicarbazide moiety raises the biological activities of such compounds [2].

By virtue of the unique structural features of 4-[N,N-(dimethyl)amino]benzaldehyde, it finds several applications in the fields of analytical chemistry and corrosion inhibition processes. Karthikeyan *et al*[3] proposed 4-[N,N-(dimethyl)amino]benzaldehyde thiosemicarbazone (DMABT) as an analytical reagent for the extractive spectrophotometric determination of copper(II). Parameshwara *et al*[4] also reported that DMABT can function as a sensitive and selective sensor for the spectrophotometric determination of palladium(II).

However, a detailed literature survey revealed that no work has been reported on 4-[N,N-(dimethyl)amino]benzaldehyde N(4) di-substituted thiosemicarbazone (HL) (Fig.1). Hence, in the current work the complexes of Co(II), Ni(II), Cu(II), Zn(II) and Cd(II) with this ligand were prepared and characterized.

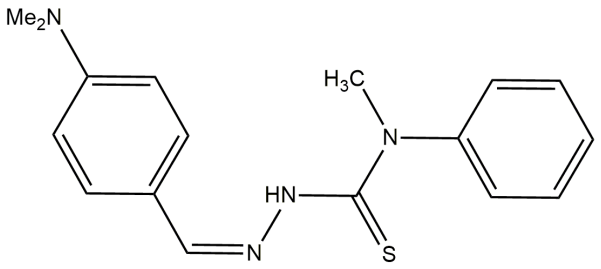

Fig.1. 4-[N,N-(Dimethyl)amino]benzaldehyde N(4)-methyl(phenyl)thiosemicarbazon (HL)

*IUPAC Name: (*Z*)-2-(4-(dimethylamino)benzylidene)-*N*-methyl-*N*-phenylhydrazinecarbothioamide

2. Experimental

2.1. Materials and methods

A detailed description about the materials, methods and characterization techniques used in this work are given in Chapter II of Part I.

2.2. Preparation of the ligand (HL)

N(4)-methyl(phenyl)thiosemicarbazide (0.1mol) dissolved in hot ethanol was added slowly to a hot ethanolic solution of 4-[N,N-(dimethyl)amino]benzaldehyde (0.1mol) and stirred for 15 minutes in the presence of 2-3 drops of glacial acetic acid. The resulting yellow coloured solution was kept for evaporation. The solid mass obtained was filtered and washed several times with ethanol and followed by diethyl ether. It was dried under vacuum. The product was

recrystallized from ethanol (Yield = 65%, M.P = 172^0C). The synthetic pathway of the ligand is shown below in Scheme 1.

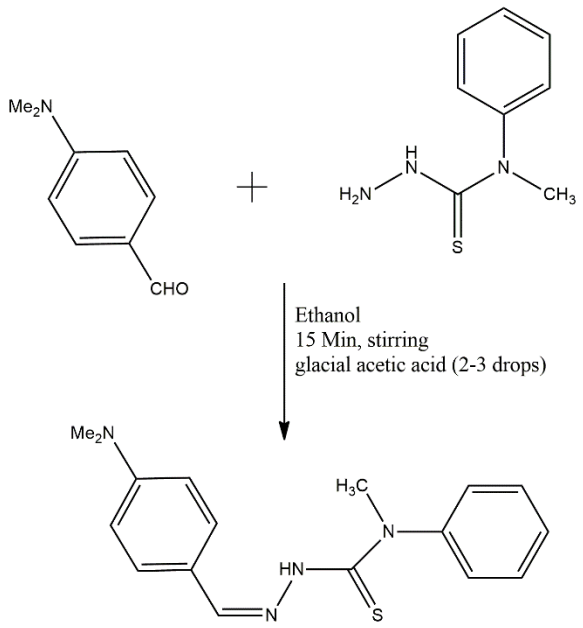

Scheme 1. Synthetic pathway of 4-[N,N-(dimethyl)amino] benzaldehyde N(4)-methyl(phenyl)thiosemicarbazone (HL)

2.3. Preparation of the metal complexes

Hot solution of metal chloride (0.001 M) in ethanol ($20cm^3$) was added to a hot solution of the ligand (0.002 M) in ethanol ($20cm^3$). The solution mixture was heated under reflux on a water bath for 4hr. On cooling, the coloured complexes precipitated out. The complexes obtained were filtered, washed with ethanol and diethyl ether and dried. The purity of the complexes were checked by TLC method.

3. Results and discussion

The data obtained from the characterization studies have been correlated to explain the properties, structures and bondings of the compounds.

3.1. Characterization of the ligand (HL)

3.1.1. Micro analytical data

The intense yellow coloured ligand in powder form registered a melting point of 172^0C. It was soluble in chloroform, DMF, DMSO and partially soluble in ethanol. The suggested formula for the ligand, $C_{17}H_{20}N_4S$ was in good agreement with the CHNS percentages (Table 1).

Table 1. Physico-chemical and analytical data of HL

Compound (Empirical Formula)	**Yield (%)**	**Melting Point (^{0}C)**	**Colour**	**CHNS Analysis Found % (Calculated)%**			
				C	**H**	**N**	**S**
$C_{17}H_{20}N_4S$	65	172^0C	Intense Yellow	65.01 (65.38)	6.12 (6.41)	17.20 (17.95)	9.99 (10.25)

3.1.2. Spectroscopic analysis

a) Electronic spectrum

The electronic absorption spectrum of the ligand in DMF was recorded in the range 200–900 nm (Fig.2). It shows two absorption maxima. The intense absorption peak at 264 nm is due to $\pi \rightarrow \pi^*$ transition. The band

at 363 nm in the ligand spectrum may be attributed to n→π* transition. The data are given in Table 2.

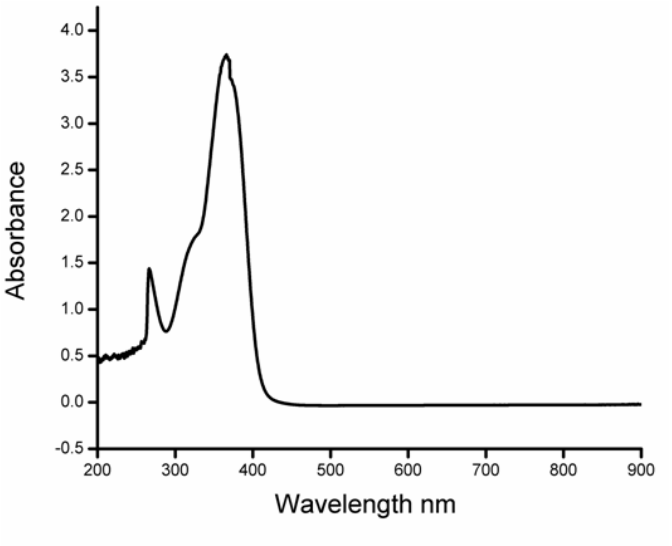

Fig.2. Electronic spectrum of HL

Table 2. Electronic spectral bands of HL

Spectral bands (nm)	**Assignments**
264	π→π* transition
363	n →π* transition

b) Infrared spectrum

IR spectra of the ligand is depicted in the Fig.3 and the spectral data are listed in the Table 3. In the spectra of the ligand, the absorption bands due to υ(N-H) appear at 3252 and 3166 cm^{-1}. Usually, thiosemicarbazones can coordinate as either a neutral (thione) or as a mono-anionic(thiolate) ligand[5]. The band at 815 cm^{-1} corresponds to

υ(C=S). The presence of an intense band at 1596 cm^{-1} is characteristic of an azomethine (>C=N) group. The band due to υ(C=S)+ υ(C= N) + υ(C-N) vibration observed at 1370 cm^{-1} and that due to υ(N-C-S)+ υ(C-S) vibration was present at 1175 cm^{-1}. (N-N) bending vibration occurred at 1062 cm^{-1}. The absence of an absorption band in the region, 2600-2500 cm^{-1} (corresponding to υ(S-H) group) indicates that the thione form of the ligand exists in the solid state[6]. Most of the vibrational bands appear to be strongly overlapped and only the major ones are indicated in Table 3.

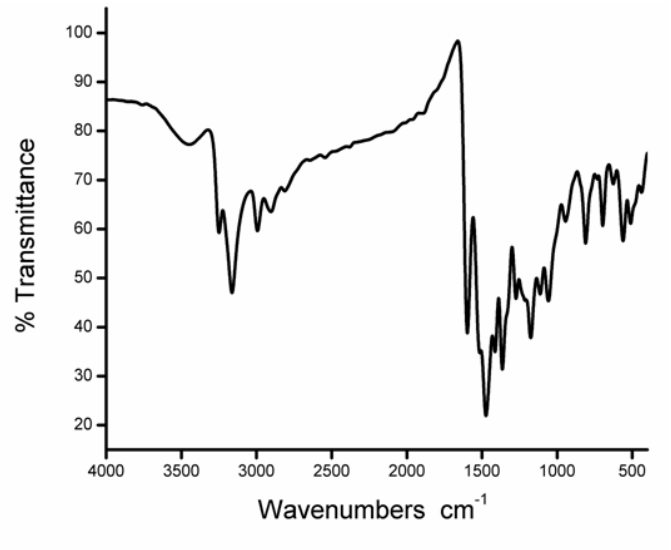

Fig.3. IR spectrum of HL

Table 3. IR spectral assignments (in cm^{-1}) of HL

Bands (cm^{-1})	**Assignments**
3252, 3166	υ(N-H)
2992	υ(C-H) (aromatic)
1596	υ(C=N)
1370	υ(C=S)+ υ(C= N) + υ(C-N)
1175	υ(N-C-S)+ υ(C-S)
1062	δ (N-N)
815	υ(C=S)

C) ^{1}H NMR spectrum

The NMR spectrum of the ligand was recorded in $CDCl_3$. The major NMR shifts are shown in Table 4. The spectrum showed a sharp singlet at 11.63 ppm. This may be due to hydrazide N-H proton. According to literature reports, it is expected between 13-15ppm for the E form and between 9-12ppm for the Z form and therefore, in the present case the ligand exists as the *Z* isomer[7]. There is no signal of thiol proton (-SH group) which is expected around 4 ppm confirming thione form of the ligand in a polar solvent. The azomethine proton showed a sharp singlet peak at 9.13 ppm. The peak at 3.56 ppm corresponds to protons of the methyl group on the terminal nitrogen. The peak at 2.97 ppm is attributed to methyl protons of dimethyl amino groups which are chemically and magnetically equivalent ones.

Table 4. ^{1}H NMR data of HL

δ (ppm)	**Assignment**
11.63	N-H proton
7.94 – 6.72 (m)	Aromatic protons
9.135	Azomethine proton
3.568	-CH_3 group on terminal nitrogen atom
2.97	-CH_3 protons (NMe_2)

3.2. Characterization of the metal complexes

Ligand formed stable complexes with Co(II), Ni(II), Cu(II), Zn(II) and Cd(II) ions. All the complexes were found to be non-hygroscopic and stable at room temperature. These complexes were insoluble in ethanol and water, but were readily soluble in chloroform, DMSO, DMF, etc.

3.2.1. Analytical data of metal complexes

The analytical data and physical properties of the ligand and its complexes are listed in Table 5. All the complexes were intensely coloured due to the presence of sulphur-to-metal charge-transfer bands. Elemental analytical data of all complexes were in good agreement with the suggested molecular formulae. The complexes were found to have a general formula $[M(HL)_2Cl_2]$, where M = Ni(II), Cu(II) or Zn(II) and for the Co(II) complex, formula was found to be $[Co(HL)_2]Cl_2.H_2O$, where HL is the bidentate neutral ligand. However, in the case of Cd(II) complex, the formula was found to be, $Cd(L)_2$ where L^- is the bidentate monoanion of HL.

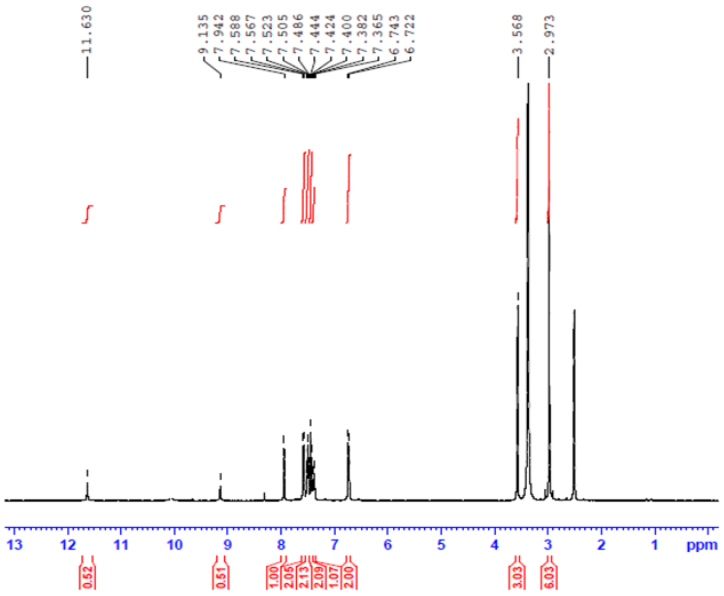

Fig.4. ^{1}H NMR spectrum of HL

Table 5. Physico-chemical and analytical data of the complexes

Compound	Colour	Yield (%)	MP (^{0}C)	Elemental Analysis (%) found (calculated)				
				C	H	N	S	Metal
$C_{17}H_{20}N_4S$	Intense yellow	70	172	65.01 (65.38)	6.12 (6.41	17.20 (17.95)	9.99 (10.25)	-
$[Co(HL)_2]Cl_2.H_2O$	Dark brown	68	182	52.81 (52.86)	5.56 (5.18)	14.51 (14.51)	8.25 (8.29)	7.80 (7.63)
$Ni(HL)_2Cl_2$	Brownish black	74	184	54.01 (54.09)	5.12 (5.30)	14.25 (14.84)	8.12 (8.48)	7.68 (7.78)
$Cu(HL)_2Cl_2$	Black	78	179	53.28 (53.79)	5.05 (5.27)	14.02 (14.76)	8.14 (8.43)	8.01 (8.37)
$Zn(HL)_2Cl_2$	Light yellow	82	186	52.53 (53.66)	5.04 (5.26)	14.21 (14.73)	8.07 (8.41)	8.41 (8.59)
$Cd(L)_2$	White	76	181	55.01 (55.40)	4.99 (5.43)	14.89 (15.21)	8.21 (8.69)	16.75 (15.26)

3.2.2. Electronic spectra and magnetic moments

The electronic spectra of the ligand and its complexes (Fig.8) were recorded in solid state. The absorption band positions and band assignments of the complexes are given in the Table 8. The Co(II) complex showed absorption bands at 363 and 535 nm. The dark colour of the Co(II) complex together with weak and broad bands in the spectra are characteristic of square planar geometry. In this study, the Co(II) showed a broad band at 535 nm which can be assigned to $^2A_1 \rightarrow {}^2E$ transition. The band at 363 nm can be assigned to intra-ligand charge-transfer transition. The magnetic moment value of this complex, 1.72 BM, confirmed the square planar environment around the metal ion[8].

Octahedral Ni(II) ion with d^8 configuration has $^3A_{2g}$ ground state. The spin-allowed transitions and bands present in the spectrum of the present Ni(II) complex are,

$^3A_{2g}(F) \rightarrow {}^3T_{2g}(F) \sim 880$ nm

$^3A_{2g}(F) \rightarrow {}^3T_{1g}(F) \sim 685$ nm

$^3A_{2g}(F) \rightarrow {}^3T_{1g}(P) \sim 517$ nm

The bands present at 356 and 254 nm can be assigned to intra-ligand charge-transfer transitions, $n \rightarrow \pi^*$, $\pi \rightarrow \pi^*$ respectively. Its effective magnetic moment value, 2.83 B.M is consistent with the spin-only value expected for two unpaired electrons of an octahedral Ni(II) complex[9].

The spectroscopic ground state term of copper(II) is ^2D. In an octahedral field it splits into two levels, $^2T_{2g}$ and ^2E_g. The present Cu(II) complex showed a broad band at 597 nm. It may be due to $^2E_g \rightarrow {}^2T_{2g}$ transition [10], typical of a Cu(II) complex with distorted octahedral geometry. The Cu(II) complexes with distorted octahedral geometry have magnetic moment values slightly higher than the spin-only value of, 1.73 B.M[11]. The Cu(II) complex obtained here showed a magnetic moment of 1.95 B.M. On the basis of electronic spectra and magnetic susceptibility measurements, a distorted octahedral geometry is suggested for the present Cu(II) complex. As expected, the Zn(II) and Cd(II) complexes have no characteristic absorption bands in the visible region and are diamagnetic in nature. On the basis of analytical data, the Zn(II) and Cd(II) complexes are assigned octahedral- and tetrahedral geometries, respectively[12].

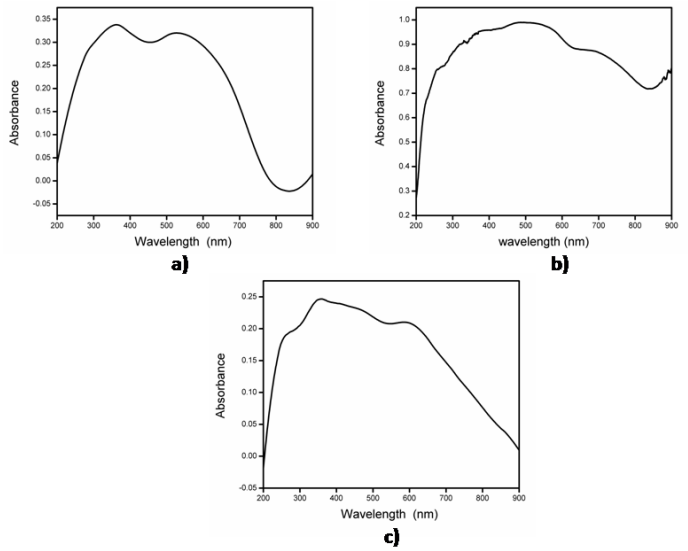

Fig.5. Electronic spectra of a) $[Co(HL)_2]Cl_2.H_2O$ b) $Ni(HL)_2Cl_2$ c) $Cu(HL)_2Cl_2$

Table 6. Electronic spectral bands and their assignments of the complexes

Compound	**Spectral bands** λ_{max} **(nm)**	**Assignments**
$[Co(HL)_2]Cl_2.H_2O$	535br	$^2A_1 \rightarrow {}^2E$
$Ni(HL)_2Cl_2$	254	$\pi \rightarrow \pi^*$
	356	$n \rightarrow \pi^*$
	517	$^3A_{2g}(F) \rightarrow {}^3T_{1g}(P)$
	685	$^3A_{2g}(F) \rightarrow {}^3T_{1g}(F)$
	880	$^3A_{2g}(F) \rightarrow {}^3T_{2g}(F)$
$Cu(HL)_2Cl_2$	597br	$^2E_g \rightarrow {}^2T_{2g}$

3.2.3. Infrared spectra and mode of bonding

The spectral analyses were performed on the ligand and its complexes in the same experimental conditions to compare the frequency changes on coordination. Generally, the absorption bands of ligand undergo shift from their positions to lower frequency region upon coordination to metal centers. This in turn helps to identify the coordinated atoms of the ligand. The significant IR spectra of the ligand (Fig.3) and complexes (Fig.6) along with their probable assignments are depicted in the Table 6.

A sharp band at 1596 cm^{-1}in the ligand spectrum is found to be shifted to about 10-21 cm^{-1} lower frequency region on complexation. This indicates the involvement of azomethine nitrogen in coordination [13, 14]. This is further supported by the appearance of weak new bonds around 518 cm^{-1} in the spectra of the complexes due to υ(M-N).

A medium intensity band at 815 cm^{-1} in the ligand spectrum can be assigned to pure υ(C=S) mode. The shift of this band to lower frequency region (around 800 cm^{-1}) in the spectra of all the complexes,

except that of Cd(II) supports the participation of the thiocarbonyl sulphur (C=S) in coordination to the central metal ions [15]. However, in the spectrum of Cd(II) complex, this band supports a large lowering (approximately 190 cm^{-1}). The position of a new band at 625 cm^{-1} in the spectrum of this complex suggests the presence of C-S-M, formed by the enolisation of –NH-C=S group in the ligand to –N=C-SH and coordinations to the Cd(II) through S^- after deprotonation. Therefore, the ligand coordinates as a neutral, bidentate (through the imino nitrogen and thiocarbonyl sulphur) one in the complexes of Co(II), Ni(II), Cu(II) and Zn(II). However, in the case of Cd(II), the ligand coordinates in a bidentate monoanionic (through the imino nitrogen and thiolate sulphur) manner.

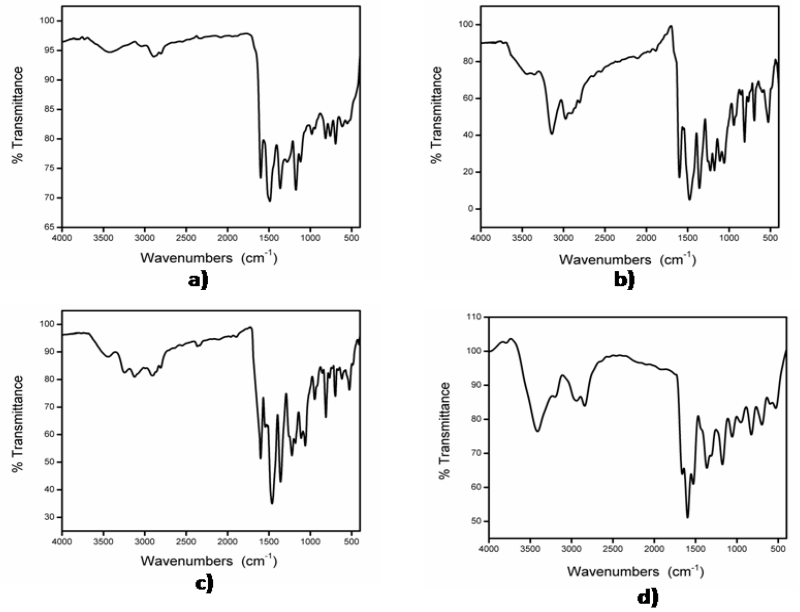

Fig.6. IR spectra of a) $[Co(HL)_2]Cl_2.H_2O$ b) $Ni(HL)_2Cl_2$ c) $Zn(HL)_2Cl_2$ d) $Cd(HL)_2$

Table 7. IR spectral assignments of metal complexes

Compound	$C_{17}H_{20}N_4S$	$[Co(HL)Cl_2.H_2O$	$[Ni(HL)_2Cl_2]$	$[Cu(HL)_2Cl_2]$	$[Zn(HL)_2Cl_2]$	$[Cd(L)_2]$
υ(NH)	3252 3166	3433	3373 3136	3301	3448 3115	3413
υ (C-H) (Ar)	2992	2899	2941	2920	2910	2848
υ (C=N)	1596	1586	1586	1583	1585	1575
ν(C=S)+ ν(C=N) + ν(C-N)	1370	1350	1349	1329	1359	1349
ν(N-C-S)+ν(C-S)	1175	1164	1154	1164	1113	1169
δ(N-N)	1062	1124	1175	1103	1052	1062
υ(C=S)	815	758	806	755	806	-
υ(M-N)	-	487	476	497	467	518

3.2.4. Electron paramagnetic resonance (EPR) spectrum

The ESR spectrum of Cu(II) complex in DMSO at 77 K at X-band was recorded. EPR measurement was made with microwave radiations in the region, 8.75- 9.65 GHz with 100 kHz field modulation (Fig.7). The Cu(II) ion (S=3/2, m_s= ±1/2) leads to a doubly degenerate spin state in the absence of magnetic field. In the presence of magnetic field, the degeneracy is lifted between these two states. The energy difference between them is given by $E = h\nu = g\beta B$, where h is the Planck's constant, ν is the frequency, g is the Lande's splitting factor, equals to 2.0023 for a free electron), β is the Bohr magneton and B is the magnetic field. As both g and β are constant, this equation implies that the splitting of the energy levels is directly proportional to the magnetic field strength. The solution spectrum of the complex at 77

K in DMSO is axial and shows four hyperfine lines characteristic of a monomeric Cu(II) complex. They correspond to −3/2, −1/2, 1/2 and 3/2 which arise from the coupling of the odd electron with copper nucleus (I = 3/2). The value of $g\|$ is 2.47 and $g^{\perp}$ is 2.06. This complex showed $g\|$> 2.3 which is characteristic of an ionic environment. The trend $g\|$> $g^{\perp}$> 2.0023 observed for the complex indicates that the unpaired electron is localised in $d_{x^2-y^2}$ orbital of the Cu(II) ion. Therefore, a distorted octahedral geometry is proposed for the complex. The exchange interaction between the copper centers in polycrystalline sample is explained by Hathaway expression G= ($g\|$-2)/(g⊥-2). Here, the value of G = 7.83, indicates negligible exchange coupling in the complex. No signal at half field was observed in the spectrum, ruling out the possibility of a dimeric form.

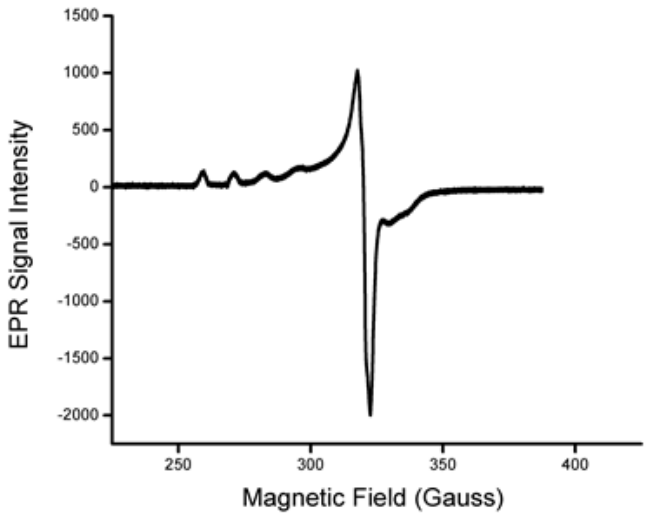

Fig.7. X-Band ESR spectrum of $Cu(HL)_2Cl_2$ complex at LNT in DMSO

3.2.5. ^{1}H NMR Spectrum of $[Zn(HL)_2Cl_2]$

The NMR spectrum of the Zn complex was run in DMSO-*d6*. Aromatic protons exhibit multiplet signals in the range, 6.638–8.000 ppm. The sharp singlet at 10.862 ppm is assigned to –NH proton. A singlet observed at 10.07 ppm can be assigned to azomethine proton. The peak at 2.85 ppm corresponds to methyl protons on terminal nitrogen atom. The peak at 3.36 ppm is attributed to methyl protons of dimethyl amino group. The peak observed at 2.50 ppm may be due to DMSO. Fig.8 represents the ^{1}H NMR spectrum of $[Zn(HL)_2Cl_2]$.

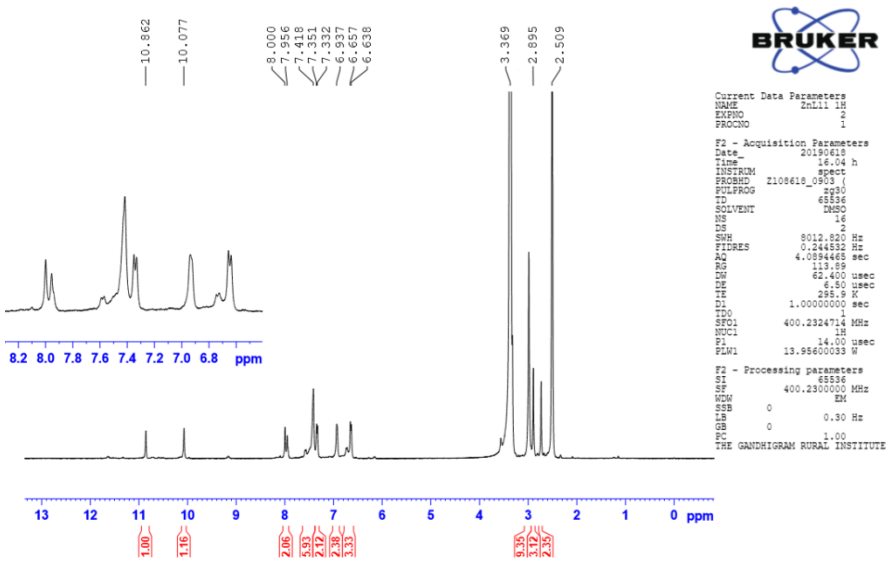

Fig.8. ^{1}H NMR of Zn(II) complex

3.2.6. Thermo gravimetric analysis

Thermo gravimetric analysis (TG) of a compound is used to check its purity and thermal stability. According to the results obtained, the

complexes are not volatile and their decomposition occur in more than one step. A typical thermogram of Co(II) complex is shown in the Fig.9. The analysis was done under at nitrogen atmosphere in a temperature range, 30–500^{0}C and at a heating rate of 10^0 C min^{-1}. Generally, water molecules in complexes are of two types, lattice water and coordinated water[16]. The lattice water will be lost at low temperature (60-120^{0}C) whereas the loss of coordinated water molecule is observed at high temperature (150-200^{0}C).

For $[Co(HL)_2]Cl_2.H_2O$, the first stage of decomposition occurred at 67^{0}C with weight loss 1.92% (calcd. 2.33%). It may be due to the loss of one molecule of lattice water. The second stage of decomposition occurred in the temperature range, 145–296°C which may be due to the decomposition of the ligand moiety (weight loss 33%). The residual mass (9%) observed at 500°C indicated the non- volatile metal oxide formed.

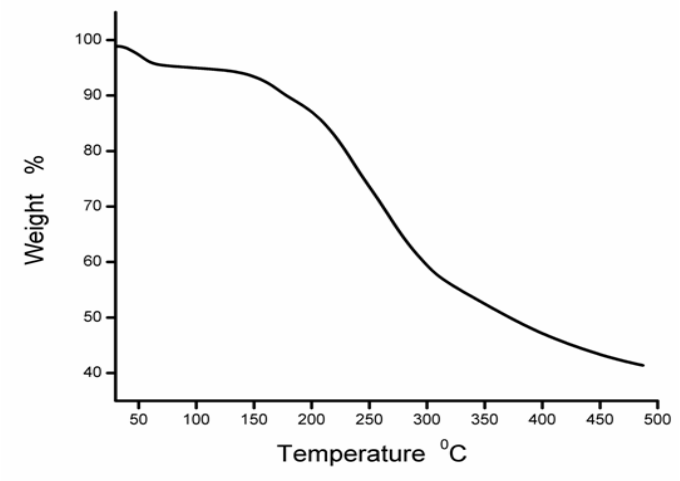

Fig.9. TG curve of Co(II) complex

4. Conclusions

In the present investigation, the synthesis and characterization of the ligand, 4-[N,N-(dimethyl)amino]benzaldehyde N(4)-methyl(phenyl) thiosemicarbazone and its Co(II), Ni(II), Cu(II), Zn(II) and Cd(II) complexes have been discussed. The ligand behaved as an N, S bidentate neutral one coordinating through azomethine nitrogen and thione sulphur in Co(II), Ni(II), Cu(II) and Zn(II) complexes and as bidentate monoanionic one in the case of Cd(II) complex. The mode of coordination of the ligand was clearly determined from the IR spectral studies. Based on the magnetic moment measurements and electronic spectral studies, Co(II) complex was assigned square planar geometry as shown in Fig.10. The complexes of Ni(II), Cu(II) and Zn(II)were found to have octahedral geometries with a general molecular formula, $[M(HL)_2Cl_2]$, where M = Ni(II), Cu(II) or Zn(II) (Fig.11). A tetrahedral geometry was assigned to the Cd(II) complex as given in Fig.12.

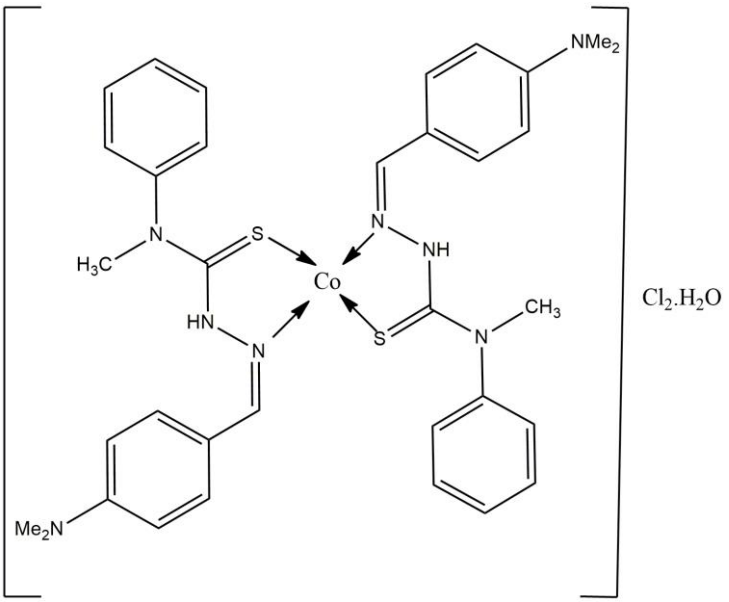

Fig.10. Proposed structure of the Co(II) complex,

$[Co(HL)_2]Cl_2.H_2O$

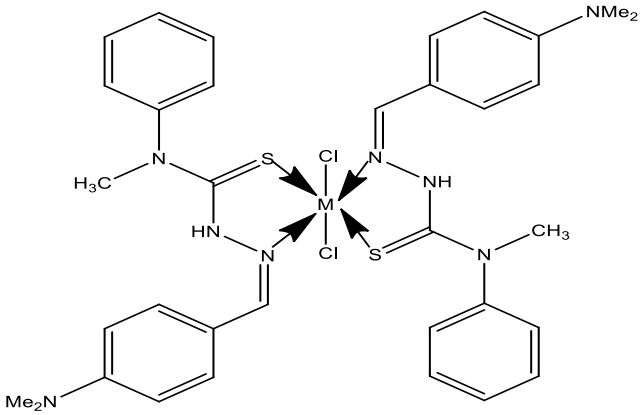

Fig.11. Proposed structure of the complexes,

$[M(HL)_2Cl_2]$

M= Ni(II), Cu(II) or Zn(II).

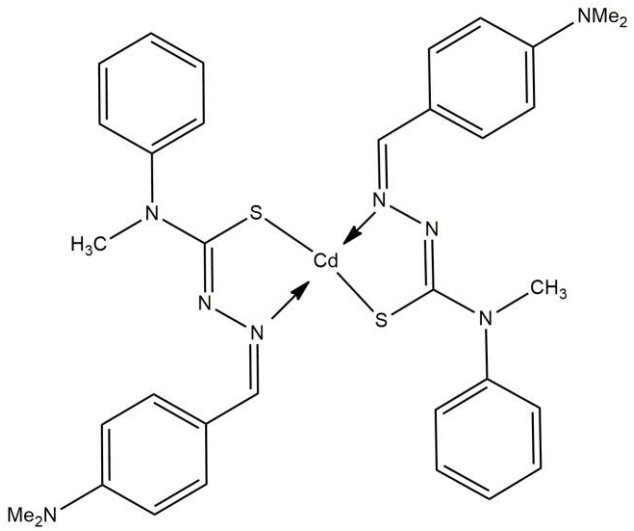

Fig.12. Proposed structure of the Cd(II) complex, $[Cd(L)_2]$

References

[1] T.S. Lobana, S. Khanna, R.J. Butcher, The Influence of the Methyl Substituents at C2 Carbon of Thiosemicarbazones {R1R2C2= N3-N2H-C1 (=S) N1H2} on Bonding and Structures of Copper (I) Complexes, Zeitschrift für anorganische und allgemeine Chemie 633(11-12) (2007) 1820-1826.

[2] E.M. Jouad, A. Riou, M. Allain, M.A. Khan, G.M. Bouet, Synthesis, structural and spectral studies of 5-methyl 2-furaldehyde thiosemicarbazone and its Co, Ni, Cu and Cd complexes, Polyhedron 20(1-2) (2001) 67-74.

[3] J. Karthikeyan, P.P. Naik, A.N. Shetty, A rapid extractive spectrophotometric determination of copper (II) in environmental samples, alloys, complexes and pharmaceutical samples using 4-N, N (dimethyl) amino] benzaldehyde thiosemicarbazone, Environmental monitoring and assessment 176(1-4) (2011) 419-426.

[4] P. Parameshwara, J. Karthikeyan, A.N. Shetty, P. Shetty, 4-(N, N-Diethylamino) Benzaldehyde Thiosemicarbazone in the Spectrophotometric Determination of Palladium, Annali di Chimica: Journal of Analytical, Environmental and Cultural Heritage Chemistry 97(10) (2007) 1097-1106.

[5] T.S. Lobana, R. Sharma, G. Bawa, S. Khanna, Bonding and structure trends of thiosemicarbazone derivatives of metals—an overview, Coordination Chemistry Reviews 253(7-8) (2009) 977-1055.

[6] R.H. Borges, A. Abras, H. Beraldo, Synthesis, characterization and Mössbauer studies of Fe (II) and Fe (III) complexes of 2-acetylpyridine thiosemicarbazone, Journal of the Brazilian Chemical Society 8(1) (1997) 33-38.

[7] Z. Afrasiabi, E. Sinn, P.P. Kulkarni, V. Ambike, S. Padhye, D. Deobagakar, M. Heron, C. Gabbutt, C.E. Anson, A.K. Powell, Synthesis and characterization of copper (II) complexes of 4-alkyl/aryl-1, 2-naphthoquinones thiosemicarbazones derivatives as potent DNA cleaving agents, Inorganica Chimica Acta 358(6) (2005) 2023-2030.

[8] F.A. Cotton, G. Wilkinson, C.A. Murillo, M. Bochmann, R. Grimes, Advanced inorganic chemistry, Wiley New York1988.

[9] B.N. Figgis, Introduction to ligand fields, Interscience publishers1966.

[10] A.P. Lever, Inorganic electronic spectroscopy, Studies in physical and theoretical chemistry 33 (1984).

[11] A.K. El-Sawaf, D.X. West, F.A. El-Saied, R.M. El-Bahnasawy, Iron(III), Cobalt(II), Nickel(II), Copper(II) and Zinc(II) Complexes of 4-Formylantipyrine Thiosemicarbazone, Synthesis and Reactivity in Inorganic and Metal-Organic Chemistry 27(8) (1997) 1127-1147.

[12] M. Imran, J. Iqbal, S. Iqbal, N. Ijaz, In vitro antibacterial studies of ciprofloxacin-imines and their complexes with Cu (II), Ni (II), Co (II), and Zn (II), Turkish journal of biology 31(2) (2007) 67-72.

[13] M. Satpathy, B. Pradhan, Synthesis and characterization of Copper(II) and Nickel(II) complexes withschiff bases derived from aromatic diamines and heterocyclic aldehydes, Journal of the Indian Chemical Society 75(9) (1998) 518-519.

[14] N. Raman, S. Sobha, A. Thamaraichelvan, A novel bioactive tyramine derived Schiff base and its transition metal complexes as selective DNA binding agents, Spectrochimica acta. Part A, Molecular and biomolecular spectroscopy 78(2) (2011) 888-98.

[15] N. Saha, N. Mukherjee, Synthesis, characterisation and coordinating properties of a new pyrazole-derived thiosemicarbazone, a potential antiviral agent: Co (III), Ni (II) and Cu (II) complexes of neutral and deprotonated 5 (3)-methylpyrazole-3 (5)-aldehydothiosemicarbazone, Polyhedron 3(9-10) (1984) 1135-1140.

[16] A. Nikolaev, V. Logvinenko, L. Myachina, Thermographic study of the structures of some simple, mixed and binuclear chelates of EDTA, Thermal analysis, Elsevier (1969), 779-791.

CHAPTER V

SYNTHESIS AND CHARACTERIZATION OF TRANSITION METALCOMPLEXES OF 4-BENZYLOXYBENZALDEHYDE N(4)-METHYL(PHENYL)THIOSEMICARBAZONE

1. Introduction

As ligands, thiosemicarbazones of substituted aromatic aldehydes and heterocyclic carbonyl compounds haven't received much attention as they actually deserve. In pursuit of our studies on thiosemicarbazones of aromatic aldehydes, our attention was drawn to that of 4-benzyloxybenzalde [1-3]. Despite the fact that metal complexes of thiosemicarbazones of 4-benzyloxybenzaldehyde have been studied, there are no reports on complexes of 4-benzyloxybenzaldehyde N(4)-disubstituted thiosemicarbazone. Reports on 4-benzyloxybenzaldehyde thiosemicarbazones revealed that they show good antioxidant and antibacterial activities [4]. Therefore, in this chapter, we present our studies on the synthesis and characterization of 4-benzyloxybenzaldehyde N(4)-methyl(phenyl)thiosemicarbazone (HL) and its complexes with a few first row transition metal ions. The structure of the ligand is given in Fig.1.

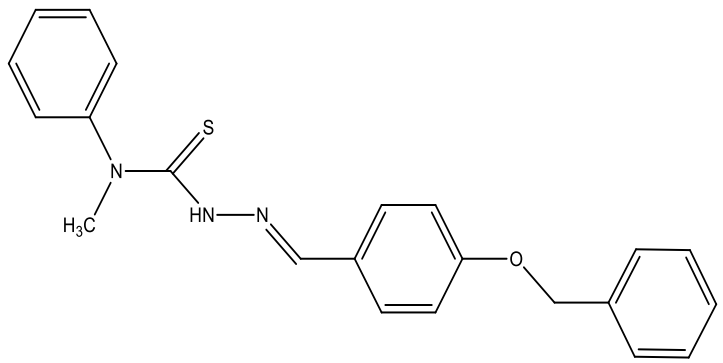

Fig.1. 4-Benzyloxybenzaldehyde N(4)-methyl(phenyl)thiosemi carbazone (HL)

* IUPAC Name: (*E*)-2-(4-(benzyloxy)benzylidene)-*N*-methyl-*N*-phenylhydrazinecarbothioamide

2. Experimental

2.1. Materials and methods

A detailed description about the materials, methods and physico-chemical techniques used in this study are given in Chapter II of Part I.

2.2. Preparation of the ligand (HL)

A solution of N(4)-methyl(phenyl)thiosemicarbazide in ethanol (0.1 mol, 250 ml) was added to 4-benzyloxybenzaldehyde in ethanol (0.1 mol, 250 ml) with 2 or 3 drops of glacial acetic acid and refluxed for 3hr with stirring. The scheme is shown below. The resulting intense yellow coloured solution was concentrated, cooled filtered and washed several times with ethanol. The solid product obtained was kept in a desiccator under reduced pressure over anhydrous calcium chloride. The product was recrystallized from ethanol. (Yield: 60%, M.P = 139ºC).

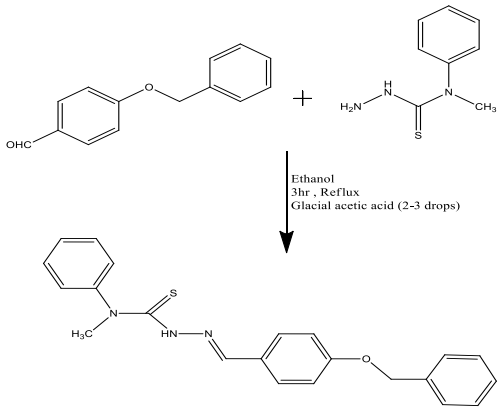

Scheme 1. Synthetic pathway of 4-benzyloxybenzaldehyde N(4)-methyl(phenyl)thiosemicarbazone (HL)

2.3. Preparation of complexes

Hot solution of metal chloride in ethanol (20 cm^3) was added to a hot solution of the ligand in ethanol. All the complexes were synthesized by mixing stoichiometric quantities of the ligand (0.002M) and the metal salts (0.001M). Then mixture was heated under reflux on a water bath for 3hr. On cooling the contents, coloured complexes precipitated out. Complexes obtained were filtered, washed with ethanol and diethyl ether and then dried and kept under reduced pressure over fused calcium chloride. The purity of the complex was checked by TLC.

3. Results and discussion

The data obtained from the analytical- and physico-chemical studies have been correlated to explain the properties, structure and bonding of the compounds.

3.1. Characterization of the ligand (HL)

The ligand, intense yellow coloured powder, having a melting point of 139^0C, was soluble in chloroform, acetonitrile, dimethylformamide, etc. TLC technique was adopted for testing its homogeneity and purity. It was characterized by elemental analysis (Table 1), IR- (Table 2 and Fig.2), electronic- (Table 3 and Fig.3) and ^{1}H NMR- (Table 4 and Fig.4) spectral studies.

3.1.1. Micro analytical data

The elemental analysis of the ligand was performed on a EUROVECTOR EA 3000. The experimentally found out- and calculated percentages of C, H, N and S were in good agreement with the molecular formula of the ligand, $C_{22}H_{21}N_3OS$.

Table 1. Physico-chemical and analytical data of HL

Compound (Empirical Formula)	Yield (%)	Melting Point (^{0}C)	Colour	CHNS Analysis Found % (Calculated)%			
				C	H	N	S
$C_{22}H_{21}N_3OS$	60	139	Yellow	70.32 (69.02)	5.59 (5.25)	11.18 (10.46)	8.52 (8.05)

3.1.2. Spectroscopic analysis

a) Vibrational spectrum

IR spectral data of the ligand with the tentative assignments of the bands are given in the Table 2 and Fig.2. Due to the presence of –NH-C (=S)-NR_2 group, in this type of ligands there is a possibility of thione-thiol tautomerism. However, the absence of a band ~ 2500 cm^{-1}, characteristic of thiol form, excluded this possibility in the present case [5]. Moreover, there is a band at 820 cm^{-1}, characteristic of ν(C=S), denoting that the free ligand exists in thione form. The band at 3341 cm^{-1} in the ligand spectrum takes into account for N-H stretching vibration [6]. The bands at 2939 and 2871 cm^{-1} represent the asymmetric- and symmetric stretching vibrations of –CH group, respectively [7]. The band at 3042 cm^{-1} may be due to C-H (aromatic) stretching vibration. The band at 1617 cm^{-1} represents the azomethine

stretching vibration [8]. The band at 1001cm^{-1} may be assigned to N-N bending vibration [9].

Table 2. IR spectral assignments (in cm^{-1})of HL

Bands (cm^{-1})	**Assignments**
3341	υ(N-H)
3042	υ(C-H) (aromatic)
2939	υ(C-H) (asymmetric)
2871	υ(C-H) (symmetric)
1617	υ(C=N)
1001	δ (N-N)
820	υ(C=S)

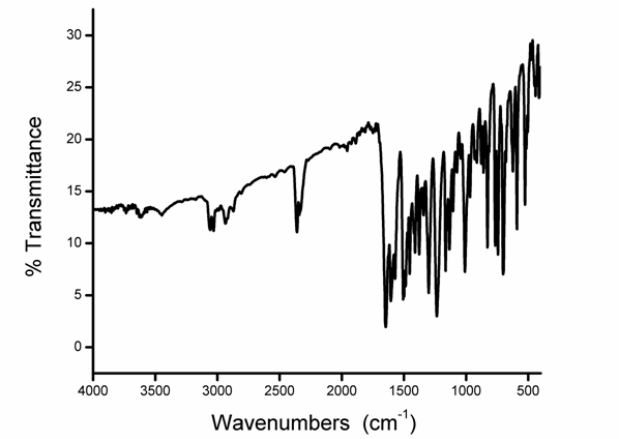

Fig.2. FT-IR spectrum of HL

b) Electronic spectrum

The electronic spectrum of the ligand showed an intense band at 286 nm which can be attributed to π→ π* transition. Similarly, a band at 335 nm in the ligand spectrum may be due to n →π* transition of the azomethine group. The data are given in Table 3.

Table 3. Electronic spectral bands of HL

Spectral Bands	**Assignments**
λ_{max} (nm)	
286	$\pi \rightarrow \pi^*$ transition
335	$n \rightarrow \pi^*$ transition

c) ^{1}H NMR spectrum

The formation of the 4-benzyloxybenzaldehyde N(4)-methyl (phenyl)thiosemicarbazone was confirmed by analyzing its ^{1}H NMR spectrum recorded in DMSO-d_6 using TMS as internal standard. The ^{1}H NMR spectrum of the ligand showed a multiplet between 7.81- 6.99 ppm, which was due to aromatic protons. A sharp singlet at 9.071 ppm was attributed to the -NH proton. The triplet that appeared at 2.47 ppm was assignable to -CH_3 protons on the terminal N-atom of the thiosemicarbazone moiety. The signal that appeared at 3.12 ppm was due to the –OCH_2 group. The azomethine hydrogen appeared as a sharp singlet at 5.11 ppm [4].

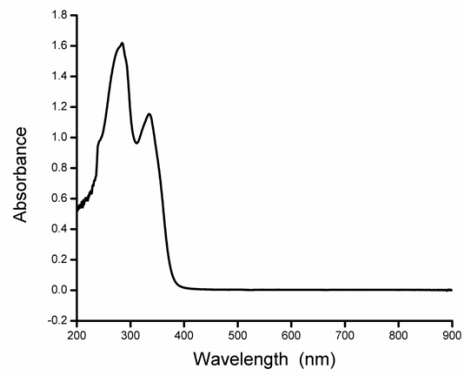

Fig.3. Electronic spectrum of HL

Table 4. ^{1}H NMR data of HL

δ (ppm)	**Assignments**
9.701	-NH group
7.81-6.99(m)	Aromatic Protons
5.11	Azomethine hydrogen
3.12	-OCH_2 group
2.472	-CH_3 group on terminal nitrogen atom

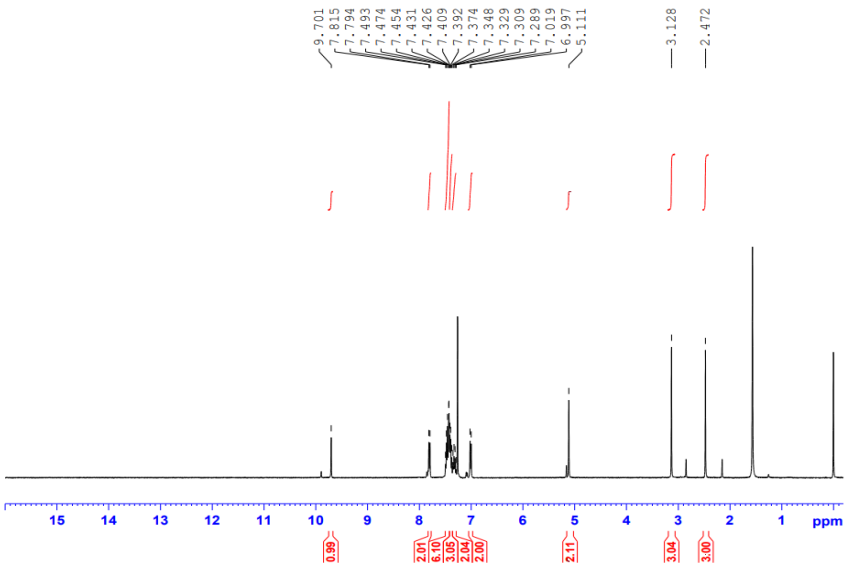

Fig.4. ^{1}H NMR spectrum of HL

3.2. Characterization of the complexes

All the complexes of 4-benzyloxybenzaldehyde N(4)-methyl(phenyl)thiosemicarbazone were stable under atmospheric conditions. They were non-hygroscopic and soluble in chloroform, DMSO and DMF, but sparingly soluble in other common organic

solvents like methanol and ethanol. Elemental analyses, magnetic moment measurements, FT-IR, electronic- and EPR spectral studies and TG analysis were used to characterize them.

3.2.1. Elemental analysis

The analytical data and physical properties of the ligand (HL) and its complexes are listed in Table 5. The complexes were found to have a general formula $[M(HL)_2Cl_2].H_2O$, when M=Co(II), Ni(II), Zn(II) or Cd(II), n = 0 and when M= Cu(II), n=1.

3.2.2. Electronic spectra and magnetic moments

The important electronic spectral bands of Co(II), Ni(II) and Cu(II) complexes and their possible assignments are given in the Table 6.

Table 5. Physico-chemical and analytical data of complexes

Compound	Colour	Yield (%)	MP (^{0}C)	Elemental Analysis (%) found (calculated)				
				C	H	N	S	Metal
$C_{22}H_{21}N_3OS$	Yellow	60	139	69.50 (70.32)	5.10 (5.59)	11.01 (11.18)	8.21 (8.52)	-
$[Co(HL)_2Cl_2]$	Brownish black	62	152	52.92 (53.40)	4.01 (4.24)	8.18 (8.49)	6.20 (6.47)	4.96 (5.96)
$[Ni(HL)_2Cl_2]$	Brown	65	158	53.02 (53.42)	4.05 (4.24)	8.15 (8.49)	6.19 (6.47)	5.25 (5.93)
$[Cu(HL)_2Cl_2].H_2O$	Black	61	164	52.76 (53.16)	4.01 (4.23)	8.17 (8.45)	6.18 (6.44)	5.51 (6.30)
$[Zn(HL)_2Cl_2]$	Yellow	65	148	52.89 (53.06)	4.20 (4.22)	8.40 (8.44)	6.20 (6.43)	6.38 (6.57)
$[Cd(HL)_2Cl_2]$	White	66	151	50.01 (50.66)	3.93 (4.03)	7.95 (8.06)	6.03 (6.14)	10.48 (10.79)

In the present case, Co(II) complex has three spin allowed transitions at 295, 407 and 893 nm characteristic of octahedral geometry of the

complex. The Co(II) complex registered a magnetic moment value of 4.82 B.M. This value, conformed a high-spin octahedral geometry around Co(II) ion.

In the present case, three intense spin allowed transitions, $^3A_{2g}(F) \rightarrow {}^3T_{2g}(F)$, $^3A_{2g}(F) \rightarrow {}^3T_{1g}(F)$ and $^3A_{2g}(F) \rightarrow {}^3T_{1g}(P)$ with bands at 645, 423 and 264 nm, respectively, indicate octahedral geometry around Ni(II) ion. It has registered a magnetic moment value of 2.82 B.M indicating its octahedral geometry.

In the present copper complex, a band at 635 nm may be due to $^2E_g \rightarrow {}^2T_{2g}$ transition, indicating an octahedral geometry for the complex. The Cu(II) complex registered a magnetic moment of 1.98 B.M, indicating its 6-coordinate octahedral geometry. The complexes of Zn(II) and Cd(II) were found to be diamagnetic.

3.2.3. IR spectra and mode of bonding

The FT-IR spectra of the complexes provide information about the binding sites of the ligands with the metal ions. The important IR spectral bands in the ligand spectrum usually undergo shift from their positions upon coordination to metal ions in the complexes. The important IR spectral bands of the ligand (Fig.2) and the complexes (Fig.5) together with their probable assignments are given in Table 7.

Table 6. Electronic spectral bands and their assignments of the complexes

Compound	**Spectral bands**	**Assignments**
	λ_{max} (nm)	
$[Co(HL)_2Cl_2]$	295	$^4T_{1g}(F) \rightarrow {}^4T_{1g}(P)$
	407	$^4T_{1g}(F) \rightarrow {}^4A_{2g}(F)$
	893	$^4T_{1g}(F) \rightarrow {}^4T_{2g}(F)$
$[Ni(HL)_2Cl_2]$	264	$^3A_{2g}(F) \rightarrow {}^3T_{1g}(P)$
	423	$^3A_{2g}(F) \rightarrow {}^3T_{1g}(F)$
	645	$^3A_{2g}(F) \rightarrow {}^3T_{2g}(F)$
$[Cu(HL)_2Cl_2].H_2O$	635br	$^2E_g \rightarrow {}^2T_{2g}$

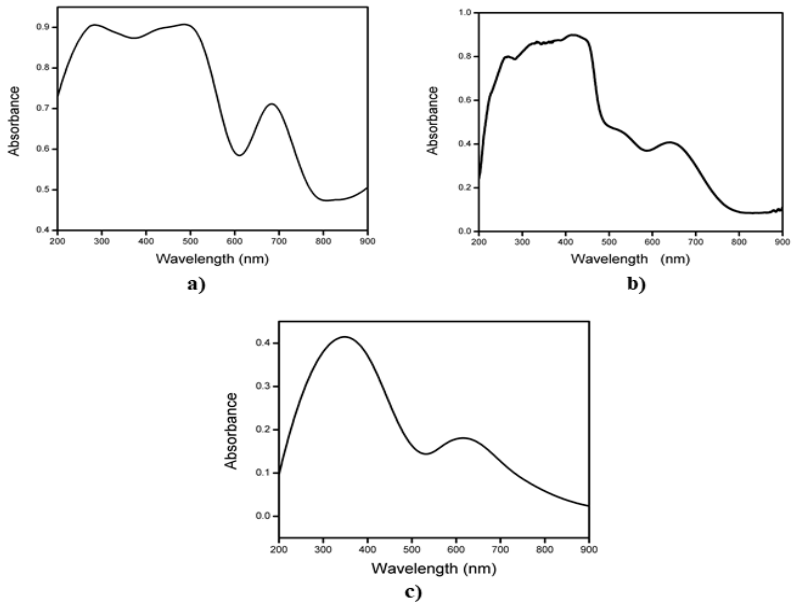

Fig.5. Electronic spectra of a) $[Co(HL)_2Cl_2]$ b) $[Ni(HL)_2Cl_2]$ and c) $[Cu(HL)_2Cl_2].H_2O$

The broad band at 3341 cm^{-1} in the ligand spectrum, assigned to the stretching of -NH group [10] remained in the spectra of all the complexes almost at the same positions, indicating the absence of enolisation of –NH-C=S group. The strong bands due to ν(C=N) are found to be shifted to downfield by a few cm^{-1} in the complexes due to the coordination of nitrogen [11]. The IR spectrum of the ligand showed typical bands in the range of 2800-2900 cm^{-1}, which can be attributed to the symmetric- and asymmetric stretching vibrations of –CH group [7]. These bands remained almost at the same position in the spectra of the complexes. The medium intensity band observed at 1001 cm^{-1}in the ligand spectrum due to δ(N-N) vibration has been found to be shifted to higher wave numbers, 1113-11169 cm^{-1} in the spectra of all the complexes. The bands due to υ(C=S) group in the spectra of the complexes shifted to lower frequency region, supporting the participation of the thiocarbonyl sulphur (C=S) in coordination to the central metal ions. These shifts indicated the coordination of the ligand through azomethine nitrogen and thione sulphur atom in all these complexes. The bands observed in the range, 507-520 cm^{-1} in the spectra of all the metal complexes may be assigned to υ(M-N)[12]. Therefore, the FTIR data indicated that the ligand functioned as neutral, bidentate (coordinating through the imino nitrogen and thiocarbonyl sulphur) in all the complexes.

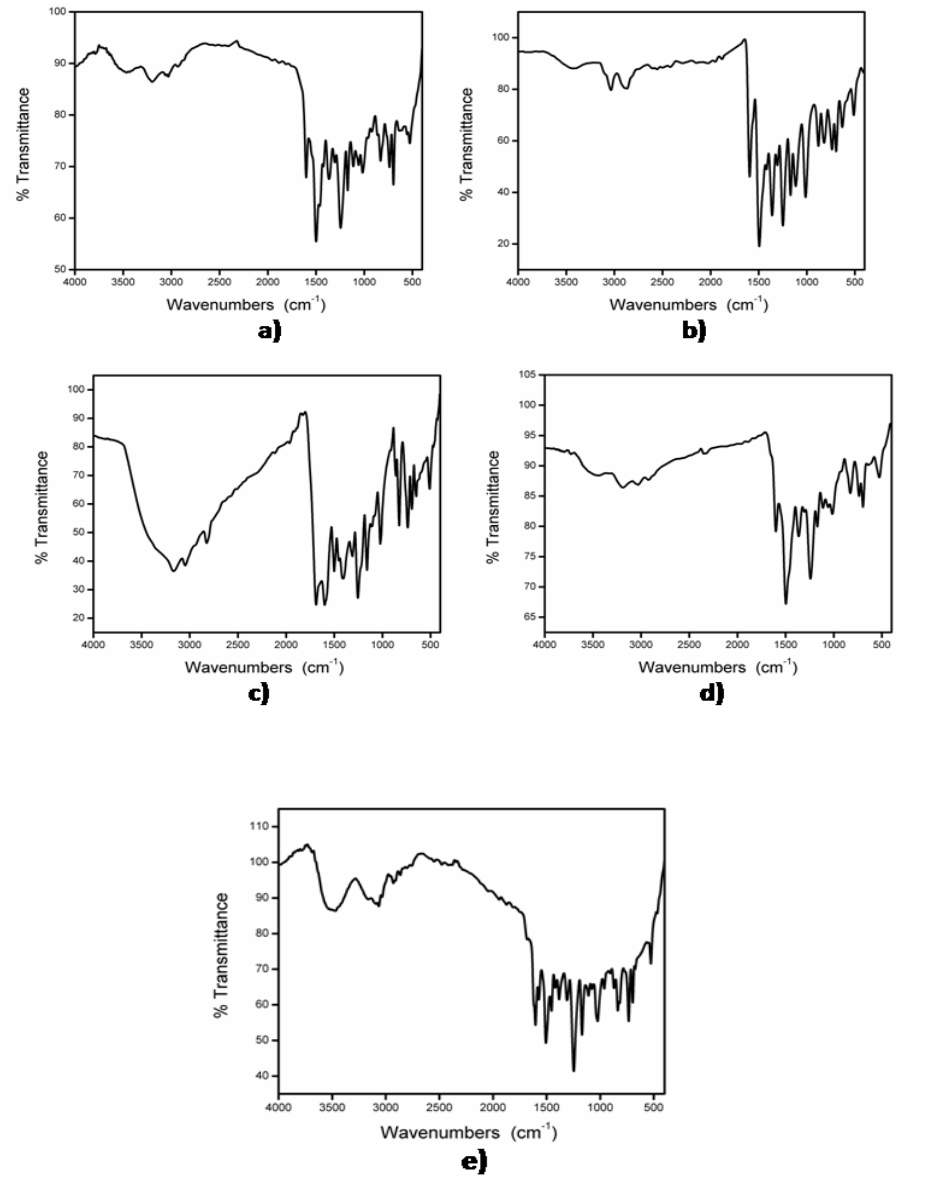

Fig.6. IR spectra of (a) $[Co(HL)_2Cl_2]$b) $[Ni(HL)_2Cl_2]$ c) $[Cu(HL)_2Cl_2].H_2O$ d) $[Zn(HL)_2Cl_2]$and e) $[Cd(HL)_2Cl_2]$

Table 7. IR spectral assignments of the ligand and complexes

Compound	$C_{22}H_{21}N_3OS$	$[Co(HL)_2Cl_2]$	$[Ni(HL)_2Cl_2]$	$[Cu(HL)_2Cl_2].H_2O$	$[Zn(HL)_2Cl_2]$	$[Cd(HL)_2Cl_2]$
υ (NH)	3341	3464	3445	3328	3454	3496
υ (C-H) (asymmetric)	2939	2910	2890	2825	2920	2925
υ (C-H) (symmetric)	2871	2848	2797	2737	2785	2755
υ (C=N)	1617	1609	1596	1608	1589	1605
δ(N-N)	1001	1169	1164	1155	1113	1154
υ(C=S)	820	815	759	789	815	796
υ(M-N)	-	518	508	518	520	507

3.2.4. Electron paramagnetic resonance (EPR) spectrum

ESR spectrum of the Cu(II) complex was recorded at 77K in DMSO solution, on the X-band at 8.75-9.65 GHz with 100 kHz field modulation in liquid nitrogen temperature (LNT) and spectrum is presented in Fig.7. The spectrum shows well- resolved signals. The analysis of the spectrum gives $g\|\| = 2.50$ and $g\perp = 2.07$. The complex under study showed the trend $g\|\| > g\perp > 2.0023$, indicating that the unpaired electron is localized in $d_{x^2-y^2}$ orbital of the Cu(II) ion[13]. In addition, exchange coupling interaction between two Cu(II) ions is explained by Hathaway expression, $G= (g\|\|-2)/(g\perp-2)$. Here, the value of G>4.0, indicates the absence of considerable exchange coupling interaction in complex (G=7.14). Normally, a value of $g\|\| = 2.3$ or higher, indicates an ionic environment; while g|| less than 2.3 shows a covalent environment around Cu(II) ion. The $g\|\|$ value for the present Cu(II) complex is 2.50, indicating its ionic character.

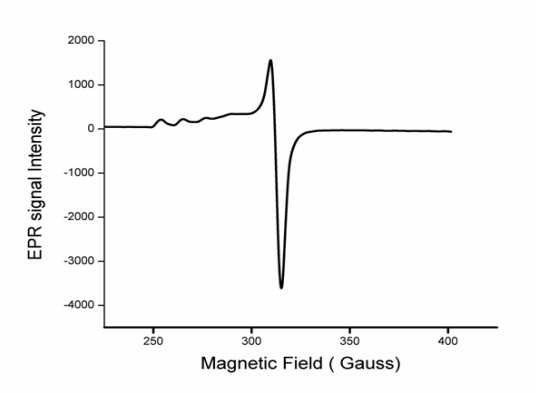

Fig.7. X-Band ESR spectrum of Cu(II) complex at LNT in DMSO

3.2.5. ^{1}HNMR spectrum of $[Zn(HL)_2Cl_2]$

The ^{1}H NMR spectrum of the Zn(II) complex was recorded in DMSO at room temperature (Fig.8). A singlet at 11.08 ppm can be assigned to N–H proton. A singlet observed at 10.02 ppm can be assigned to azomethine proton. Aromatic protons showed a multiplet peaks in the region, 8.63–5.6 ppm. $-CH_3$ protons absorbed at 3.57-3.11 ppm. The peaks in the range, 2.50-2.49 ppm may be assigned to solvent protons.

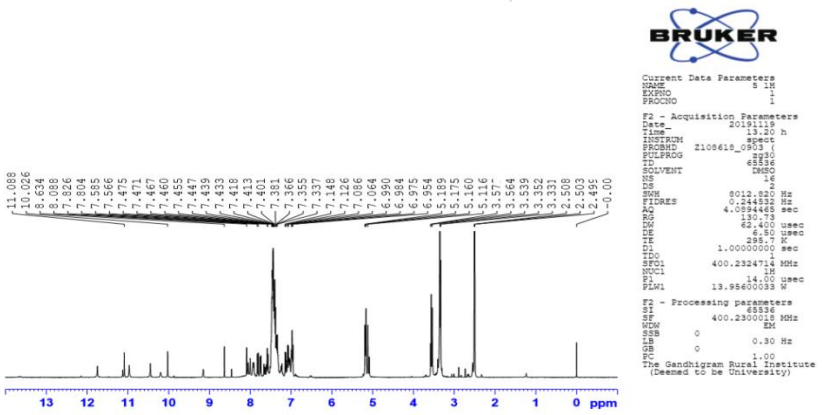

Fig.8. ^{1}H NMR spectrum of $[Zn(HL)_2Cl_2]$

3.2.6. Thermo gravimetric analysis

Thermo gravimetric analyses are useful techniques to understand thermal stabilities and purities of the complexes and to confirm the presence and nature of water molecules whether coordinated or lattice held ones in the complexes.

The $[Ni(HL)_2Cl_2]$ complex showed three stages of decomposition which may be due to the successive degradation of ligand molecule. A residual mass of 9.67% was left which may be due to the formation of NiS (calcd. 10.30%).

For $[Cu(HL)_2Cl_2].H_2O$, two decomposition stages were observed. Initial mass loss (61^0C) corresponded to the loss of one lattice water molecule with a mass loss of 1.73% (Calcd. 1.99%). The second stage occurred between 101–352°C with a mass loss of 46.2%. A residual mass of 7.43% may be due to the formation of copper oxide(calcd. 8.4%).

For $[Zn(HL)_2Cl_2]$, the first stage was between 169–186°C and demonstrated a mass loss of 8.67%. The second stage occurred at 225–374°C with a mass loss of 38.5%. A residual mass of 8.7% may be due to the formation of ZnS (calcd. 10.82%).

For $[Cd(HL)_2Cl_2]$ complex, the first stage decomposition occurred at 263-358^0C with weight loss of 39.1%. It may be attributed to the degradation of the ligand molecules. The absence of any thermal change before this temperature demonstrated its high thermal stability.

A residual mass of 12.05% may be due to the formation of CdO (calcd. 13.74%).

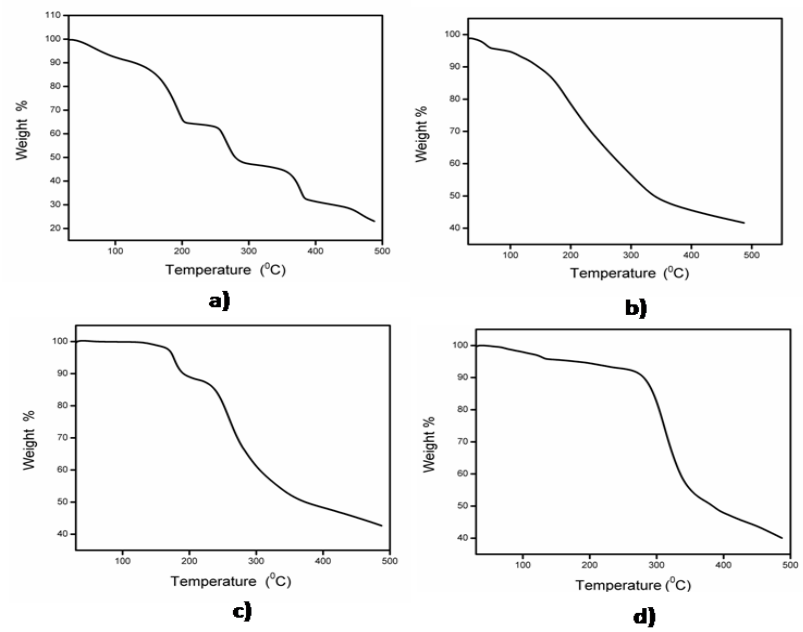

Fig.9. TG curves of a) $[Ni(HL)_2Cl_2]$ b) $[Cu(HL)_2Cl_2].H_2O$ c) $[Zn(HL)_2Cl_2]$ and d) $[Cd(HL)_2Cl_2]$

4. Conclusions

The synthesis and characterisation of Co(II), Ni(II), Cu(II), Zn(II) and Cd(II) complexes of 4-benzyloxybenzaldehyde N(4)-methyl(phenyl) thiosemicarbazone (HL) were discussed. Based on the elemental analyses, IR and NMR spectral data, all the complexes were assigned octahedral geometry (Fig.10). According to IR and ^1H NMR spectral data, HL was found to function as neutral bidentate ligand.

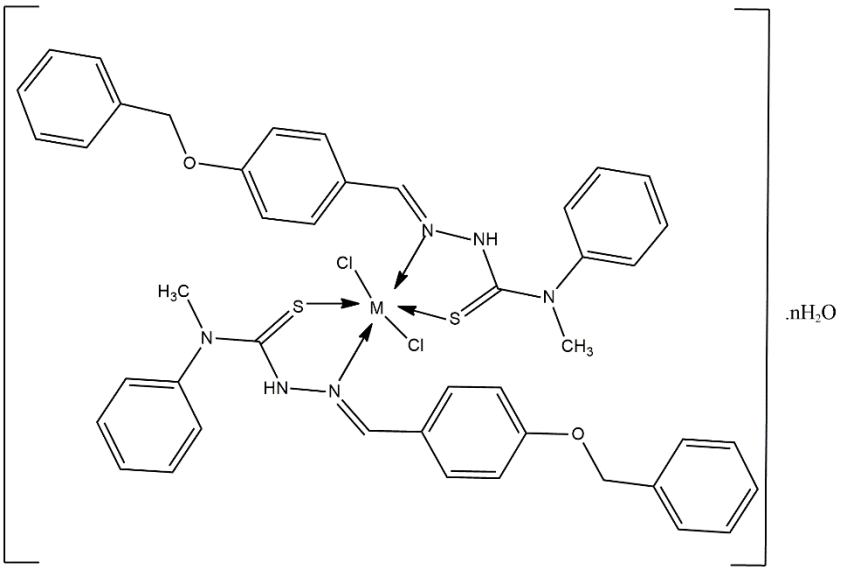

Fig.10. Proposed structures of the complexes, $[M(HL)_2Cl_2].nH_2O$, when M= Co(II), Ni(II), Zn(II) or Cd(II); n=0 and when M= Cu(II); n=1.

References

[1] S. Padhye, G.B. Kauffman, Transition metal complexes of semicarbazones and thiosemicarbazones, Coordination Chemistry Reviews 63 (1985) 127-160.

[2] D.X. West, S.B. Padhye, P.B. Sonawane, Structural and physical correlations in the biological properties of transition metal heterocyclic thiosemicarbazone and S-alkyldithiocarbazate complexes, Complex Chemistry, Springer1991, 1-50.

[3] E. Labisbal, K.D. Haslow, A. Sousa-Pedrares, J. Valdés-Martínez, S. Hernández-Ortega, D.X. West, Copper (II) and nickel (II) complexes of 5-methyl-2-hydroxyacetophenone N (4)-substituted thiosemicarbazones, Polyhedron 22(20) (2003) 2831-2837.

[4] B. Prathima, Y.S. Rao, S.A. Reddy, Y. Reddy, A.V. Reddy, Copper (II) and nickel (II) complexes of benzyloxybenzaldehyde-4-phenyl-3-thiosemicarbazone: Synthesis, characterization and biological activity, Spectrochimica Acta Part A: Molecular and Biomolecular Spectroscopy 77(1) (2010) 248-252.

[5] B.S. Garg, M.P. Kurup, S.K. Jain, Y.K. Bhoon, Spectral studies of iron (III) complexes of substituted thiosemicarbazones of 2-acetylpyridine, Transition Metal Chemistry 13(4) (1988) 247-249.

[6] K.P. Deepa, K.K. Aravindakshan, Synthesis and characterization of metal complexes of N-methyl-and N-ethylacetoacetanilide semicarbazones, Synthesis and Reactivity in Inorganic and Metal-Organic Chemistry 31(1) (2001) 43-56.

[7] Y. Sharma, Elementary organic spectroscopy, S. Chand Publishing (2007).

[8] H. Aliyu, H. Abdullahi, Synthesis and characterisation of Manganese (II), Cobalt (II), Nickel (II) and Copper (II) N, N'-bis (Benzoin) ethylenediiminato complexes, Bayero Journal of Pure and Applied Sciences 2(2) (2009) 110-112.

[9] P. Kalsi, Spectroscopy of organic compounds, New Age International (2007).

[10] K. Aravindakshan, C. Nair, Preparation and characterization of vanillin thiosemicarbazone complexes with Co (II), Ni (II), Cu (II), Zn (II), Cd

(II) and Hg (II), Proceedings of the Indian Academy of Sciences-Chemical Sciences, Springer, (1984) 111-115.

[11] K. Nakanishi, Infrared Absorption Spectroscopy, Nankodo Co, Ltd., Tokyo (1962).

[12] T. Yousef, T. Rakha, U. El Ayaan, G.A. El Reash, Synthesis, spectroscopic characterization and thermal behavior of metal complexes formed with (Z)-2-oxo-2-(2-(2-oxoindolin-3-ylidene) hydrazinyl)-N-phenylacetamide (H2OI), Journal of Molecular Structure 1007 (2012) 146-157.

[13] K.B. Gudasi, S.A. Patil, R.S. Vadavi, R.V. Shenoy, M. Nethaji, Crystal structure of 2-[2-hydroxy-3-methoxyphenyl]-3-[2-hydroxy-3-methoxybenzylamino]-1, 2-dihydroquinazolin-4 (3H)-one and the synthesis, spectral and thermal investigation of its transition metal complexes, Transition metal chemistry 31(5) (2006) 586-592.

CHAPTER VI

SYNTHESIS AND CHARACTERIZATION OF TRANSITION METAL COMPLEXES OF 4-HYDROXY-3-METHOXYACETOPHENONE N(4)-METHYL(PHENYL)THIOSEMICARBAZONE

1. Introduction

The ligands with electronegative donor atoms like sulphur, nitrogen and oxygen play prominent role in the formation of coordination compounds. Out of numerous versatile multifunctional ligands with these donor atoms, thiosemicarbazones are potent. Traces of interest of thiosemicarbazones date back to the beginning of the 20th century. Thiosemicarbazones are getting more attraction due to their antitumor-[1], antibacterial-[2], antifungal-[3], and antiviral-[4] activities and these activities have been shown to enhance on coordinating with metal ions [5, 6]. A variety of thiosemicarbazones can be synthesized by using different carbonyl compounds and by diversely substituting at N(4) position of the thiosemicarbazide moiety [7]. When these ligands coordinate with metal ions, they either act as neutral bidentate- or as anionic bidentate ligands. Very rarely, they can act as mono dentate ligands by binding through sulphur alone [8].

Our literature survey revealed that acetophenone- and substituted acetophenone thiosemicarbazones and their transition metal complexes showed good antibacterial-[9], antioxidant-[10], antifungal-[11], cytotoxic-[12] activities. However, there are no reports on the coordination behaviour of N-subsituted thiosemicarbazones of 4-hydroxy-3-methoxyacetophenone. The present chapter portrays the synthesis and characterization of Co(II), Ni(II), Cu(II), Zn(II) and Cd(II) complexes with a novel thiosemicarbazone (HL) derived from the condensation of 4-hydroxy-3-methoxyacetophenone and N(4)-methyl(phenyl)thiosemicarbazide. The structure of the ligand is given in Fig.1.

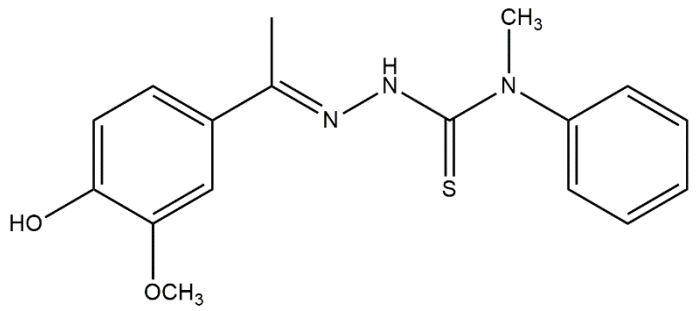

Fig.1. 4-Hydroxy-3-methoxyacetophenone N(4)-methyl(phenyl) thiosemicarbazone, (HL)

*IUPAC Name: (*E*)-2-(1-(4-hydroxy-3-methoxyphenyl)ethylidene)-*N*-methyl-*N*-phenylhydrazinecarbothioamide

2. Experimental

2.1. Materials and methods

The details about the chemicals used, the procedures adopted for the synthesis of precursors and the methods of characterization are described in Chapter II.

2.2. Preparation of the ligand (HL)

N(4)-methyl(phenyl)thiosemicarbazide (0.1mol, 250 ml) dissolved in hot ethanol was added slowly to an ethanolic solution of 4-hydroxy-3-methoxyacetophenone (0.1mol, 250 ml) under constant stirring. A white coloured solution was formed after refluxing the mixture for about 4hr in the presence of a catalytic amount of glacial acetic acid. A white coloured compound was obtained on evaporating the solvent. It was dried under reduced pressure (Yield=78%, M.P=149^{0}C). The

synthetic pathway of the ligand, 4-hydroxy 3-methoxyacetophenone N(4)-methyl(phenyl)thiosemicarbazone (HL) is shown in Scheme 1.

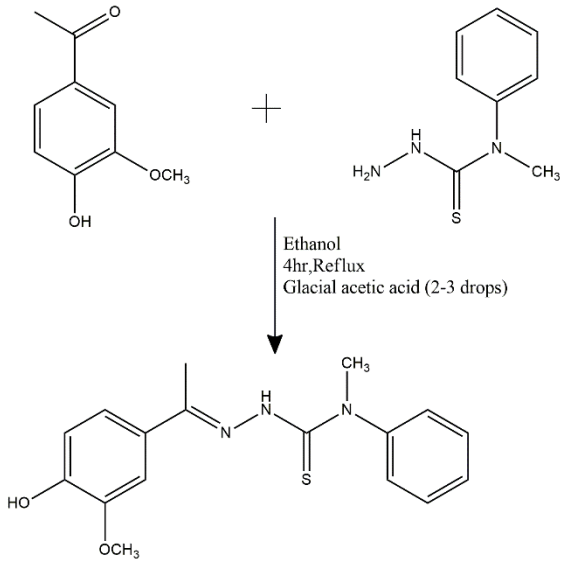

Scheme 1. Synthetic pathway of 4-hydroxy-3-methoxyacetophenone N(4)-methyl(phenyl)thiosemicarbazone (HL)

2.3. Preparation of the metal complexes

A methanolic solution of metal chloride (0.025mol in 20 ml) was slowly added to a methanolic solution of HL (0.05mol in 40 ml) and the mixture was refluxed for 4hr. The resulting mixture was concentrated and cooled. The complex precipitated was filtered off, washed several times with methanol and dried under reduced pressure. All the complexes were prepared using a reaction mixture containing metal chloride and ligand in 1:2 molar ratio. Yields and melting points of the complexes were noted.

3. Results and discussion

The physical properties, elemental analytical-, and spectral data have been used to explain the structure and bonding of the compounds.

3.1. Characterization of the ligand (HL)

3.1.1. Micro analytical data

The white coloured ligand, 4-hydroxy-3-methoxyacetophenone N(4) methyl(phenyl)thiosemicarbazone (HL) was soluble in chloroform, DMSO, DMF, etc. The compound was stable under atmospheric conditions. It was non-hygroscopic in nature. It was characterized analytically and further by FT- IR, UV-Vis- and ^{1}H NMR spectral techniques. CHNS percentages were in agreement with the suggested molecular formula, $C_{17}H_{19}N_3O_2S$ of the ligand.

Table 1. Physico-chemical and analytical data of HL

Compound (Emperical formula)	**Yield (%)**	**Melting point (^{0}C)**	**Colour**	**CHNS Analysis Found% (Calculated)%**			
				C	**H**	**N**	**S**
$C_{17}H_{19}N_3O_2S$	78	149^{0}C	White	61.20 (61.94)	5.32 (5.76)	12.32 (12.75)	9.50 (9.71)

3.1.2. Spectroscopic analysis

a) Vibrational spectrum

Infrared spectroscopy brings important information in the preliminary conformation of the structural aspects of new molecules in the absence of the crystallographic data. The FT-IR spectrum of the compound was recorded in the region, 4000–400 cm^{-1} and is presented as Fig.2. A

sharp band observed at 3454 cm^{-1} may be due to -OH stretching vibration [13]. The band at 3217 cm^{-1} may be assigned to NH stretching vibration. A weak absorption band observed at 2950 cm^{-1} was due to C-H stretching vibration. The non- existence of a band around 2560 cm^{-1} [assigned to υ(S–H)] indicated the existence of the ligand as thione tautomer in the solid state [14]. A sharp band at 1593 cm^{-1} was assigned for the stretching mode of C=N bond of the ligand. The band appeared at 1482 cm^{-1} was assigned the C=C stretching vibration. A medium intensity band found at 1344 cm^{-1} may be attributed to υ(C=S)+ υ(C=N) + υ(C-N). The band at 1206 cm^{-1} in the ligand spectrum may be assigned to υ(NH–C=S). Absence of any characteristic band due to υ(C=O) in the region, 1725-1705cm^{-1} confirmed the condensation of carbonyl compound. The band at 857 cm^{-1} corresponded to υ(C=S).

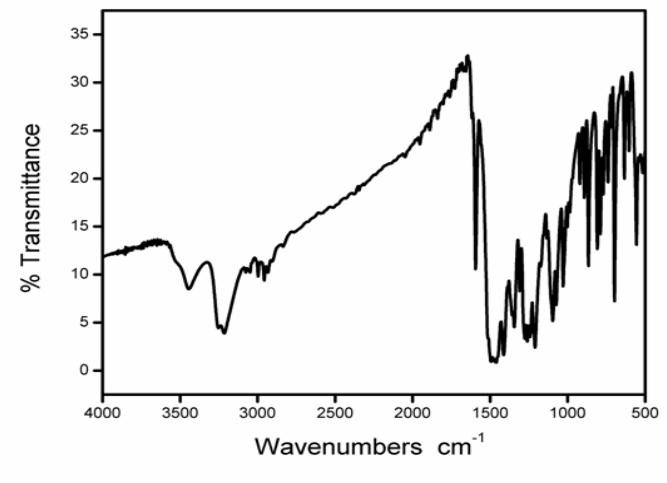

Fig.2. IR spectrum of HL

Table 2. IR spectral assignments (in cm^{-1}) of HL

Bands (cm^{-1})	**Assignments**
3454	υ(-OH)
33217	υ (-NH)
1 1593	υ(C=N)
1344	υ(C=S)+ υ(C=N) + υ(C-N)
1206	υ(NH-C=S)
1103	δ(N-N)
857	υ(C=S)

b) Electronic spectrum

The electronic absorption spectrum of the ligand was recorded in solid state in the range of 200–900 nm (Fig.3). The strong peak at 267 nm can be attributed to π→π* transition. Similarly, a peak at 329 nm may be due to n→π* transitions. The data are given in Table 3.

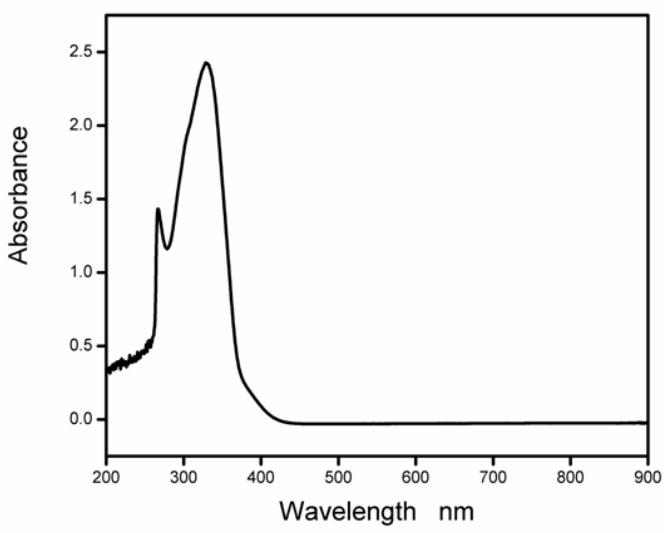

Fig.3. Electronic spectrum of HL

Table 3. Electronic spectral bands of HL

Spectral bands (nm)	**Assignments**
267	π→π* transition
329	n→π* transition

c) ^{1}H NMR spectrum

The ^{1}H NMR spectrum of the ligand is presented in Fig.4.The spectrum showed a singlet at 10.802 ppm which can be assigned to N–H proton. A sharp singlet at 10.551 ppm may be assigned to -OH proton. A sharp singlet at 9.463 ppm may be assigned to aromatic proton adjacent to methoxy group. A doublet at 9.338-9.317 ppm may be attributed to the aromatic proton near to imine bond. The remaining aromatic protons showed multiplet peaks in the region 7.555–6.791 ppm. Singlet at 3.831 ppm may be assigned to methoxy protons. ^{4}N–CH_3 protons absorbed at 3.575 ppm. A singlet at 2.276 ppm may be attributed to three methyl protons on azomethine carbon.

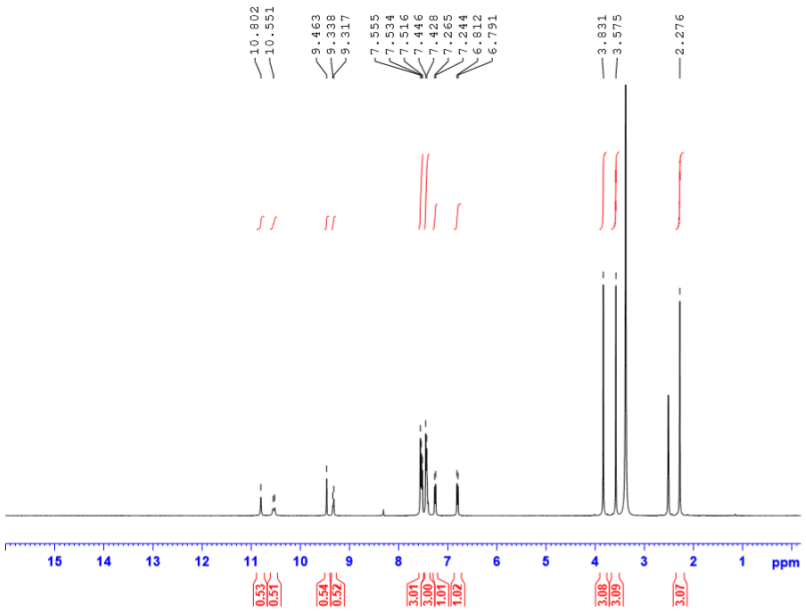

Fig.4. ^{1}H NMR spectrum of HL

Table 4. ^{1}H NMR data of HL

δ (ppm)	**Assignments**
10.802	O-H proton
10.551	N-H proton
9.463	Azomethine proton
7.555–6.791	Aromatic Protons
3.831	Methoxy Protons
3.575	-CH_3 group on terminal nitrogen atom
2.276	-CH_3 group on azomethine carbon.

3.2. Characterization of the metal complexes

All the complexes of 4-hydroxy-3-methoxyacetophenone N(4)-methyl(phenyl)thiosemicarbazone (HL) were stable under atmospheric conditions. They were soluble in DMSO, chloroform, DMF, etc., and sparingly soluble in methanol and ethanol. The micro analytical data of the complexes were obtained on the CHNS analyser. FT-IR, UV-Vis, magnetic measurements, ^{1}H NMR, TG and ESR studies were carried out for the characterization and structural elucidation of the complexes.

3.2.1. Analytical data of metal complexes

The micro analytical data of all the complexes agreed well with their proposed molecular formulae. The physico-chemical and analytical data of the complexes are presented in Table 5.

Table 5. Physico-chemical and analytical data of the complexes

Compound	Yield (%)	Colour	M.P (^{0}C)	Elemental Analysis (%) found (calculated)				
				C	H	N	S	Metal
$C_{17}H_{19}N_3O_2S$	78	White	149	61.20 (61.94)	5.32 (5.76)	12.32 (12.75)	9.50 (9.75)	-
$[Co(HL)Cl_2]$	66	Dark green	179	44.02 (44.43)	4.12 (4.14)	9.14 (9.15)	7.00 (6.97)	12.35 (12.83)
$[Ni(HL)_2Cl_2].H_2O$	74	Brown	182	50.26 (50.60)	4.51 (4.71)	10.21 (10.42)	8.00 (7.93)	7.12 (7.27)
$[Cu(HL)Cl_2].H_2O$	72	Black	178	42.24 (42.34)	3.89 (3.94)	8.95 (8.72)	6.25 (6.64)	13.45 (13.19)
$[ZnL(H_2O)Cl]$	78	Yellow	172	45.39 (45.62)	4.41 (4.47)	9.28 (9.39)	7.15 (7.16)	14.58 (14.62)
$[Cd(L)_2]$	75	White	175	52.51 (52.92)	4.71 (4.67)	10.81 (10.89)	8.12 (8.30)	14.02 (14.58)

3.2.2. Electronic spectra and magnetic moments

The electronic spectra of the metal complexes were recorded in solid state and their assignments are given in Table 6.

The tetrahedral Co(II) with $^4A_2$ ground state showed three transitions, $^4A_2 \rightarrow {}^4T_2(F)$, $^4A_2 \rightarrow {}^4T_1(F)$ and $^4A_2 \rightarrow {}^4T_1(P)$. The first one is not usually observed since it occurs in the region, 3300–2000 nm. $^4A_2 \rightarrow {}^4T_1(P)$ transition appears as an intense broad band in the visible region. Here, Co(II) complex showed absorption bands at 675 and 451 nm due to $^4A_2 \rightarrow {}^4T_1(P)$ and $^4A_2 \rightarrow {}^4T_1(F)$ transitions, respectively. Tetrahedral Co(II) complexes show magnetic moments in the range, 3.8–4.7 B.M, while octahedral complexes in the range, 4.8–5.6 B.M. The low-spin square planar Co(II) complexes have magnetic moments in the range, 2.1–2.9 B.M. Here, the magnetic moment of the Co(II) complex was 3.86 B.M. The electronic spectrum, dark green colour and the magnetic moment of the complex confirmed its tetrahedral geometry.

Octahedral Ni(II) complexes with d^8 configuration have a ground state, $^3A_{2g}$. In this study, broad bands at 413, 623 and 875 nm may be assigned to three spin-allowed transitions $^3A_{2g}(F) \rightarrow {}^3T_{1g}(P)$, $^3A_{2g}(F) \rightarrow {}^3T_{1g}(F)$ and $^3A_{2g}(F) \rightarrow {}^3T_{2g}(F)$, respectively, indicating the octahedral geometry of Ni(II) complex. The magnetic moment of the complex was 2.92 B.M which supported its octahedral geometry.

Most of the square planar Cu(II) complexes exhibit a single broad asymmetric d–d band in the region, 625–1388 nm [15] and the broadness of the band is due to the combination of the three spin-

allowed transitions, $^2B_{1g} \rightarrow {}^2A_{1g}$, $^2B_{1g} \rightarrow {}^2B_{2g}$, and $^2B_{1g} \rightarrow {}^2E_g$. Here, the Cu(II) complex showed a broad band at 369 nm, assigned to $\pi \rightarrow \pi^*$ transition of aromatic rings and another one at 647 nm. As the four lower orbitals are so close in energy, individual transitions will not be prominent and therefore, all the three vibronically induced transitions appeared as a broad single absorption band. The magnetic moment value of the complex was found to be 1.87 BM, which supported its square planar structure.

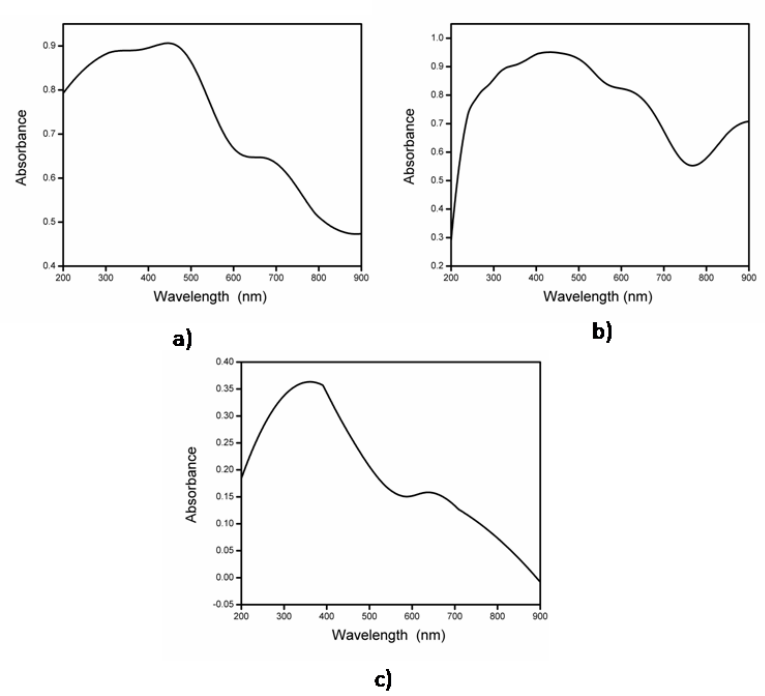

Fig.5. Electronic spectra of (a) $[Co(HL)Cl_2]$ b) $[Ni(HL)_2Cl_2].H_2O$ and c) $[Cu(HL)Cl_2].H_2O$

Table 6. Electronic spectral bands and their assignments of the complexes

Compound	Spectral bands λ_{max} (nm)	Assignments
$[Co(HL)Cl_2]$	675br	$^4A_2 \rightarrow {}^4T_1$ (P)
$[Ni(HL)_2Cl_2].H_2O$	413	$^3A_{2g}(F) \rightarrow {}^3T_{1g}$ (P)
	623	$^3A_{2g}$ (F) $\rightarrow {}^3T_{1g}$(F)
	875	$^3A_{2g}$ (F) $\rightarrow {}^3T_{2g}$ (F)
$[Cu(HL)Cl_2].H_2O$	647br	$^2B_{1g} \rightarrow {}^2A_{1g}$, $^2B_{1g} \rightarrow {}^2B_{2g}$ and $^2B_{1g} \rightarrow {}^2E_g$

br = broad

3.2.3. IR spectra and mode of bonding

The bonding of the ligands to metal ions has been studied by careful comparison of the infrared spectra of the complexes with those of the free ligands. It can be observed that the significant absorption bands in the ligands spectrum generally undergoes shift upon coordination to metal ions in the complexes. The significant IR spectral bands of ligand and its metal complexes with their assignments are depicted in the Table 6. The infrared spectrum of 4-hydroxy-3-methoxyacetophenone N(4)-methyl(phenyl)thiosemicarbazone (HL) and its metal complexes are mainly characterized by the absorptions due to the vibrations of -NH, -OH, –C=S, –C=N and –N-N groups. The broad bands present in the region, 3454 cm^{-1} in the spectra of all the complexes are assigned to υ(OH) group. The band due to the stretching of secondary -NH group of the thiosemicarbazone moiety observed at 3217 cm^{-1} in the ligand spectrum. It was found to be retained nearly at the same position in the spectra of all the complexes

except those of Zn(II) and Cd(II) complexes. This suggested the coordination of thioamide in the thione form itself [19]. In Zn(II) and Cd(II) complexes, the medium intensity band at 3217 cm^{-1} in the ligand spectrum, due to the secondary –NH of the thioamide group was not observed, indicating the loss of H-atom *via* enolisation of –NH-C=S to –N=C-SH and subsequent coordination through the thiolate sulphur atom to the metal ion.

The ligand can exhibit thione–thiol tautomerism since it contains thioamido (–NH–C=S) functional group. There was no characteristic band due to υ(S-H) in the range 2700-2500 cm^{-1} in ligand and its metal complexes. The band at 1593 cm^{-1} assigned to the azomethine group in the ligand spectrum, was shifted towards lower frequency in the spectra of all the complexes, indicating the involvement of the azomethine nitrogen atom in coordination [16]. The bands near 1344 and 857 cm^{-1} in the spectrum of the free ligand were assigned to υ(NH–C=S) and υ(C=S). These bands are seen to be shifted to lower wave numbers in the spectra of all the complexes, confirming the coordination of sulphur with the metal ions. However, in the spectra of Zn(II) and Cd(II) complexes, the bands corresponding to υ(C=S) are found to be shifted to lower wave numbers to a greater extend (approximately 192 and 182 cm^{-1}). The position of the new bands at 726 and 730 cm^{-1} in the spectra of these complexes suggested the presence of C-S-M, formed by the enolisation of -NH-C=S group in the ligand to -N=C-SH and subsequent coordination to the Zn(II) and Cd(II) through S^- after deprotonation. In the case of Zn(II) complex, the presence of broad band in the region of 3500 cm^{-1} due to –OH stretching modes of water molecule present in the compound. The

presence of coordinated water molecule was supported by the appearance of new bond at 445 cm^{-1} due to υ(M-O). This was further confirmed by ^{1}H NMR of the complexes.

The band observed at 1103 cm^{-1} in the ligand spectrum due to υ(N-N) has been found to be shifted to higher wave numbers in the spectra of all the complexes. The IR spectra of all the complexes showed new band at 439-497 cm^{-1} assigned to υ(M–N). Thus, the IR spectra suggest that the ligand coordinates as a neutral, bidentate (through the imino nitrogen and thiocarbonyl sulphur) one in the complexes of Co(II), Ni(II) and Cu(II). But in the case of Zn(II) and Cd(II), ligand coordinates in bidentate monoanionic (through the imino nitrogen and thiolate sulphur) manner.

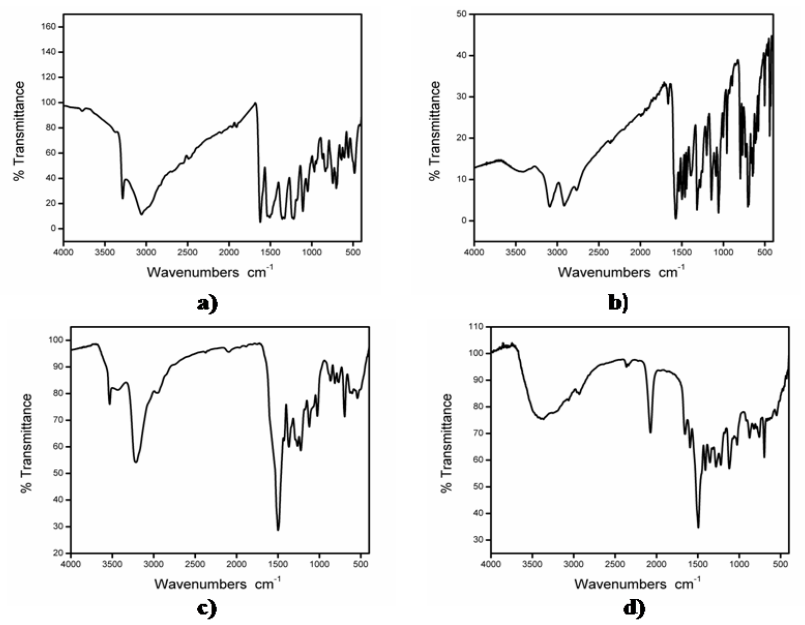

Fig.6. IR spectra of (a)[$Co(HL)Cl_2$] b)[$Ni(HL)_2Cl_2$].H_2O c) [$Cu(HL)Cl_2$].H_2O and d) [$Cd(L)_2$]

Table 7. IR spectral assignments of the metal complexes

Compound	$C_{17}H_{19}N_3O_2S$	$Co(HL)CL_2$	$Ni(HL)_2Cl_2.H_2O$	$Cu(HL)Cl_2.H_2O$	$ZnL(H_2O)Cl$	$Cd(L)_2$
υ(OH)	3454	3301	3424	3424	3351	3373
υ(NH)	3217	3054	3094 2920	3229 2950	-	-
υ(C=N)	1593	1554	1575	1528	1529	1510
υ(C=S)+υ(C=N) + ν(C-N)	1344	1338	1319	1278	1335	1339
δ(N-N)	1103	1103	1145	1103	1109	1113
υ(C=S)	857	825	795	815	665	675
υ(M-N)	-	476	497	539	446	496

3.2.4. Electron paramagnetic resonance (EPR) spectrum

ESR spectrum of copper complex recorded in DMSO at liquid nitrogen temperature (LNT) and is presented in Fig.7. It is exhibited a typical monomeric spectrum with a set of four well resolved signals. The ground state can be derived from *g-tensor* value. The $g\|$ and $g\perp$values were 2.428, 2.04, respectively. The trend in $g\| > g\perp >$ 2.0023 suggests that the unpaired electron lies predominantly in the $d_{x^2-y^2}$ orbital, with $^2B_{1g}$ as the ground state. In the present case, it was found that $g\| > g\perp >$ 2 and therefore, the unpaired electron is likely to be in the $d_{x^2-y^2}$orbital, indicating square planar geometry around copper(II) ion [17, 18]. ESR spectrum showed that the $g\|$ value of complex was greater than 2.3, indicating a small amount of ionic character of the copper-ligand bond. In addition, the g values are related to the G-factor by Hathaway expression, $G = (g\|\text{-}2.0023/g\perp\text{-}2.0023)$. This relation gives exchange interaction between the copper centers in polycrystalline samples. Here, the value of G was greater than 4, indicating absence of

exchange interaction between copper(II) centers. The absence of half field signal in the spectrum, indicated the monomeric form of the complex.

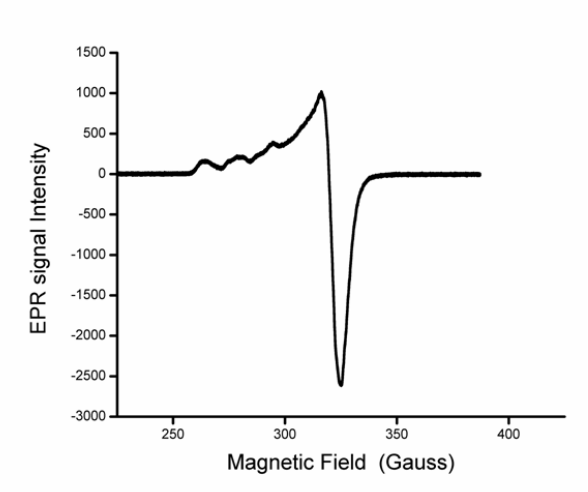

Fig.7. X-Band ESR spectrum of Cu(II) complex at LNT in DMSO

3.2.5. ^{1}H NMR spectra of Zn(II) and Cd(II) complexes

a) Zn(II) complex

The ^{1}H NMR spectrum of the Zn(II) complex in DMSO was recorded with TMS as internal standard. The spectrum is given in Fig.8. The singlet at 10.806 ppm was assigned to –OH group. A sharp singlet at 9.999 ppm may be assigned to aromatic proton adjacent to methoxy group. A doublet at 9.347-9.334 ppm was attributed to aromatic protons nearto imine bond. The remaining aromatic protons showed resonance peaks at 7.546-6.779 ppm. The singlet peak at 3.81 ppm may be due to methoxy protons. ^{4}N–CH_3 protons absorbed at 3.714

ppm. The singlet peak at 3.36 ppm may be due to coordinated water molecules. The ^{1}H NMR spectrum registered a peak with three protons intensity at 2.505-2.483 ppm which may be assigned to three methyl protons on azomethine carbon. The peak due to N-H was not observed, indicating the loss of H-atom *via* enolisation of –NH-C=S to –N=C-SH and subsequent coordination through the thiolate sulphur atom to the metal ion.

b) Cd(II) complex

The ^{1}H NMR spectrum of Cd(II) in DMSO was carried out with TMS as internal standard. The spectrum is given in Fig.9. The singlet at 10.469 ppm was assigned to –OH group. A sharp singlet at 9.614 ppm may be assigned to aromatic proton adjacent to methoxy group. A doublet at 9.473-9.257 ppm may be attributed to aromatic protons near to imine bond. The remaining aromatic protons showed resonance peaks at 7.596-6.631 ppm. The peak at 3.861 ppm may be due to methoxy protons. ^{4}N–CH_3 protons absorbed at 3.749 ppm. The ^{1}H NMR spectrum has shown a peak of three protons intensity at 2.890-2.731 ppm assignable to three methyl protons on azomethine carbon. The peak due to N-H was not observed, indicating the loss of H-atom *via* enolisation of –NH-C=S to –N=C-SH and subsequent coordination through the deprotonated sulphur (S^-) to the Cd(II) ion.

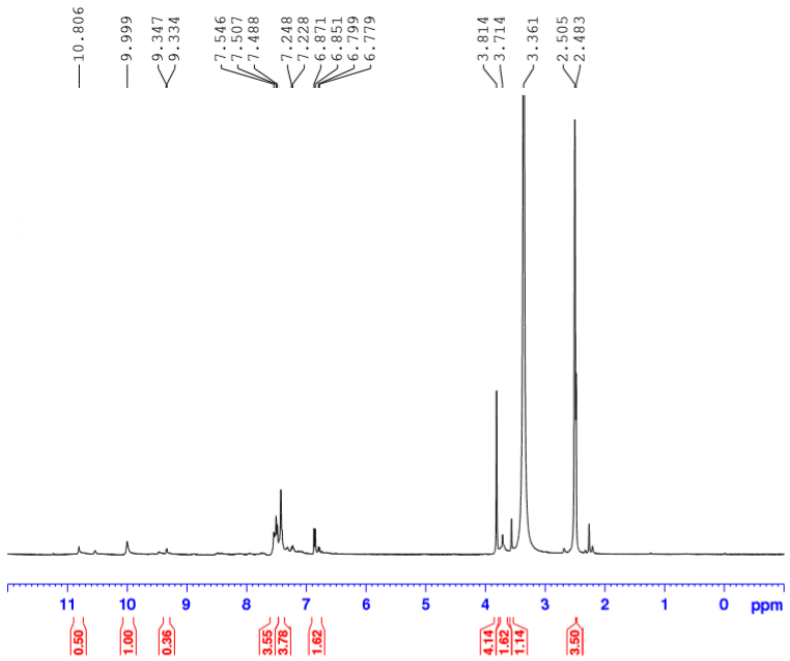

Fig.8. ^{1}H NMR spectrum of Zn(II) complex

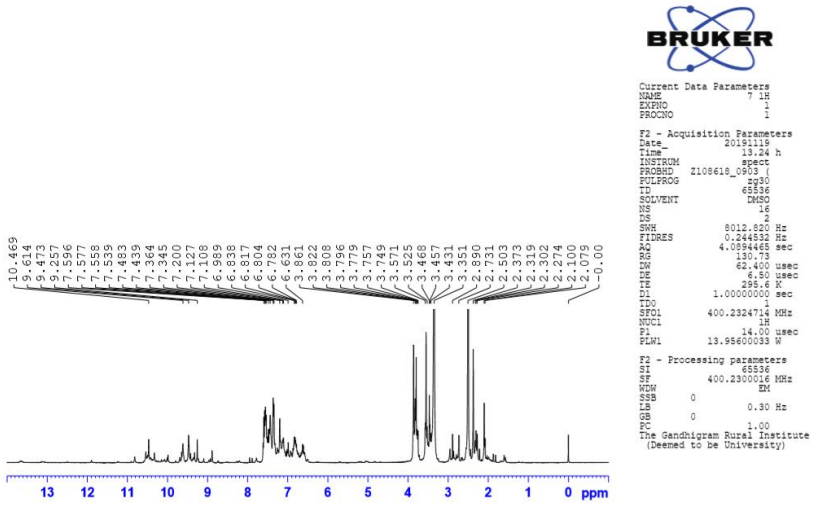

Fig.9. ^{1}H NMR spectrum of Cd(II) complex

3.2.6. Thermo gravimetric analysis

Thermo gravimetric analysis is used to find out the thermal stability of the complexes. It is also used to assess the status of the water-, or solvent molecules in the complex. In the present study, Ni(II) and Cu(II) complexes were chosen as representative examples for thermal analysis.

For $[Ni(HL)_2Cl_2].H_2O$, decomposed in two stages. The first stage was observed in the temperature range, 70.2-181.5^{0}C. It demonstrated a mass loss of 3%, corresponding to the loss of lattice water. The second stage occurred in the temperature range, 197-365.3 ^{0}C with a mass loss of 37%, which may be due to the decomposition of the ligand moiety. A residual mass of 10% was observed at 500°C which may be due to the formation of nickel sulphide (calcd. 11.51%).

In $[Cu(HL)Cl_2].H_2O$ showed a two staged decomposition pattern. The first stage decomposition observed at 96^{0}C with mass loss of 2.09%. It corresponded to the loss of lattice water molecule. The second stage occurred in the temperature range, 151-307 ^{0}C with a mass loss of 27.49% which may be due to the decomposition of the ligand moiety. The residual mass of 19.28% was observed at 347-484°C which may be due to the formation of CuS (19.83%).

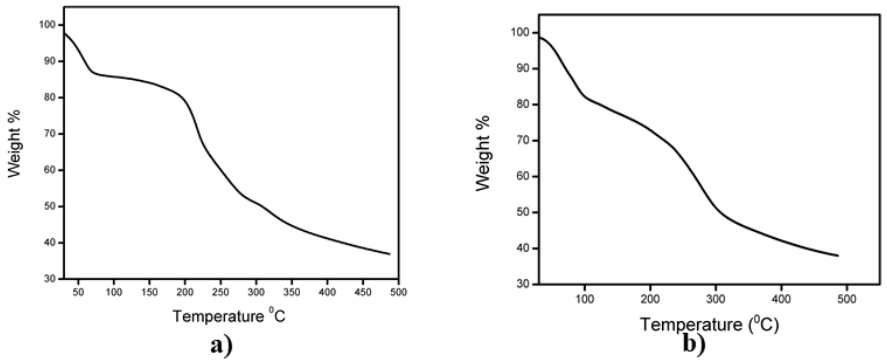

Fig.10. TG curves of a) $[Ni(HL)_2Cl_2].H_2O$ and b) $[Cu(HL)Cl_2].H_2O$

4. Conclusions

The synthesis and characterization of Co(II), Ni(II), Cu(II), Zn(II) and Cd(II) complexes of 4-hydroxy-3-methoxyacetophenone N(4)-methyl (phenyl)thiosemicarbazone (HL) have been discussed. According to IR and ^1H NMR analyses, the ligand acted as neutral bidentate one in Co(II), Ni(II) and Cu(II) complexes. Based on the elemental analytical-, magnetic moment- and spectral data, the Co(II), Zn(II) and Cd(II) complexes were assigned tetrahedral geometries. Octahedral geometry was assigned for the Ni(II) complex. Cu(II) complex was assigned square planar geometry. The proposed structures of the complexes are shown in Fig.11-15.

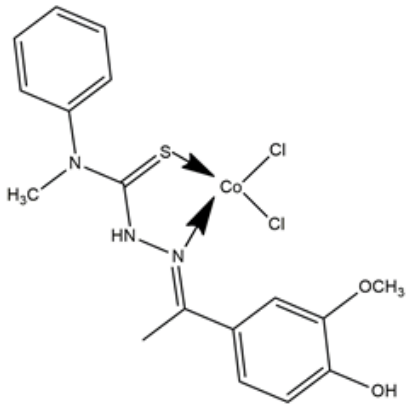

Fig.11. Proposed structure of the complex, $[Co(HL)Cl_2]$

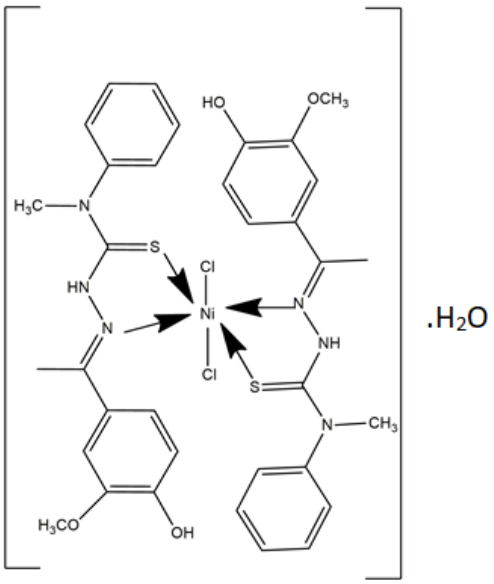

Fig.12. Proposed structure of the complex, $[Ni(HL)_2Cl_2].H_2O$

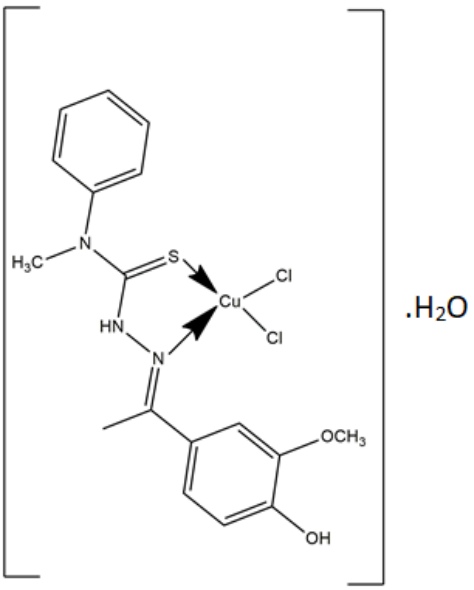

Fig.13. Proposed structure of the complex, $[Cu(HL)Cl_2].H_2O$

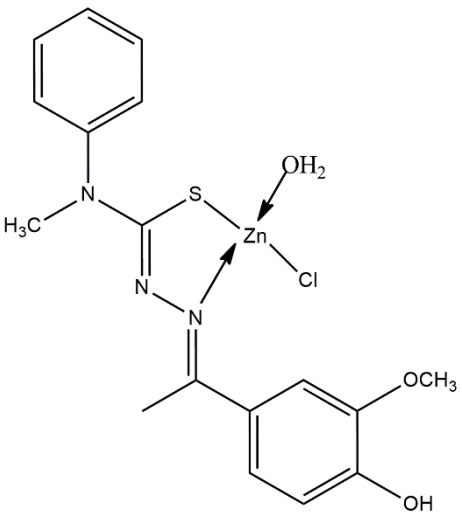

Fig.14. Proposed structure of the complex, $[ZnL(H_2O)Cl]$

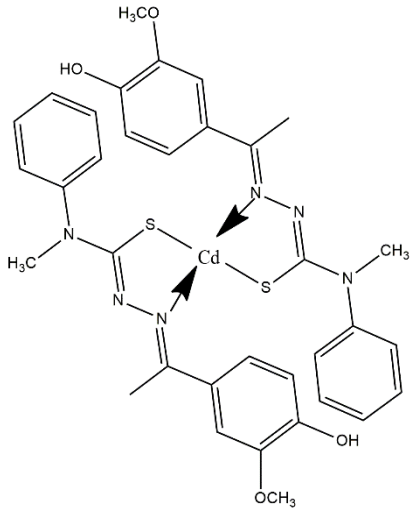

Fig.15. Proposed structure of the complex, $[Cd(L)_2]$

References

[1] A.G. Quiroga, J.M. Pérez, I. López-Solera, J.R. Masaguer, A. Luque, P. Román, A. Edwards, C. Alonso, C. Navarro-Ranninger, Novel tetranuclear orthometalated complexes of Pd (II) and Pt (II) derived from p-isopropylbenzaldehyde thiosemicarbazone with cytotoxic activity in cis-DDP resistant tumor cell lines. Interaction of these complexes with DNA, Journal of medicinal chemistry 41(9) (1998) 1399-1408.

[2] H. Govender, C. Mocktar, H.M. Kumalo, N.A. Koorbanally, Synthesis, antibacterial activity and docking studies of substituted quinolone thiosemicarbazones, Phosphorus, Sulfur, and Silicon and the Related Elements 194(11) (2019) 1074-1081.

[3] S. Chandra, S. Raizada, M. Tyagi, A. Gautam, Synthesis, Spectroscopic, and Antimicrobial Studies on Bivalent Nickel and Copper Complexes of Bis(thiosemicrbazone), Bioinorganic Chemistry and Applications (2007) 51483.

[4] C. Shipman Jr, S.H. Smith, J.C. Drach, D.L. Klayman, Antiviral activity of 2-acetylpyridine thiosemicarbazones against herpes simplex virus, Antimicrobial Agents and Chemotherapy 19(4) (1981) 682.

[5] R.A. Finch, M.C. Liu, A.H. Cory, J.G. Cory, A.C. Sartorelli, Triapine (3-aminopyridine-2-carboxaldehyde thiosemicarbazone; 3-AP): an inhibitor of ribonucleotide reductase with antineoplastic activity, Adv Enzyme Regul 39 (1999) 3-12.

[6] W. Antholine, J. Knight, H. Whelan, D.H. Petering, Studies of the reaction of 2-formylpyridine thiosemicarbazone and its iron and copper complexes with biological systems, Molecular Pharmacology 13(1) (1977) 89-98.

[7] S.B. Novaković, G.A. Bogdanović, V.M. Leovac, Transition metal complexes with thiosemicarbazide-based ligands. Part L. Synthesis, physicochemical properties and crystal structures of Co (II) complexes with acetone S-methylisothiosemicarbazone, Polyhedron 25(5) (2006) 1096-1104.

[8] P.M. Krishna, K.H. Reddy, Synthesis, single crystal structure and DNA cleavage studies on first 4N-ethyl substituted three coordinate copper (I) complex of thiosemicarbazone, Inorganica Chimica Acta 362(11) (2009) 4185-4190.

[9] M. Jagadeesh, M. Lavanya, S.K. Kalangi, Y. Sarala, C. Ramachandraiah, A.V. Reddy, Spectroscopic characterization, antioxidant and antitumour studies of novel bromo substituted thiosemicarbazone and its copper (II), nickel (II) and palladium (II) complexes, Spectrochimica Acta Part A: Molecular and Biomolecular Spectroscopy 135 (2015) 180-184.

[10] R. Kothari, B. Sharma, Synthesis, characterization, antibacterial, antifungal, antioxidant and dna interaction studies of thiosemicarbazone transition metal complexes, World J. Pharm. Pharm. Sci 3(7) (2014) 1067-1080.

[11] N.D. Thanh, H.T. Duc, V.T. Duyen, P.M. Tuong, N. Van Quoc, Synthesis and antibacterial and antifungal activities of N-(tetra-O-acetyl-β-d-glucopyranosyl)thiosemicarbazones of substituted 4-formylsydnones, Chem Cent J 9 (2015) 60-60.

[12] N.R. Jyothi, N.M. Farook, M. Cho, J. Shim, Cytotoxic activities of thiosemicarbazones and their metal complexes, Asian Journal of Chemistry 25(10) (2013) 5841.

[13] P. Bamfield, The reaction of cobalt halides with N-arylsalicylideneimines, Journal of the Chemical Society A: Inorganic, Physical, Theoretical (0) (1967) 804-808.

[14] S.A. Khan, M. Yusuf, Synthesis, spectral studies and in vitro antibacterial activity of steroidal thiosemicarbazone and their palladium (Pd (II)) complexes, European journal of medicinal chemistry 44(5) (2009) 2270-2274.

[15] M. Joseph, M. Kuriakose, M.P. Kurup, E. Suresh, A. Kishore, S.G. Bhat, Structural, antimicrobial and spectral studies of copper (II) complexes of 2-benzoylpyridine N (4)-phenyl thiosemicarbazone, Polyhedron 25(1) (2006) 61-70.

[16] N. Raman, S. Sobha, A. Thamaraichelvan, A novel bioactive tyramine derived Schiff base and its transition metal complexes as selective DNA binding agents, Spectrochimica acta. Part A, Molecular and biomolecular spectroscopy 78(2) (2011) 888-98.

[17] O.I. Singh, M. Damayanti, N.R. Singh, R.H. Singh, M. Mohapatra, R. Kadam, Synthesis, EPR and biological activities of bis (1-n-butylamidino-O-alkylurea) copper (II) chloride complexes: EPR

evidence for binuclear complexes in frozen DMF solution, Polyhedron 24(8) (2005) 909-916.

[18] T. Yousef, G.A. El-Reash, O. El-Gammal, R. Bedier, Co (II), Cu (II), Cd (II), Fe (III) and U (VI) complexes containing a NSNO donor ligand: synthesis, characterization, optical band gap, in vitro antimicrobial and DNA cleavage studies, Journal of Molecular Structure 1029 (2012) 149-160.

CHAPTER VII

SYNTHESIS AND CHARACTERIZATION OF TRANSITION METAL COMPLEXES OF CROTONALDEHYDE ISONICOTINOYLHYDRAZONE

1. Introduction

Isonicotinoylhydrazone, formed by the condensation of isonicotinoylhydrazide (isoniazide) with different types of carbonyl compounds, are typical examples of aroylhydrazones containing heterocyclic nitrogen atom. The coordination chemistry of aroylhydrazone, particularly that of isonicotinoylhydrazones is a fascinating research area due to their diverse pharmacological application [1]. It has been reported that isonicotinoylhydrazones are better antitubercular agents than isoniazide [2]. Apart from this, these compounds exhibit antibacterial-, antifungal-, antiviral- and antitumour activities [3-5]. Literature survey showed that only a little work has been done on metal complexes of aroylhydrazones of unsaturated aliphatic aldehydes. Crotonaldehyde (2-Butenal) is a typical unsaturated aliphatic aldehyde. It has many industrial applications. It is used as an intermediate solvent for accelerators, for the purifications of mineral oils and as insecticides.

In this chapter, we report crotonaldehyde isonicotinoylhydrazone (HL) (Fig.1) synthesized *via* conventional synthesis synthetic method. Its crystal structure has been determined by single crystal X-ray diffraction analysis. Moreover, its ligational behaviour has been ascertained by preparing and characterizing its Co(II), Ni(II), Cu(II), Zn(II) and Cd(II) complexes.

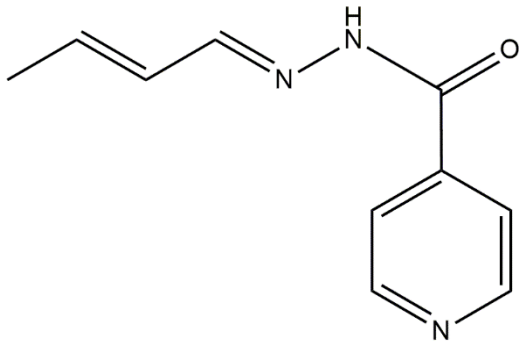

Fig.1. Crotonaldehyde isonicotinoyldrazone (HL)

*IUPAC Name:(*E*)-*N'*-((*E*)-but-2-en-1-ylidene)isonicotinohydrazide

2. Experimental

2.1. Materials and methods

Details regarding the chemicals used and the methods adopted for the characterization of the compounds are described in Chapter II.

2.2. Preparation of the ligand (HL)

To a hot solution of isonicotinic acid hydrazid in ethanol (0.05mol), an ethanolic solution of crotonaldehyde (0.05mol) was added slowly. The reaction mixture was refluxed in the presence of catalytic amount of glacial acetic acid on a water bath for 4hr. The solid compound, crotonaldehyde isonicotinoylhydrazone, formed was filtered and dried (Yield 79%, M.P 176^0C). The synthetic procedure of the ligand is shown in Scheme 1.

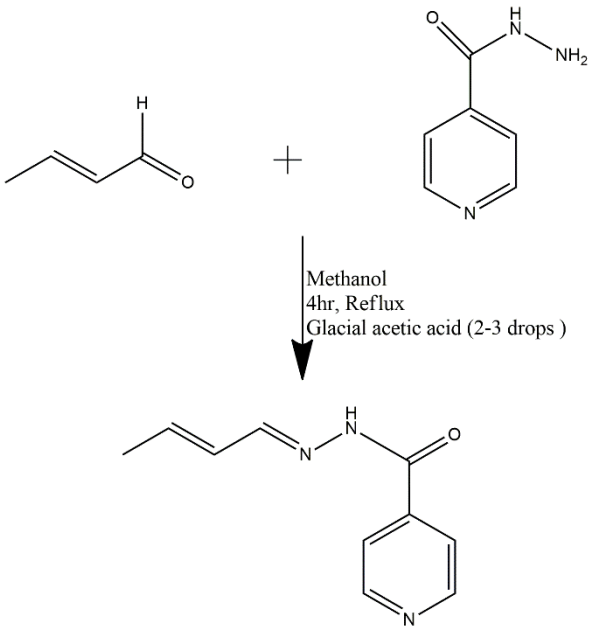

Scheme 1. Synthetic pathway of crotonaldehyde isonicotinoyldrazone (HL)

2.3. Preparation of the complexes

An ethanolic solution of the metal chloride (0.05mol in 20ml) was added drop wise to an ethanolic solution of HL (0.1mol in 20ml) and refluxed for 4hr. The resulting product was kept aside for slow evaporation. It was filtered, the precipitate was washed several times with ethanol and dried under reduced pressure.

3. Results and discussion

The data obtained from the analytical and physico-chemical methods have been used to assign the structures and geometries of the compounds.

3.1. Characterization of the ligand (HL)

The ligand (HL) was characterized by single crystal X-ray analysis, IR, UV-Vis and ^{1}H NMR spectral techniques.

3.1.1. Micro analytical data

The ligand obtained as white crystals with an empirical formula, $C_{10}H_{11}N_3O$. CHNS percentages were in agreement with the suggested formula (Table 1). It was non-hygroscopic and stable at normal atmospheric conditions. It was soluble in DMSO, DMF, chloroform, etc.

Table 1. Physico-chemical and analytical data of the ligand

Compound (Empirical Formula)	**Yield (%)**	**Melting Point (^{0}C)**	**Colour**	**CHNS Analysis Found % (Calculated)%**			
				C	**H**	**N**	**O**
$C_{10}H_{11}N_3O_2S$	79	176^{0}C	White	63.01 (63.42)	5.21 (5.81)	22.02 (22.19)	8.28 (8.45)

3.1.2. Single crystal X-ray crystallography

A crystal with dimensions, 0.60 x 0.30 x 0.20 mm was selected for collecting the data. It crystallized with one molecule per asymmetric unit into monoclinic crystal system with a space group of C c. X-ray crystallographic data were collected at 296(2) K on a Bruker Model Kappa Apex II diffractometer employing graphite monochromated Mo $K\alpha$ (λ = 0.71073 Å) radiation. Direct methods were used to solve the structure and refined by least square on F^2 using SHELXL-97 [6]. The

crystallographic tools PLATON[7], DIAMOND3.2d[8], ORTEP [9] and MERCURY3.5.1[10] for windows were used for structure analysis and presentation of the results. All non-hydrogen atoms were refined anisotropically. The details of the X-ray data and structure refinements are given in Table 2.Bond distances and angles are listed in Table 3. The PLATON diagram of HL with the atom numbering scheme is shown in Fig.2.

Table 2. Crystal data and structural refinement parameters for compound, HL

Identification code	shelx		
Empirical formula	$C_{10}H_{11}N_3O$	Theta range for data collection	2.845- 28.423 deg.
Formula weight	189.22	R indices (all data)	R1 = 0.0430, wR2 = 0.1130
Temperature	296(2) K	Goodness-of-fit on F^2	0.952
Refinement method	Full-matrix least-squares on F^2	Limiting indices	-12<=h<=12, -16<=k<=16, -12<=l<=6
Wavelength	0.71073 A	Extinction coefficient	n/a
Crystal size	0.60x0.30 x 0.20 mm	Completeness to theta	25.242 99.6 %
Crystal system, space group	Monoclinic, C c	Reflections collected	3984
Unit cell dimensions		Independent reflections	2064 [R(int) = 0.0200]
a (A^0)	9.5031(16) A	Max. and min. transmission	0.983 and 0.951
b (A^0)	12.5545(16)	Data / restraints / parameters	2064 / 2 / 132
c (A^0)	9.1639(10)	Absorption coefficient	0.085 mm^{-1}
α(°)	90 deg	F(000)	400
β(°)	113.469(7) deg	Z	4, 1.253Mg/m^3
γ(°)	90 deg.	Volume	1002.9(2) A^3

Table 3. Bond distances and bond angles of HL

Bond length (Å)		Bond Angle (°)	
C(1)-C(2)	1.374(4)	C(2)-C(1)-C(5)	118.7(2)
C(1)-C(5)	1.374(3)	C(2)-C(1)-H(1)	120.6
C(1)-H(1)	0.9300	C(5)-C(1)-H(1)	120.6
C(2)-N(1)	1.323(4)	N(1)-C(2)-C(1)	123.8(2)
C(2)-H(2)	0.9300	N(1)-C(2)-H(2)	118.1
C(3)-N(1)	1.328(3)	C(1)-C(2)-H(2)	118.1
C(3)-C(4)	1.386(3)	N(1)-C(3)-C(4)	123.2(2)
C(3)-H(3)	0.9300	N(1)-C(3)-H(3)	118.4
C(4)-C(5)	1.378(3)	C(4)-C(3)-H(3)	118.4
C(4)-H(4)	0.9300	C(5)-C(4)-C(3)	118.5(2)
C(5)-C(6)	1.506(3)	C(5)-C(4)-H(4)	120.7
C(6)-O(1)	1.217(3)	C(3)-C(4)-H(4)	120.7
C(6)-N(2)	1.339(3)	C(4)-C(5)-C(1)	118.49(19)
N(2)-N(3)	1.381(2)	C(4)-C(5)-C(6)	122.70(18)
N(2)-H(1N)	0.84(3)	C(1)-C(5)-C(6)	118.79(18)
N(3)-C(7)	1.265(3)	O(1)-C(6)-N(2)	124.86(19)
C(7)-C(8)	1.435(3)	O(1)-C(6)-C(5)	121.35(19)
C(7)-H(7)	0.9300	N(2)-C(6)-C(5)	113.79(17)
C(8)-C(9)	1.332(4)	C(6)-N(2)-N(3)	119.73(17)
C(8)-H(8)	0.9300	C(6)-N(2)-H(1N)	120.4(19)
C(9)-C(10)	1.469(4)	N(3)-N(2)-H(1N)	119.7(19)
C(9)-H(9)	0.9300	C(7)-N(3)-N(2)	114.35(19)
C(10)-H(10A)	0.9600	N(3)-C(7)-C(8)	122.7(2)
C(10)-H(10B)	0.9600	N(3)-C(7)-H(7)	118.7
C(10)-H(10C)	0.9600	C(8)-C(7)-H(7)	118.7
		C(9)-C(8)-C(7)	120.9(3)
		C(9)-C(8)-H(8)	119.6
		C(7)-C(8)-H(8)	119.6
		C(9)-C(10)-H(10B)	109.5
		H(10A)-C(10)-H(10B)	109.5
		C(9)-C(10)-H(10C)	109.5
		H(10A)- C(10)-H(10C)	109.5
		H(10B)-C(10)-H(10C)	109.5
		C(3)-N(1)-C(2)	117.2(2)

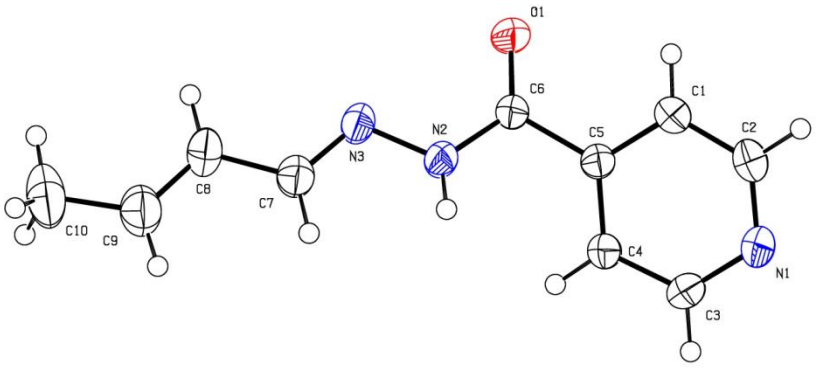

Fig.2. The PLATON diagram of HL with atom numbering scheme

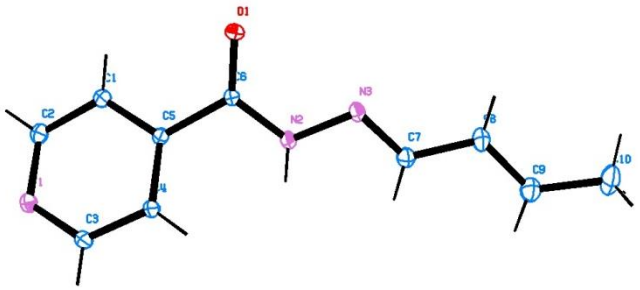

Fig.3. Ortep diagram of HL

The bond distances, C(7)–N(3) and N(2)–N(3) were1.265(3) Å and 1.381(2) Å, respectively. They were found to be intermediate between the analogous single [C–N, 1.47 Å; N–N, 1.45 Å] and double bonds [C=N, 1.28 Å; N=N, 1.25 Å][11]. Similarly C(6)-O(1) bond distance, was 1.217(3) A^0 also consistent with the C=O double bond (1.23 Å). The bond distance, C(7)-C(8) was 1.435(3), which was in between single bond (1.54 Å) and double bond (1.34 Å). The angle N2–C6–O1

(124.86) was significantly larger than C5–C6–O1 (121.35) possibly to relive repulsion between lone pairs of electrons on N3 and O1 atoms. The bond angles, C6-C5-C1, N3-N2-C6, C7-N3-N2, C9-C8-C7 and C6-C5-C4 were $118.79(18)^0$, $119.73(17)^0$, $114.35(19)^0$, $120.9(3)^0$ and $122.70(18)^0$, respectively. O1- and the hydrazinic N3 atoms were *trans* with respect to C6–N2 bond. These structural data revealed quasi coplanarity of the entire molecular skeleton with localization of the double bonds in the central chain which has an E-configuration with respect to the double bond of the hydrazone bridge [12]. A *s-trans* configuration was shown around the N2–N3 (1.381A˚) single bond [13]. The phenolic ring maintained coplanarity with the central –C=N–N–C=O moiety.

3.1.3. Spectroscopic analysis

a) Electronic spectrum

The ligand showed intense bands at 266 nm and 318 nm which may be attributed to $\pi \rightarrow \pi^*$ and $n \rightarrow \pi^*$ transitions, respectively. This may be due to azomethine chromophore and the amide part of the hydrazone moiety. The data are given in Table 4.

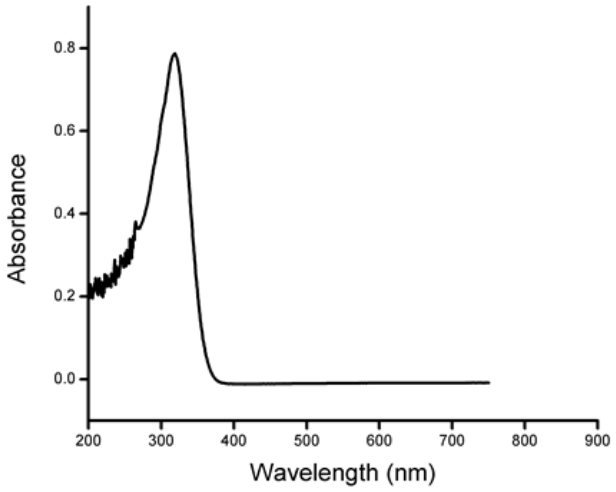

Fig.4. Electronic spectrum of HL

Table 4. Electronic spectral bands of HL

Spectral bands (nm)	**Assignments**
266	$\pi \rightarrow \pi^*$ transition
318	$n \rightarrow \pi^*$ transition

b) Vibration spectrum

IR spectroscopy is an important technique that provides information about various vibrations of functional groups present in the compound. The IR spectral assignments of the ligand are shown in Fig.5 and listed in Table 5.

The characteristic bands in the region 3400-3200 cm^{-1} may be attributed to the symmetric- and asymmetric stretching vibrations of -

NH group. The medium intensity bands at 2998 and 2849 cm^{-1} may be assigned to asymmetric- and symmetric =CH stretching frequencies, respectively. The ligand showed a strong band at 1568 cm^{-1}, which is characteristic of υ(>C=N) group [14]. A sharp band at 1677 cm^{-1} can be assigned to υ(C=O). This ruled out the existence of thiol tautomer of the compound. The band observed at 1139 cm^{-1} in the spectrum of the ligand may be assigned to δ(N-N) vibration.

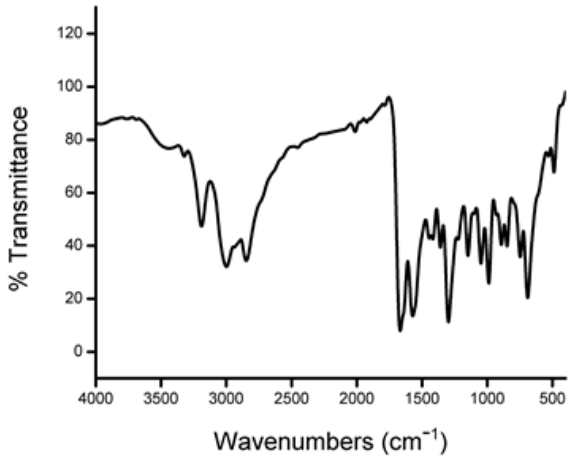

Fig.5. IR spectrum of HL

Table 5. Significant IR spectral bands (in cm^{-1}) of HL

Bands (cm^{-1})	**Assignments**
3482, 3202	υ(N-H)
2998	υ(C-H) (asymmetric)
2849	υ(C-H) (symmetric)
1677	υ(C=O)
1568	υ(C=N)
1139	δ(N-N)

c) ^{1}H NMR spectrum

^{1}H NMR spectral measurement of the ligand in DMSO was carried out with TMS as internal standard. The spectrum is given in Fig.6 and spectral data in Table 6. -NH proton resonated in the downfield region with a chemical shift at 11.702 ppm integrating for one proton. The doublet at 8.736-8.725 ppm was assigned to azomethine proton. The peak observed at 8.075–8.031 ppm may be assigned to the pyridine moiety. These may be a doublet, merged together due to two equivalent protons. The doublet at 7.796–7.785 ppm may be assigned to olefinic =CH proton near the imine bond. The quartet at 6.296-6.236 ppm was attributed to olefinic =CH proton adjacent to the -CH_3 group. The resonance peak due to methyl hydrogens appeared as a sharp signal up field of NMR spectrum at 1.919 -1.904 ppm, integrated for three hydrogens, as expected. The peak observed between 2-3 ppm may be due to the solvent used.

Table 6. ^{1}H NMR assignments of HL

δ (ppm)	**Assignments**
11.702	N-H proton
8.736-8.725	Azomethine proton
8.075-8.031	Hydrogens on hydrazone moiety
7.796-7.785	Hydrogen adjacent to azomethine group
6.296-6.236	Hydrogen adjacent to methyl protons
1.915-1.904	-CH_3 group on terminal nitrogen atom

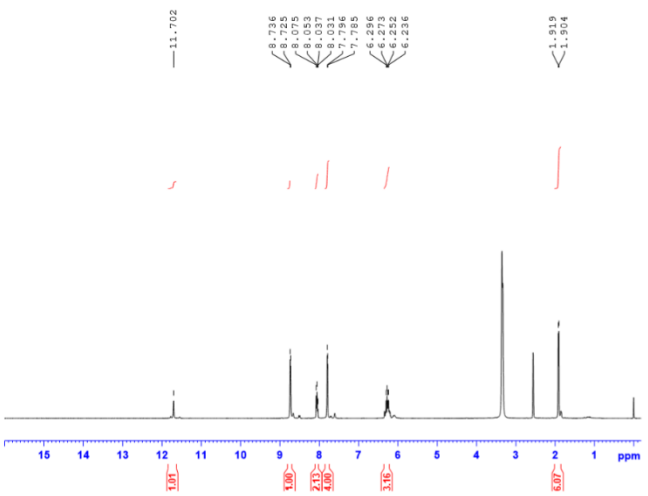

Fig.6. ^{1}H NMR spectrum of HL

3.1.4. Mass spectrum

In the ESI-mass spectrum of the ligand (Fig.7) showed a well-defined peak at m/z 190 (100%)(M+1) which coincided with the molecular weight of the proposed structure, (Mw: 189.22g).

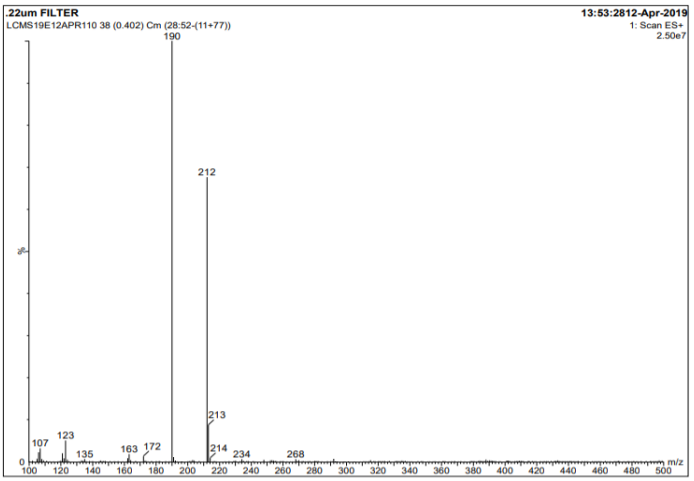

Fig.7. Mass spectrum of HL

3.2. Characterization of the complexes

Crotonaldehyde isonicotinoylhydrazone (HL) formed stable complexes with Co(II), Ni(II), Cu(II), Zn (II) and Cd(II). Their physical- and analytical data are presented in Table 7. These complexes were soluble in chloroform, DMSO, DMF, etc and partially soluble in common organic solvents like ethanol, methanol, etc. They were non-hygroscopic in nature. These complexes were characterized as follows:

3.2.1. Analytical data of the metal complexes

Elemental analytical data of all the complexes were in good agreement with the suggested molecular formulae. The general formula of the complexes was found to be $[M(HL)_2Cl_2]$, where M=Co(II), Ni(II) or Cu (II). The Zn(II) and Cd(II) complexes were of the types, $[Zn(HL)Cl_2]$ and $[Cd(L)_2]$, where HL acted as a neutral bidentate ligand and L^- acted as monoanionic bidentate ligand. FT-IR and electronic spectral studies and magnetic moment measurements were performed for the structure elucidation of the complexes.

Table 7. Physico-chemical and analytical data of complexes

Compound	Colour	Yield (%)	M.P (^{0}C)	Elemental Analysis (%) found (calculated)				
				C	H	N	O	Metal
$C_{10}H_{11}N_3O$	White	79	176	63.01 (63.42)	5.21 (5.81)	22.02 (22.19)	8.28 (8.45)	-
$[Co(HL)_2Cl_2]$	Brown	72	184	47.01 (47.26)	4.01 (4.33)	16.50 (16.54)	6.08 (6.30)	11.09 (11.60)
$[Ni(HL)_2Cl_2]$	Black	68	187	47.08 (47.28)	4.29 (4.33)	16.32 (16.52)	6.28 (6.30)	11.38 (11.56)
$[Cu(HL)_2Cl_2]$	Green	70	183	46.54 (46.83)	4.21 (4.29)	16.27 (16.39)	6.21 (6.24)	12.31 (12.40)
$[Zn(HL)Cl_2]$	White	78	189	36.74 (36.89)	3.09 (3.38)	12.81 (12.91)	4.84 (4.92)	19.91 (20.09)
$[Cd(L)_2]$	Yellow	69	187	48.80 (48.94)	4.01 (4.49)	17.07 (17.13)	6.31 (6.52)	22.51 (22.92)

3.2.2. Electronic spectra and magnetic moments

The electronic spectral measurements of the ligand and the complexes were performed in solid state. The absorption regions and tentative band assignments of the complexes are given below. The present octahedral Co(II) complex showed three spin allowed transitions at 627, 386 and 264 nm assigned to $^4T_{1g}(F)\rightarrow{}^4T_{2g}(F)$, $^4T_{1g}(F)\rightarrow{}^4A_{2g}(F)$ and $^4T_{1g}(F)\rightarrow{}^4T_{1g}(P)$ transitions, respectively. Among these, $^4T_{1g}(F)\rightarrow{}^4T_{1g}(P)$ has highest energy. As $^4T_{1g}(P)$ and $^4A_{2g}(F)$ levels are very close, the transitions to them are almost of same energy. The lower energy transition, $^4T_{1g}(F)\rightarrow{}^4T_{2g}(F)$ is observed generally in the near infrared region. The magnetic moment value of this complex was 4.46 BM, as expected value for an octahedral d^7 Co(II) complex [15].

The present octahedral Ni(II) complex showed bands at 870 and 585 nm in the visible region. They may be assigned to $^3A_{2g}(F)\rightarrow{}^3T_{1g}(F)$ and $^3A_{2g}(F)\rightarrow{}^3T_{1g}(P)$ transitions, respectively. $^3A_{2g}(F)\rightarrow{}^3T_{2g}(F)$ is usually observed in the infrared region. It is out of range of the spectrophotometer used. The other bands present at 397 and 267 nm may be assigned to intra-ligand charge-transfer transitions which can be attributed to $n\rightarrow\pi^*$ and $\pi\rightarrow\pi^*$ transitions, respectively. The complex registered a magnetic moment of 2.92 B.M confirming its octahedral geometry.

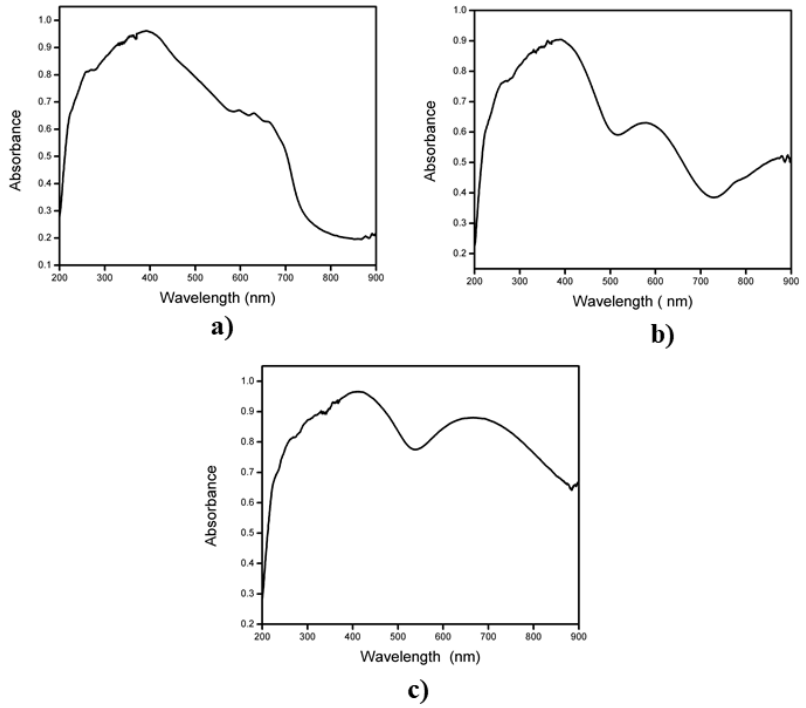

Fig.8. Electronic spectra of a) $[Co(HL)_2Cl_2]$ b) $[Ni(HL)_2Cl_2]$ and c) $[Cu(HL)_2Cl_2]$

All Cu(II) complexes are generally blue or green in colour, due to absorption bands in the range, 600-900 nm. $[Cu(HL)_2Cl_2]$ registered a magnetic moment of 1.96 B.M. The band observed at 404 nm may be assigned to $^2B_{1g} \rightarrow {}^2E_g$ transition. Another broad band at 669 nm attributed to $^2B_{1g} \rightarrow {}^2B_{2g}$ transition was characteristic of distorted octahedral Cu(II) complex. As expected, the diamagnetic Zn(II) and Cd(II) complexes did not show any characteristic absorption bands in the visible region. On the basis of analytical and spectral data, the Zn(II) and Cd(II) complexes were assigned tetrahedral geometry.

3.2.3. Infrared spectra and mode of bonding

The FTIR spectra of the ligand and its metal complexes were recorded in the range 4000-400 cm^{-1}. The significant IR spectral bands of the complexes (Fig.9) along with their probable assignments are given in the Table 7. The vibrational frequencies of ligand were compared with vibrational frequencies of complexes and the changes were ascertained**.** Crotanaldehyde isonicotinoylhydrazone existed as keto tautomer with strong bands at 3482, 1677 and 1568 cm^{-1} corresponding to υ(N-H), υ(C=O) and the azomethine υ(C=N) group, respectively. A sharp band due to υ(C=N) in the ligand spectrum was found to be shifted to lower frequency region upon complexation. This shows the coordination through azomethine nitrogen to metal ions. The broad band around 3400 cm^{-1} in the ligand spectrum due to υ(N-H) stretching vibration was not found in the spectrum of Cd(II) complex. This pointed out that the ligand might have undergone enolisation of –N–NH-C=O to –N–N=C-OH and its subsequent coordination through the deprotonated oxygen to the metal ion might have occurred. The bands due to υ(C=O) were found to be shifted to lower frequencies in the spectra of all the complexes, except that of Cd(II) complex, indicating the coordination through C=O in those complexes. The new bands at 422-462 cm^{-1} in the spectra of the metal complexes may be assigned to υ(M–N) [16].

Table 7. IR spectral assignments of the metal complexes

Compound	$C_{10}H_{11}N_3O$	$[Co(HL)_2Cl_2]$	$[Ni(HL)_2Cl_2]$	$[Cu(HL)_2Cl_2]$	$[Zn(HL)Cl_2]$	$[Cd(L)_2]$
υ(N-H)	3482,3202	3380	3404	3407	3445	-
$\upsilon_{=CH}$ (aromatic)	2998 2849	3158 3055	3042 2833	3042 2898	3197 3042	3224 3028
υ(C=O)	1677	1608	1635	1621	1647	-
υ(C=N)	1568	1545	1529	1556	1541	1543
δ(N-N)	1139	1061	1086	1177	1073	1191
υ(M-N)	-	422	425	461	462	453

3.2.4. Electron paramagnetic resonance (EPR) spectrum

The ESR spectrum of Cu(II) complex in DMSO at X -band frequency in the region 8.75- 9.65 GHz with 100 kH field modulation was recorded. The spectrum of sample was measured at liquid nitrogen temperature (77K). The values of $g\|$ and $g^{\perp}$ were 2.478 and 2.051, respectively. The fact that $g\| > g^{\perp} > 2.0023$ for complex indicated that the unpaired electron is localised in $d_{x^2-y^2}$ orbital of the Cu(II) ion. Thus, a distorted octahedral geometry was proposed for the complex [17]. The $g\|$ value was found to be slightly higher than 2.3, indicating the absence of considerable covalent character in copper-ligand bond. The G parameter, [$G = (g\| - 2) / (g^{\perp} - 2)$] was found to be greater than 4, suggesting the absence of considerable interaction between adjacent molecules in the solid state (G=9.37). No signal at half field was observed in the spectrum, ruling out the possibility of a dimeric form [18].

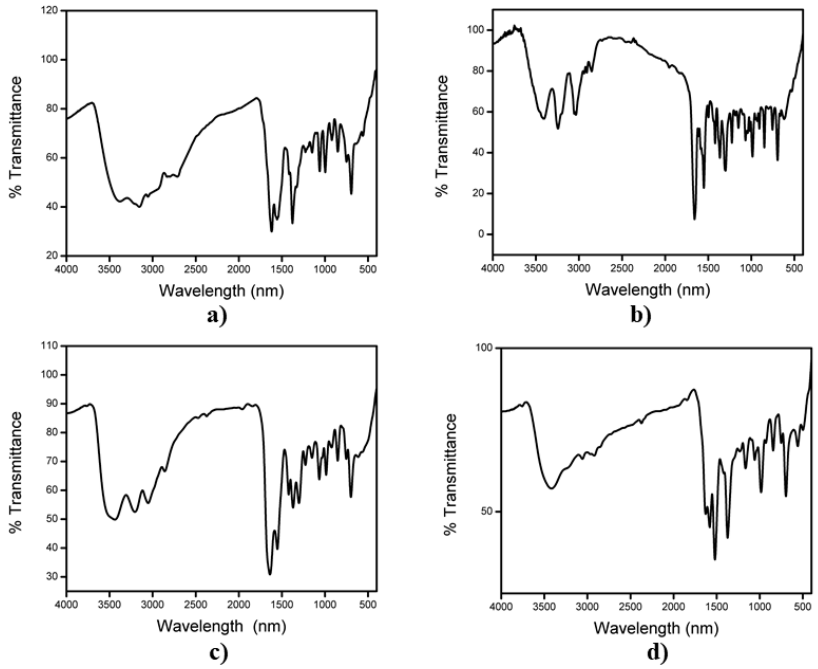

Fig.9. IR spectra of a) $[Co(HL)_2Cl_2]$ b) $[Ni(HL)_2Cl_2]$ c) $[Cu(HL)_2Cl_2]$ and d) $[Cd(L)_2]$

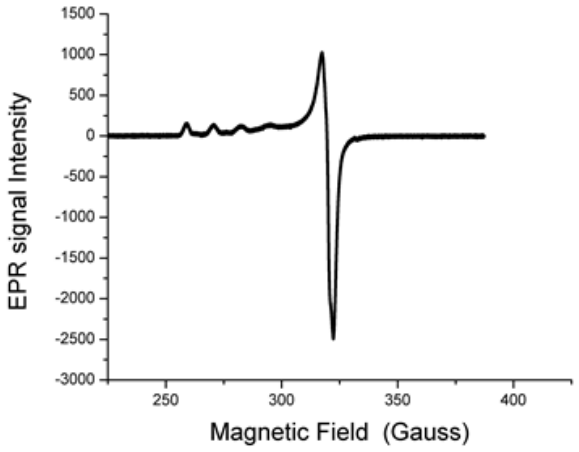

Fig.10. X-Band ESR spectrum of $Cu(HL)_2Cl_2$ complex at LNT in DMSO

3.2.5. ^{1}H NMR spectrum of [Zn(HL)Cl_2]

The ^{1}H NMR spectrum of the Zn(II) complex was recorded in DMSO at room temperature (Fig.11). A broad singlet at 11.712 ppm can be assigned to N–H proton. A doublet observed at 8.759-8.754 ppm can be assigned to azomethine proton. The peaks at 7.821 and 6.285 ppm may be assigned to aromatic protons on hydrazone moiety. The methyl protons absorbed at 1.876 ppm. The peak at 2.507 ppm may be due to the solvent.

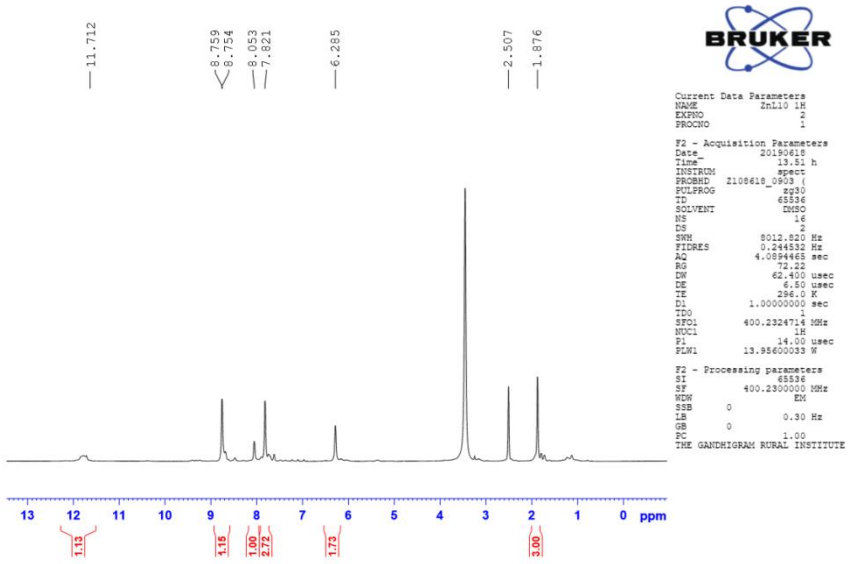

Fig.11. ^{1}H NMR of [Zn(HL)Cl_2]

4. Conclusions

The synthesis and characterization of Co(II), Ni(II), Cu(II), Zn(II) and Cd(II) complexes of crotonaldehyde isonicotinoyldrazone(HL) have been discussed. According to IR and ^{1}H NMR analysis, ligand acted as

neutral bidentate one in all the complexes, except in Cd(II) complex. Based on the elemental analytical-, magnetic moment- and spectral data, the Co(II), Ni(II) and Cu(II) complexes were assigned octahedral geometry. The Zn(II) and Cd(II) complexes were assigned a tetrahedral geometry. The proposed structures of the complexes are shown in Fig.12-14.

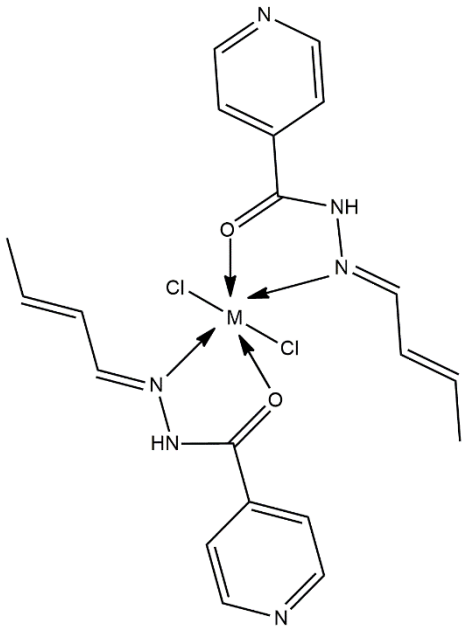

Fig.12. Proposed structure of the complexes, $[M(HL)_2Cl_2]$ where M=Co(II), Ni(II) or Cu(II).

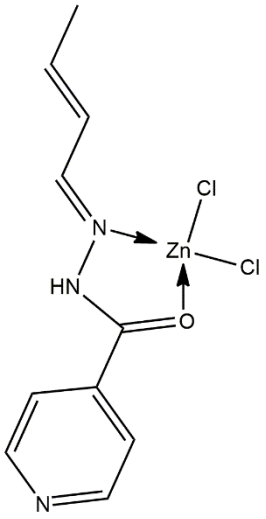

Fig.13. Proposed structure of the complex, $[Zn(HL)Cl_2]$

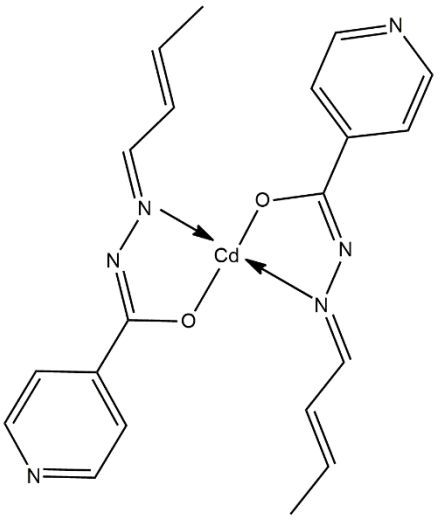

Fig.14. Proposed structure of the complex, $[Cd(L)_2]$

Reference

[1] P. Mazza, F. Zani, M. Orcesi, C. Pelizzi, G. Pelizzi, G. Predieri, Synthesis, structure, antimicrobial, and genotoxic activities of organotin compounds with 2,6-diacetylpyridine nicotinoyl-and isonicotinoylhydrazones, Journal of inorganic biochemistry 48(4) (1992) 251-270.

[2] A. Walcourt, M. Loyevsky, D.B. Lovejoy, V.R. Gordeuk, D.R. Richardson, Novel aroylhydrazone and thiosemicarbazone iron chelators with anti-malarial activity against chloroquine-resistant and-sensitive parasites, The international journal of biochemistry & cell biology 36(3) (2004) 401-407.

[3] V. Velezheva, P. Brennan, P. Ivanov, A. Kornienko, S. Lyubimov, K. Kazarian, B. Nikonenko, K. Majorov, A. Apt, Synthesis and antituberculosis activity of indole–pyridine derived hydrazides, hydrazide–hydrazones, and thiosemicarbazones, Bioorganic & Medicinal Chemistry Letters 26(3) (2016) 978-985.

[4] V. Angelova, V. Karabeliov, P.A. Andreeva-Gateva, J. Tchekalarova, Recent developments of hydrazide/hydrazone derivatives and their analogs as anticonvulsant agents in animal models, Drug Development Research 77(7) (2016) 379-392.

[5] M.N. Koopaei, M.J. Assarzadeh, A. Almasirad, S.F. Ghasemi-Niri, M. Amini, A. Kebriaeezadeh, N.N. Koopaei, M. Ghadimi, A. Tabei, Synthesis and analgesic activity of novel hydrazide and hydrazine derivatives, Iranian journal of pharmaceutical research: IJPR 12(4) (2013) 721.

[6] G. Sheldrick, SHELXL-97, Program for crystal-structure refinement (1997).

[7] A. Spek, P.A.M.C. Tool, University of Utrecht, The Netherlands (1999).

[8] C. Impact, DIAMOND-Crystal and Molecular Structure Visualization (Version 4), (2009).

[9] L.J. Farrugia, WinGX and ORTEP for Windows: an update, Journal of Applied Crystallography 45(4) (2012) 849-854.

[10] C.F. Macrae, I.J. Bruno, J.A. Chisholm, P.R. Edgington, P. McCabe, E. Pidcock, L. Rodriguez-Monge, R. Taylor, J. Streek, P.A. Wood, Mercury CSD 2.0–new features for the visualization and investigation of crystal structures, Journal of Applied Crystallography 41(2) (2008) 466-470.

[11] G.J. Palenik, D. Rendle, W. Carter, The crystal and molecular structures of thiosemicarbazones; an antitumor agent 5-hydroxy-2-formylpyridine thiosemicarbazone sesquihydrate and the inactive acetone thiosemicarbazone, Acta Crystallographica Section B: Structural Crystallography and Crystal Chemistry 30(10) (1974) 2390-2395.

[12] P. Sreeja, A. Sreekanth, C.R. Nayar, M.P. Kurup, A. Usman, I. Razak, S. Chantrapromma, H. Fun, Synthesis, spectral studies and structure of 2-hydroxyacetophenone nicotinic acid hydrazone, Journal of Molecular Structure 645(2-3) (2003) 221-226.

[13] V. Vrdoljak, G. Pavlović, T. Hrenar, M. Rubčić, P. Siega, R. Dreos, M. Cindrić, Cobalt(iii) complexes with tridentate hydrazone ligands: protonation state and hydrogen bond competition, RSC Advances 5(127) (2015) 104870-104883.

[14] V. Malik, G. Solanki, V. Singh, Four and six coordinate complexes of divalent nickel, Oriental Journal of Chemistry 26(1) (2010) 301.

[15] W. Ferenc, K. Czapla, J. Sarzy, Magnetic, thermal and spectral characterization of 2, 4-dimethoxybenzoates of Mn (II), Co (II) and Cu (II), Eclética Química 32(3) (2007) 7-12.

[16] J. Liu, B. Zhang, B. Wu, K. Zhang, S. Hu, The direct electrochemical synthesis of Ti (II), Fe (II), Cd (II), Sn (II), and Pb (II) complexes with N, N-bis (Salicylidene)-o-phenylenediamine, Turkish Journal of Chemistry 31(6) (2007) 623-629.

[17] A. Jaggi, S. Chandra, K. Sharma, Stereochemical versatility of Cu (II): Cu (II) complexes of benzyl methyl ketone semicarbazone, Polyhedron 4(1) (1985) 163-168.

[18] N. Raman, R. Jeyamurugan, M. Subbulakshmi, R. Boominathan, C.R. Yuvarajan, Synthesis, DNA binding, and antimicrobial studies of novel metal complexes containing a pyrazolone derivative Schiff base, Chemical Papers 64(3) (2010) 318-328.

CHAPTER VIII

SYNTHESIS AND CHARACTERIZATION OF TRANSITION METAL COMPLEXES OF 4-[N,N-(DIMETHYL)AMINO]BENZALDEHYDE ISONICOTINOYLHYDRAZONE

1. Introduction

The remarkable biological activities of aroylhydrazones have been of significant interest. Metal complexes of isonicotinoylhydrazones haven't received as much attention as they actually deserve. In search of isonicotinoylhydrazone of different aromatic aldehydes, our attention was drawn to 4-[N,N-(dimethyl)amino]benzaldehyde. It is used as biological and analytical reagent [1]. Therefore, many researchers use to study it as a target structure and evaluated its biological activities. It can easily coordinate to the metal ions forming stable complexes [2].

Manav Malhotra *et al*[3] reported the synthesis and characterization of (E)-N-(substituted benzylidene)isonicotinohydrazide derivatives as potent antimicrobial and hydrogen peroxide scavenging agents. Literature survey revealed that more research work is still need to be done on the metal complexes of 4-[N,N-(dimethyl)amino] benzaldehyde isonicotinoylhydrazone. Therefore, in this chapter we present our studies on the synthesis and characterization of 4-[N,N-(dimethyl)amino]benzaldehyde isonicotinoylhydrazone (HL) (Fig.1) and its complexes with Co(II), Ni(II), Cu(II), Zn(II) and Cd(II).

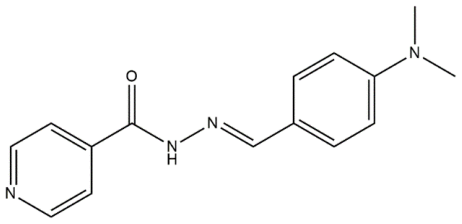

Fig.1. 4-[N,N-(Dimethyl)amino]benzaldehyde isonicotinoylhydrazone (HL)

*IUPAC Name:(E)-N'-(4-(dimethylamino) benzylidene) isonicotinohydrazide

2. Experimental

2.1. Materials and methods

A detailed description about the materials, methods and characterization techniques used in this work are given in Chapter II of Part I.

2.2. Preparation of the ligand (HL)

To a hot solution of isonicotinic acid hydrazide in methanol (0.1mol), an methanolic solution of 4-[N,N-(dimethyl)amino]benzaldehyde (0.1mol) was added slowly. The reaction mixture was stirred for 15 min in the presence of catalytic amount of glacial acetic acid. The solid compound, 4-[N,N-(dimethyl)amino]benzaldehyde isonicotinoylhydrazone (HL)formed was filtered and dried under reduced pressure (Yield 75%, M.P 208^0C). The scheme is shown below.

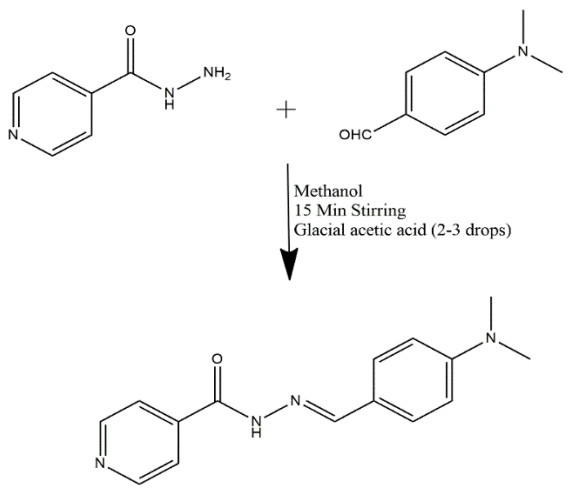

Scheme 1. Synthesis of 4-[N,N-(dimethyl)amino]benzaldehyde isonicotinoylhydrazone (HL)

2.3. Preparation of metal complexes

Hot solution of metal chloride in ethanol (20 cm^3) was added to a hot solution of the ligand, 4-[N,N-(dimethyl)amino]benzaldehyde isonicotinoylhydrazone (HL) in ethanol (20 cm^3). All the complexes were synthesized by mixing stoichiometric quantities of the ligand (0.002M) and the metal chlorides (0.001M). Then mixture was heated under reflux on a water bath for 4hr. On cooling, the coloured complexes precipitated out. Complexes obtained were filtered, washed with ethanol and diethyl ether and then dried. The purity of the complexes were checked by TLC method.

3. Results and discussion

The data obtained from the elemental analyses, physico-chemical- and spectral investigations have been used to explain the properties, structures and bonding of the compounds.

3.1. Characterization of the ligand

3.1.1. Micro analytical data

The ligand, HL was an intense yellow coloured solid. It was sparingly soluble in common organic solvents such as alcohol, acetone, ether and benzene, but soluble in acetonitrile, DMF, DMSO, chloroform, etc. The homogeneity and purity of the ligand were checked by thin-layer chromatographic (TLC) method. It was characterized by elemental analysis (Table 1), and further by UV-Vis (Table 2), IR- (Table 3), ^{1}H NMR (Table 4) and ESI-MS spectral techniques. The data obtained

from these studies were correlated to explain the structure of the ligand.

Table 1. Physico-chemical and analytical data of HL

Compound (Empirical Formula)	**Yield (%)**	**Melting Point (^{0}C)**	**Colour**	**CHNS Analysis Found % (Calculated)%**		
				C	**H**	**N**
$C_{15}H_{16}N_4O$.	75	208^{0}C	Yellow	67.01 (67.16)	5.21 (5.97)	20.78 (20.89)

3.1.2. Mass spectrum

In the ESI-mass spectrum of the ligand (Fig.3) showed a well-defined peak at m/z = 269 (100%) (M+1), which is in good agreement with the molecular weight (Mw: 268.31g) according to the proposed structure.

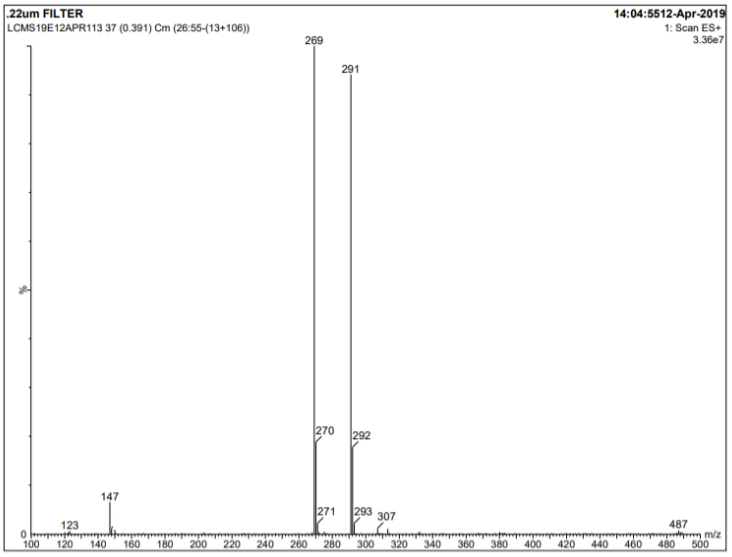

Fig.2. ESI-MS spectrum of HL

3.1.3. Spectroscopic analysis

a) Electronic spectrum

The electronic spectrum of the ligand showed a strong absorption at 264 nm which can be attributed to π→π* transition. Similarly, a band at 369 nm may be due to n→π* transition from the azomethine group and amide part of the hydrazone moiety. The spectral data are given in Table 2.

Table 2. Electronic spectral bands of HL

Spectral bands (nm)	**Assignments**
264	π→π* transition
369	n→π* transition

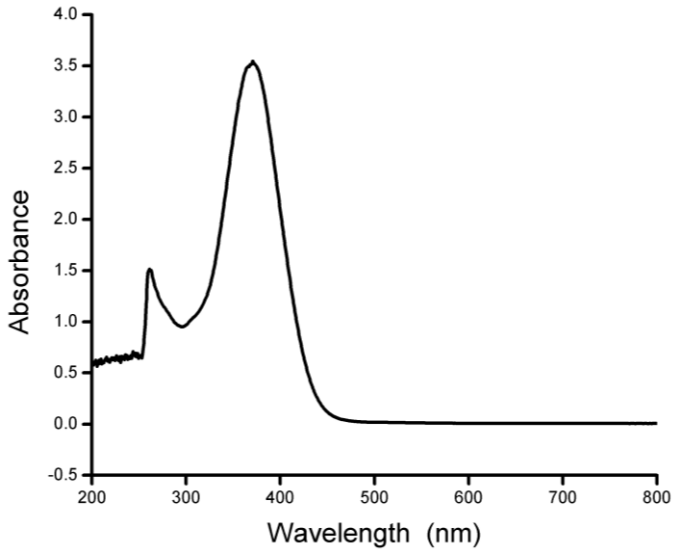

Fig.3. Electronic spectrum of HL

b) Infrared spectrum

IR spectroscopy is an important technique in the structural elucidation of a compound. The significant IR spectral bands (Fig.4) and assignments of the ligand are presented in Table 3. The IR spectrum of the ligand showed two bands, at 3398 and 3144 cm^{-1} which may be attributed to υ(N–H). Another band appeared at 1666 cm^{-1} may be assigned to υ(C=O). The band at 1613 cm^{-1} may be assigned to azomethine υ(C=N)[4]. These characteristic bands ruled out the presence of thiol-tautomer of ligand in the solid state. The medium intensity bands found at 2970 and 2835 cm^{-1} may be assigned to asymmetric- and symmetric =CH stretching frequencies, respectively. The presence of a band at 1169 cm^{-1} in the spectrum of the ligand can be assigned to δ(N-N).

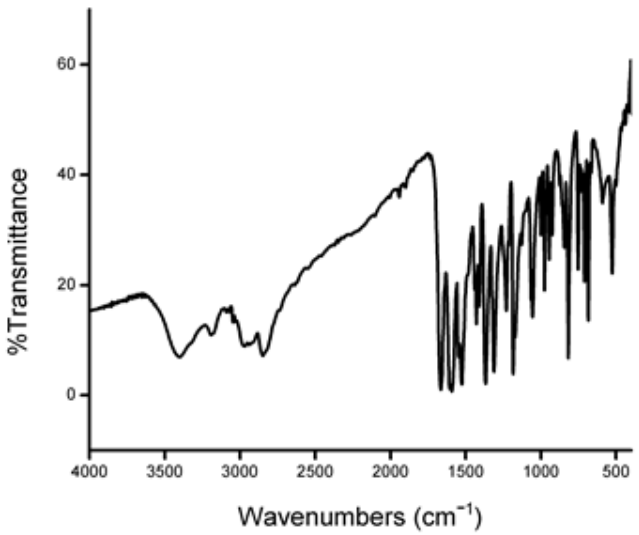

Fig.4. IR spectrum of HL

Table 3. Significant IR spectral bands (in cm^{-1}) of HL

Bands (cm^{-1})	**Assignments**
3398,3144	υ(N-H)
2970	υ(C-H) (asymmetric)
2835	υ(C-H) (symmetric)
1666	υ(C=O)
1613	υ(C=N)
1169	δ(N-N)

c) ^{1}H NMR spectrum

The formation of the ligand, 4-[N,N-(dimethyl)amino]benzaldehyde isonicotinoylhydrazone (HL) was confirmed by the singlet at δ 8.32 ppm assigned to the azomethine proton in ^{1}H NMR spectrum. Beside this, the ^{1}H NMR spectrum of the ligand showed a signal at δ 11.77 ppm assigned to amide (-HN-N=) proton. The peaks observed at δ8.77–8.76(d, 2H) and δ7.81-7.80(d, 2H) ppm may be assigned to pyridine moiety. The peaks at 7.57-7.55(d, 2H) and 6.77-6.75(d, 2H) ppm, may be attributed to benzylidene protons. A singlet due to six protons at δ2.98 ppm was assigned to the protons of the two methyl groups which are chemically and magnetically equivalent.

Table 4. ^{1}H NMR assignments of HL

δ (ppm)	**Assignments**
11.777	N-H proton
8.774-8.762	(d, 2H) pyridine moiety
8.322	Azomethine proton
7.814-7.7802	(d, 2H,) pyridine moiety
7.577-7.555	(d, 2H) benzylidene protons
6.777-6.756	(d, 2H) benzylidene protons
2.983	(s, 6H) methyl protons

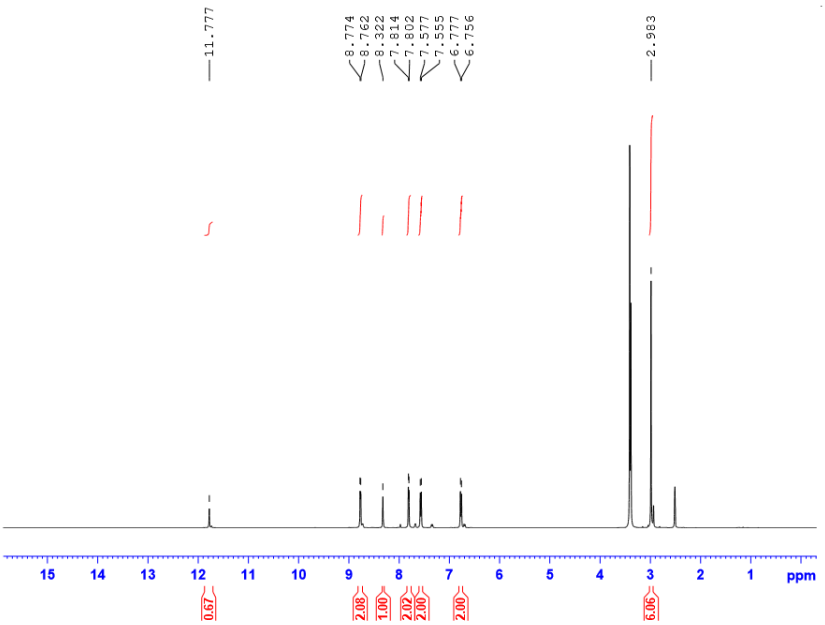

Fig.5. ^{1}H NMR spectrum of HL

3.2. Characterization of the complexes

4-[N,N-(Dimethyl)amino]benzaldehyde isonicotinoylhydrazone (HL) formed stable complexes with Co(II), Ni(II), Cu(II), Zn (II) and Cd(II) ions. These complexes were coloured powders and soluble in chloroform, DMSO, DMF, etc but partially soluble in common organic solvents like ethanol, methanol, etc. They are non-hygroscopic in nature. The physico-chemical and analytical data obtained for the ligand and its complexes are presented in Table 5. These complexes were characterized as follows:

3.2.1. Analytical data of metal complexes

Elemental analytical data of all the complexes were in good agreement with the suggested molecular formulae. The general formula of the complexes were found to $[M(HL)_2Cl_2]$, where M=Co(II) or Ni(II). The Cu(II) and Zn(II) complexes had a formula, $[M(HL)Cl_2]$. The Cd(II) complex was found to be of the type, $[Cd(L)_2]$, where L^- can acted as a monoanionic bidentate ligand. FT-IR, electronic and EPR spectral studies and magnetic moment measurements were performed for assigning the structures of the complexes.

Table 5. Physico-chemical and analytical data of the complexes

Compound	**colour**	**Yield (%)**	**M.P (^{0}C)**	**Elemental Analysis (%) found (calculated)**				
				C	**H**	**N**	O	Metal
$C_{15}H_{16}N_4O$	Intense yellow	75	208	667.01 (67.16)	5.21 (5.97)	20.78 (20.89)	5.90 (5.97)	-
$[Co(HL)_2Cl_2]$	Dark Brown	71	216	54.03 (54.07)	4.01 (4.81)	16.13 (16.82)	4.80 (4.81)	8.41 (8.85)
$[Ni(HL)_2Cl_2]$	Crimson Red	69	>212	54.21 (54.09)	4.90 (4.81)	16.81 (16.83)	4.79 (4.81)	8.81 (8.82)
$[Cu(HL)Cl_2]$	Black	70	>216	44.21 (44.73)	3.49 (3.97)	13.86 (13.91	3.89 (3.97)	15.56 (15.79)
$[Zn(HL)Cl_2]$	Light Yellow	59	219	44.09 (44.52)	3.90 (3.96)	13.58 (13.85)	3.91 (3.96)	16.01 (16.17)
$[Cd(L)_2]$	White	78	216	55.01 (55.52)	4.29 (4.93)	17.01 (17.27)	4.87 (4.93)	17.01 (17.33)

3.2.2. Electronic spectra and magnetic moments

The electronic spectral data and the magnetic moments were used to identify the geometries of the complexes. The electronic spectra are shown in Fig.6. The significant electronic spectral bands and probable assignments are discussed below. For the Co(II) complex , the absorption bands observed at 635 and 376 nm, may be assigned to $^4T_{1g}(F)\rightarrow{}^4A_{2g}(F)$ and $^4T_{1g}(F)\rightarrow{}^4T_{1g}(P)$ transitions of an octahedral complex. The lower energy transition, $^4T_{1g}(F)\rightarrow{}^4T_{2g}(F)$ is found generally in the near infrared region and this was not observed in the present case due to limited range of the instrument used. The magnetic moment value of this complex was 4.49 BM, as expected for an octahedral d^7 Co(II) complex.

The electronic spectrum of Ni(II) complex registered three bands at 306, 577 and 872 nm assignable to $^3A_{2g}(F) \rightarrow {}^3T_{1g}(P)$, $^3A_{2g}(F) \rightarrow {}^3T_{1g}(F)$ and $^3A_{2g}(F) \rightarrow {}^3T_{2g}(F)$ transitions, respectively, characteristic of an octahedral complex. It registered a magnetic moment value of 2.77 B.M which was in agreement with octahedral geometry.

The broad band of Cu(II) complex due to the combination of three spin–allowed transitions, $^2B_{1g} \rightarrow {}^2A_{1g}$, $^2B_{1g} \rightarrow {}^2B_{2g}$, and $^2B_{1g} \rightarrow {}^2E_g$, indicate a square planar geometry. Here, the Cu(II) complex showed band at 376 nm, assigned to $\pi \rightarrow \pi^*$ transition of aromatic rings. A broad band at 635 nm, was characteristic of its square planar geometry. The magnetic moment value of the complex was found to be 1.85 B.M., which supported its monomeric square planar structure.

As expected, the diamagnetic Zn(II) and Cd(II) complexes did not show any characteristic absorption bands in the visible region. On the basis of analytical and spectral data, the Zn(II) and Cd(II) complexes were assigned tetrahedral geometry.

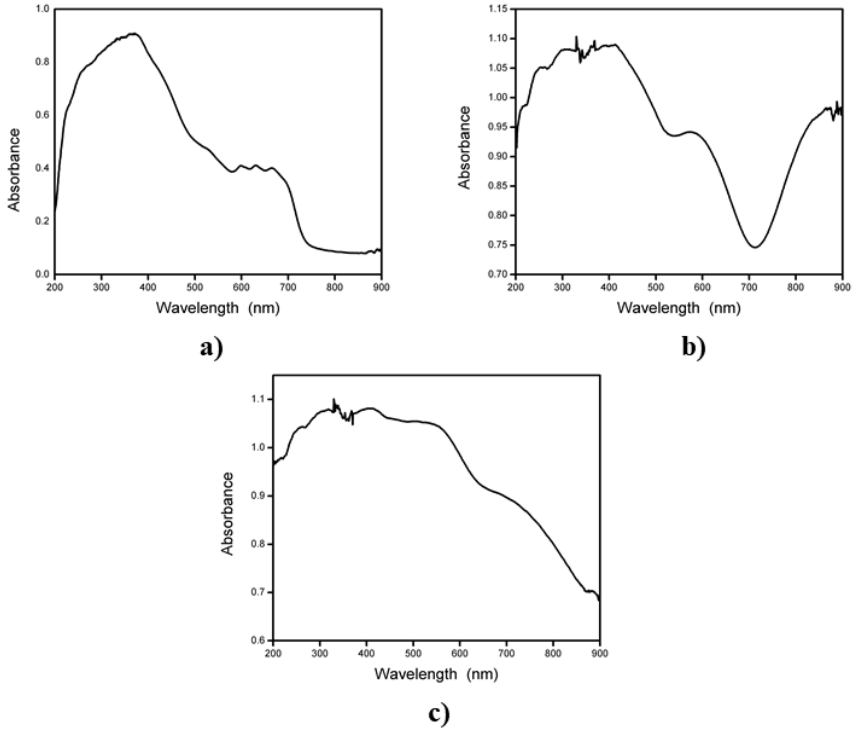

Fig.6. Electronic spectra of a) $[Co(HL)_2Cl_2]$ b) $[Ni(HL)_2Cl_2]$ and c) $[Cu(HL)Cl_2]$

Table 6. Electronic spectral bands and their assignments of the complexes

Compound	Spectral bands λ_{max} (nm)	Assignments
$[Co(HL)_2Cl_2]$	376	$^4T_{1g}(F) \rightarrow {}^4T_{1g}(P)$
	635	$^4T_{1g}(F) \rightarrow {}^4A_{2g}(F)$
$[Ni(HL)_2Cl_2]$	306	$^3A_{2g}(F) \rightarrow {}^3T_{1g}(P)$
	577	$^3A_{2g}(F) \rightarrow {}^3T_{1g}(F)$
	872	$^3A_{2g}(F) \rightarrow {}^3T_{2g}(F)$
$[Cu(HL)Cl_2]$	635br	$^2B_{1g} \rightarrow {}^2A_{1g}$, $^2B_{1g} \rightarrow {}^2B_{2g}$ and $^2B_{1g} \rightarrow {}^2E_g$

3.2.3. Infrared spectra and mode of bonding

The characteristic IR spectral bands of the ligand and the complexes (Fig.7) along with their tentative assignments are given in the Table 7. The IR spectral analysis gave information about the mode of coordination of the ligand to the metal ions. On analysing the infrared spectra of the metal complexes of 4-[N,N-(dimethyl)amino] benzaldehyde isonicotinoylhydrazone, it was observed that the absorption band due to υ(N-H) was found in the spectra of all the complexes except that of Cd(II). This indicated that the ligand had not undergone enolisation of –N–NH-C=O to –N–N=C-OH during the formation of these complexes. The vibrational frequencies due to υ(C=O) of all these complexes are found to be shifted to lower frequencies, which indicated the coordination of –N–NH-C=O in the keto form to metal centres. This band was not seen in the spectrum of Cd(II) complex. This pointed out that the ligand might have undergone enolisation of –N–NH-C=O to –N–N=C-OH and subsequently coordinated through the deprotonated oxygen to Cd(II). Thus, the appearance of a new band at 1229 cm^{-1} in the spectrum of this complex due to υ(C-O) confirmed this observation.

The coordination through azomethine nitrogen was suggested by the shift of υ(C=N) from 1613 cm^{-1} in the ligand spectrum towards lower wave numbers in the spectra of all the complexes. The band found at 1169 cm^{-1} in the ligand spectrum due to δ(N-N), shifted to higher or lower wave numbers in the spectra of all the complexes. Thus, the hydrazone coordinated to the metal ions through the amide oxygen and

azomethine nitrogen in all the complexes. This type of bonding was supported by the appearance of new bands in the low frequency regions, 444-475 cm^{-1} in the spectra of all the metal complexes which can be assigned to υ(M-N). Thus, the ligand, 4-[N,N(dimethyl) amino]benzaldehyde isonicotinoylhydrazone (HL) acted as a neutral bidentate in all the complexes except that of Cd(II). In the Cd(II) complex, it functioned as bidentate monoanionic one (L^-).

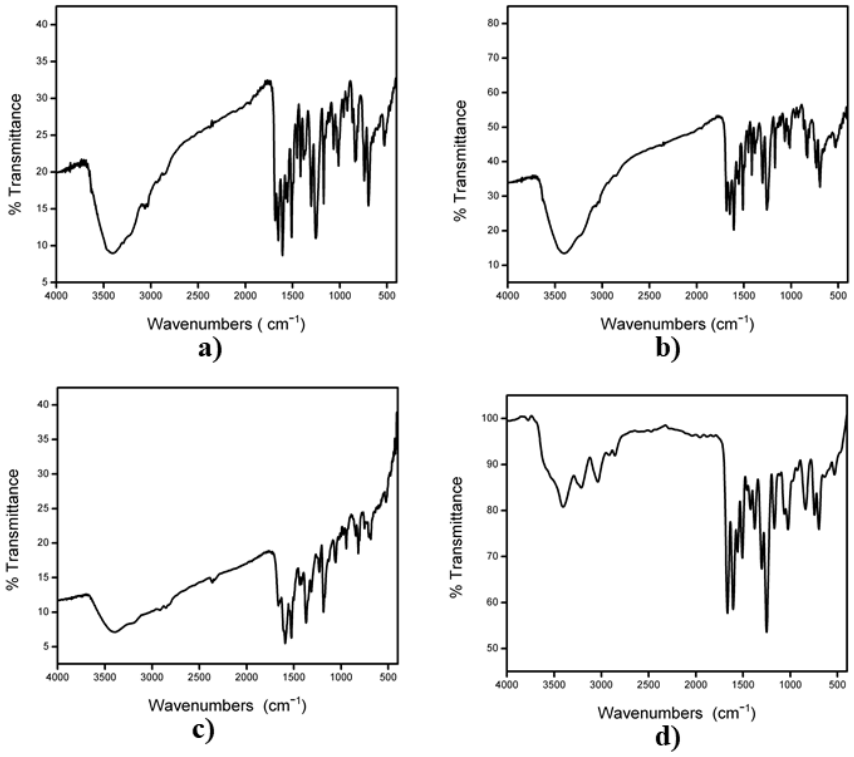

Fig.7. IR spectra of a) $[Co(HL)_2Cl_2]$ b) $[Ni(HL)_2Cl_2]$ c) $[Cu(HL)Cl_2]$ and d) $[Zn(HL)Cl_2]$

Table 7. IR spectral assignments of the metal complexes

Compound	$C_{15}H_{16}N_4O$	$[Co(HL)_2Cl_2]$	$[Ni(HL)_2Cl_2]$	$[Cu(HL)Cl_2]$	$[Zn(HL)Cl_2]$	$[Cd(L)_2]$
υ(N-H)	3398 3144	3413	3401	3390	3413 3213	-
$\upsilon_{=CH}$ (aromatic)	2970 2835	3022 2875	3037 2870	2958 2848	3026 2882	3069 859
υ(C=O)	1666	1639	1661	1662	1661	-
υ(C=N)	1613	1559	1593	1594	1605	1594
δ(N-N)	1169	1156	1174	1185	1174	1172
υ(M-N)	-	444	463	475	451	452

3.2.4. Electron paramagnetic resonance (EPR) spectrum

The ESR spectrum (X-band) of $[Cu(HL)Cl_2]$ was recorded at liquid nitrogen temperature (77K) in DMSO solution. On analysing the spectrum, $g\|$ and $g\perp$ values were found to be 2.467 and 2.065, respectively. The trend in $g\| > g\perp > 2.0023$ suggested that the unpaired electron occupied predominantly in the $d_{x^2-y^2}$ orbital, with $^2B_{1g}$ as the ground state, it is characteristic of square planar geometry of copper(II) complex. According to Neiman and Kivelson[5], if $g\|$ is less than 2.3, a covalent character- and greater than 2.3, an ionic character of the metal-ligand bond in complex is indicated. Here, the $g\|$ value of the complex was greater than 2.3, indicating a partial ionic character of the copper-ligand bond.

The geometric parameter, G i.e. the measurement of exchange interaction between the copper centres in a polycrystalline compound, is calculated by using the expression, $G = [(g\|-2)/(g\perp-2)]$. In the present case, it was found to be 7.18, suggesting the absence of considerable interaction between adjacent molecule in the solid state [6]. Absence of half field signal in the spectrum ruled out the

possibility of a dimeric form [7]. ESR spectrum, together with electronic spectrum suggested a square planar geometry for $[Cu(HL)Cl_2]$.

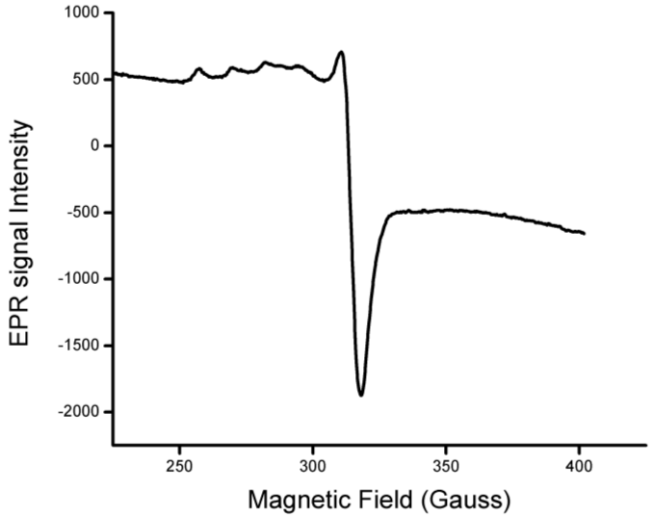

Fig.8. X-Band ESR spectrum of $[Cu(HL)Cl_2]$ complex at LNT in DMSO

3.2.5. ^{1}H NMR spectrum of $[Zn(HL)Cl_2]$

The azomethine proton absorbed at δ7.969 ppm in the ^{1}H NMR spectrum which indicated coordination of the ligand to Zn(II) through azomethine nitrogen. Another signal at δ11.754 ppm was assigned to the amide (-HN-N=) proton. The peak observed at δ8.77–6.687 ppm may be assigned to aromatic protons. A peak of six protons at δ2.990-2.939 ppm was assigned to the methyl group protons.

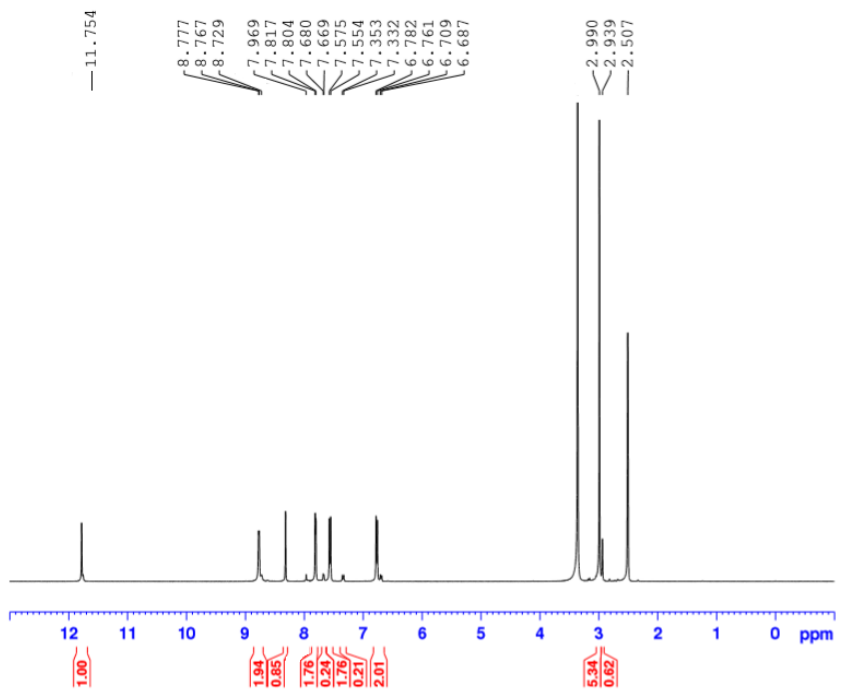

Fig.9. ^{1}H NMR spectrum of [Zn(HL)Cl_2]

4. Conclusions

The synthesis and characterization of Co(II), Ni(II), Cu(II), Zn(II) and Cd(II) complexes of 4-[N,N-(dimethyl)amino]benzaldehyde isonicotinoylhydrazone (HL) have been discussed. According to IR and ^{1}H NMR spectral analyses, the ligand acted as neutral bidentate in all the complexes except that of Cd(II). In the Cd(II) complex, the ligand functioned as bidentate monoanionic one. The Co(II) and Ni(II) complexes showed octahedral geometry (Fig.10). Cu(II) complex was assigned square planar geometry (Fig.11). The Zn(II)(Fig.12) and Cd(II) (Fig.13) complexes were assigned tetrahedral geometry.

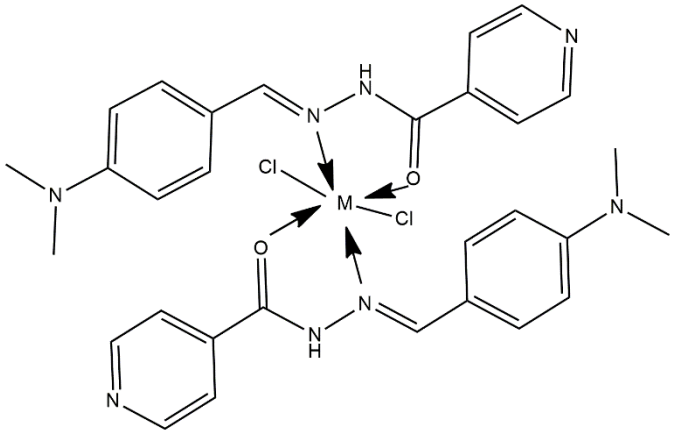

Fig.10. Proposed structure of the complexes, $[M(HL)_2Cl_2]$, where M=Co(II) or Ni(II).

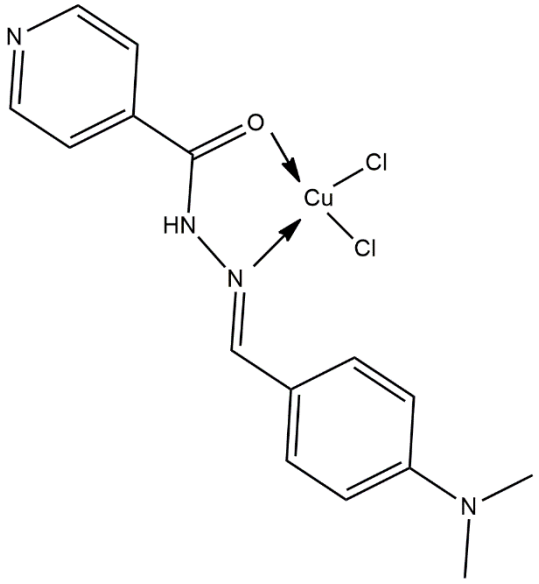

Fig.11. Proposed structure of the complex, $[Cu(HL)Cl_2]$

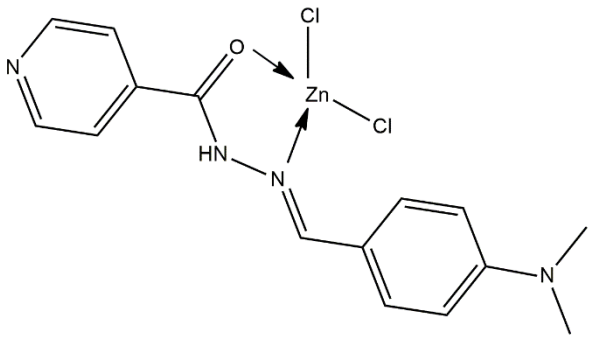

Fig.12. Proposed structure of the complex, $[Zn(HL)Cl_2]$

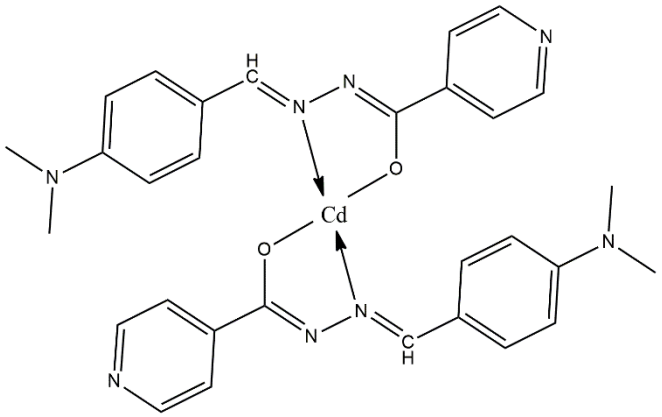

Fig.13. Proposed structure of the complex, $[Cd(L)_2]$

References

[1] O. Adegoke, Analytical, biochemical and synthetic applications of para-dimethylaminobenzaldehyde, International Journal of Pharmaceutical Sciences Review and Research 11 (2011) 17-29.

[2] R.K. Agarwal, R.K. Sarin, Synthesis and characterization of some lanthanide (III) perchlorato complexes of hydrazones of isonicotinic acid hydrazide, Polyhedron 12(19) (1993) 2411-2415.

[3] M. Malhotra, G. Sharma, A. Deep, Synthesis and characterization of (E)-N′-(substituted benzylidene)isonicotinohydrazide derivatives as potent antimicrobial and hydrogen peroxide scavenging agents, Acta poloniae pharmaceutica 69 (2012) 637-44.

[4] A.P. Mishra, L. Pandey, Synthesis, characterization and solid state structural studies of oxovanadium (IV)-O, N donor Schiff base chelates, Indian Journal of Chemistry-Section A Inorganic, Physical, Theoretical and Analytical Chemistry 44 (2005) 94-97.

[5] D. Kivelson, R. Neiman, ESR studies on the bonding in copper complexes, The Journal of Chemical Physics 35(1) (1961) 149-155.

[6] B. Hathaway, D. Billing, The electronic properties and stereochemistry of mono-nuclear complexes of the copper (II) ion, Coordination Chemistry Reviews 5(2) (1970) 143-207.

[7] N. Raman, R. Jeyamurugan, M. Subbulakshmi, R. Boominathan, C.R. Yuvarajan, Synthesis, DNA binding, and antimicrobial studies of novel metal complexes containing a pyrazolone derivative Schiff base, Chemical Papers 64(3) (2010) 318-328.

CHAPTER IX

SYNTHESIS AND CHARACTERIZATION OF TRANSITION METAL COMPLEXES OF 4-HYDROXY-3-METHOXYACETOPHENONE ISONICOTINOYLHYDRAZONE

1. Introduction

4-Hydroxy-3-methoxyacetophenone, also known as acetovanillone is a natural organic compound structurally related to vanillin. It has been isolated from a variety of plant sources and is being studied for its variety of pharmacological properties. It has distinct anti-inflammatory capabilities due to its ability to selectively prevent the formation of radicals, oxygen ions and peroxides in the body. It has been extensively studied for its disease-fighting capabilities and applications.

Isonicotinoylhydrazones have four potential coordination sites, *via* ring nitrogen, primary and secondary amino nitrogen atoms and carbonyl oxygen and can exhibit potential coordination variabilities. They are generally bidentate ligands, binding through amide oxygen and imine nitrogen of hydrazone moiety. However, if an additional donor site is present on the carbonyl compound used, isonicotinoylhydrazone can function as a tridentate ligand forming stable complexes with transition metal ions. The C=O groups enhances the electron delocalization of such ligands [1].

Our literature survey revealed that there are no reports on the coordination complexes of 4-hydroxy-3-methoxyacetophenone isonicotinoylhydrazone (HL) (Fig.1). Hence it seems to be worthwhile and interesting to prepare some complexes of this compound and to characterize them.

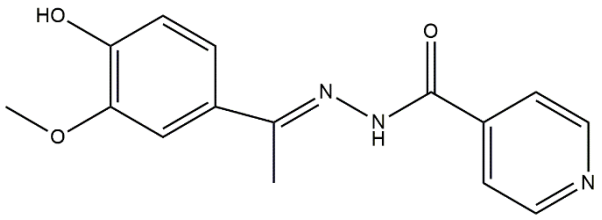

Fig.1. 4-Hydroxy-3-methoxyacetophenone isonicotinoylhydrazone (HL)

*IUPAC Name: (*E*)-*N'*-(1-(4-hydroxy-3-methoxyphenyl) ethylidene) isonicotinohydrazide

2. Experimental

2.1. Materials and methods

A detailed description about the materials, methods and characterization techniques used in this work are given in Chapter II of Part I.

2.2. Preparation of the ligand (HL)

To a hot solution of isonicotinoylhydrazide in ethanol (0.05mol), an ethanolic solution of 4-hydroxy-3-methoxyacetophenone (0.05mol) was added slowly. The reaction mixture, in the presence of catalytic amount of glacial acetic acid was refluxed on a water bath for 4hr. The solid compound, 4-hydroxy-3-methoxyacetophenone isonicotinoylhydrazone formed was filtered and dried under reduced pressure (Yield 75%, M.P 201^{0}C). The synthetic pathway of the ligand is shown in Scheme 1.

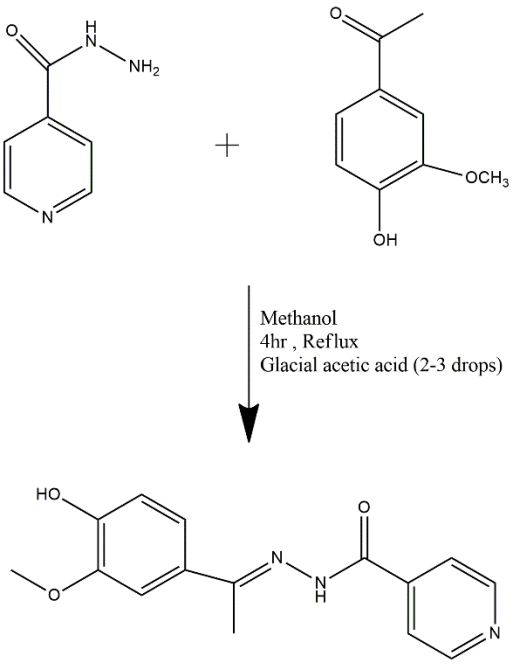

Scheme 1. Synthetic pathway of 4-hydroxy-3-methoxyacetophenone isonicotinoylhydrazone (HL)

2.3. Preparation of metal complexes

Hot solution of metal chloride in ethanol ($20cm^3$) was added to a hot solution of the ligand, 4-hydroxy-3-methoxyacetophenone isonicotinoylhydrazone (HL) in ethanol ($20cm^3$). All the complexes were synthesized by mixing stoichiometric quantities of the ligand (0.002M) and the metal salts (0.001M). Then mixture was heated under reflux on a water bath for 4 hr. On cooling, the coloured complexes precipitated out. Complexes obtained were filtered, washed with ethanol and diethyl ether and then dried. The purity of the complexes were checked by TLC method.

3. Results and discussion

The data obtained from the elemental analyses, physico-chemical- and spectral investigations have been used to explain the properties, structure and bonding of the compounds.

3.1. Characterization of the ligand (HL)

3.1.1. Micro analytical data

The ligand, HL was a white coloured solid, sparingly soluble in common organic solvents such as ethanol, acetone, ether and benzene but soluble in DMF, DMSO, chloroform, etc. The homogeneity and purity of the ligand were checked by thin-layer chromatographic (TLC) method. It was characterized by elemental analyses (Table 1), mass spectrum and further by UV-Vis- (Table 2), IR- (Table 3) and ^{1}H NMR (Table 4) spectral techniques. The data obtained from these were correlated to elucidate the structure of the ligand.

Table 1. Physico-chemical and analytical data of HL

Compound (Empirical Formula)	**Yield (%)**	**Melting Point (^{0}C)**	**Colour**	**CHNS Analysis Found % (Calculated)%**			
				C	**H**	**N**	**O**
$C_{15}H_{15}N_3O_3$.	75	201^{0}C	White	63.02 (63.08)	5.02 (5.25)	14.20 (14.72)	16.42 (16.82)

3.1.2. Mass spectrum

In the ESI-mass spectrum of the ligand (Fig.2) showed a well-defined peak at m/z 286 which coincided with the molecular weight calculated as per the proposed structure, (Mw: 285.31g).

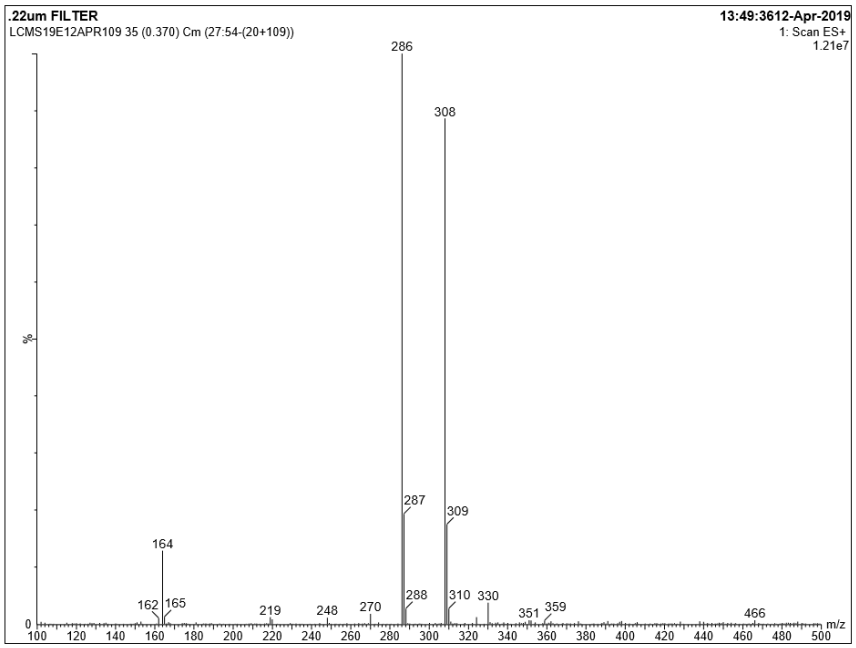

Fig.2. ESI-MS spectrum of HL

3.1.3. Spectroscopic analysis

a) Electronic spectrum

Solid state reflectance spectral data showed a band at 273 nm which can be attributed to $\pi \rightarrow \pi^*$ transition. Similarly, a strong band at 320

nm in the ligand spectrum may be due to n→π* transition from the azomethine group and amide part of the hydrazone moiety.

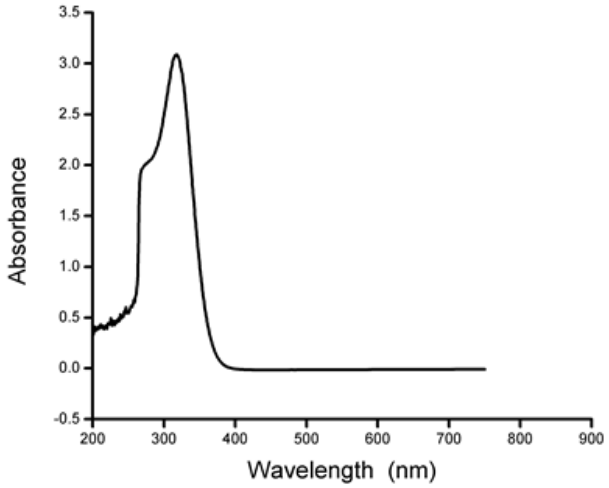

Fig.3. Electronic spectrum of HL

Table 2. Electronic spectral bands of HL

Spectral bands (nm)	**Assignments**
273	π→π* transition
320	n→π* transition

b) Infrared spectrum

Significant IR bands of the compound and their probable assignments are discussed here. A sharp band at 3472 cm^{-1} may be due to the O-H stretching. The ligand band at 3181 cm^{-1} may be due to υ(N-H). The band at 1661 cm^{-1} corresponds to υ(C=O). A strong band at 1598 cm^{-1},

may be assigned to azomethine (>C=N) group [2]. The presence of a band at 1183 cm^{-1} in the spectrum of the ligand may be assigned to δ(N-N).

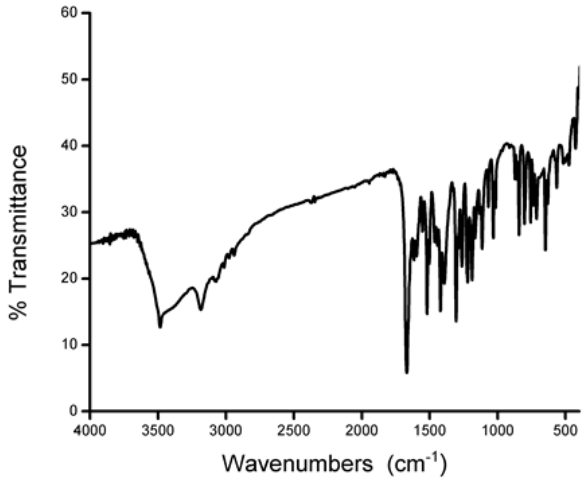

Fig.4. IR spectrum of HL

Table 3. IR spectral assignments (in cm^{-1}) of HL

Bands (cm^{-1})	**Assignments**
3491	υ(O-H)
3181	υ(N-H)
1661	υ(>C=O)
1598	υ(>C=N)
1183	δ(N-N)

C) ^{1}H NMR spectrum

The formation of the 4-hydroxy-3-methoxyacetophenone isonicotinoylhydrazone (HL) was confirmed by analysing its ^{1}H NMR

spectrum. The complete assignment of the ^{1}H NMR spectrum of ligand is given in Table 4. A singlet at 10.949 ppm can be assigned to N–H proton. A sharp singlet peak at 9.491ppm may be attributed to O-H proton. Aromatic protons showed multiplet peaks in the region 8.767–6.827 ppm. Singlet at 3.828 ppm is assigned to methoxy protons. Methyl protons absorbed at 2.325 ppm.

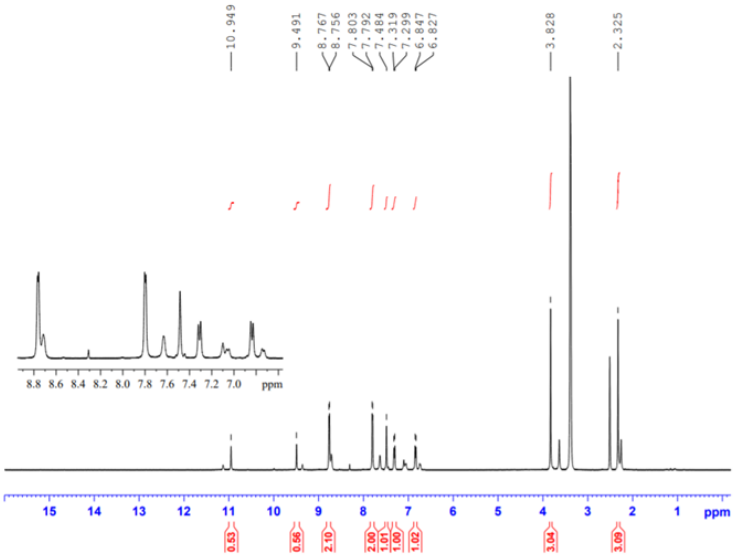

Fig.5. ^{1}H NMR spectrum of HL

Table 4. ^{1}H NMR assignments of HL

δ (ppm)	**Assignments**
10.949	N-H proton
9.491	O-H proton
8.767- 6.827 (m)	Aromatic protons
3.828	Methoxy protons
2.325	Methyl protons

3.1.4. Powder X-ray diffraction (PXRD) analysis

Since we couldn't get the single crystals of HL, we recorded its powder XRD pattern. It revealed the crystallanity of the compound.

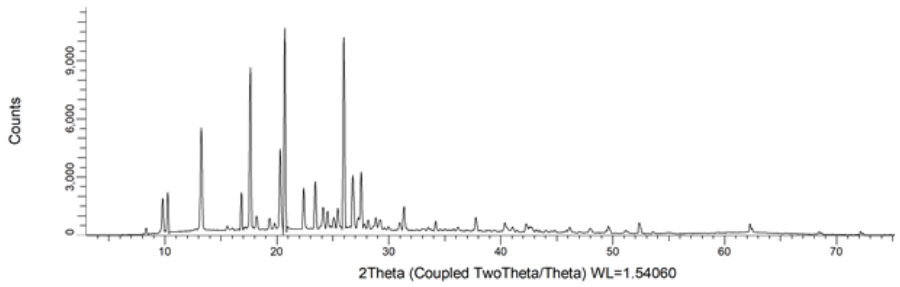

Fig.6. PXRD spectrum of HL

3.2. Characterization of the metal complexes

All the complexes of 4-hydroxy-3-methoxyacetophenone isonicotinoylhydrazone (HL) were stable under normal atmospheric conditions. All the mononuclear complexes were powders. They were soluble in acetonitrile, DMF, chloroform and DMSO, but insoluble or partially soluble in other common organic solvents like methanol, acetone and ethanol. Elemental analysis, magnetic moment measurements, electronic spectral-, FT-IR, ^{1}H NMR, EPR and TG studies were employed to characterize them.

3.2.1. Analytical data of metal complexes

The analytical data and physical properties of the ligand, HL and its complexes are listed in Table 5. Elemental analytical data of all the complexes were in good agreement with the suggested molecular

formulae. In the complexes, the ligand was found to be coordinated to neutral bidentate form. The complexes were found to have a general formula $[M(HL)_2Cl_2]$, where M = Ni(II), Cu(II), Zn(II) or Cd(II). The Co(II) complex was found to have tetrahedral structure, $[Co(HL)_2]Cl_2$.

Table 5. Physico-chemical and analytical data of the complexes

Compound	**Colour**	**Yield (%)**	**M.P (^{0}C)**	**Elemental Analysis (%) found (calculated)**				
				C	**H**	**N**	**O**	**Metal**
$C_{15}H_{15}N_3O_3$	White	75	201	63.02 (63.08)	5.02 (5.25)	14.20 (14.72)	16.42 (16.82)	-
$[Co(HL)_2]Cl_2$	Dark green	73	210	51.01 (51.39)	3.56 (3.97)	11.28 (11.99)	13.20 (13.70)	8.19 (8.41)
$[Ni(HL)_2Cl_2$	Light pink	68	212	50.98 (51.41)	3.49 (3.99)	11.25 (11.99)	13.12 (13.71)	8.10 (8.38)
$[Cu(HL)_2Cl_2]$	Dark brown	69	214	50.28 (51.06)	3.55 (3.97)	11.02 (11.91)	13.34 (13.61)	9.03 (9.01)
$[Zn(HL)_2Cl_2]$	Yellow	70	>209	50.52 (50.92)	3.64 (3.96)	11.21 (11.88)	13.47 (13.58)	9.06 (9.25)
$[Cd(HL)_2Cl_2]$	White	71	>212	47.01 (47.74)	3.64 (3.71)	11.06 (11.14)	12.18 (12.73)	14.29 (14.91)

3.2.2. Electronic spectra and magnetic moments

The electronic spectra of the complexes were recorded in solid state and their probable assignments are given in Table 6. The Co(II) complex showed absorption bands at 704 and 451 nm due to $^4A_2 \rightarrow {}^4T_1(P)$ and intra-ligand charge-transfer transitions respectively. It registered a magnetic moment value of 4.78 B.M. This value clearly indicated a tetrahedral geometry for $[Co(HL)_2]Cl_2$ complex.

In the case of octahedral Ni(II) complexes three spin-allowed transitions, $^3A_{2g}(F) \rightarrow {}^3T_{2g}(F)$, $^3A_{2g}(F) \rightarrow {}^3T_{1g}(F)$ and $^3A_{2g}(F) \rightarrow {}^3T_{1g}(P)$, are expected. In the electronic spectrum of $[Ni(HL)_2Cl_2]$, the bands at 568 and 336 nm may be assigned to $^3A_{2g}(F) \rightarrow {}^3T_{1g}(F)$ and $^3A_{2g}(F) \rightarrow {}^3T_{1g}(P)$, transitions, respectively. $^3A_{2g}(F) \rightarrow {}^3T_{2g}(F)$ is usually found in the near IR region. It was not observed in the present case as it may be out of the range of the spectrophotometer used. The electronic spectrum together with the magnetic moment value of 3.28 B.M supported an octahedral geometry for $[Ni(HL)_2Cl_2]$.

In the present investigation, the spectrum of $[Cu(HL)_2Cl_2]$ showed a broad band at 718 nm, which may be due to $^2T_{2g} \rightarrow {}^2E_g$transition [3], expected for an octahedral Cu(II) complex. A magnetic moment value of 1.89 B.M also supported its octahedral structure.

Table 6. Electronic spectral bands and their assignments of the complexes

Compound	**Spectral bands**	**Assignments**
	λ_{max} (nm)	
$[Co(HL)_2Cl_2]$	361	C-T
	704br	$^4A_2 \rightarrow {}^4T_{1g}(P)$
$[Ni(HL)_2Cl_2]$	336	$^3A_{2g}(F) \rightarrow {}^3T_{1g}(P)$
	568br	$^3A_{2g}(F) \rightarrow {}^3T_{1g}(F)$
$[Cu(HL)_2Cl_2]$	718br	$^2T_{2g} \rightarrow {}^2E_g$

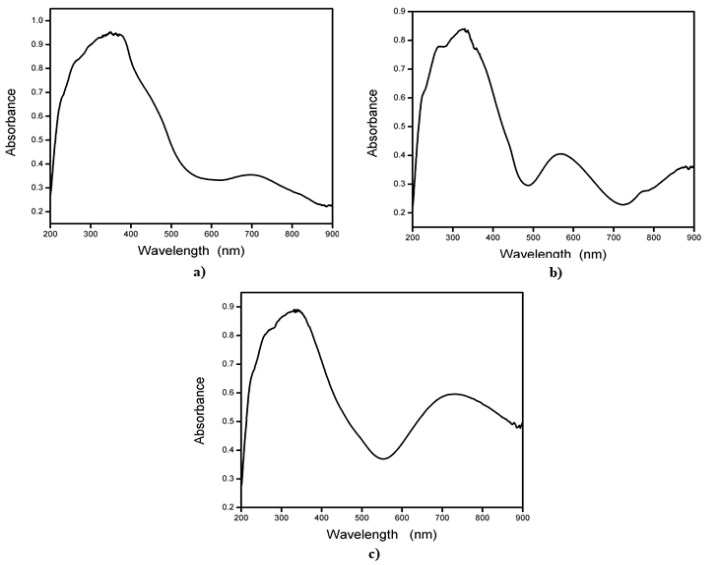

Fig.7. Electronic spectra of a)$[Co(HL)_2]Cl_2$ b) $[Ni(HL)_2Cl_2]$ and c) $[Cu(HL)_2Cl_2]$

3.2.3. Infrared spectra and mode of bonding

The assignments of the characteristic IR bands are presented in Table 7. A sharp band due to (C=O) at 1661 cm^{-1} in the ligand spectrum was found to be shifted to about a few cm^{-1} lower frequency region on complexation. This indicated the involvement of amide oxygen (C=O) in coordination. IR spectra are given in Fig.8. The band at 1598 cm^{-1} in the spectrum of the free ligand was assigned to υ(C=N). However, in the spectra of the complexes the band was shifted to lower wave numbers indicating the participation of azomethine nitrogen in coordination. The band observed at 1183 cm^{-1} in the ligand spectrum due to υ(N-N) has been found to be remained in the spectra of all the complexes. This type of bonding was supported by the appearance of new bands in the low frequency region, 518-575 cm^{-1} in the spectra of all the metal complexes which can be assigned to υ(M-N).

Table 7. IR spectral assignments of the metal complexes

Compound	$C_{15}H_{15}N_3O_3$	$[Co(HL)_2]Cl_2$	$[Ni(HL)_2Cl_2]$	$[Cu(HL)_2Cl_2]$	$[Zn(HL)_2Cl_2]$	$[Cd(HL)_2Cl_2]$
υ OH/NH	3472	3379	3320	3448	3435	3470
υ (C=O)	1661	1650	1656	1624	1652	1658
υ(C=N)	1598	1585	1583	1590	1568	1574
δ(N-N)	1183	1194	1113	1172	1198	1191
υ(M-N)	-	599	553	575	546	518

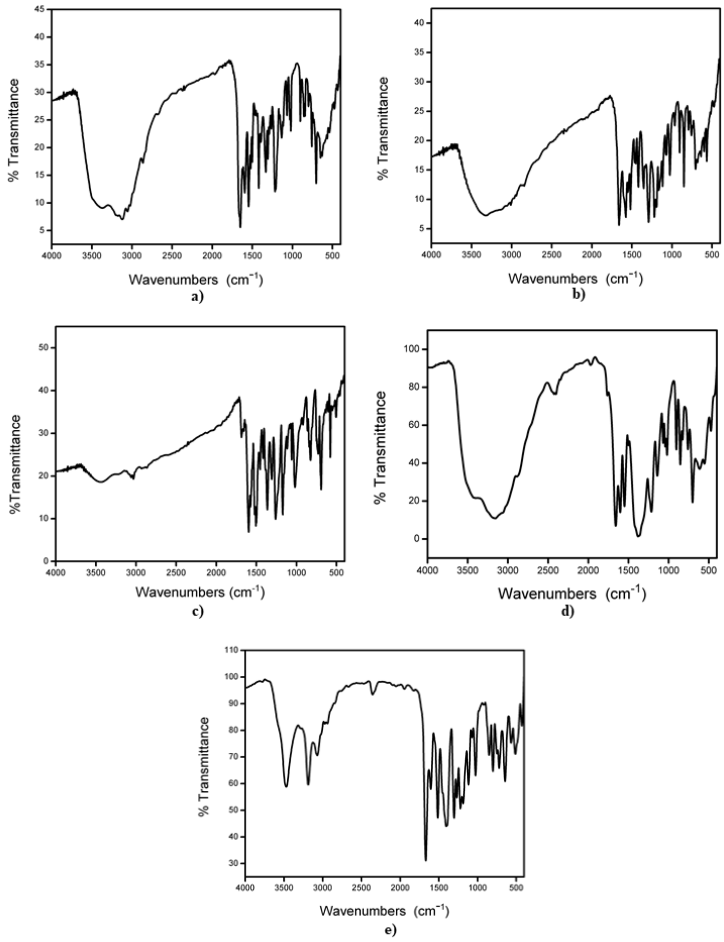

Fig.8. IR spectra of a) $[Co(HL)_2]Cl_2$ b) $[Ni(HL)_2Cl_2]$ c) $[Cu(HL)_2Cl_2]$ d) $[Zn(HL)_2Cl_2]$ and e) $[Cd(HL)_2Cl_2]$

3.2.4. Electron paramagnetic resonance (EPR) spectrum

The X band ESR spectrum was recorded in dimethyl sulfoxide at LNT (Fig.9). In the absence of magnetic field, the Cu(II) ion has an effective spin of S = 3/2 and is associated with a spin angular momentum, m_s = ±1/2, leading to a doubly degenerate spin state. The solution spectrum of the complex showed four hyperfine lines characteristic of a monomeric Cu(II) complex. They corresponded to −3/2, −1/2, 1/2 and 3/2 which arose from the coupling of the odd electron with copper nucleus (I = 3/2). The value of $g\|$ was 2.511 and that of $g^{\perp}$ was 2.054. This complex showed $g\|$ > 2.3 which was characteristic of anion environment. The trend, $g\|$ > $g^{\perp}$> 2.0023 indicated that the unpaired electron was localised in $d_{x^2-y^2}$ orbital of the Cu(II) ion [4]. Thus, a distorted octahedral geometry was proposed for the complex. The exchange interaction between the copper centers in sample was explained by Hathaway expression, G= ($g\|$-2)/($g\perp$-2). Here, a value of G>4.0, indicated negligible exchange coupling in the complex (G= 9.46). No signal at half field was observed in the spectrum, ruling out the possibility of a dimeric form [5].

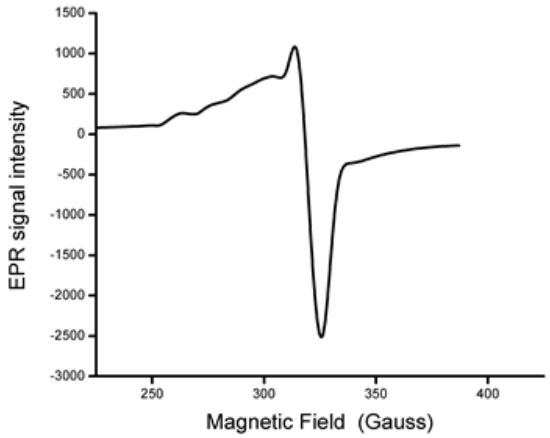

Fig.9. X-Band ESR spectrum of $[Cu(HL)_2Cl_2]$ complex at LNT in DMSO

3.2.5. ^{1}H NMR Spectrum of $[Zn(HL)_2Cl_2]$

The peak at 11.964-11.924 ppm was attributed to N–H proton. A singlet peak at 8.409 ppm may be assigned to O-H proton. Aromatic protons showed multiplet signals in the region 8.791–7.029 ppm. Singlet at 3.364 ppm was assigned to methoxy protons. Methyl protons absorbed at 2.509-2.505 ppm. Fig.11 represents the ^{1}H NMR spectrum of $[Zn(HL)_2Cl_2]$.

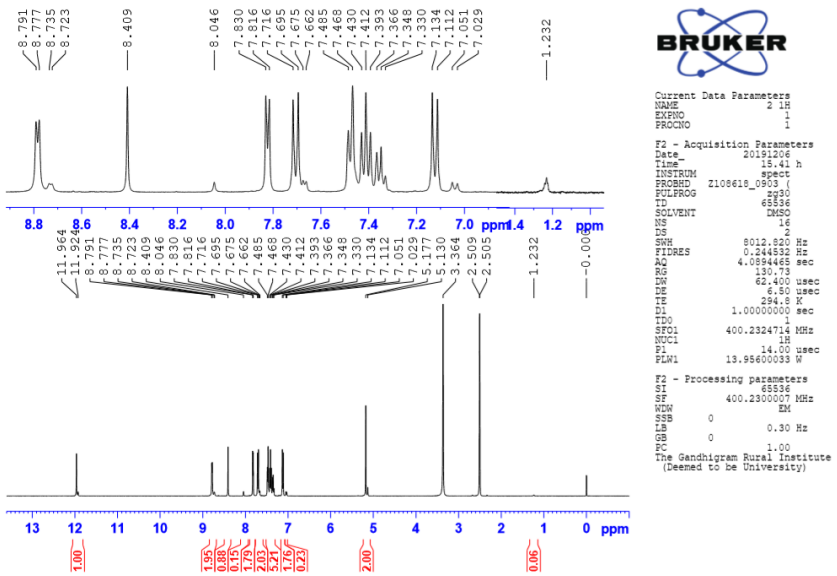

Fig.10. ^{1}H NMR Spectrum of $[Zn(HL)_2Cl_2]$

3.3.6. Thermo gravimetric analysis

In the present study, Ni(II) and Cd(II) complexes were chosen as representative compounds for thermal analysis.

For $[Ni(HL)_2Cl_2]$, three stages of decomposition occurred. The first decomposition stage was in the temperature range, 202–254°C with a 1.5% mass loss. The second decomposition observed at 290-356^{0}C with mass loss of 4.52%, which may be due to the partial decomposition of the ligand moiety. The third decomposition stage occurred at 385-492^{0}C. The residual mass of 10.67% may be due to the formation of NiO (calc. 11.01%).

The Cd(II) complex showed two stages of decomposition. The first stage of decomposition observed at 98^0C may be due to moisture. At 299^0C it showed with a mass loss of 32.42% which may be due to the decomposition of the ligand moiety. A residual mass loss of 15.87% may be due to the formation of CdO (calcd.16.91%).

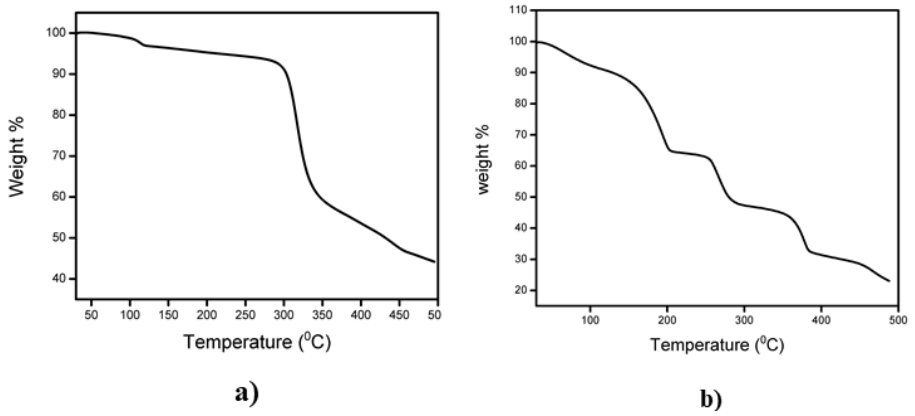

Fig.11. TG curves of a) $[Ni(HL)_2Cl_2]$ and b) $[Cd(HL)_2Cl_2]$

4. Conclusions

Based on the above spectral, physico-chemical and thermal studies, an octahedral environment around Ni(II),Cu(II), Zn(II) and Cd(II) ions was proposed. However, the Co(II) complex was found to be tetrahedral in geometry. In all the complexes, the ligand acts as neutral bidentate coordinating through carbonyl oxygen and imine nitrogen. The proposed structural formulae are given in Fig.12 and 13.

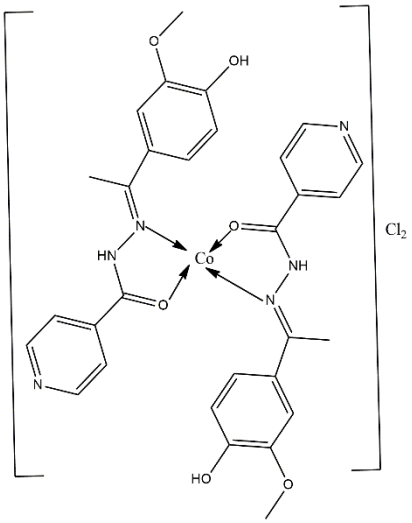

Fig.12. Proposed structure of the complex, $[Co(HL)_2]Cl_2$

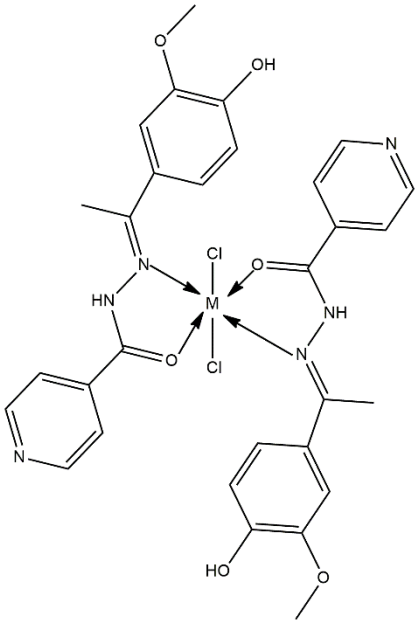

Fig.13. Proposed structure of the complexes,

$[M(HL)_2Cl_2]$

where, M= Ni(II), Cu(II), Cd(II) or Zn(II).

References

[1] S. Tandon, S. Chander, L. Thompson, Ligating properties of tridentate Schiff base ligands, 2-[[(2-pyridinylmethyl) imino] methyl] phenol (HSALIMP) and 2-[[[2-(2-pyridinyl) ethyl] imino] methyl] phenol (HSALIEP) with zinc (II), cadmium (II), nickel (II) and manganese (III) ions. X-ray crystal structures of the [Zn (SALIEP)(NO3)] 2 dimer,[Mn (SALIEP) 2](ClO4), and [Zn (AMP) 2 (NO3) 2], Inorganica Chimica Acta 300 (2000) 683-692.

[2] S.M. Khalil, H. Seleem, B. El-Shetary, M. Shebl, Mono-and bi-nuclear metal complexes of schiff-base hydrazone (ONN) derived from o-hydroxyacetophenone and 2-amino-4-hydrazino-6-methyl pyrimidine, Journal of Coordination Chemistry 55(8) (2002) 883-899.

[3] B. Hathaway, The correlation of the electronic properties and stereochemistry of mononuclear {CuN 4–6} chromophores, Journal of the Chemical Society, Dalton Transactions (12) (1972) 1196-1199.

[4] A. Jaggi, S. Chandra, K. Sharma, Stereochemical versatility of Cu (II): Cu (II) complexes of benzyl methyl ketone semicarbazone, Polyhedron 4(1) (1985) 163-168.

[5] N. Raman, R. Jeyamurugan, M. Subbulakshmi, R. Boominathan, C.R. Yuvarajan, Synthesis, DNA binding, and antimicrobial studies of novel metal complexes containing a pyrazolone derivative Schiff base, Chemical Papers 64(3) (2010) 318-328.

CHAPTER X

SYNTHESIS, STRUCTURAL CHARACTERIZATION, HIRSHFELD SURFACE AND DFT BASED REACTIVITY, UV FILTER AND NLO STUDIES OF SCHIFF BASE ANALOGUE OF 4-AMINOANTIPYRINE

1. Introduction

Schiff bases are nitrogen analogues of aldehydes or ketones with a growing interest due to their RC=N group and are also known as azomethines. They are usually prepared by the condensation of primary amines with carbonyl compounds under specific conditions. In general, aldehydes take part faster than ketones in condensation reactions because the reaction centre of an aldehyde is sterically less hindered than that of a ketone. Schiff bases of aliphatic aldehydes are relatively unstable and readily polymerize, while those of aromatic aldehydes, having an effective conjugation system, are more stable. Schiff bases are generally bi-or tri- dentate ligands capable of forming very stable complexes with transition metal ions. In organic synthesis, Schiff base formation reactions are useful in making carbon-nitrogen bonds. They have been extensively studied because of their exciting biological activities such as antitumor-[1], antimicrobial-[2] and antioxidant-[3] activities. These wide ranges of biological applications are due to the imine groups present in them [4].

Generally, pyrazolones comprise a group of organic compounds, which are heterocycles, and process a five- membered lactam ring with an additional keto group. Among pyrazolone analogues, synthetically important compounds derived from 4-aminoantipyrine have received much attention because they exhibit attractive multi-functional properties including antifungal-, antibacterial-, antimalarial-, antiviral-, anti-inflammatory- and antipyretic properties. Nowadays,4-aminoantipyrine derivatives have been treated as important model compounds in the biological- and medical fields [5]. Generally Schiff

bases are crystalline and feebly basic. They are characterized by the presence of an azomethine group, –RC=NR', where R and R' are alkyl-, cycloalkyl-, aryl- or heterocyclic groups. Schiff bases are widely designed by varying the chemical environment around the –C=N- group. The presence of a lone pair of an electron in the sp^2 hybridized orbital on the imino nitrogen atom makes the azomethine group more significant.

Recently, Density Functional Theory (DFT) has been recognized as a better auxiliary tool in the study of biological- and chemical properties of several active compounds than the *ab initio* methods used in the past. It has been endorsed as a well-known post-HF approach for the computational calculations of structural characteristics, vibrational frequencies and energies of compounds. It has been proved to be a reliable and potent tool with accuracy and cost effectiveness. We decided to explore the spectroscopic- and quantum chemical properties of the title compound, which were calculated using the DFT-B3LYP method at 6-311++G(d,p) Basis set level [6]. These data were compared with experimental results.

A search through the literature revealed that no work has been done on the Schiff base formed by the condensation of 4-aminoantipyrine with 4-benzyloxybenzaldehyde. Therefore, it was considered to be worthwhile to report the synthesis, characterization and theoretical studies, crystal structure of the novel Schiff base, 4-(4-benzyloxybenzalidene)amino-2,3-dimethyl-1-phenyl-3-pyrazol-5-one (L), (Fig.1). The structural- and geometrical properties, NLO activity,

molecular electrostatic potential, Hirshfeld surface- and fingerprint plot analyses were studied. The frontier molecular orbital calculations of the compound were also made.

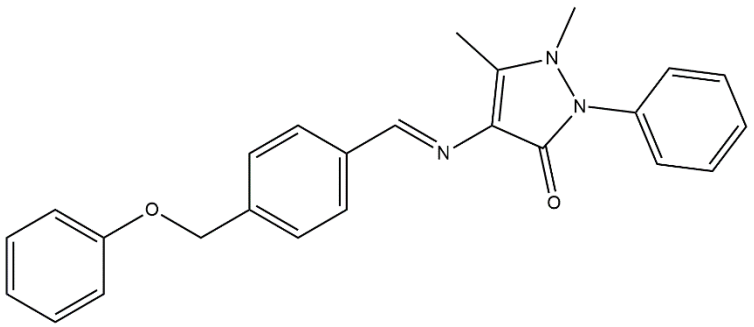

Fig.1. 4-(4-benzyloxybenzalidene)amino-2,3-dimethyl-1-phenyl-3-pyrazol-5-one (L)

*IUPAC Name: (*E*)-1,5-dimethyl-4-((4-(phenoxymethyl)benzylidene) amino)-2-phenyl-1*H*-pyrazol-3(*2H*)-one

2. Experimental

2.1. Materials and methods

Details regarding the chemicals used and the methods adopted for the characterization of the compounds are described in Chapter II.

2.2. Synthesis of the Schiff base (L)

The compound was synthesised by refluxing an equimolar ethanolic solution of 4-aminoantipyrine (2.03g, 0.01mol) and 4-benzyloxybenzaldehyde (2.12g, 0.01mol) in the presence of a few drops of acetic acid for 4hr on a water bath. The resulting solution was allowed to evaporate slowly and the precipitate formed was filtered,

washed with ethanol and dried under vacuum. The solid obtained was recrystallized from ethanol to yield yellow needle like single crystals. The reaction sequence of the formation of the novel Schiff base ligand (L) is outlined in Scheme 1.

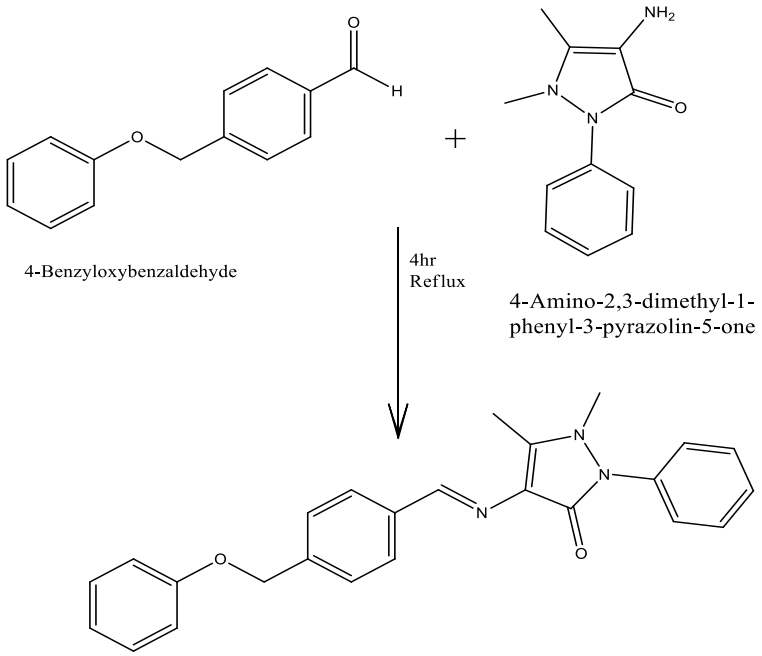

Scheme 1. 4-(4-Benzyloxybenzalidene) amino-2,3-dimethyl-1-phenyl-3-pyrazol-5-one (L)

2.3. Single crystal structure determination

The single crystal X-ray diffraction measurements were carried out at 296(2) K on a Bruker Kappa Apex II diffractometer. The final refinements for the structure were obtained with the Full-matrix least-squares method and X Shell Structure Solution Software. Table 2

summarizes the crystal data collected and refinement data for the structural analysis.

2.4.Computational details

To obtain more information of chemical interest, we have performed the theoretical calculations of structural, spectral and the density derived properties of the Schiff base using the Gaussian 09 program [7]. The molecular structural data of the compound obtained from the XRD data in the RES file format were converted to GJF file format using Open Babel utility[8]. The geometrical optimization was carried out at DFT/B3LYP levels with 6-311++G(d,p) Basis set. B3LYP [9]represents Becke's three parameters hybrid functional method with Lee-Yang-Parr (LYP) correlation functional which are best for predicting the results of molecular geometry and vibrational wavenumbers of a moderately larger molecule.

The optimization was achieved without any symmetry constraints. Further, vibrational frequency calculations were done to confirm the true minima on the calculated potential surface. The calculated harmonic vibrational frequencies were scaled by 0.960 in the high wave number region and by 0.961 in the low wave number region (below 1800 cm^{-1}) for B3LYP/6-311++G(d,p) level, since the B3LYP functional tends to overestimate the fundamental vibrational mode. Solvent effects on the calculated structures were investigated with the Self-Consistent Reaction Field (SCRF) method, *via* the Integral Equation Formalism Polarized Continuum Model (IEF-PCM). Ethanol was used as a solvent environment (ε=32.61) in order to reproduce the

same solvent used in the experiment. In order to understand the electronic properties, theoretical UV-Vis spectra have been investigated by TD-DFT method with 6-311++G (d,p) Basis set for ethanol and gas phase. Furthermore, to understand the UV-screening nature of the molecule under study, rational understanding of electronic transitions is one of the prerequisites. Quantitative analysis of molecular surface has been carried out. Surface properties such as, surface area, enclosed volume, average value and standard of mapped functions were computed for overall molecular surface or local surfaces. Local minima and maxima of mapped functions on the surface were also be located. Molecular surface analysis was also done by carrying out Molecular Electrostatic Potential (MEP) map and Hirshfeld analysis [10] as well as fingerprint analysis. Furthermore, the fukui analysis of the compound was also carried out to assess its the probable reactive sites. MultiWFN software was used for their Fukui, MEP and DD analysis. The non-linear optical response of the molecule was also evaluated.

3. Results and discussion

The novel Schiff base was characterized with respect to its composition by elemental analysis and showed a good agreement with the theoretical values.

3.1. Characterization of the ligand (L)

The ligand (L) was characterized by single crystal X-ray analysis, ESI-MS, IR, UV-Vis and ^{1}H NMR spectral techniques.

3.1.1. Micro analytical data

The ligand was yellow coloured needle like single crystals of 4-(4-benzyloxybenzalidene)amino-2,3-dimethyl-1-phenyl-3-pyrazol-5-one (L). CHNS percentages were in good agreement with the suggested molecular formula, $C_{25}H_{23}N_3O_2$ (Table 1). It is non-hygroscopic and stable at normal atmospheric conditions. It melted at 153^oC and soluble in DMSO, DMF, chloroform, etc.

Table 1. Physico-chemical and analytical data of L

Compound (Empirical Formula)	**Yield (%)**	**Melting Point (^0C)**	**Colour**	**CHNS Analysis Found % (Calculated)**		
				C	**H**	**N**
$C_{25}H_{23}N_3O_2$	76	153	Yellow	75.475 (75.88)	5.786 (5.78)	10.566 (10.46)

3.1.2. Mass spectrum

In the ESI - mass spectrum of L (Fig.2)**,** the molecular ion peak at m/z 398.28 (100%) (M+1), coincided with its formula weight (Mw: 397.48g), which confirmed the formation of the 4-(4-benzyloxybenzalidene)amino-2,3-dimethyl-1-phenyl-3-pyrazol-5-one (L).

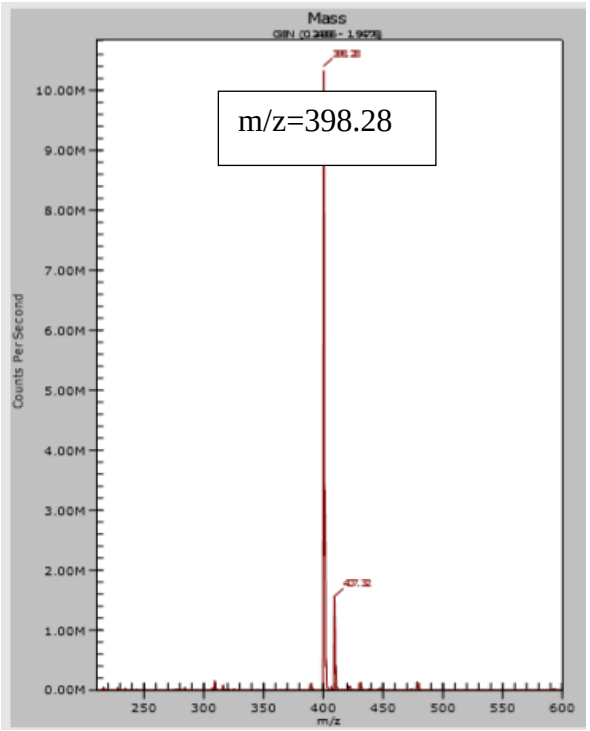

Fig.2. Mass spectrum of L

3.1.3. ^{1}H NMR spectrum

The^{1}H NMR spectrum of the Schiff base, L (Fig.3) showed two sharp peaks at δ3.15ppm and δ 2.49 ppm with integration equivalent to three hydrogens corresponding to the N-CH_3 and C-CH_3 groups, respectively. The presence of an electronegative oxygen, nitrogen and sp^2 hybridized carbon tends to shift the NMR signal of nearby protons slightly downfield[11]. The azomethine hydrogen showed a sharp singlet at δ9.73 ppm. The multiplet signals observed in the range, δ7.02-7.84 ppm may be due to aromatic protons of L[12].

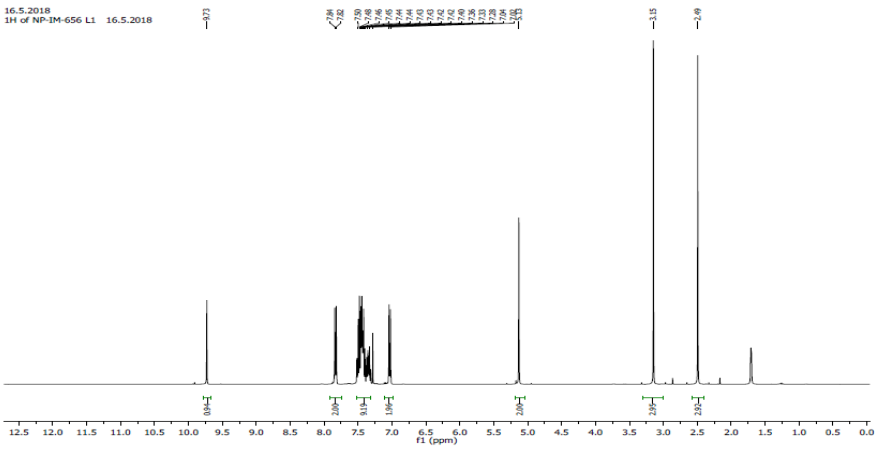

Fig.3. ^{1}H NMR spectrum of L

3.1.4. ^{13}C NMR spectrum

The prominent peaks in the ^{13}C NMR spectrum of L (Fig.4) are: C(14)-160.48, C(17)-160.94, C(15)-114.75, C(1)-124.15, C(24)-134.77, C(25)-10.03, C(26)-35.89, C(18)-136.57, C(22)-129.05, C(21)-118.78**.** The spectrum confirmed the formation of the Schiff base.

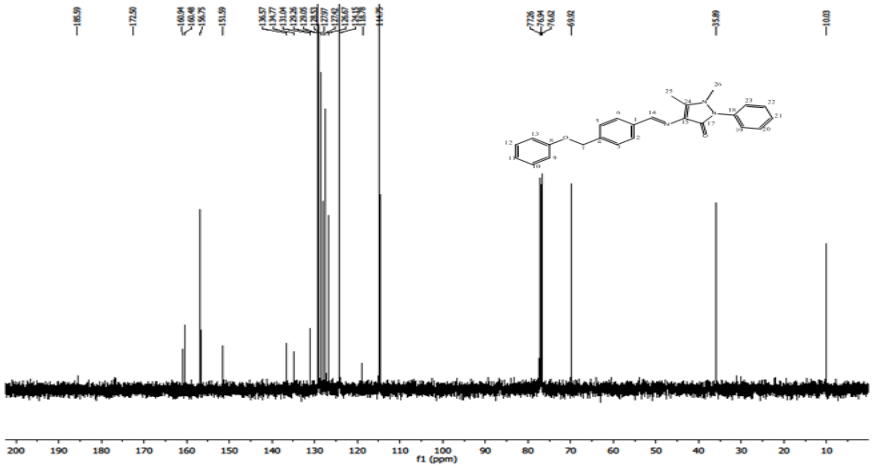

Fig.4. ^{13}C NMR spectrum of L

3.1.5. Thermo gravimetric analysis

Thermo gravimetric analysis (TG) of a compound is used to establish its purity and thermal stability. The analysis was carried out in nitrogen atmosphere over a temperature range of 30–500^{0}C and at a heating rate of 10^{0}C min^{-1} (Fig.5). The compound was stable upto 295^{0}C. The estimated mass loses at 296^{0}C was 50%, which may be due to the successive decomposition of $C_{25}H_{23}N_3O_2$.

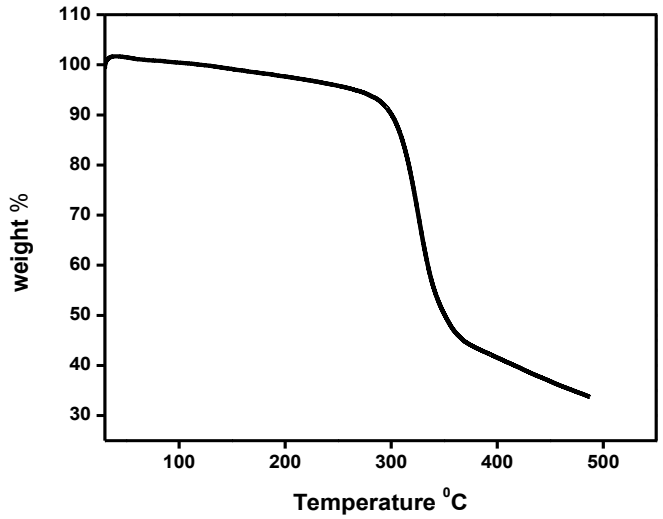

Fig.5. TG curve of L

3.2. Computational results

3.2.1. Molecular structure

The process of optimization of compound has led to a confirmer that has the lowest energy and highest stability. This is evident from the

frequency calculation, which shows no imaginary frequencies. The optimized structure of L is shown in Fig.7 and the values of the geometrical parameters are listed in Table 4 with experimental results. The atomic numbering scheme of the molecule was done by Ortep-3 format (Fig.6). We used GaussView Atomic Numbering Scheme for all results other than comparison of experimental geometrical parameters with computational results. For the reliability of geometry calculations, the Pearson Correlation Analyses of Experimental and Theoretical Geometrical parameters of the compound was performed. From Table 2, it is clear that the theoretical results are in almost same harmony with the experimental results. The computed and experimental values of Root Means Square Deviations (RMSD) of bond distances and bond angles from experimental value were 0.03 Å and 1.04°, respectively. The correlations observed for calculated and experimental geometrical parameters were 0.93, 0.98 and 0.86 for bond length, bond angle and dihedral angle, respectively.

Table 2. Summary of crystal and structural refinement data for L

Identification code	Shelx
Empirical formula	C_{25} H_{23} N_3 O_2
Formula weight	397.46
Temperature	296(2) K
Wavelength	0.71073 A^0
Crystal system, space group	Orthorhombic, P 21 21 21
Unit cell dimensions	a = 6.5188(4) A alpha = 90 deg. b = 18.6606(15) A beta = 90 deg. c = 35.390(3) A gamma = 90 deg.
Volume	4305.0(5) A^3
Calculated density absorption coefficient, Z	8,1.226 Mg/m^3
Crystal size	0.500 x 0.350 x 0.350 mm
Theta range for data collection	1.151 to 28.405 deg
Limiting indices	-8<=h<=5, -24<=k<=24, -47<=l<=46
Absorption correction	Semi-empirical from equivalents
Max. and min. transmission	0.973 and 0.962
Refinement method	Full-matrix least-squares on F^2
Extinction coefficient	0.0137(17)

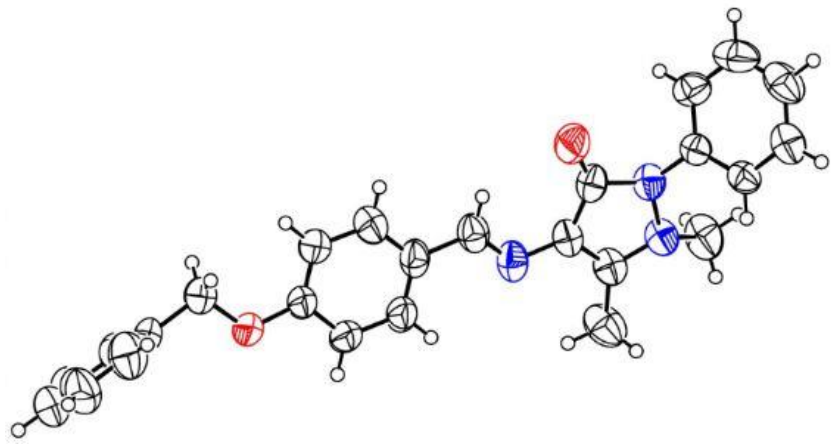

Fig.6. Ortep diagram of L

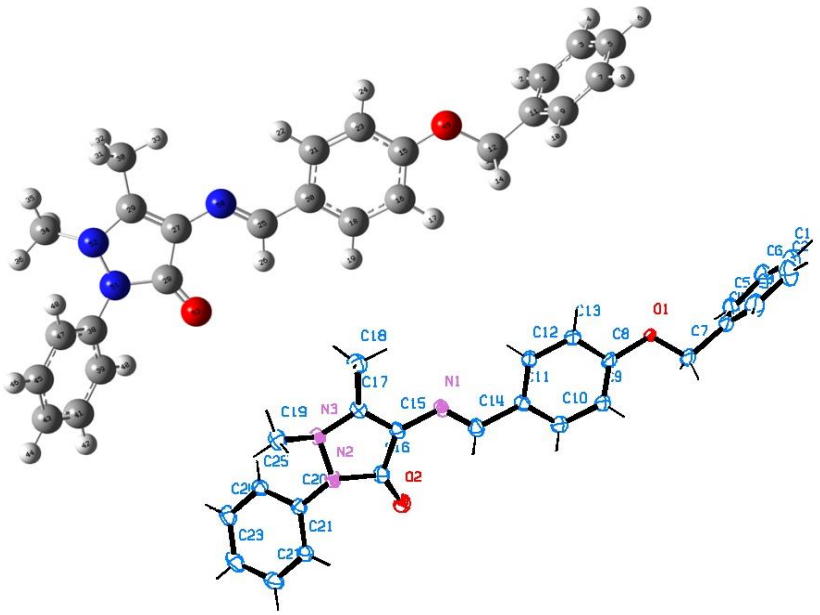

Fig.7. The theoretical geometric structure (B3LYP/6-311++G (d, p) level) of 4-(4-benzyloxybenzalidene)amino-2,3-dimethyl-1-phenyl-3-pyrazol-5-one (L) along with the molecular structure of 4-(4-benzyloxybenzalidene)amino-2,3-dimethyl-1-phenyl-3-pyrazol-5-one (L), showing 50% probability displacement ellipsoids and the atom-numbering scheme.

3.2.2. Description of crystal structure

The compound, L crystallized in the orthorhombic space group P21 21 21 with Z = 8 in the unit cell. The bond lengths andangles are within normal ranges and these values are comparable with those observed in other similar antipyrine Schiff bases. The selected bond lengths and bond angles are listed in Table 3. In this case, the C14 =N1 bond length, 1.286(7) Å conforms the double bond between C14 and N1. The distance between C15 and N1 is 1.387(6) Å, which is intermediate

between classical C-N and C=N bond lengths, because of the molecular conjugative effect. As expected, the molecule adopts a *trans*- configuration about the imine bond, C14 = N1.

Table 3. Selected molecular structural parameters of L

Bond length			bond angle			Dihedrals		
Atoms	XRD	DFT-gas	Atoms	XRD	DFT-gas	Atoms	XRD	DFT-gas
C(1)-C(6)	1.32	1.39	C(6)-C(1)-C(2)	120.20	119.83	C(6)-C(1)-C(2)-C(3)	0.30	-0.03
C(1)-C(2)	1.35	1.39	C(1)-C(2)-C(3)	119.30	119.99	C(1)-C(2)-C(3)-C(4)	1.00	0.06
C(2)-C(3)	1.39	1.39	C(4)-C(3)-C(2)	120.20	120.58	C(2)-C(3)-C(4)-C(5)	-1.70	0.01
C(3)-C(4)	1.36	1.40	C(5)-C(4)-C(3)	118.40	119.01	C(2)-C(3)-C(4)-C(7)	-178.90	-179.04
C(4)-C(5)	1.34	1.40	C(5)-C(4)-C(7)	117.90	120.40	C(3)-C(4)-C(5)-C(6)	1.10	-0.11
C(4)-C(7)	1.49	1.50	C(3)-C(4)-C(7)	123.60	120.57	C(7)-C(4)-C(5)-C(6)	178.50	178.95
C(5)-C(6)	1.36	1.39	C(4)-C(5)-C(6)	121.30	120.57	C(2)-C(1)-C(6)-C(5)	-1.00	-0.06
C(7)-O(1)	1.40	1.44	C(1)-C(6)-C(5)	120.60	120.01	C(4)-C(5)-C(6)-C(1)	0.30	0.14
C(8)-C(9)	1.34	1.40	O(1)-C(7)-C(4)	107.60	108.27	C(5)-C(4)-C(7)-O(1)	-102.60	-83.97
C(8)-O(1)	1.38	1.36	C(9)-C(8)-O(1)	125.90	124.83	C(3)-C(4)-C(7)-O(1)	74.60	95.07
C(8)-C(13)	1.37	1.41	C(9)-C(8)-C(13)	119.10	119.64	O(1)-C(8)-C(9)-C(10)	-178.60	179.94
C(9)-C(10)	1.38	1.39	O(1)-C(8)-C(13)	115.00	115.53	C(13)-C(8)-C(9)-C(10)	1.00	0.01
C(10)-C(11)	1.37	1.40	C(8)-C(9)-C(10)	120.00	119.37	C(8)-C(9)-C(10)-C(11)	-1.40	0.01
C(11)-C(12)	1.36	1.41	C(11)-C(10)-C(9)	122.20	121.68	C(9)-C(10)-C(11)-C(12)	0.80	-0.03
C(11)-C(14)	1.46	1.46	C(12)-C(11)-C(10)	117.00	118.06	C(9)-C(10)-C(11)-C(14)	-178.90	-179.94
C(12)-C(13)	1.38	1.38	C(12)-C(11)-C(14)	122.60	122.57	C(10)-C(11)-C(12)-C(13)	0.00	0.03
C(14)-N(1)	1.29	1.29	C(10)-C(11)-C(14)	120.50	119.38	C(14)-C(11)-C(12)-C(13)	179.70	179.93
C(15)-C(17)	1.35	1.37	C(11)-C(12)-C(13)	121.10	120.94	C(11)-C(12)-C(13)-C(8)	-0.30	-0.01
C(15)-N(1)	1.39	1.38	C(12)-C(13)-C(8)	120.50	120.32	C(9)-C(8)-C(13)-C(12)	-0.20	-0.01
C(15)-C(16)	1.44	1.47	N(1)-C(14)-C(11)	119.70	121.99	O(1)-C(8)-C(13)-C(12)	179.40	179.95
C(16)-O(2)	1.23	1.22	C(17)-C(15)-N(1)	121.40	123.24	C(12)-C(11)-C(14)-N(1)	-4.80	0.31
C(16)-N(2)	1.39	1.42	C(17)-C(15)-C(16)	108.70	107.64	C(10)-C(11)-C(14)-N(1)	174.90	-179.78
C(17)-N(3)	1.36	1.39	N(1)-C(15)-C(16)	129.70	129.07	C(17)-C(15)-C(16)-O(2)	175.80	-176.39
C(17)-C(18)	1.47	1.49	O(2)-C(16)-N(2)	123.50	124.35	N(1)-C(15)-C(16)-O(2)	0.60	1.01
C(19)-N(3)	1.45	1.47	O(2)-C(16)-C(15)	132.10	130.91	C(17)-C(15)-C(16)-N(2)	-3.20	1.46
C(20)-C(21)	1.36	1.40	N(2)-C(16)-C(15)	104.40	104.70	N(1)-C(15)-C(16)-N(2)	178.40	178.86
C(20)-C(25)	1.38	1.40	C(15)-C(17)-N(3)	110.30	110.95	N(1)-C(15)-C(17)-N(3)	174.10	174.99
C(20)-N(2)	1.41	1.42	C(15)-C(17)-C(18)	128.90	127.67	C(16)-C(15)-C(17)-N(3)	-1.60	2.60
C(21)-C(22)	1.37	1.39	N(3)-C(17)-C(18)	120.70	121.37	N(1)-C(15)-C(17)-C(18)	-8.20	5.43
C(22)-C(23)	1.38	1.39	C(21)-C(20)-C(25)	120.10	120.06	C(16)-C(15)-C(17)-C(18)	176.10	176.98
C(23)-C(24)	1.36	1.39	C(21)-C(20)-N(2)	118.10	118.91	C(25)-C(20)-C(21)-C(22)	-0.50	-0.24
C(24)-C(25)	1.37	1.39	C(25)-C(20)-N(2)	121.80	121.02	N(2)-C(20)-C(21)-C(22)	178.70	179.32
			C(20)-C(21)-C(22)	119.50	119.54	C(20)-C(21)-C(22)-C(23)	-0.40	1.01
			C(21)-C(22)-C(23)	120.70	120.94	C(21)-C(22)-C(23)-C(24)	0.00	-0.76
			C(24)-C(23)-C(22)	119.80	119.48	C(22)-C(23)-C(24)-C(25)	1.20	-0.26
			C(23)-C(24)-C(25)	119.60	120.45	C(23)-C(24)-C(25)-C(20)	-2.10	-178.11
			C(24)-C(25)-C(20)	120.30	119.76	C(21)-C(20)-C(25)-C(24)	1.70	-0.76
						N(2)-C(20)-C(25)-C(24)	179.80	179.69

3.2.3. Vibrational analysis

The theoretical IR spectrum was compared with the experimental FT-IR spectrum (Fig.8). They showed most of the bands at same position with almost the same shapes and intensities. However, a few of them were found to be slightly shifted. The selected bands in the IR spectrum confirmed the formation of the novel Schiff base, L. The experimental infrared spectrum of L showed a strong, intense band at 1573 cm^{-1} (due to υC=N) indicating the presence of azomethine group. The band at 1621 cm^{-1} was due to υ(C=O). The high value of υ(C=N) was due to high conjugation (resonance effect) of the substituted double bonds. Generally, C-H vibrations appear in the range 3100-3000 cm^{-1} [13]. The bands at 3043and 2930 cm^{-1} were due to symmetric- and asymmetric stretching vibrations of aromatic C-H group [14]. The theoretical vibrations frequencies were studied by using DFT/ B3LYP method and 6-311++G(d,p) basis set level and showed good agreements with the experimental results.

3.2.4. Electronic spectrum and Frontier Molecular Orbital analysis

The Gauss-Sum 3.0 Program was used to calculate group contributions to the molecular orbitals (HOMO and LUMO) and to prepare the density of the state (DOS), as shown in Fig.9. The experimental and simulated electronic absorption spectra of the compound are shown in Fig.10. The computed electronic spectrum of the molecule was in good agreement with the reported experimental spectrum. Experimental studies showed that the molecule had specific UV spectrum with an absorption maximum at 340.5 nm. Similarly, computed spectrum in

ethanol showed an absorption maxima at 346.29 nm (28877.53 cm^{-1}). This result enlightened the UV filter activity of studied compound because according to literature, the potential candidate for UVB absorber should have molar extinction coefficient greater than 10000 and λ_{max} in between 280 to 400 nm. The molecular orbital distribution in each absorption further gave an insight into the electronic nature of the UV filter activity of the compound.

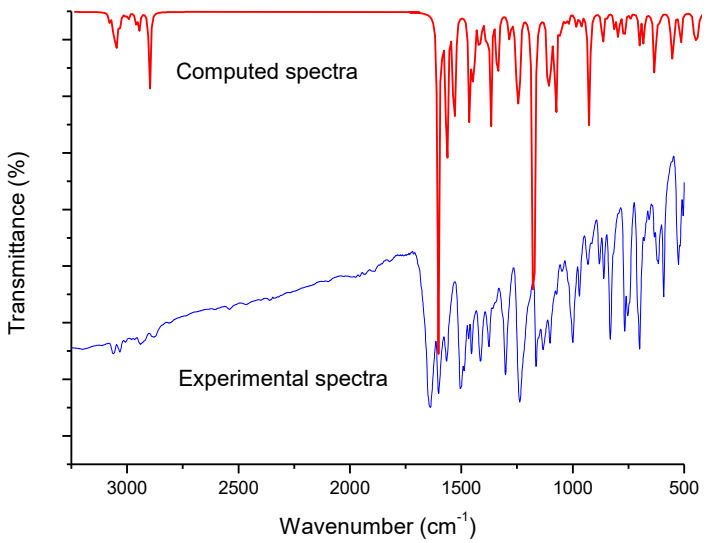

Fig.8. FT-IR spectra of L (calculated and experimental)

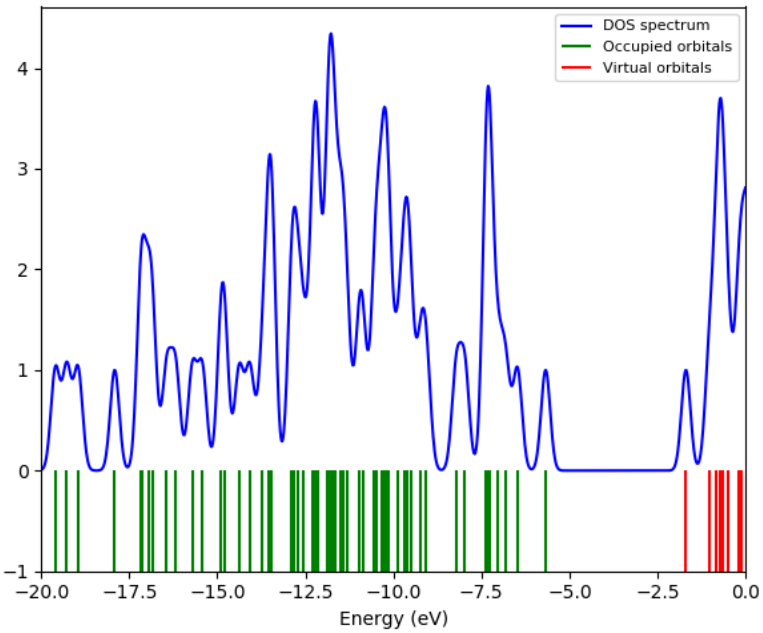

Fig.9. The density of the states of L

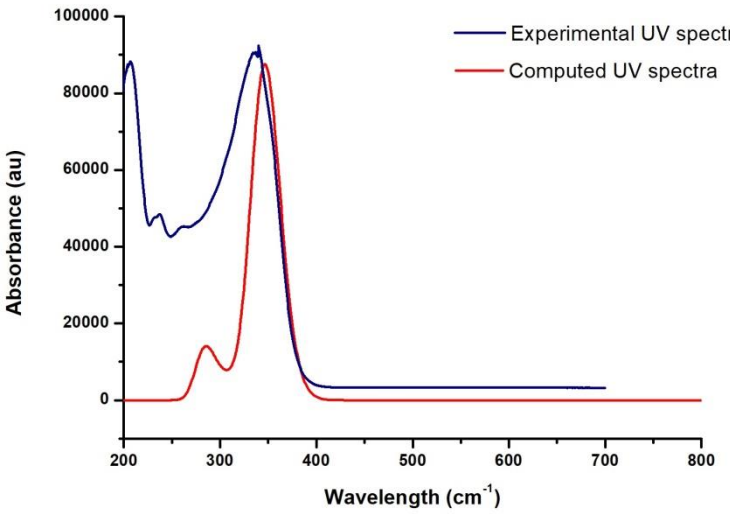

Fig.10. UV-Vis spectra of L (theoretical and experimental)

TD-DFT data provided absorption maxima, oscillator strengths and information on orbitals which are involved in the excitation. The percentage contribution of a molecular orbital (MO) configuration to the resulting excited state TD-DFT wave function is generally obtained as 100 x C x C x 2, where C is the coefficient printed by Gaussian for each excitation. The major absorption features, which are used to understand the electronic transition, such as, absorption wavelength (nm), oscillator strength (f), major transition and assigned charge transfer are listed in Table 4. Electronic spectrum of L recorded in ethanol showed sharp and intense bands at 331 and 231 nm which were attributed to $n \rightarrow \pi^*$ and $\pi \rightarrow \pi^*$ transitions, respectively. The spectrum displayed bands in this range due to the non-bonding electrons present on the nitrogen of the azomethine group of the Schiff base. The theoretical absorption bands in ethanol were obtained at 346.29, 308.38 and 301.08 nm with an oscillator strength of 1.206, 0.053 and 0.018, respectively. Similar bands were observed in experimental spectrum. The IEF-PCM calculations revealed that the absorption bands in ethanol have slight red-shifts compared to those obtained in the gas phase calculations made by TD-DFT method and these are very close to the experimental counterpart.

Surfaces of the frontier orbitals were drawn to understand the bonding scheme of the compound. Here, six important molecular orbitals (MO) were examined. The third, second highest and highest occupied MOs are represented, respectively, by HOMO-2, HOMO-1 and HOMO. The lowest, second and third lowest unoccupied MOs are denoted as

LUMO, LUMO+1 and LUMO+2, respectively. The topologies of frontier orbitals can be seen in Fig.11. The low-energy bands are mainly described by the HOMO to LUMO, HOMO-2 to LUMO and HOMO-1 to LUMO transitions. These absorption peaks appear significantly more intense than the peak due to HOMO-1 to LUMO+1 transition. The overlap between the π and π^* orbitals involved in the electronic transitions is a major requirement to increase oscillator strengths (i.e., to increase band intensities). Among these, HOMO to LUMO transitions exhibit relatively high oscillator strengths, mainly due to better overlapping of these orbitals. This observation is well explained by the HOMO-LUMO contours; here both MOs are distributed on the pyrazolone-and phenyl rings adjacent to azomethine group. The excellent overlap of HOMO and LUMO makes the transition more intense with high oscillator strength.

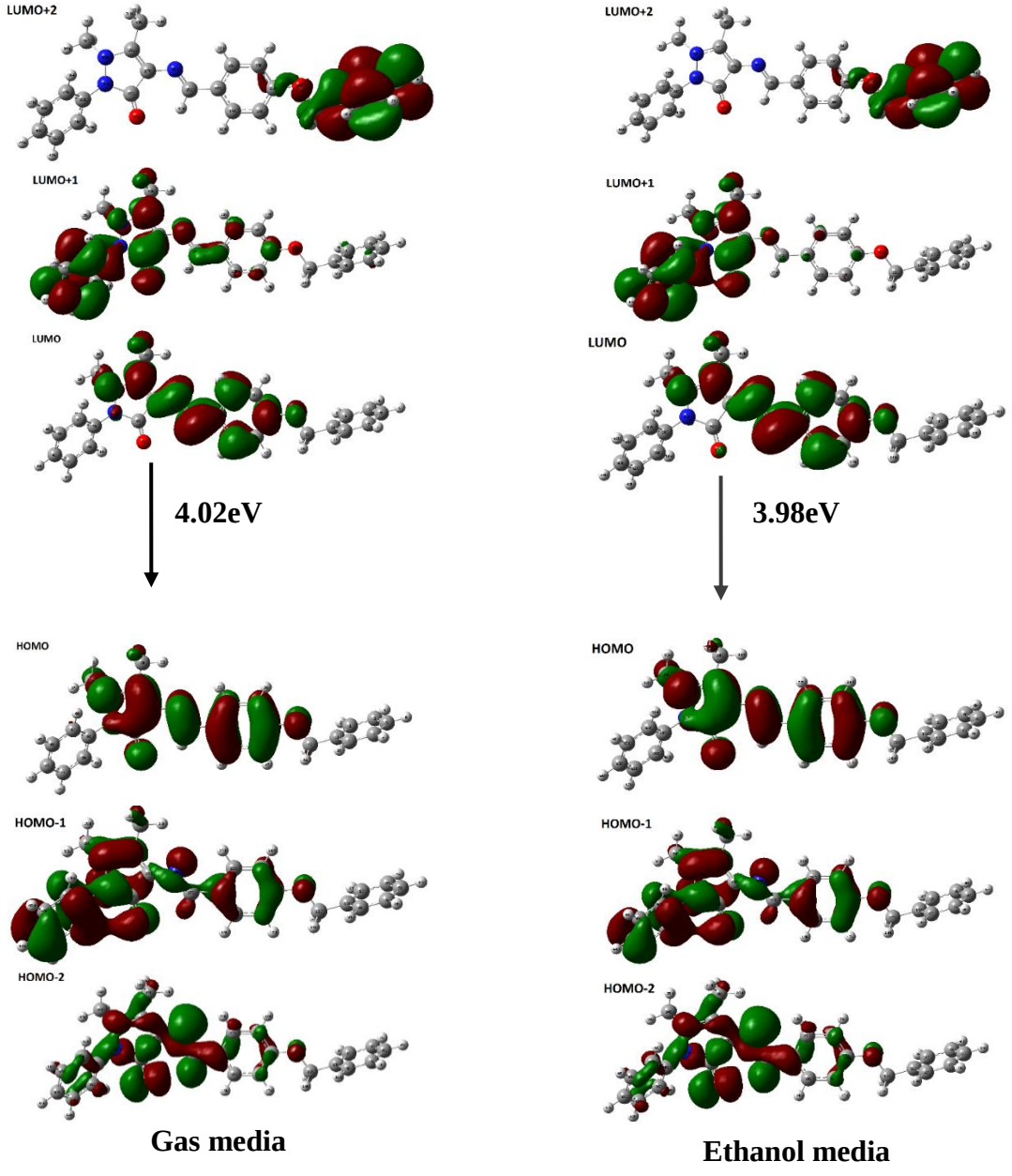

Fig.11. Electronic scheme showing the topology of frontier orbitals involved in the first π-π* transitions of L

Table 4. Theoretical absorption wavelengths λ (nm) and oscillator strengths of L in the gas- and ethanol media at the B3LYP/6-311++G (d,p) level of theory

	Energy (cm^{-1})	Wavelength (nm)	Oscillator Strength	Major contributions
Ethanol	28877.87	346.29	1.206	HOMO->LUMO (97%)
	32427.52	308.38	0.053	H-2->LUMO (62%), H-1->LUMO (31%)
	33213.91	301.08	0.018	HOMO->L+1 (93%)
	34902.03	286.52	0.021	H-2->LUMO (17%), H-1->LUMO (33%), HOMO->L+4 (30%)
	35244.01	283.74	0.155	H-2->LUMO (12%), H-1->LUMO (30%), HOMO->L+4 (32%)
	35469.04	281.94	0.007	HOMO->L+3 (87%)
Gas	30902.33	323.60	1.035	HOMO->LUMO (96%)
	32890.48	304.04	0.0011	H-2->LUMO (66%), H-1->LUMO (27%)
	33636.55	297.30	0.008	HOMO->L+1 (95%)
	34753.62	287.74	0.0004	HOMO->L+2 (95%)
	35929.58	278.32	0.015	H-1->LUMO (16%), HOMO->L+3 (12%), HOMO->L+4 (37%), HOMO->L+5 (11%)
	36641.77	272.91	0.1444	H-2->LUMO (14%), H-1->LUMO (42%), HOMO->L+4 (30%)

3.2.5. Molecular Electrostatic Potential (MEP)

The molecular electrostatic potential (MEP) map is a plot of electrostatic potential mapped on to the constant electron density surface. Interpretation of MEP maps plays a key role in the identification of active sites in the molecule and it can be used to visualize and locate the reactive sites for electrophilic and nucleophilic

attack. It has applications in chemical bonding and in the synthesis of new compounds. Molecular Electrostatic Potential (MEP) was elucidated using the B3LYP/ 6-311++G(d,p) method to examine the reactive sites of the novel Schiff base ligand. The MEP of the L with the same level of theory is shown in Fig.11 (A). The negative regions (red) are mainly localized over the oxygen atom of the C=O group on the pyrazolone ring. Hence, this atom is the most reactive site for the electrophilic attack. FMO contours also support this result. HOMO contours can be seen over this C=O group while LUMO contours are not seen. The positive regions (blue) are localized over the H-atoms of the phenyl- and methyl groups, which are the reactive sites for nucleophilic attack. When the MEP of optimized geometry is examined, it can be seen that oxygen atom of keto group of the pyrazolone ring (most negative region) and H- atoms of methyl- and phenyl groups on pyrazolone moiety (most positive region) are encoded regions and give equivalent results to the partial charge values obtained by Hirshfeld population analysis. Molecular structure and surface extrema are plotted in Fig.11 (B) and energy values of each surface extrema and their Cartesian coordinates are given in Table 5. Red and blue spheres correspond to surface maxima and minima, respectively.

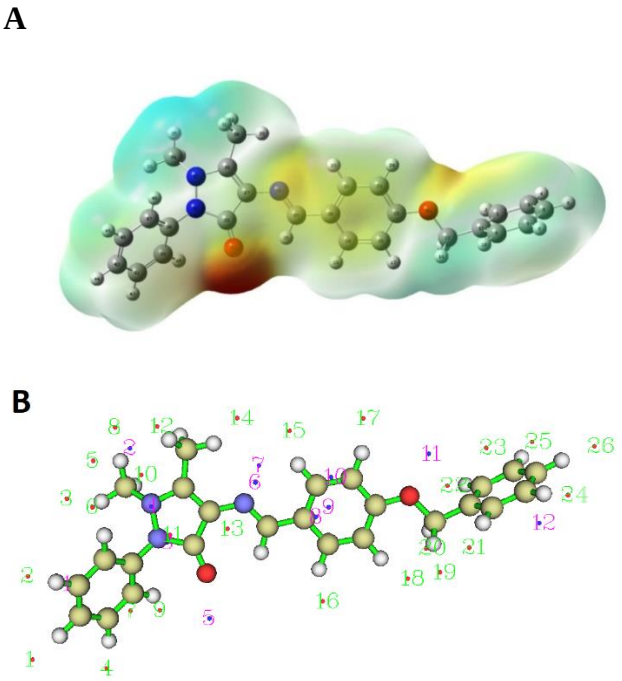

Fig.11.(A). Molecular electrostatic potentials (MEP) 3D mapped on the electron density surface of L; (B). Molecular structure and surface extrema.

Minimum 5(-43.16kcal/mol) is the global minimum on the surface. The large negative value is owing to the lone pair of electrons on oxygen. Maximum 8 (24.66kcal/mol) is global maximum arising from the positively charged H35. The MEP at this point is much larger than those at other maxima (where the MEP ranges from 10 to 15kcal/mol) (Table 5). This is because of the presence of nitrogen on the pyrazolone ring, which attracts the electron from H35.

Moreover, surface properties such as surface area, enclosed volume, average value and standard of mapped functions for overall molecular surface are given in Table 6. Local minima and maxima of mapped functions on the surface can also be seen in Table 6.

Table 5. Quantitative analysis of molecular surface of L

The number of surface minima: 12						
Sl No.	a.u.	eV	kcal/mol	X	Y	Z
1	-0.01999	-0.54386	-12.5418	-8.6846	-0.96607	-1.11623
2	0.02411	0.656079	15.12955	-5.52255	3.951808	-2.06783
3	-0.01317	-0.35843	-8.26549	-4.71862	-0.02365	-2.29753
4	-0.01134	-0.30844	-7.11285	-4.62239	1.409078	2.013036
5	**-0.06879**	**-1.87176**	**-43.1637**	**-3.40207**	**-3.19827**	**-0.19382**
6	-0.03979	-1.08266	-24.9668	-0.66082	1.623099	1.721559
7	-0.03782	-1.02926	-23.7354	-0.50164	2.344626	-1.20809
8	-0.02735	-0.74428	-17.1634	1.356252	-0.03166	1.930148
9	-0.02732	-0.74354	-17.1465	1.881086	0.238874	2.036793
10	-0.02639	-0.71799	-16.5572	2.245565	1.405443	-1.83931
11	-0.04454	-1.21198	-27.949	6.032039	1.583489	0.619086
12	-0.01913	-0.52054	-12.0039	9.922552	-1.79863	-0.47572
The number of surface maxima: 26						
Sl No.	a.u.	eV	kcal/mol	X	Y	Z
1	0.022626	0.615675	14.19781	-10.1591	-3.47632	1.187112
2	0.025051	0.681669	15.71967	-9.36536	-0.31817	3.196317
3	0.027404	0.745691	17.19606	-8.11795	2.344626	-0.57153
4	0.020481	0.557311	12.85191	-7.9104	-4.53471	-1.65816
5	0.028895	0.786276	18.13198	-6.97041	3.675769	-1.38036
6	0.026338	0.716701	16.52752	-6.73061	1.757872	2.421516
7	-0.02606	-0.70923	-16.3553	-6.12652	-2.28568	1.539941
8	**0.039298**	**1.069366**	**24.66018**	**-5.6825**	**4.69187**	**0.187327**
9	0.01004	0.273215	6.300486	-5.53827	-2.6892	-2.72211
10	0.026925	0.732674	16.89589	-5.36635	2.873803	-3.05748
11	0.000531	0.014449	0.333201	-4.17802	0.252168	1.554564
12	0.031741	0.863713	19.91771	-4.22961	4.579149	-1.45127
13	-0.0111	-0.30216	-6.96796	-2.20468	0.093814	-1.93179
14	0.015325	0.417011	9.616506	-0.95464	4.186531	0.823074
15	0.011768	0.320222	7.384493	0.926872	3.362413	0.71491
16	0.016659	0.453301	10.45337	1.065463	-3.37727	-1.13572
17	0.014955	0.406933	9.384116	3.789317	3.328221	0.913089
18	0.030708	0.835608	19.2696	4.516005	-3.06655	-0.86237
19	0.025332	0.689309	15.89587	5.605306	-2.90344	1.384732
20	0.024792	0.674618	15.55707	5.551615	-2.08819	-2.38662
21	0.025678	0.698725	16.11299	6.690038	-2.1056	2.839969
22	0.02463	0.670205	15.45532	6.92925	0.249056	-3.21186
23	-0.02232	-0.60741	-14.0072	8.233172	1.423769	0.72597
24	0.025355	0.689955	15.91076	10.46241	-0.83287	3.490079
25	0.02534	0.689528	15.90092	10.58914	1.409718	-2.70965
26	0.025634	0.697535	16.08555	12.33829	0.76385	0.596604

Table 6. Summary of surface analysis of L

Volume	510.79562Å^2
Estimated density according to mass and volume	1.2921 g/cm^3
Minimal value	-43.16374 kcal/mol
Maximal value	24.66018 kcal/mol
Overall surface area	458.27601Å^2
Positive surface area	232.80628 Å^2
Negative surface area	225.46973 Å^2

3.2.6. Fukui function and dual descriptor

Fukui function is a real space function, which is commonly studied using visualization of isosurface. It is used to predict where the most electrophilic- and nucleophilic sites of a molecule are present. The countour graph of nucleophilic- electrophilic Fukui function and dual descriptor were generated and are given in Fig. 12 A, B and C, respectively.

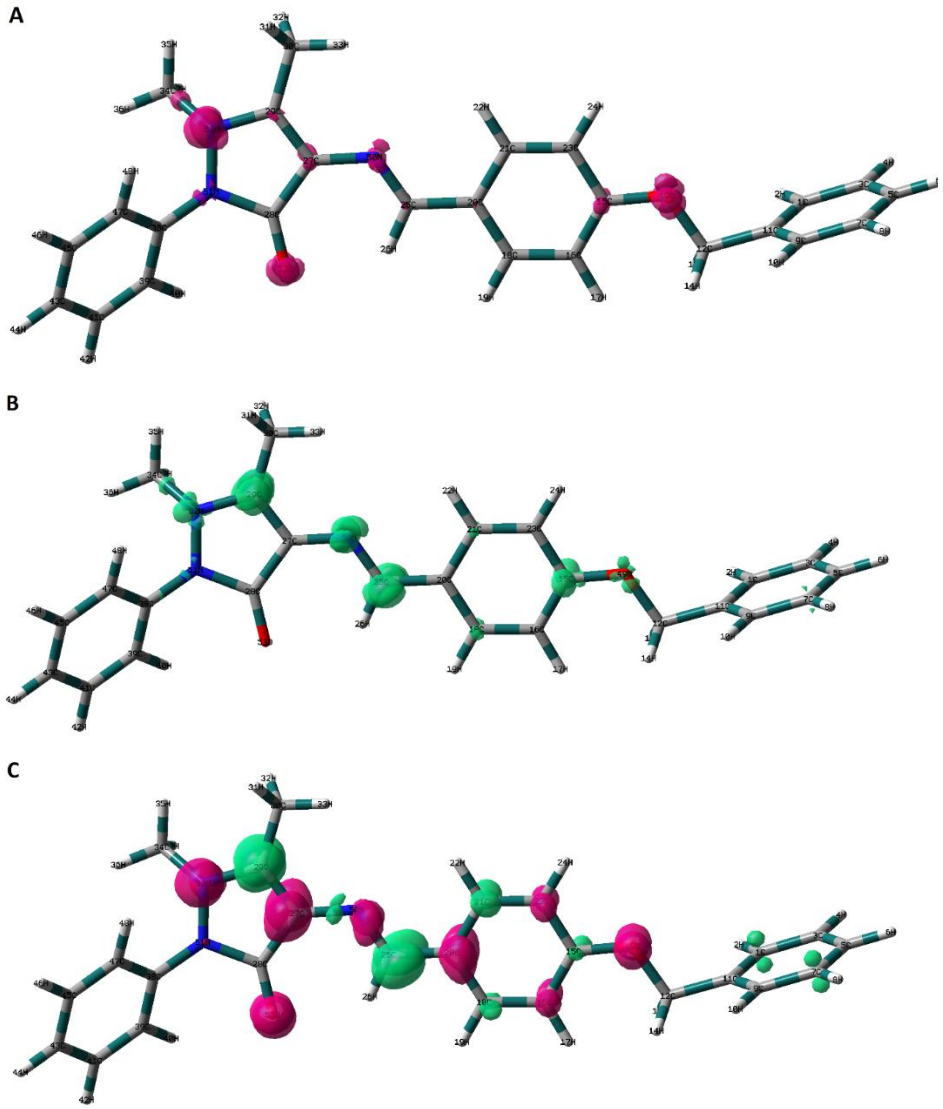

Fig.12. The countour graph of nucleophilic Fukui function (A), electrophilic Fukui function (B) and dual descriptor (C) of L

From Fig.12, it is clear that most of f^- functions are localized on O53, N52, N50, C27 and O49 and *ipso* and *meta* carbon atoms of the central phenyl ring. Therefore, these positions of the Schiff base (L) ligand are reactive sites for the electrophilic attack and this observation is in

agreement with the MEP map. While in the case of *f*+ function, most of the contours are focused on C29, C25, C15 and N50 indicating that the nucleophilic attack can take place on these sites. Fig.12(C) indicates dual descriptor contours. The region covered by negative isosurfaces (red) suggest that nitrogen and oxygen are activated for the electrophilic attack; this conclusion is in well agreement with Fukui function. The region covered by positive isosurfaces (green) suggest the possibility of a nucleophilic attack. From Fig.12, it can be concluded that C29 and C25 are major nucleophilic sites.

The quantitative nature of reactive sites of compound can be estimated by "condensed" version of Fukui function and dual descriptor. In the condensed version, the amount of electron density distribution around an atom can be represented by population number. For this purpose, we have used the Hirshfeld charge, which is one of the most recommended method for population analyses and highly suitable to calculate condensed Fukui function and dual descriptor. The atomic charges for all atoms in the Schiff base in its N, N+1 and N-1 electronic states and condensed f^- and f^+ and dual descriptor (Δf) are listed in Table 7. It has been reported that if $\Delta f > 0$, the site is favourable for a nucleophilic attack, whereas if $\Delta f < 0$, the site is favourable for an electrophilic attack.

The order of Nucleophilic reactivity is: 25(C) > 29(C) > 50(N) > 15(C) > 31(H)

Electrophilic reactivity is: 53(O) > 52(N) > 27(C) > 49(O) > 15(C) > 50(N)

The attack for free radicals is: 38(C) > 11(C)> 10(H) > 47(C) > 40(H) The dual descriptor order is: 25(C)> 29(C)> 31(H)> 1(C)> 7(C)……. 49(O) > 27(C) > 52(N) > 53(O)

Table 7 shows that for f^-, the two highest values occur at 53 (O) and 52 (N). Therefore, these atoms are favourable sites for the electrophilic attack. For f^+, the two highest values occur at C25 and C29. Therefore, these atoms are favourable sites for nucleophilic attack. The central part of the Schiff base which includes the phenyl- and pyrazolone rings is favourable for nucleophilic-, electrophilic- and radical attacks. The dual descriptors also show a similar trend. For dual descriptor, the most positive values occur at C25 and C29, suggesting that they are the most unfavourable sites for the electrophilic attack. O53 and N52 have large negative values and hence are favoured by the attack of electrophilic reactants. Lower values of f^- and f^+, occur on atoms of two phenyl rings at the end of the molecule, Fukui functions for sites located on two end phenyl ring moieties mainly have low indices. These sites are susceptible to neither nucleophilic- nor electrophilic attack. Reactions on sites with the high value of Fukui functions are frontier-controlled, while on those with low Fukui functions and high net charge values are charge-controlled.

Table 7. The atomic charges for all atoms in L in its N, N+1 and N-1 electronic states and condensed f^- and f^+ and dual descriptor (Δf)

Atom	N	N+1	N-1	f^+	f^-	f^0	Δf
1(C)	-0.035	-0.051	-0.034	0.016	0.001	0.009	0.015
2(H)	0.042	0.033	0.043	0.009	0.000	0.005	0.009
3(C)	-0.037	-0.053	-0.027	0.016	0.010	0.013	0.007
4(H)	0.042	0.030	0.050	0.012	0.008	0.010	0.004
5(C)	-0.036	-0.055	-0.022	0.019	0.014	0.017	0.005

6(H)	0.042	0.028	0.052	0.014	0.010	0.012	0.004
7(C)	-0.037	-0.061	-0.027	0.023	0.010	0.017	0.013
8(H)	0.042	0.027	0.050	0.015	0.008	0.012	0.006
9(C)	-0.036	-0.045	-0.034	0.009	0.002	0.006	0.007
10(H)	0.041	0.035	0.043	0.006	0.001	0.004	0.005
11(C)	-0.002	-0.004	-0.011	0.002	-0.008	-0.003	0.010
12(C)	0.033	0.026	0.040	0.007	0.007	0.007	0.000
13(H)	0.035	0.024	0.045	0.010	0.010	0.010	0.000
14(H)	0.035	0.027	0.045	0.008	0.010	0.009	-0.002
15(C)	0.076	0.034	0.122	0.042	0.046	0.044	-0.004
16(C)	-0.069	-0.092	-0.033	0.024	0.035	0.030	-0.012
17(H)	0.037	0.020	0.059	0.017	0.022	0.019	-0.004
18(C)	-0.031	-0.063	0.004	0.032	0.035	0.034	-0.003
19(H)	0.044	0.025	0.063	0.018	0.020	0.019	-0.001
20(C)	-0.021	-0.038	0.014	0.018	0.035	0.026	-0.017
21(C)	-0.028	-0.058	-0.003	0.029	0.025	0.027	0.004
22(H)	0.039	0.022	0.054	0.017	0.015	0.016	0.001
23(C)	-0.053	-0.077	-0.020	0.023	0.034	0.028	-0.010
24(H)	0.044	0.025	0.067	0.019	0.023	0.021	-0.004
25(C)	0.039	-0.031	0.075	0.070	0.036	0.053	0.034
26(H)	0.031	0.006	0.047	0.025	0.016	0.020	0.009
27(C)	-0.018	-0.036	0.030	0.018	0.048	0.033	-0.030
28(C)	0.134	0.125	0.157	0.009	0.023	0.016	-0.014
29(C)	0.047	-0.011	0.083	0.058	0.036	0.047	0.022
30(C)	-0.078	-0.095	-0.066	0.017	0.012	0.014	0.005
31(H)	0.041	0.006	0.060	0.035	0.019	0.027	0.017
32(H)	0.041	0.020	0.059	0.021	0.017	0.019	0.004
33(H)	0.046	0.034	0.055	0.012	0.009	0.010	0.002
34(C)	-0.031	-0.051	-0.011	0.020	0.020	0.020	0.001
35(H)	0.046	0.027	0.062	0.020	0.015	0.017	0.004
36(H)	0.041	0.020	0.058	0.021	0.017	0.019	0.004
37(H)	0.035	0.003	0.058	0.033	0.023	0.028	0.010
38(C)	0.040	0.044	0.032	-0.004	-0.008	-0.006	0.004
39(C)	-0.040	-0.046	-0.035	0.006	0.005	0.006	0.000
40(H)	0.044	0.039	0.048	0.005	0.004	0.005	0.001
41(C)	-0.034	-0.048	-0.018	0.014	0.016	0.015	-0.002
42(H)	0.043	0.031	0.056	0.012	0.013	0.012	-0.001
43(C)	-0.044	-0.066	-0.020	0.021	0.024	0.023	-0.003
44(H)	0.040	0.023	0.056	0.017	0.016	0.016	0.001
45(C)	-0.040	-0.053	-0.024	0.014	0.016	0.015	-0.002
46(H)	0.041	0.026	0.054	0.015	0.013	0.014	0.002
47(C)	-0.052	-0.057	-0.048	0.005	0.004	0.005	0.000
48(H)	0.036	0.026	0.040	0.010	0.004	0.007	0.006
49(O)	-0.126	-0.145	-0.079	0.018	0.047	0.033	-0.029
50(N)	-0.149	-0.192	-0.108	0.043	0.041	0.042	0.003
51(N)	0.000	-0.008	0.017	0.007	0.017	0.012	-0.010
52(N)	-0.003	-0.025	0.054	0.022	0.057	0.040	-0.035
53(O)	-0.296	-0.317	-0.229	0.021	0.067	0.044	-0.046

3.2.7. Hirshfeld Surface and Fingerprint Plot Analysis on Schiff base

Hirshfeld surface analysis and the associated two-dimensional fingerprints calculations were performed using Crystal Explorer 17.5 [16]. This method is used to reveal weak interactions between monomers in the complex- or in molecular crystals. The analysis of the 2D fingerprint plot with Hirshfeld surface provides an idea of the interactions within the crystal structures in a quantitative manner. The Hirshfeld surface parameters, d_e and d_i are described to visualize the properties of a molecule on the Hirshfeld surface. The term d_e and *di,* are the distances from the surface to the nearest nucleus external to the surface and internal to the surface, respectively [17]. The normalised contact distance, d_{norm} that include d_e and d_i and Van der Waals radius of an atom are represented by Eq.1 [18]. A small value of d_{norm} indicates close intermolecular contact and implies evident interaction.

$$d_{norm} = \frac{d_i - r_i^{vdw}}{r_i^{vdw}} + \frac{d_e - r_e^{vdw}}{r_e^{vdw}} \quad (1)$$

In Hirshfeld surface, intermolecular contacts closer than the sum of Van der Waals radii will be highlighted in red on the d_{norm} surface. Longer contacts are represented by blue and contacts around the sum of Van der Waals radii are plotted in white (Fig.13).

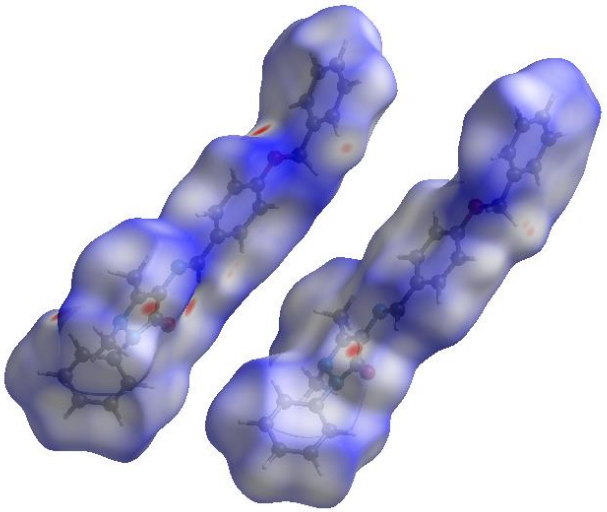

Fig.13. The Hirshfeld surface of the compound mapped with $d_{norm,}$ the red spots represent C – H···N donor-acceptor interactions

Fingerprint plot of Hirshfeld surface analysis [19] is handy for investigating the non-covalent interactions in molecular crystals. The fingerprint plot for the title compound is presented in Fig.14. In this plot, X and Y correspond to d_i and d_e, respectively. The H···H interactions appear in the middle of the scattered points in the two-dimensional fingerprint plots with overall Hirshfeld surface of 54.3%. The H···C/C···H contacts are given in S6. These contacts are represented as regions in the bottom right ($d_e < d_{i,}$ C···H) of the related plots. It can be seen that there is one spike at the bottom left of the plot (i.e., short d_i and d_e) in H···N/N···H and H···O/O···H contacts. This observation suggests that Schiff base behaves as H-bond acceptor rather than hydrogen bond donor (the lower spike, $d_i > d_e$).

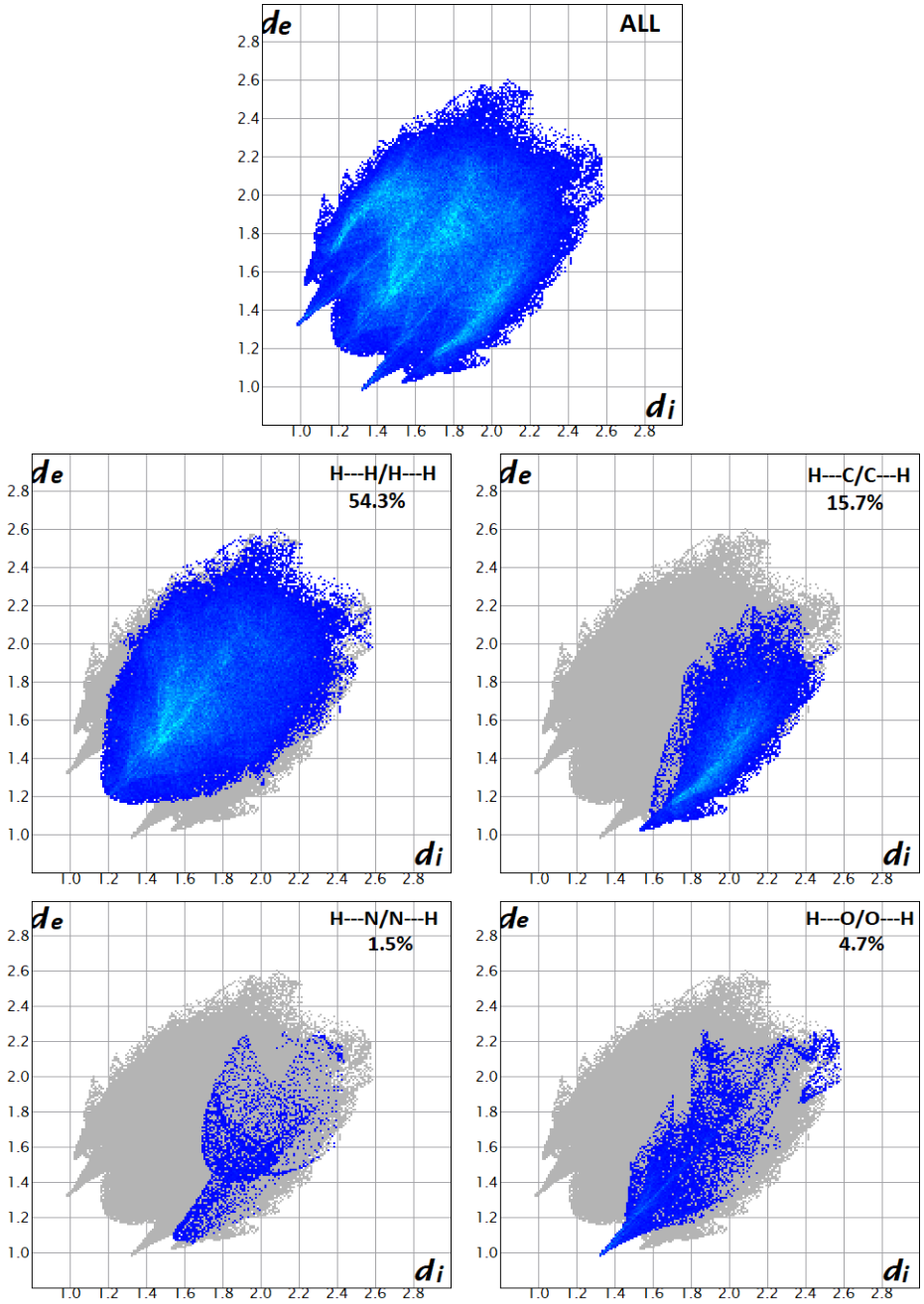

Fig.14. Fingerprint plots of L and H···H, H···C, H···N and H···O contacts, showing the percentages of contacts contributing to the total Hirshfeld surface area

3.2.8. Non-Linear Optical (NLO) Properties

DFT has been extensively used as an effective method to investigate organic NLO materials. In this work, the polar properties of the Schiff base, L are also calculated at B3LYP/6-311++G(d,p) level using the Gaussian 09W program package. The electric dipole moment, polarizability and first-order hyperpolarizability of L are listed inTable 8. Urea is one of the prototypical molecules used in the study of the NLO properties of the molecular systems. Therefore, it was often used as a threshold value for comparative purposes. The calculated values of α_{tot} and β_{tot} for the title compound are, respectively, 5.59×10^{-23} and 1.04×10^{-29} esu, which are about 11.4 and 13.1 times higher than the α_{tot} and β_{tot} values of urea, which are, respectively, 4.91×10^{-24} and 7.91×10^{-31}esu obtained by the same method. Therefore, the title compound is a right candidate for NLO applications.

Table 8. The electric dipole moment, polarizability and first-order hyperpolarizability of L calculated at B3LYP/6-311++G(d,p) level

Dipole moment	**L**	**urea**	**First-order hyperpolarizability**	**L**	**urea**
μ_x	-5.5×10^{-19}	0.00	β_{xxx}	7.05×10^{-30}	2.1×10^{-36}
μ_y	2.36×10^{-18}	-4.48×10^{-18}	β_{xxy}	3.49×10^{-32}	-3.1×10^{-31}
μ_z	-2.5×10^{-19}	2.50×10^{-21}	β_{xyy}	2.57×10^{-30}	-3.9×10^{-36}
μ_{tot}	2.44×10-[18]	4.48×10^{-18}	β_{yyy}	-7.4×10^{-32}	7.67×10^{-31}
Polarizability	**L**	**urea**	β_{xxz}	5.29×10^{-31}	-1×10^{-35}
α_{xx}	8.88×10^{-23}	5.46×10^{-24}	β_{xyz}	-8.2×10^{-31}	5.17×10^{-35}
α_{xy}	-2.4×10^{-25}	-8.2×10^{-31}	β_{yyz}	-6.6×10^{-32}	-7.3×10^{-35}
α_{yy}	4.48×10^{-23}	5.71×10^{-24}	β_{xzz}	6.74×10^{-31}	-1.5×10^{-36}
α_{xz}	-1.3×10^{-24}	-3.5×10^{-29}	β_{yzz}	-1.6×10^{-31}	3.3×10^{-31}
α_{yz}	1.41×10^{-24}	1.69×10^{-28}	β_{zzz}	7.76×10^{-31}	-2.4×10^{-34}
α_{zz}	3.41×10^{-23}	3.56×10^{-24}	β_{tot}	1.04×10^{-29}	7.91×10^{-31}
α_{tot}	5.59×10^{-23}	4.91×10^{-24}			

4. Conclusions

A novel Schiff base ligand, 4-(4-benzyloxybenzalidene)amino-2,3-dimethyl-1-phenyl-3-pyrazol-5-one (L) was synthesized and structurally characterized by elemental analysis, SCXRD analysis, UV–VIS absorption, FT-IR, ESI-MS, ^{13}C- and ^{1}H NMR techniques. It was stable up to 296^{0}C. The analysis of XRD data revealed its polycrystalline, orthorhombic structure with a space group of P 21 21 21. The Hirshfeld surface and corresponding Fingerprint plot of the compound revealed weak interactions between monomers in in the molecular crystal of L. DFT calculations at B3LYP/6-311++G(d,p) provided detailed information of its molecular structure, electronic properties vibrational spectra, chemical reactivity, UV-filter activity and NLO effects. The results show that L can act as both UV-filter and NLO material and can be used as a promising optical material in future.

References

[1] J. Lu, H. Guo, X. Zeng, Y. Zhang, P. Zhao, J. Jiang, L. Zang, Synthesis and characterization of unsymmetrical oxidovanadium complexes: DNA-binding, cleavage studies and antitumor activities, Journal of inorganic biochemistry 112 (2012) 39-48.

[2] S. Sumathi, P. Tharmaraj, C. Sheela, R. Ebenezer, Synthesis, spectral, NLO studies, and antimicrobial activities of curcumin diketimine metal complexes, Journal of Coordination Chemistry 65(3) (2012) 506-515.

[3] M.-F. Wang, Z.-Y. Yang, Z.-C. Liu, Y. Li, T.-R. Li, M.-H. Yan, X.-Y. Cheng, Synthesis and crystal structure of a Schiff base derived from two similar pyrazolone rings and its rare earth complexes: DNA-binding and antioxidant activity, Journal of Coordination Chemistry 65(21) (2012) 3805-3820.

[4] R.M. Issa, A.M. Khedr, H.F. Rizk, UV–vis, IR and 1H NMR spectroscopic studies of some Schiff bases derivatives of 4-aminoantipyrine, Spectrochimica Acta Part A: Molecular and Biomolecular Spectroscopy 62(1-3) (2005) 621-629.

[5] T. Bansal, M. Singh, G. Mishra, S. Talegaonkar, R.K. Khar, M. Jaggi, R. Mukherjee, Concurrent determination of topotecan and model permeability markers (atenolol, antipyrine, propranolol and furosemide) by reversed phase liquid chromatography: utility in Caco-2 intestinal absorption studies, Journal of Chromatography B 859(2) (2007) 261-266.

[6] Y. Li, H. Zhang, Y. Liu, F. Li, X. Liu, Synthesis, characterization, and quantum chemical calculation studies on 3-(3-nitrophenylsulfonyl) aniline, Journal of Molecular Structure 997(1-3) (2011) 110-116.

[7] R.A. Gaussian09, 1, mj frisch, gw trucks, hb schlegel, ge scuseria, ma robb, jr cheeseman, g. Scalmani, v. Barone, b. Mennucci, ga petersson et al., gaussian, Inc., Wallingford CT 121 (2009) 150-166.

[8] N.M. O'Boyle, M. Banck, C.A. James, C. Morley, T. Vandermeersch, G.R. Hutchison, Open Babel: An open chemical toolbox, Journal of cheminformatics 3(1) (2011) 33.

[9] C. Lee, W. Yang, R.G. Parr, Development of the Colle-Salvetti correlation-energy formula into a functional of the electron density, Physical review B 37(2) (1988) 785.

[10] M.A. Spackman, D. Jayatilaka, Hirshfeld surface analysis, CrystEngComm 11(1) (2009) 19-32.

[11] S.T.D. R. Biju bennie, M. Sivasakthi, S. Asha Jeba Mary, M. Seethalakshmi, S. Daniel Abraham, C. Joel and R. Antony, Synthesis, Spectral Characterization and Antimicrobial Studies of Schiff base Transition Metal Complexes derived from Cuminaldehyde and 4-Aminoantipyrine, Chem Sci Trans., 3(3) (2014) 937-944.

[12] R.J. Anderson, D.J. Bendell, P.W. Groundwater, Organic spectroscopic analysis, Royal Society of Chemistry2004.

[13] N.E. Eltayeb, F. Şen, J. Lasri, M.A. Hussien, S.E. Elsilk, B.A. Babgi, H. Gökce, Y. Sert, Hirshfeld Surface analysis, spectroscopic, biological studies and molecular docking of (4E)-4-((naphthalen-2-yl) methyleneamino)-1, 2-dihydro-2, 3-dimethyl-1-phenylpyrazol-5-one, Journal of Molecular Structure 1202 (2020) 127315.

[14] N.K.I.S.o.I.a.C.C.W. and, p.-. Sons: New York, Infrared Spectra of Inorganic and Coordination Compounds;, Wiley and Sons: New York, (1986) 248-249].

[15] R.G. Parr, W. Yang, Density functional approach to the frontier-electron theory of chemical reactivity, Journal of the American Chemical Society 106(14) (1984) 4049-4050.

[16] V. CrystalExplorer, 3.0, SK Wolff, DJ Grimwood, JJ McKinnon, MJ Turner, D, Jayatilaka, MA Spackman, University of Western Australia (2012).

[17] J.J. McKinnon, M.A. Spackman, A.S. Mitchell, Novel tools for visualizing and exploring intermolecular interactions in molecular crystals, Acta Crystallographica Section B: Structural Science 60(6) (2004) 627-668.

[18] J.J. McKinnon, D. Jayatilaka, M.A. Spackman, Towards quantitative analysis of intermolecular interactions with Hirshfeld surfaces, Chemical Communications (37) (2007) 3814-3816.

[19] M.A. Spackman, J.J. McKinnon, Fingerprinting intermolecular interactions in molecular crystals, CrystEngComm 4(66) (2002) 378-392.

[20] Y.-X. Sun, Q.-L. Hao, W.-X. Wei, Z.-X. Yu, L.-D. Lu, X. Wang, Y.-S. Wang, Experimental and density functional studies on 4-(3, 4-dihydroxybenzylideneamino) antipyrine, and 4-(2, 3, 4-trihydroxybenzylideneamino) antipyrine, Journal of Molecular Structure: THEOCHEM 904(1-3) (2009) 74-82.

CHAPTER XI

REACTIVITY AND NLO STUDIES OF N(4)-DISUBSTITUTED THIOSEMICARBAZONES AND ISONICOTINOYLHYDRAZONES

1. Introduction

Theoretical chemistry utilizes various efficient computational programs to quantitatively calculate accurate structures, thermochemical properties and interactions of molecules. There are various methods in computational chemistry, such as *ab initio*, semi-empirical and density functional theory (DFT) for theoretically predicting the structural characteristics of molecules. DFT is one of the most popular and versatile method among them. It has been recognized as a promising auxiliary tool in investigating the interactions and biological- and chemical properties of biologically active compounds. It has been proved to be a reliable and potent tool with accuracy and cost effectiveness which account for its great success in the study of large systems.

In this study, theoretical geometry optimization was done by DFT/B3LYP level with 6-311++G(d,p) Basis set in the ground state using the Gaussian 09W program and GAUSS-VIEW 5.0.9 visualization program. The conformational studies were done with the aim of providing comprehensive structures, reactivities and stabilities of the ligands. The structural- and geometrical properties, frontier molecular orbital calculations, molecular electrostatic potential, chemical reactivity and NLO activity of most of the ligands synthesized during the present research program are performed and discussed in this chapter.

2. Applications of DFT method

2.1. Geometry optimization

The process of optimization of compound led to a confirmer that has the lowest energy and highest stability. This was evident from the frequency calculation, which showed no imaginary frequencies. Geometrical optimization was done by using experimental and X-ray diffraction data of the molecules, whenever possible. DFT method, proposed by Hohenberg and Kohn [1], was used for the gas phase structure optimization process.

2.2. GAUSSVIEW–GUI for GAUSSIAN 09W program

It is a well featured graphical user interface for GAUSSIAN 09W program [2]. One can prepare input by using GAUSS-VIEW 5.0.9 visualization program [3] and submit it to Gaussian for processing and can explain the output by Gaussian. GAUSS-VIEW can graphically portray the results of various calculations, such as molecular orbitals, atomic charges, surfaces from the electron density, electrostatic potential, NMR shielding density and many other properties. Surfaces may be displayed in solid-, translucent- and wire mesh modes.

2.3. HOMO and LUMO analysis

The highest occupied molecular orbital (HOMO) and lowest unoccupied molecular orbital (LUMO) are the two important molecular orbitals which identify the chemical behaviour of a compound. The analysis of HOMO–LUMO interaction in a molecule

can be used to describe various chemical properties such as reactivity, stability, biological activity, kinetics and so on of a molecule [4]. Knowledge of HOMO-LUMO energies is used to calculate important reactivity indices of a compound [5]. The small energy gap normally suggests a high chemical reactivity and low kinetic stability of a compound.

2.4. Global descriptors

According to the Koopmans' theorem [6], gas-phase vertical ionization energies (IP) and vertical electron affinities (EA) of the isomers are related to HOMO-LUMO energies through the equations, EA = $-E_{LUMO}$, IP = $-E_{HOMO}$. The potential of a ligand to accept precisely one electron from a donor is referred as electron affinity. Electronegativity (χ) represents the power to attract electrons and is equal to the negative of the chemical potential. By using HOMO and LUMO energy values, global descriptors such as chemical hardness (η), [$\eta = (I - A)/2$], chemical softness (ζ), [$\zeta = 1/2\eta$], chemical potential (μ), [$\mu = (E_{LUMO} + E_{HOMO})/2$] and the global electrophilicity index (ω), [$\omega = \mu^2/2\eta$] can also be calculated.

2.5. Molecular electrostatic potential

The molecular electrostatic potential (MEP) map is a plot of electrostatic potential mapped on a constant electron density surface and can be used to visualize and locate the reactive sites for electrophilic- and nucleophilic attacks as well as biological activity and hydrogen bonding interactions [7]. The MEP at a given point in the

vicinity of a molecule can be expressed in terms of the interaction energy between the electrical charges generated by the molecule's electrons, nucleus and a positive test charge (a proton) located at the same point. MEP maps are colour-coded images of the calculated electron density surface. MEP maps display the charge distributions of the molecules and allow one to see the different charge regions. The charge distribution information is used to determine charge-dependent properties and interactions of molecules with each other. Interpretation of MEP maps plays a key role in the identification of active sites in a molecule. It has applications in chemical bonding and in the synthesis of new compounds. Moreover, MEP can simultaneously display molecular size, shape as well as positive, negative and neutral electrostatic potential regions in terms of colour grading. The order of the electrostatic potential is as follows: red < orange< yellow< green < blue. Negative regions of MEP are rich in electrons and are focused on electronegative atoms. Positive regions are electrons deficient and these sites are mainly around hydrogen atoms.

2.6. Fukui functions

Fukui functions have been widely used for the identification and prediction of the probable reactive sites in DFT calculations. Fukui function is defined as [8];

$$f(r) = \left[\frac{\partial \rho(r)}{\partial N} \right]_{\nu \, S}$$

Here, number of electrons present in a system is represented by the term N, electron density is denoted by ρ and the constant term in the partial derivative, v is the external potential acting on an electron due to all other electrons and nuclei. Generally, the reactive site has a larger value of Fukui function than the other regions. The dual descriptor is another function used to reveal reactive sites. It is defined as the difference between nucleophilic- and electrophilic Fukui functions.

$$\Delta f(r) = f^{+}(r) - f^{-}(r)$$

Fukui function and dual descriptor can be quantified based on population analysis techniques and can be termed as "condensed" version of Fukui function. In the condensed version, the atomic population number is used to represent the amount of electron density distribution around an atom. The condensed Fukui function and dual descriptor for an atom, k can be written as the following 4 equations:

Nucleophilic attack: $f_k^+ = q_k\,(N + 1) - q_k\,(N)$ (1)

Electrophilic attack: $f_k^- = q_k\,(N) - q_k\,(N - 1)$ (2)

Radical attack: $f_k^0 = (q_k(N+1) - q_k(N-1))/2$ (3)

Dual descriptor: $\Delta f(k) = [f_k^+ - f_k^-]$ (4)

where q_k is the electronic population of atom, k in neutral (N), anionic (N+1) or cationic (N-1) chemical species, f^- measures reactivity towards electrophilic attack or the tendency of the compound to donate electrons, whereas f^+ measures reactivity towards nucleophilic attack

or tendency of the compound to accept electrons. Fukui function is a real space function which is commonly studied by visualization of isosurface and are used to predict where the most electrophilic- and nucleophilic sites of a molecule are present. Morrel *et al* [9] have proposed a new dual descriptor, Δf_k for nucleophilicity and electrophilicity. If $\Delta f_k > 0$, the site is electrophilic and if $\Delta f_k < 0$, the site is nucleophilic. If the dual descriptor provides a positive value for a site, it is favourable for a nucleophilic attack and a negative value for electrophilic attack.

2.7. Non-linear optical properties

The π-electron conjugated compounds with asymmetric polarization induced by electron donor and acceptor groups are good candidates for non-linear optical (NLO) applications in optical signal processing, telecommunication, optical computing, optical switching and other photonic technologies [10, 11]. NLO effects originate from the interactions of electromagnetic fields in various media to produce new fields altered in phase, frequency, amplitude or other propagation characteristics from the incident fields [12]. Particles with expansive optical non-linearities have turned into a focal point of the recent research in perspective of their potential applications in different photonic technologies, including, all-optical exchanging and information preparation such as frequency shifting, optical modulation, optical switching, optical logic and optical memory. It has been discovered that organic molecules that exhibit extended π conjugation, in particular, show enhanced second order NLO properties with ultra-

fast response times, lower dielectric constants, better processability characteristics and enhanced NLO responses as compared to the traditional inorganic solids. Hence, the search for novel organic molecules with extended π conjugation, capable of manipulating photonic signals, is currently an intense area of research. DFT has been extensively used as an effective method to investigate organic NLO materials.

The non-linear optical response of an isolated molecule can be derived from its energy terms, which can be written as Taylor expansion concerning uniform external electric field, F,

$$E(F) \equiv E(0) - \mu_0 F - \frac{1}{2}\alpha F^2 - \frac{1}{6}\beta F^3 - \frac{1}{24}\gamma F^4 ...$$

where μ is permanent dipole moment, which is a vector; α is polarizability, which is a matrix (second rank tensor) and β is first-order hyperpolarizability, which is a third rank tensor and known as second-order non-linear optical response coefficient. It can be described by a 3*3*3 matrix. (Hyper) polarizability tensors are directly correlated to the frequency of external field, F. If F has zero-frequency (static electric field), the (hyper) polarizability is known as static or frequency-independent one. The dynamic or frequency-dependent (hyper) polarizabilities correspond to those at external electromagnetic fields with non-zero frequency. For static case, since all of the three indices are exchangeable, the remaining ten components are unique. According to Kleinman symmetry [13], the 27 components of the 3D

matrix can be reduced to ten components for a molecule with no symmetry. The components of β are defined as the coefficients in the Taylor series expansion of the energy in the external electric field. The calculation of the terms, α_{tot} and β_{tot} are defined as follows:

$$\beta_x = \beta_{xxx} + \beta_{xyy} + \beta_{xzz}$$

$$\beta_y = \beta_{yxx} + \beta_{yyy} + \beta_{yzz}$$

$$\beta_z = \beta_{zxx} + \beta_{zyy} + \beta_{zzz}$$

$$\beta_{tot} = \sqrt{\beta_x^2 + \beta_y^2 + \beta_z^2}$$

$$\alpha_{tot} = \frac{\alpha_{xx} + \alpha_{yy} + \alpha_{zz}}{3}$$

Since the values of the polarizabilities (α) and first-order hyperpolarizabilities (β) of Gaussian 09W output are reported in atomic units (a.u.), the calculated values have been converted into electrostatic units (esu) (1 a.u. = 0.1482 × 10^{-24} esu for α; 1 a.u. = 8.6393 × 10^{-33} cm^5/esu for β) [14]. Urea is one of the prototypical molecules used in the study of the NLO properties of molecular systems. Therefore, its μ, α_{tot} and β_{tot} values are used frequently as threshold ones for comparative purposes. The μ, α_{tot} and β_{tot} of urea are 1.3732 Debye, 4.91×10^{-24} and 7.91×10^{-31} esu, respectively, as obtained by B3LYP/6-311++G(d,p) method.

3. Computational details

To obtain more information of chemical interest, the geometrical parameters of the compounds in the ground state was optimized by DFT/B3LYP levels with 6-311++G(d,p) Basis set using the Gaussian 09W program and GAUSS-VIEW 5.0.9 visualization program. The starting molecular structure of the compound was obtained from the XRD data [RES file format was converted to GJF file format using Open Babel utility] or by drawing structures using Gauss view program. B3LYP [15] represents Becke's three parameters hybrid functional method with Lee-Yang-Parr (LYP) correlation functional which is best for predicting results of molecular geometry and vibrational wavenumbers of a moderately large molecule. In order to know more about the compounds, HOMO–LUMO energy gap, global reactivity descriptors, MEP map and local reactivity descriptors were computed using the same method. To explore NLO properties, total static dipole moment (μ), linear polarizability (α) and mean first-order hyperpolarizability (β_{tot}) were calculated using the above mentioned method.

4. Results and discussion

The following ligands were selected for computational studies:

1. 2,4-Dihydroxybenzaldehyde N(4)-methyl(phenyl)thiosemicarbazone (DBMPTSC)
2. 4-[N,N(Dimethyl)amino]benzaldehyde N(4)-methyl(phenyl)thiosemicarbazone (PDBMPTSC)

3. 4-Benzyloxybenzaldehyde N(4)-methyl(phenyl)thiosemicarbazone (BBMPTSC)

4. 4-Hydroxy-3-methoxyacetophenone N(4)-methyl(phenyl)thiosemicarbazone (AMPTSC)

5. Crotonaldehyde isonicotinoylhydrazone (CINH)

6. 4-[N,N(Dimethyl)amino]benzaldehyde isonicotinoylhydrazone (PDBINH)

7. 4-Hydroxy-3-methoxyacetophenone isonicotinoylhydrazone (AINH).

4.1. 2,4-Dihydroxybenzaldehyde N(4)-methyl(phenyl) thiosemicarbazone (DBMPTSC)

4.1.1. Optimized structure, MEP and Global descriptive parameters

The initial geometry of the molecule was chosen from X-ray refinement data. The optimized molecular structure, HOMO-, LUMO- and MEP plots of the compound have been done at B3LYP/6-311++G(d,p) using the GAUSS-VIEW 5.0.9 program and are shown in Fig.1. The optimized geometry showed an energy of -1293.7692 a.u. Global descriptors such as chemical hardness, chemical softness, chemical potential, electronegativity and global electrophilic index were calculated using HOMO-LUMO energy values are tabulated in Table 1. The negative chemical potential value indicates the stability of the compound. The MEP surfaces obtained at B3LYP/6-311++G(d,p)

calculations are shown in Fig.1.The electronegative region extends over oxygen atoms of hydroxyl groups and sulphur atom bonded to carbon through double bond indicating that they are potential sites for electrophilic process. The electropositive region is found to be spread over the hydrogen atoms of the compound. These are sites for nucleophilic attack. The relatively high negative value of HOMO indicates the high capacity of the compound to donate electrons to appropriate acceptor. Theoretically, HOMO– LUMO energy gap is found to be 4.074 eV. The lower HOMO-LUMO energy gap promotes charge transfer within the molecule which may impart biological activity to the molecule. The lower energy band gap implies high reactivity of the molecule and better non-linear optical activity too.

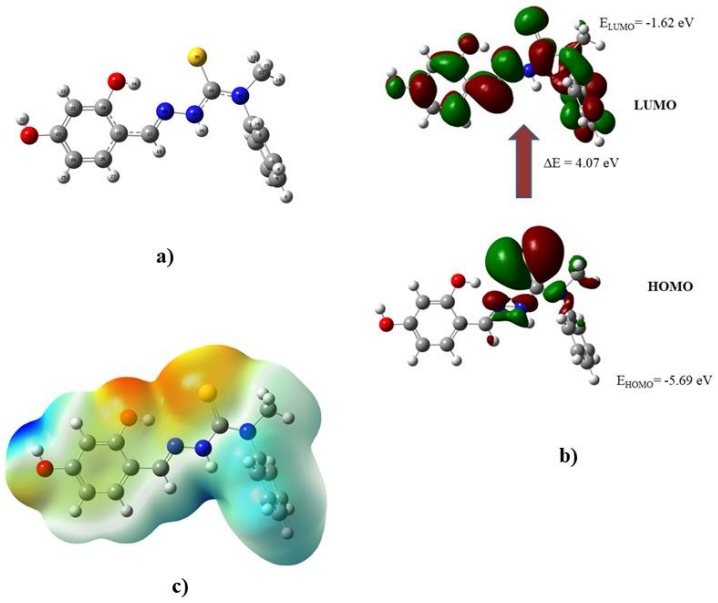

Fig.1. a) Optimized molecular structure, b) HOMO-, LUMO- and c) MEP plot of DBMPTSC

Table 1. Global descriptive parameters

E_{HOMO}	-5.6950	Softness ζ	0.2454
E_{LUMO}	-1.6207	Chemical potential μ	-3.6579
Ionization potential IP	5.6950	Electronegativity χ	3.6579
Electron affinity EA	1.6207	Global electrophilic index ω	3.2839
Hardness η	2.0371	Dipole moment	6.6828D

4.1.2. Fukui functions of DBMPTSC

The calculated Fukui functions for the charged- (N+1 and N-1) as well as the neutral species (N) and dual descriptor $\Delta f(k)$ of DBMPTSC are summarized in Table 2. Mulliken population analysis performed on the compound showed that S35 and N30 have highest values of f^-. This indicates that these positions of the compound are good reactive sites for the electrophilic attack and this observation is in agreement with the MEP map. The O31 and O33 have low f^-values, indicating that these sites are not much nucleophilic compared to S35 and N30. The dual descriptors of S35 and N30 atoms are less than zero and therefore, these sites are favourable for electrophilic attack.

Table 2. The atomic charges for all atoms in DBMPTSC in its N, N-1 and N+1 electronic states and condensed f^- and f^+ and dual descriptor (Δf)

Atom	N	N-1	N+1	f^+	f^-	f^0	Δf
C1	0.192111	0.20719	0.068179	-0.12393	-0.01508	-0.06951	-0.10885
C3	0.029698	0.069971	-0.05082	-0.08052	-0.04027	-0.0604	-0.04025
C5	0.031295	0.105504	-0.02606	-0.05736	-0.07421	-0.06578	0.016853
C7	0.004666	0.04575	-0.02765	-0.03232	-0.04108	-0.0367	0.008768
C9	0.199269	0.212439	0.021398	-0.17787	-0.01317	-0.09552	-0.1647
C11	-0.18792	-0.15331	-0.15493	0.032992	-0.03461	-0.00081	0.067605
C12	0.425514	0.451999	0.376813	-0.0487	-0.02649	-0.03759	-0.02222
C16	0.105276	0.148681	-0.06834	-0.17362	-0.04341	-0.10851	-0.13021
C17	-0.1657	0.076205	-0.11222	0.053486	-0.24191	-0.09421	0.295395
C19	0.380616	0.397359	0.364139	-0.01648	-0.01674	-0.01661	0.000266
C20	0.235709	0.257611	0.214303	-0.02141	-0.0219	-0.02165	0.000496
C21	-0.07664	-0.02528	-0.13119	-0.05455	-0.05136	-0.05295	-0.00319
C23	-0.20761	-0.19511	-0.23487	-0.02727	-0.0125	-0.01988	-0.01477
C24	-0.10308	-0.03743	-0.13306	-0.02998	-0.06565	-0.04781	0.035674
C26	-0.5355	-0.50233	-0.58049	-0.04498	-0.03317	-0.03908	-0.01181
N28	-0.13371	-0.04128	-0.23491	-0.10121	-0.09243	-0.09682	-0.00878
N29	0.612111	0.565717	0.684375	0.072264	0.046394	0.059329	0.02587
N30	0.298504	0.256772	0.31522	0.016716	0.041732	0.029224	-0.02502
O31	-0.6762	-0.67712	-0.69762	-0.02142	0.000921	-0.01025	-0.02234
O33	0.197886	0.144555	0.10555	-0.09233	0.053331	-0.04617	-0.14566
S35	-0.57296	-0.36122	-0.69781	-0.12486	0.21174	-0.1683	-0.3366

4.1.3. Non-linear optical effects of DBMPTSC

The computed electric dipole moment, polarizability and first-order hyperpolarizability of DBMPTSC are presented in Table 3. Usually, urea is used as a reference for the characterization of organic non-linear materials. The calculated values of α_{tot} and β_{tot} for the compound are, respectively, 3.87×10^{-23} and 1.33×10^{-29} esu, which are about 7.9 and 16.8 times higher than those of urea obtained by the same method. The dipole moment of the compound is 4.86 times higher than that of urea. The higher first-order hyperpolarizability of the compound than

that of urea indicates that it could be a potential molecule for future studies of non- linear optical properties.

Table 3. The electric dipole moment, polarizability and first-order hyperpolarizability of DBMPTSC calculated at B3LYP/6-311++G(d,p) level

Dipole moment	**DBMPTSC**	**urea**	**First-order hyperpolarizability**	**DBMPTSC**	**urea**
μ_x	4.03×10^{-18}	0.00	β_{xxx}	1.09×10^{-29}	2.1×10^{-36}
μ_y	-5.32×10^{-18}	-4.48×10^{-18}	β_{xxy}	1.16×10^{-30}	-3.1×10^{-31}
μ_z	-3.07×10^{-19}	2.50×10^{-21}	β_{xyy}	2.07×10^{-30}	-3.9×10^{-36}
μ_{tot}	6.68×10^{-18}	4.48×10^{-18}	β_{yyy}	-2.65×10^{-30}	7.67×10^{-31}
Polarizability	**DBMPTSC**	**urea**	β_{xxz}	-3.05×10^{-31}	-1×10^{-35}
α_{xx}	5.39×10^{-23}	5.46×10^{-24}	β_{xyz}	7.88×10^{-33}	5.17×10^{-35}
α_{xy}	7.58×10^{-25}	-8.2×10^{-31}	β_{yyz}	-1.43×10^{-32}	-7.3×10^{-35}
α_{yy}	3.96×10^{-23}	5.71×10^{-24}	β_{xzz}	3.06×10^{-31}	-1.5×10^{-36}
α_{xz}	-1.14×10^{-24}	-3.5×10^{-29}	β_{yzz}	4.76×10^{-31}	3.3×10^{-31}
α_{yz}	7.14×10^{-25}	1.69×10^{-28}	β_{zzz}	4.53×10^{-32}	-2.4×10^{-34}
α_{zz}	2.32×10^{-23}	3.56×10^{-24}	β_{tot}	1.33×10^{-29}	7.91×10^{-31}
α_{tot}	3.87×10^{-23}	4.91×10^{-24}			

4.2. 4-[N,N-(Dimethyl)amino]benzaldehyde N(4)-methyl(phenyl)thiosemicarbazone (PDBMPTSC)

4.2.1. Optimized structure, MEP and Global descriptive parameters

The initial geometry of the molecule was drawn by using GAUSS-VIEW 5.0.9 program. The optimized molecular geometry, HOMO-, LUMO- and MEP plots of the compound have been done at B3LYP/6-311++G(d,p) and are shown in Fig.2. The optimized geometry showed an energy -1277.2598 a.u. Global descriptors such as ionization potential, chemical hardness, chemical softness, chemical potential, electronegativity and global electrophilicity index were calculated by using HOMO-LUMO energy values and are tabulated in Table 4. The

ease of electron donation is represented by ionization potential (IP). The compound with low IP may be more active. The stability of a compound is related to chemical potential, μ. The observed μ value of this compound (-3.3252), indicates the high stability of the compound. The red region mainly stretches over sulphur atom bonded to carbon through double bond and nitrogen atoms of thiosemicarbazone moiety. These are probable sites for electrophilic attack. The blue region of the compound is over hydrogen atoms which are potential sites for nucleophile attack.

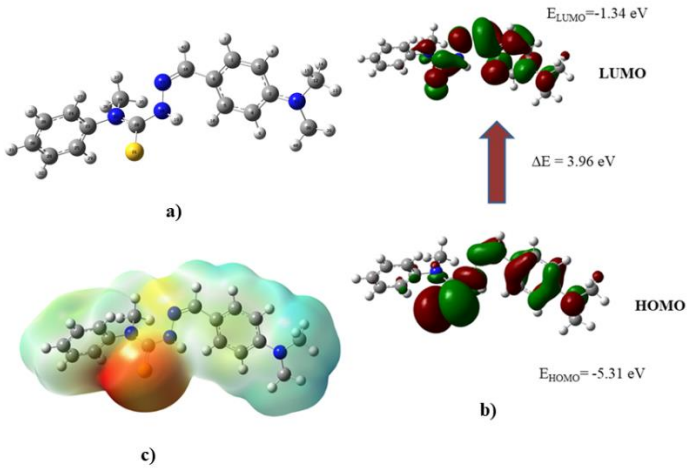

Fig.2. a) Optimized molecular structure, b) HOMO-, LUMO- and c) MEP plot of PDBMPTSC

Table 4. Global descriptive parameters

E_{HOMO}	-5.3051	Softness ζ	0.2525
E_{LUMO}	-1.3453	Chemical potential μ	-3.3252
Ionization potential IP	5.3051	Electronegativity χ	3.3252
Electron affinity EA	1.3453	Global electrophilic index ω	2.7923
Hardness η	1.9799	Dipole moment	6.0827D

4.2.2. Fukui functions of PDBMPTSC

The calculated Fukui indices for cationic, anionic and neutral species of the compound are tabulated in Table 5. The high f^- values of S21 and N17 indicate that these sites are prone to electrophilic attack. The negative dual descriptor values also concede that these sites are nucleophilic. The f^+values of C16 and C24 are, 0.590 and 0.668, respectively. $\Delta f > 0$ showed that these sites are electrophilic. All these results are in good agreement with the MEP map of the compound.

Table 5. The atomic charges for all atoms in PDBMPTSC in its N, N+1 and N-1 electronic states and condensed $f^+$and f^- and dual descriptor (Δf)

Atom	**N**	**N-1**	**N+1**	f^+	f^-	f^0	Δf
C1	-0.20117	0.085866	-0.0588	0.142372	-0.28704	-0.07233	0.429407
C2	-0.09646	-0.04621	0.090797	0.187258	-0.05025	0.068503	0.23751
C3	-0.70073	-0.32481	-0.68579	0.014943	-0.37592	-0.18049	0.390865
C4	0.04366	-0.06954	-0.11493	-0.15859	0.113202	-0.02269	-0.27179
C5	0.176532	0.058557	0.042223	-0.13431	0.117975	-0.00817	-0.25228
C6	-0.17267	-0.81471	-0.87946	-0.70679	0.642034	-0.03238	-1.34882
N11	0.145107	0.07039	-0.09685	-0.24195	0.074717	-0.08362	-0.31667
C12	0.10337	0.1985	-0.09278	-0.19615	-0.09513	-0.14564	-0.10102
C16	0.66458	1.14492	1.254981	0.590401	-0.48034	0.055031	1.070741
N17	-0.01252	-0.23535	-0.30697	-0.29445	0.222827	-0.03581	-0.51728
N18	0.405085	0.352494	0.332604	-0.07248	0.052591	-0.00994	-0.12507
C20	-0.14998	-0.10508	-0.0907	0.059279	-0.0449	0.007189	0.10418
S21	-0.49624	-1.5492	-1.60748	-1.11124	1.052965	-0.02914	-2.16421
N22	0.529923	0.566472	0.613894	0.083971	-0.03655	0.023711	0.12052
C23	-0.36808	-0.29914	-0.66123	-0.29315	-0.06894	-0.18104	-0.22421
C24	0.069321	0.705053	0.737549	0.668228	-0.63573	0.016248	1.30396
C25	-0.045	0.350563	0.296089	0.341093	-0.39557	-0.02724	0.73666
C26	-0.10412	0.177603	0.100681	0.204797	-0.28172	-0.03846	0.486516
C28	0.122144	0.071915	-0.0028	-0.12495	0.050229	-0.03736	-0.17517
C30	-0.13269	0.070025	-0.06784	0.064857	-0.20272	-0.06893	0.267574
C34	0.112891	0.40866	0.341367	0.228476	-0.29577	-0.03365	0.524245
C38	0.107045	0.183016	-0.14458	-0.25162	-0.07597	-0.1638	-0.17565

4.2.3. Non-linear optical effects of PDBMPTSC

The calculated dipole moment (μ), linear polarizability (α_{total}) and first-order hyperpolarizability (β_{total}) of the compound, PDBMPTSC are 6.0827 Debye, 4.35×10^{-23} and 1.99×10^{-29} cm^5/esu, respectively, and are presented in Table 6. Theoretically, the linear polarizability (α_{total}) of the compound is nine times higher than that of urea. It can be noted that the first-order hyperpolarizability (β_{tot}) of the compound is twenty five times higher than that of urea. The higher value of hyperpolarizability is related with the intramolecular charge transfer, resulting between π-electronic conjugation from electron donor and accepter groups. The physical properties of this π-conjugated compound are due to high degree electron charge delocalization along the charge transfer axis and also due to small band gap. The dipole moment of the molecule is four times higher than that of urea.

Table 6. The electric dipole moment, polarizability and first-order hyperpolarizability of PDBMPTSC calculated at B3LYP/6-311++G(d,p) level

Dipole moment		**First-order hyperpolarizability**	
μ_x	5.39×10^{-18}	β_{xxx}	-2.04×10^{-29}
μ_y	-1.91×10^{-18}	β_{xxy}	6.98×10^{-30}
μ_z	2.07×10^{-19}	β_{xyy}	8.28×10^{-31}
μ_{tot}	6.08×10^{-18}	β_{yyy}	9.29×10^{-31}
Polarizability		β_{xxz}	3.94×10^{-31}
α_{xx}	6.68×10^{-23}	β_{xyz}	-1.47×10^{-31}
α_{xy}	2.30×10^{-25}	β_{yyz}	-8.25×10^{-31}
α_{yy}	3.50×10^{-23}	β_{xzz}	1.22×10^{-30}
α_{xz}	2.80×10^{-25}	β_{yzz}	-1.52×10^{-31}
α_{yz}	1.34×10^{-24}	β_{zzz}	-2.21×10^{-31}
α_{zz}	2.86×10^{-23}	β_{tot}	1.99×10^{-29}
α_{tot}	4.35×10^{-23}		

4.3. 4-Benzyloxybenzaldehyde N(4)-methyl(phenyl) thiosemicarbazone (BBMPTSC)

4.3.1. Optimized structure, MEP and Global descriptive parameters

The initial geometry of the molecule was obtained by using GAUSS-VIEW 5.0.9 program. The optimized geometry showed an energy of-1488.9101 a.u. The optimized molecular geometry, HOMO-, LUMO- and MEP plots of BBMPTSC have been generated at B3LYP/6-311++G(d,p) using the GAUSS-VIEW 5.0.9 program and are shown in Fig.3. Theoretically, HOMO– LUMO energy gap was found to be 3.735 eV. Global descriptors such as chemical hardness, chemical softness, chemical potential and the global electrophilicity index were also calculated and are listed in Table 7. The negative chemical potential value shows the stability of a compound. In the MEP map of the compound, the red region is positioned on the N and S atoms linked with carbon through double bonds, which can be considered as sites for electrophilic attack. However, the blue region of the compound is shown to be spread over the hydrogen atoms and these sites are prone to nucleophilic attack.

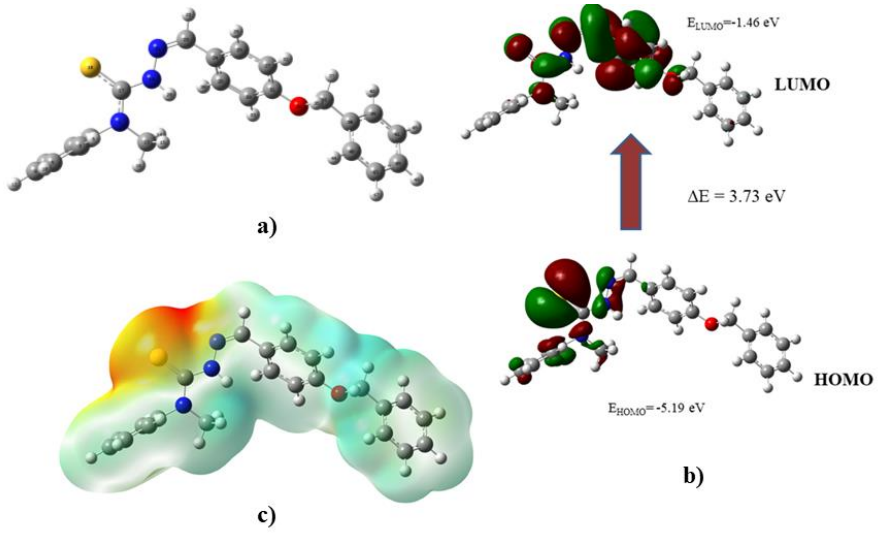

Fig.3. a) Optimized molecular structure, b) HOMO-, LUMO- and c) MEP plot of BBMPTSC

Table 7. Global descriptive parameters

E_{HOMO}	-5.1971	Softness ζ	0.2676
E_{LUMO}	-1.4615	Chemical potential μ	-3.3293
Ionization potential IP	5.1971	Electronegativity χ	3.3293
Electron affinity EA	1.4615	Global electrophilic index ω	2.9672
Hardness η	1.8677	Dipole moment	8.5239D

4.3.2. Fukui functions of BBMPTSC

The condensed Fukui functions (f_k^+), (f_k^-), (f_k^0) and dual descriptor $\Delta f(k)$ of BBMPTSC are given in Table 8. The higher values of f^- show that the nitrogen atom of imine group (N21) and thione sulphur (S18) are potential nucleophilic sites. The value of dual descriptor, $\Delta f_A < 0$ shows that these sites are more susceptible to electrophilic attack. From this it is implied that these atoms of BBMPTSC are potential

donor sites and can coordinate to metal(II) ions to form complexes. This is also conceded by electrostatic potential map of the compound. N19 and O34 have low f^+ values indicating that they are weak electrophilic sites. The dual descriptor, $\Delta f > 0$ suggest that these sites may undergo nucleophilic attack. C4 and C26 have high Δf values indicating their good electrophilic nature. These results are also conceded by MEP of the compound.

Table 8. The atomic charges for all atoms in BBMPTSC in its N, N-1 and N+1 electronic states and condensed f^- and f^+ and dual descriptor (Δf)

Atom	**N**	**N-1**	**N+1**	f^+	f^-	f^0	Δf
N1	0.466561	0.511265	0.570565	0.104004	-0.0447	0.02965	0.148708
C2	-0.79354	-1.44453	-1.47547	-0.68193	0.650992	-0.01547	-1.33292
C3	1.34223	0.452468	0.417943	-0.92429	0.889762	-0.01726	-1.81405
C4	-0.45087	0.30035	0.322311	0.773179	-0.75122	0.010981	1.524397
C5	-0.1522	0.219099	0.108294	0.260498	-0.3713	-0.0554	0.631801
C7	0.558541	0.253104	0.204693	-0.35385	0.305437	-0.02421	-0.65929
C9	-0.16964	-0.33159	-0.41411	-0.24447	0.161951	-0.04126	-0.40642
C13	0.126341	0.296458	0.20157	0.075229	-0.17012	-0.04744	0.245346
C17	-0.53998	0.103922	-0.12421	0.415776	-0.6439	-0.11406	1.05968
S18	1.22421	0.862277	0.984863	-0.23935	0.361933	0.061293	-0.60128
N19	-0.02243	0.10642	0.072208	0.094635	-0.12885	-0.01711	0.223482
N21	-0.33565	-0.67898	-0.75078	-0.41513	0.343329	-0.0359	-0.75846
C23	-0.07317	0.218448	0.141925	0.215095	-0.29162	-0.03826	0.506713
C24	-0.05339	0.001028	-0.42416	-0.37077	-0.05442	-0.21259	-0.31636
C25	-0.07789	0.087792	-0.13747	-0.05958	-0.16569	-0.11263	0.106108
C26	-0.56114	0.050719	-0.00589	0.555247	-0.61186	-0.02831	1.167106
C27	0.476962	0.354277	0.166939	-0.31002	0.122685	-0.09367	-0.43271
C29	-0.30321	0.199322	0.087656	0.390868	-0.50253	-0.05583	0.893402
C31	-0.37287	-0.62233	-0.64473	-0.27186	0.249455	-0.0112	-0.52131
O34	0.023056	0.054952	-0.00428	-0.02734	-0.0319	-0.02962	0.004557
C35	-0.19972	-0.35683	-0.35336	-0.15363	0.157103	0.001736	-0.31073
C38	0.362182	0.584307	0.554592	0.19241	-0.22213	-0.01486	0.414535
C39	0.097374	-0.05151	-0.08933	-0.18671	0.148879	-0.01891	-0.33559
C40	-0.4737	-0.03659	-0.05622	0.417484	-0.43711	-0.00981	0.854593
C41	0.02239	-0.02106	-0.1047	-0.12709	0.043452	-0.04182	-0.17055
C43	0.093811	0.000943	-0.08424	-0.17805	0.092868	-0.04259	-0.27092
C45	-0.21425	-0.11374	-0.16462	0.049635	-0.10052	-0.02544	0.15015

4.3.3. Non-linear optical effects of BBMPTSC

In the present study, NLO behaviour of BBMPTSC was investigated by the determination of the first-order hyperpolarizability (β), electric dipole moment (μ) and the polarizability (α) by using B3LYP/6-311++G(d, p) basis set using the Gaussian 09W program package. The electric dipole moment, polarizability and first-order hyperpolarizability of BBMPTSC are listed in Table 9. One of the important criteria for a molecule to behave as a good NLO material is that it should have a large value of the first-order hyperpolarizability (β). The calculated values of α_{tot} and β_{tot} for the compound are, respectively, 3.14×10^{-24} and 9.56×10^{-30} esu, which are about 0.64 and 12.1 times higher than those of urea, which are, respectively, 4.91×10^{-24} and 7.91×10^{-31} esu obtained by the same method. The dipole moment of the compound is six times higher than that of urea. The first-order hyperpolarizability of BBMPTSC is 12 times higher than that of urea and thus it could be a potential molecule for future studies of non-linear optical properties.

Table 9. The electric dipole moment, polarizability and first-order hyperpolarizability of BBMPTSC calculated at B3LYP/6-311++G(d,p) level

Dipole moment		**First-order hyperpolarizability**	
μ_x	7.28×10^{-18}	β_{xxx}	-7.78×10^{-30}
μ_y	-4.39×10^{-18}	β_{xxy}	1.14×10^{-30}
μ_z	5.97×10^{-19}	β_{xyy}	-1.46×10^{-30}
μ_{tot}	8.52×10^{-18}	β_{yyy}	1.07×10^{-30}
Polarizability		β_{xxz}	1.13×10^{-30}
α_{xx}	-6.96×10^{-23}	β_{xyz}	2.28×10^{-31}
α_{xy}	-1.58×10^{-25}	β_{yyz}	1.30×10^{-31}
α_{yy}	4.42×10^{-23}	β_{xzz}	1.16×10^{-31}
α_{xz}	-1.13×10^{-24}	β_{yzz}	1.01×10^{-32}
α_{yz}	7.27×10^{-25}	β_{zzz}	4.69×10^{-31}
α_{zz}	3.47×10^{-23}	β_{tot}	9.56×10^{-30}
α_{tot}	3.14×10^{-24}		

4.4. 4-Hydroxy-3-methoxyacetophenone N(4)-methyl(phenyl)thiosemicarbazone (AMPTSC)

4.4.1. Optimized structure, MEP and Global descriptive parameters

The initial geometry of the molecule was drawn by using GAUSS-VIEW 5.0.9 program. The optimized molecular geometry, HOMO-, LUMO- and MEP plots of the compound have been done at B3LYP/6-311++G(d,p) and are shown in Fig.4. The optimized geometry showed an energy of -1372.3935 a.u. Global descriptors such as ionization potential, chemical hardness, chemical softness, chemical potential, electronegativity and global electrophilicity index are calculated by using HOMO-LUMO energy values and are tabulated in Table 10. The

electronegative region extends over oxygen atom of hydroxyl group and sulphur atom bonded to carbon through double bond indicating that they are potential sites for electrophilic process. The electropositive region is found to be spread over the hydrogen atoms of the compound and these sites favour nucleophilic attack.

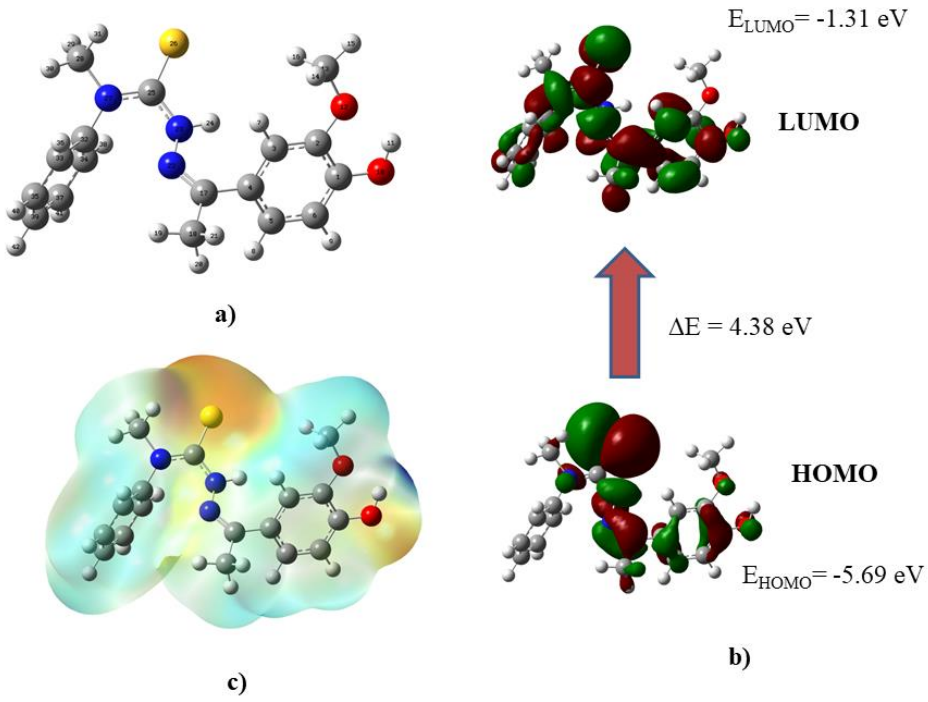

Fig.4. a) Optimized molecular structure, b) HOMO-, LUMO- and c) MEP plot of AMPTSC

Table 10. Global descriptive parameters

E_{HOMO}	-5.6877	Softness ζ	0.2283
E_{LUMO}	-1.3075	Chemical potential μ	-3.4976
Ionization potential IP	5.6877	Electronegativity χ	3.4976
Electron affinity EA	1.3075	Global electrophilic index ω	2.7928
Hardness η	2.1901	Dipole moment	6.0827D

4.4.2. Fukui functions of AMPTSC

The mulliken charges and corresponding fukui functions of the atoms in the compound are given in Table 11. The high f^- values of S26 and N22 imply that these sites are susceptible to electrophilic attack. This is also confirmed by the dual descriptor values of these atoms. O10 acts as a potential site for nucleophilic attack. These results are in accordance with MEP data of the compound. C17 shows high value of f^+ indicating that it is a potential electrophilic site. The atoms such as N23, N27, C32, and C25 are favourable for nucleophilic attack. By virtue of high electron density, sulphur and azomethine nitrogen can provide electrons to metal ions to form complexes. Thus, the ligand acts as a potential bidentate one which is confirmed by MEP and Fukui function analysis.

Table 11. The atomic charges for all atoms in AMPTSC in its N, N-1 and N+1 electronic states and condensed f^+ and f^- and dual descriptor (Δf)

Atom	**N**	**N-1**	**N+1**	f^+	f^-	f^0	Δf
C1	-0.36153	-0.34134	-0.35545	0.006083	-0.0202	-0.00706	0.026278
C2	-0.55168	-0.41442	-0.62075	-0.06907	-0.13727	-0.10317	0.068195
C3	0.432793	0.520358	0.330589	-0.1022	-0.08757	-0.09488	-0.01464
C4	0.054263	0.139491	-0.00544	-0.0597	-0.08523	-0.07246	0.025528
C5	-0.03098	0.045658	-0.16262	-0.13164	-0.07664	-0.10414	-0.055
C6	0.07247	0.121866	0.053942	-0.01853	-0.0494	-0.03396	0.030868
O10	1.124138	1.092824	1.133452	0.009314	0.031314	0.020314	-0.022
O12	-0.24146	-0.21062	-0.25751	-0.01605	-0.03083	-0.02344	0.014784
C13	0.202089	0.239701	0.167108	-0.03498	-0.03761	-0.0363	0.002631
C17	-1.15202	-1.16642	-1.10433	0.047687	0.014403	0.031045	0.033284
C18	-0.06984	0.011557	-0.17884	-0.109	-0.0814	-0.0952	-0.0276
N22	0.713297	0.679562	0.655303	-0.05799	0.033735	-0.01213	-0.09173
N23	0.204014	0.194124	0.222416	0.018402	0.00989	0.014146	0.008512
C25	0.01141	0.087931	0.03465	0.02324	-0.07652	-0.02664	0.099761
S26	0.412682	0.36191	0.380255	-0.03243	0.050772	0.009173	-0.0832
N27	0.423078	0.406685	0.430517	0.007439	0.016393	0.011916	-0.00895
C28	0.263359	0.301666	0.185889	-0.07747	-0.03831	-0.05789	-0.03916
C32	-0.93287	-0.91483	-0.7667	0.166176	-0.01804	0.074066	0.18422
C33	0.517934	0.56571	0.382489	-0.13545	-0.04778	-0.09161	-0.08767
C34	-0.70609	-0.44582	-0.94049	-0.23439	-0.26028	-0.24734	0.025882
C35	-0.17657	-0.14962	-0.24756	-0.07099	-0.02696	-0.04897	-0.04404
C37	-0.10542	-0.07135	-0.16603	-0.06061	-0.03406	-0.04734	-0.02655
C39	-0.10306	-0.05463	-0.17089	-0.06783	-0.04842	-0.05813	-0.01941

4.4.3. Non-linear optical effects of AMPTSC

The computed electric dipole moment, polarizability and first-order hyperpolarizability of AMPTSC are presented in Table 12. The calculated values of α_{tot} and β_{tot} for the compound are, respectively, 3.99×10^{-23} and 5.34×10^{-30} esu, which are about 8.13 and 6.75 times higher than those of urea obtained by the same method. The dipole moment of the compound is 2.25 times higher than that of urea.

Table 12. The electric dipole moment, polarizability and first-order hyperpolarizability of AMPTSC calculated at B3LYP/6-311++G(d,p) level

Dipole moment		**First-order hyperpolarizability**	
μ_x	-5.97×10^{-19}	β_{xxx}	-3.64×10^{-30}
μ_y	-2.03×10^{-18}	β_{xxy}	3.71×10^{-31}
μ_z	2.41×10^{-19}	β_{xyy}	-1.85×10^{-30}
μ_{tot}	3.08×10^{-18}	β_{yyy}	-2.39×10^{-30}
Polarizability		β_{xxz}	4.38×10^{-31}
α_{xx}	4.72×10^{-23}	β_{xyz}	1.13×10^{-31}
α_{xy}	2.58×10^{-25}	β_{yyz}	4.91×10^{-31}
α_{yy}	4.36×10^{-23}	β_{xzz}	5.43×10^{-31}
α_{xz}	-2.66×10^{-24}	β_{yzz}	-3.77×10^{-31}
α_{yz}	2.15×10^{-25}	β_{zzz}	3.26×10^{-32}
α_{zz}	2.89×10^{-23}	β_{tot}	5.34×10^{-30}
α_{tot}	3.99×10^{-23}		

4.5. Crotanaldehyde isonicotinoylhydrazone (CINH)

4.5.1. Optimized structure, MEP and Global descriptive parameters

The initial geometry of the molecule was confirmed from X-ray refinement data. The optimized molecular structure, HOMO-, LUMO- and MEP plots of the compound have been done at B3LYP/6-311++G(d,p) using the GAUSS-VIEW 5.0.9 program and are shown in Fig.5. The optimized geometry showed an energy of -627.2931 a.u. Global descriptors such as chemical hardness, chemical softness, chemical potential, electronegativity and global electrophilic index calculated using HOMO-LUMO energy values are tabulated in Table 13. The negative chemical potential value indicates the stability of the

compound. The MEP analysis and surfaces obtained at B3LYP/6-311++G(d,p) are shown in Fig.5 in which the electronegative region is found to be spread over oxygen atom bonded to carbon through double bond, nitrogen of the pyridine moiety and the inter linked nitrogen atoms of hydrazone moiety, indicating that they are potential sites for electrophilic process. The electropositive region is found to be spread over the hydrogen atoms of the compound. These are sites for nucleophilic attack.

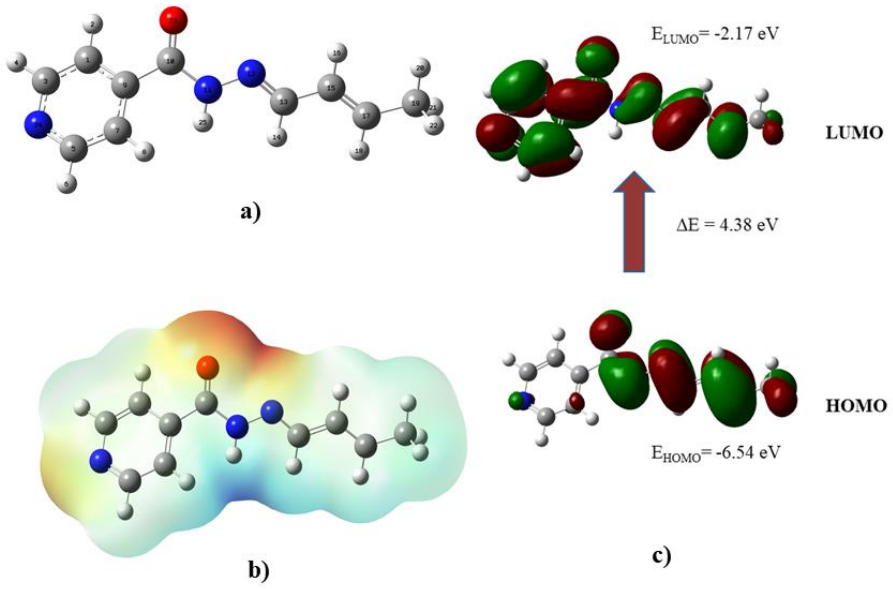

Fig.5. a) Optimized molecular structure, b) HOMO-, LUMO- and c) MEP plots of CINH

Table 13. Global descriptive parameters

E_{HOMO}	-6.5462	Softness ζ	0.2284
E_{LUMO}	-2.1690	Chemical potential μ	-4.3576
Ionization potential IP	6.5462	Electronegativity χ	4.3576
Electron affinity EA	2.1690	Global electrophilic index ω	4.3381
Hardness η	2.1886	Dipole moment	5.4087D

4.5.2. Fukui functions of CINH

The mulliken charges and corresponding fukui functions of the atoms in the compound are given in Table 14. The f^- values of O23, N12 and N24 are 0.170, 0.130 and 0.149, respectively. These values imply that these sites are susceptible to electrophilic attack. This is also confirmed by dual descriptor values of these atoms. These results are supported by MEP of the compound. C13 shows high f^+ value (0.184) which indicates that it is a potential electrophilic site. By virtue of high electron density, amide oxygen and azomethine nitrogen prefer to coordinate with metal ions to form complexes. Thus, the ligand may acts as a potential bidentate one which is confirmed by MEP and Fukui function analysis.

Table 14. The atomic charges for all atoms in CINH in its N, N-1 and N+1 electronic states and condensed f^+ and f^- and dual descriptor (Δf)

Atom	**N**	**N-1**	**N+1**	f^+	f^-	f^0	Δf
C1	0.424945	0.678569	0.43563	0.010685	-0.25362	-0.12147	0.264309
C3	0.051687	0.199393	0.032781	-0.01891	-0.14771	-0.08331	0.1288
C5	-0.32162	-0.17711	-0.39431	-0.07269	-0.1445	-0.1086	0.071814
C7	-0.23857	-0.36339	-0.40613	-0.16756	0.124819	-0.02137	-0.29238
C9	-0.12275	0.026337	-0.13097	-0.00823	-0.14908	-0.07866	0.140855
C10	-0.65093	-0.7355	-0.7195	-0.06857	0.084571	0.008002	-0.15314
N11	0.193552	0.302183	0.182915	-0.01064	-0.10863	-0.05963	0.097994
N12	-0.20643	-0.3367	-0.40841	-0.20198	0.130271	-0.03586	-0.33225
C13	0.167973	0.540031	0.35245	0.184477	-0.37206	-0.09379	0.556535
C15	0.26248	0.475665	0.16546	-0.09702	-0.21319	-0.1551	0.116165
C17	0.023844	0.333507	0.13455	0.110706	-0.30966	-0.09948	0.420369
C19	-0.00654	-0.04564	-0.29862	-0.29208	0.039098	-0.12649	-0.33118
O23	-0.25341	-0.42398	-0.49212	-0.23872	0.170575	-0.03407	-0.40929
N24	0.675762	0.526641	0.546273	-0.12949	0.149121	0.009816	-0.27861

4.5.3. Non-linear optical effects of CINH

The computed electric dipole moment, polarizability and first-order hyperpolarizability of CINH are presented in Table 15.The calculated values of α_{tot} and β_{tot} for the compound are, respectively, 2.51×10^{-23} and 1.09×10^{-29} esu, which are about 5.12 and 13.8 times higher than those of urea obtained by the same method. The dipole moment of the compound is 3.94 times higher than that of urea. The higher first-order hyperpolarizability of the compound than that of urea indicates that it could be a potential molecule for future studies of non- linear optical properties.

Table 15. The electric dipole moment, polarizability and first-order hyperpolarizability of CINH calculated at B3LYP/6-311++G(d,p) level

Dipole moment		**First-order hyperpolarizability**	
μ_x	-3.48×10^{-18}	β_{xxx}	-1.07×10^{-29}
μ_y	-3.98×10^{-18}	β_{xxy}	8.79×10^{-31}
μ_z	1.11×10^{-18}	β_{xyy}	-4.53×10^{-31}
μ_{tot}	5.41×10^{-18}	β_{yyy}	-7.55×10^{-31}
Polarizability		β_{xxz}	2.77×10^{-32}
α_{xx}	4.13×10^{-23}	β_{xyz}	-2.10×10^{-31}
α_{xy}	-2.71×10^{-24}	β_{yyz}	-1.57×10^{-31}
α_{yy}	2.11×10^{-23}	β_{xzz}	2.13×10^{-30}
α_{xz}	7.74×10^{-26}	β_{yzz}	-2.47×10^{-31}
α_{yz}	-2.39×10^{-25}	β_{zzz}	-2.18×10^{-31}
α_{zz}	130×10^{-23}	β_{tot}	1.09×10^{-29}
α_{tot}	2.51×10^{-23}		

4.6. 4-[N,N-(Dimethyl)amino]benzaldehyde isonicotinoylhydrazone (PDBINH)

4.6.1. Optimized structure, MEP and Global descriptive parameters

The initial geometry of the molecule was drawn by using GAUSS-VIEW 5.0.9 program. The optimized molecular geometry, HOMO-, LUMO- and MEP plots of the compound have been done at B3LYP/6-311++G(d,p) and are shown in Fig.6. The optimized geometry showed an energy of -875.6570 a.u. Global descriptors such as ionization potential, chemical hardness, chemical softness, chemical potential, electronegativity and global electrophilicity index are calculated by using HOMO-LUMO energy values and are tabulated in Table 16. The

energy values of HOMO-LUMO indicate the electron donating and accepting trend of a compound. Comparatively high negative energy value of HOMO indicates the high electron donating tendency of the compound. The calculated HOMO-LUMO energy gap is 3.9821 eV. It pointed out that the chemical potential of the compound is negative and it is stable. The MEP map of the surface provides idea about the electrophilic- and nucleophilic centers and mode of interactions with other compounds. The electronegative centers are mainly focussed on oxygen atom bonded to carbon through double bond, nitrogen on pyridine moiety and interlinked nitrogen atoms of hydrazone moiety. These are potential sites for electrophilic attack. The hydrogen atoms of the compound act as nucleophilic centers.

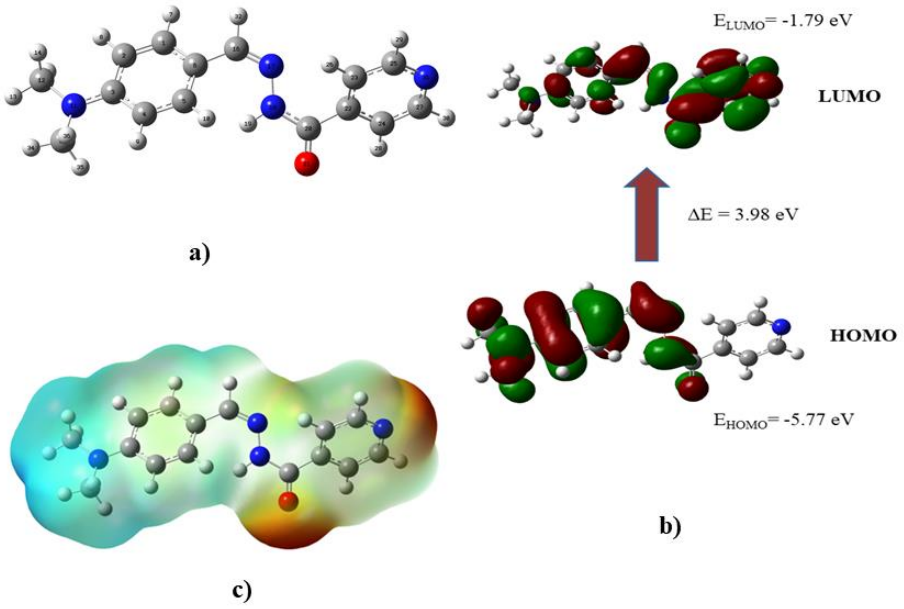

Fig.6. a) Optimized molecular structure, b) HOMO-, LUMO- and c) MEP plots of PDBINH

Table 16. Global descriptive parameters

E_{HOMO}	-5.7781	Softness ζ	0.2511
E_{LUMO}	-1.7959	Chemical potential μ	-3.7870
Ionization potential IP	5.7781	Electronegativity χ	3.7870
Electron affinity EA	1.7959	Global electrophilic index ω	3.5948
Hardness η	1.9910	Dipole moment	9.0281D

4.6.2. Fukui functions of PDBINH

The calculated Fukui functions for cationic, anionic and neutral species of the compound are tabulated in Table 17. The f^-values of O21, N31 and N17 are 0.258, 0.077 and 0.4343, respectively. These values indicate that these sites are potentially nucleophilic. The negative dual descriptor values also concede that these sites are nucleophilic. The f^+values of C22, C23, C3, N18, C16 and C2 are, 0.492, 0.139, 0.250, 0.107, 0.035 and 0.013, respectively. The values of $\Delta f > 0$ show that these sites are electrophilic. All these results are in good agreement with the MEP map of the compound.

Table 17. The atomic charges for all atoms in PDBINH in its N, N-1 and N+1 electronic states and condensed f^+ and f^- and dual descriptor (Δf)

Atom	N	N-1	N+1	f^+	f^-	f^0	Δf
C1	-0.02692	0.122504	-0.05854	-0.03163	-0.14942	-0.09052	0.11779
C2	-0.00415	-0.0277	0.008653	0.012799	0.023555	0.018177	-0.01076
C3	-0.63928	-0.23777	-0.38887	0.250403	-0.40151	-0.07555	0.65191
C4	-0.09444	-0.04092	-0.14728	-0.05284	-0.05352	-0.05318	0.000677
C5	-0.05733	-0.01178	-0.11029	-0.05296	-0.04555	-0.04926	-0.00741
C6	0.149594	0.14097	0.031507	-0.11809	0.008624	-0.05473	-0.12671
N11	0.114166	0.094829	-0.01879	-0.13296	0.019337	-0.05681	-0.1523
C12	0.076127	0.241428	-0.00242	-0.07855	-0.1653	-0.12192	0.086755
C16	-0.93684	-0.76108	-0.90285	0.033989	-0.17575	-0.07088	0.209742
N17	1.3978	0.963421	0.99292	-0.40488	0.434379	0.01475	-0.83926
N18	0.012976	0.17946	0.120406	0.10743	-0.16648	-0.02953	0.273914
C20	-0.56366	-0.64535	-0.65642	-0.09276	0.081683	-0.00554	-0.17444
O21	-0.22287	-0.48127	-0.55264	-0.32977	0.258401	-0.03569	-0.58817
C22	0.141408	0.584573	0.634041	0.492633	-0.44317	0.024734	0.935798
C23	0.111082	0.334163	0.250626	0.139544	-0.22308	-0.04177	0.362625
C24	0.768151	0.710134	0.516075	-0.25208	0.058017	-0.09703	-0.31009
C25	-0.19003	-0.17074	-0.33497	-0.14495	-0.01928	-0.08211	-0.12566
C27	-0.36016	-0.33254	-0.37989	-0.01973	-0.02762	-0.02368	0.007888
N31	0.187049	0.109879	0.030657	-0.15639	0.07717	-0.03961	-0.23356
C33	0.137301	0.227778	-0.03192	-0.16922	-0.09048	-0.12985	-0.07875

4.6.3. Non-linear optical effects of PDBINH

The computed electric dipole moment, polarizability and first-order hyperpolarizability of PDBINH are presented in Table 18. The calculated values of α_{tot} and β_{tot} for the compound are, respectively, 1.06×10^{-22} and 2.74×10^{-29} esu, which are about 21.7 and 34.6 times higher than those of urea obtained by the same method. The dipole moment of the compound is 6.57 times higher than that of urea. The smaller frontier orbital energy gap and high dipole moment of the compound are responsible for its NLO activity. The first-order hyperpolarizability of the compound is higher than that of urea and

thus it could be a potential molecule for future studies as a non- linear optical material.

Table 18. The electric dipole moment, polarizability and first-order hyperpolarizability of PDBINH calculated at B3LYP/6-311++G(d,p) level

Dipole moment		**First-order hyperpolarizability**	
μ_x	8.95×10^{-18}	β_{xxx}	2.87×10^{-29}
μ_y	-1.08×10^{-18}	β_{xxy}	3.01×10^{-30}
μ_z	5.05×10^{-19}	β_{xyy}	-6.05×10^{-31}
μ_{tot}	9.03×10^{-18}	β_{yyy}	9.79×10^{-31}
Polarizability		β_{xxz}	-1.25×10^{-30}
α_{xx}	5.64×10^{-23}	β_{xyz}	1.99×10^{-31}
α_{xy}	3.68×10^{-25}	β_{yyz}	3.36×10^{-31}
α_{yy}	2.86×10^{-23}	β_{xzz}	-1.09×10^{-30}
α_{xz}	-6.24×10^{-25}	β_{yzz}	1.04×10^{-31}
α_{yz}	5.61×10^{-25}	β_{zzz}	7.82×10^{-31}
α_{zz}	2.15×10^{-23}	β_{tot}	2.74×10^{-29}
α_{tot}	1.06×10^{-22}		

4.7. 4-Hydroxy-3-methoxyacetophenone isonicotinoylhydrazone (AINH)

4.7.1. Optimized structure, MEP and Global descriptive parameters

The initial geometry of the molecule was drawn by using GAUSS-VIEW 5.0.9 program. The optimized molecular geometry, HOMO-, LUMO- and MEP plots of the compound have been done at B3LYP/6-311++G(d,p) and are shown in Fig.7. The optimized geometry showed an energy of -970.7875 a.u. Global descriptors such as ionization

potential, chemical hardness, chemical softness, chemical potential, electronegativity and global electrophilicity index were calculated by using HOMO-LUMO energy values and are tabulated in Table 19. Electronegative region extends over oxygen atoms bonded to carbon through double bond, nitrogen on pyridine moiety, oxygen atom of hydroxyl- and methoxy groups and interlinked nitrogen atoms of hydrazone moiety, indicating that they can act as potential sites for electrophilic process. The electropositive region is found to be spread over the hydrogen atoms of the compound. These are sites for nucleophilic attack.

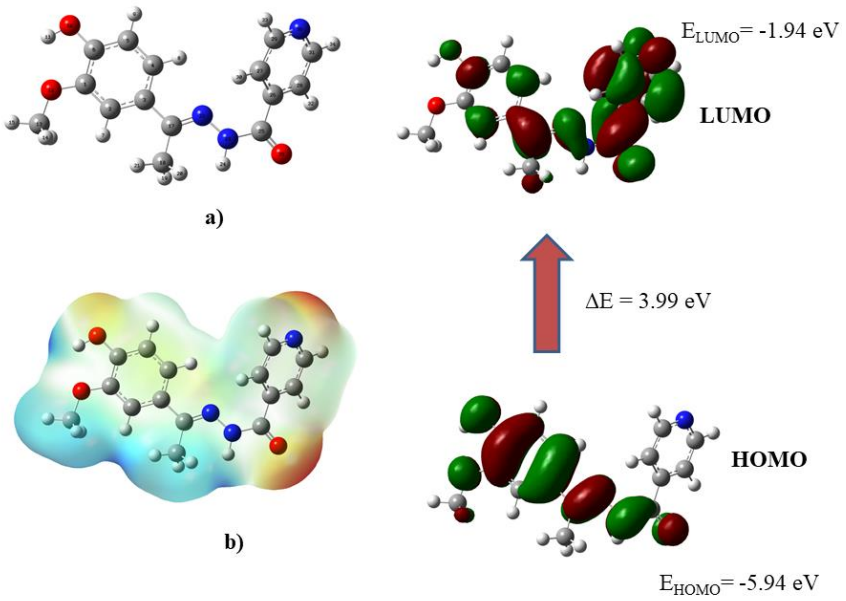

Fig.7. a) Optimized molecular structure, b) HOMO-, LUMO- and c) MEP plot of AINH

Table 19. Global descriptive parameters

E_{HOMO}	-5.9391	Softness ζ	0.25042
E_{LUMO}	-1.9458	Chemical potential μ	-3.9424
Ionization potential IP	5.9391	Electronegativity χ	3.9424
Electron affinity EA	1.9458	Global electrophilic index ω	3.9953
Hardness η	1.9966	Dipole moment	7.4177D

4.7.2. Fukui functions of AINH

The calculated Fukui indices for cationic, anionic and neutral species of the compound are tabulated in Table 20. The f^- values of O35, N22 and N36 are 0.312, 0.480 and 0.031, respectively, which indicate that these sites are potentially nucleophilic. The negative dual descriptor values also support this. O10 and O12 are also nucleophilic sites with f^- values of 0.043 and 0.147, respectively. The f^+ values of C25, C27, C6, C17, C31 and C13 are, 0.485, 0.309, 0.393, 0.216, 0.088 and 0.069, respectively. The Δf >0 showed that these sites are electrophilic and are potential sites for nucleophilic attack. All these results are in good agreement with the MEP map of the compound.

Table 20. The atomic charges for all atoms in AINH in its N, N-1 and N+1 electronic states and condensed f^+ and f^- and dual descriptor (Δf)

Atom	**N**	**N-1**	**N+1**	f^+	f^+	f^+	Δf
C1	0.52501	0.183249	0.096843	-0.42817	0.341761	-0.0432	-0.76993
C2	0.184554	0.095196	-0.03071	-0.21526	0.05583	-0.07972	-0.27109
C3	-0.23827	0.064162	-0.52344	-0.28518	0.078839	-0.10317	-0.36402
C4	-0.06912	-0.06943	-0.08583	-0.01671	-0.06825	-0.04248	0.051538
C5	-0.03842	0.064066	-0.0692	-0.03078	-0.10248	-0.06663	0.071704
C6	-0.67973	-0.32249	-0.28651	0.393223	-0.35724	0.01799	0.750467
O10	0.053314	0.010228	-0.17216	-0.22548	0.043086	-0.09119	-0.26856
O12	-0.25591	-0.40304	-0.45908	-0.20318	0.14713	-0.02802	-0.35031
C13	0.201083	0.399018	0.269914	0.068831	-0.19794	-0.06455	0.266766
C17	-0.04806	0.144332	0.168403	0.216467	-0.1924	0.012036	0.408863
C18	-0.32407	-0.10974	-0.38174	-0.05767	-0.21432	-0.136	0.15665
N22	0.575203	0.128724	-0.12644	-0.70164	0.480007	-0.11082	-1.18165
N23	0.173027	0.542051	0.011221	-0.16181	0.108865	-0.02647	-0.27067
C25	-0.51748	-0.04165	-0.03167	0.485806	-0.47583	0.004989	0.961634
C26	0.412651	-0.42403	-0.38867	-0.80132	0.836678	0.017678	-1.638
C27	0.572006	0.922441	0.881155	0.309149	-0.35044	-0.02064	0.659584
C28	0.590295	0.786807	0.571098	-0.0192	-0.19651	-0.10785	0.177315
C29	-0.56766	-0.48124	-0.57934	-0.01168	-0.08643	-0.04905	0.074749
C31	-0.31412	-0.17069	-0.22529	0.08883	-0.14343	-0.0273	0.232257
O35	0.854085	-0.31711	0.546939	-0.30715	0.312034	0.002444	-0.61918
N36	-0.03838	-0.00087	-0.1855	-0.14712	0.031049	-0.05803	-0.17817

4.7.3. Non-linear optical effects of AINH

The computed electric dipole moment, polarizability and first-order hyperpolarizability of AINH are presented in Table 21. The calculated values of α_{tot} and β_{tot} for the compound are, respectively, 3.41×10^{-23} and 3.92×10^{-29} esu, which are about 6.95 and 49.56 times higher than those of urea obtained by the same method. The dipole moment of the compound is 5.41 times higher than that of urea. Higher the dipole moment, stronger is the intermolecular interaction. The higher value of hyperpolarizability is correlated with the intramolecular charge

transfer, resulting from π-electronic conjugation from electron donor to accepter groups. The physical properties of this π-conjugated compound are governed by high degree electron charge delocalization along charge transfer axis and by small band gap. The higher first-order hyperpolarizability of the compound than that of urea indicates that it could be a potential molecule for future studies of non- linear optical properties. The smaller frontier orbital energy gap and high dipole moment of the compound may increase its NLO activity.

Table 21. The electric dipole moment, polarizability and first-order order hyperpolarizability of AINH calculated at B3LYP/6-311++G(d,p) level

Dipole moment		**First-order hyperpolarizability**	
μ_x	6.43×10^{-18}	β_{xxx}	1.38×10^{-29}
μ_y	3.67×10^{-18}	β_{xxy}	-3.28×10^{-30}
μ_z	3.81×10^{-19}	β_{xyy}	1.82×10^{-30}
μ_{tot}	7.42×10^{-18}	β_{yyy}	-2.62×10^{-30}
Polarizability		β_{xxz}	1.59×10^{-31}
α_{xx}	4.84×10^{-23}	β_{xyz}	1.83×10^{-31}
α_{xy}	-1.01×10^{-24}	β_{yyz}	2.25×10^{-31}
α_{yy}	3.44×10^{-23}	β_{xzz}	1.95×10^{-31}
α_{xz}	-2.12×10^{-24}	β_{yzz}	-4.59×10^{-31}
α_{yz}	7.32×10^{-25}	β_{zzz}	1.86×10^{-31}
α_{zz}	1.96×10^{-23}	β_{tot}	1.09×10^{-29}
α_{tot}	3.41×10^{-23}		

5. Conclusions

Geometries of all the compounds were optimized using DFT calculations at 6-311++G(d,p) level. Global reactivity descriptor parameters were calculated and analysed using HOMO–LUMO. The

MEP maps and Fukui functions show the total charge distribution and chemical reactivities of the compounds. MEP helps to understand the electron density which is useful for determining the electrophilic- and nucleophilic regions. It is found that negative potential sites are on the electronegative atoms and the positive potential sites are around the hydrogen atoms. All the compounds showed higher value of linear polarizabilities, first-order hyperpolarizabilities and the dipole moment than urea. Based on the total static dipole moment (μ), the linear polarizability (α_{tot}) and the mean first-order hyperpolarizability (β_{tot}), 4-hydroxy-3-methoxyacetophenone isonicotinoylhydrazone, 4-[N,N-(dimethyl)amino]benzaldehyde N(4)-methyl(phenyl) thiosemicarbazone and 4-[N,N-(dimethyl)amino]benzaldehyde isonicotinoylhydrazone are most suitable compounds for further investigations as NLO materials.

References

[1] P. Hohenberg, W. Kohn, Inhomogeneous electron gas, Physical review 136(3B) (1964) B864.

[2] R.A. Gaussian09, 1, mj frisch, gw trucks, hb schlegel, ge scuseria, ma robb, jr cheeseman, g. Scalmani, v. Barone, b. Mennucci, ga petersson et al., gaussian, Inc., Wallingford CT 121 (2009) 150-166.

[3] A. Frisch, H. Hratchian, R. Dennington II, T. Keith, J. Millam, B. Nielsen, A. Holder, J. Hiscocks, GaussView Version 5.0. 8, Gaussian, Inc., Wallingford, CT (2009).

[4] R.G. Parr, R.G. Pearson, Absolute hardness: companion parameter to absolute electronegativity, Journal of the American chemical society 105(26) (1983) 7512-7516.

[5] J.P. Perdew, R.G. Parr, M. Levy, J.L. Balduz, Density-Functional Theory for Fractional Particle Number: Derivative Discontinuities of the Energy, Physical Review Letters 49(23) (1982) 1691-1694.

[6] F. Jensen, Introduction to computational chemistry, John wiley & sons (2017).

[7] P. Politzer, D.G. Truhlar, Chemical applications of atomic and molecular electrostatic potentials: reactivity, structure, scattering, and energetics of organic, inorganic, and biological systems, Springer Science & Business Media (2013).

[8] R.G. Parr, W. Yang, Density functional approach to the frontier-electron theory of chemical reactivity, Journal of the American Chemical Society 106(14) (1984) 4049-4050.

[9] C. Morell, A. Grand, A. Toro-Labbe, New dual descriptor for chemical reactivity, The Journal of Physical Chemistry A 109(1) (2005) 205-212.

[10] R.R. Tykwinski, U. Gubler, R.E. Martin, F. Diederich, C. Bosshard, P. Günter, Structure−Property Relationships in Third-Order Nonlinear Optical Chromophores, The Journal of Physical Chemistry B 102(23) (1998) 4451-4465.

[11] V.M. Geskin, C. Lambert, J.-L. Brédas, Origin of high second-and third-order nonlinear optical response in ammonio/borato diphenylpolyene

zwitterions: the remarkable role of polarized aromatic groups, Journal of the American Chemical Society 125(50) (2003) 15651-15658.

[12] Y.-X. Sun, Q.-L. Hao, W.-X. Wei, Z.-X. Yu, L.-D. Lu, X. Wang, Y.-S. Wang, Experimental and density functional studies on 4-(3,4-dihydroxybenzylideneamino) antipyrine, and 4-(2, 3, 4-trihydroxybenzylideneamino) antipyrine, Journal of Molecular Structure: THEOCHEM 904(1-3) (2009) 74-82.

[13] Y.-P. Tian, W.-T. Yu, C.-Y. Zhao, M.-H. Jiang, Z.-G. Cai, H.K. Fun, Structural characterization and second-order nonlinear optical properties of zinc halide thiosemicarbazone complexes, Polyhedron 21(12-13) (2002) 1217-1222.

[14] C. Adant, M. Dupuis, J. Bredas, Ab initio study of the nonlinear optical properties of urea: electron correlation and dispersion effects, International Journal of Quantum Chemistry 56(S29) (1995) 497-507.

[15] C. Lee, W. Yang, R.G. Parr, Development of the Colle-Salvetti correlation-energy formula into a functional of the electron density, Physical Review B 37(2) (1988) 785-789.

PART II

BIOLOGICAL STUDIES

CHAPTER XII

ANTIMICROBIAL STUDIES OF N(4)-DISUBSTITUTED THIOSEMICARBAZONES, ISONICOTINOYLHYDRAZONE AND THEIR METAL COMPLEXES

1. Introduction

Thiosemicarbazones are an important class of multidentate ligands. Transition metal complexes of thiosemicarbazone have important physiological and pharmacological activities. They show anti-tumour, anti-viral and anti-bacterial activities[1, 2]. They are also used as fungicides and pesticides[3]. Thiosemicarbazones with OH group at the ortho position to azomethine group are of interest mainly due to the possibility of hydrogen bonds, either O-H...N or O...H-N type and tautomerism between enol-imine and keto-amine forms.

A detailed literature survey revealed that [ortho-(poly)hydroxybenzaldehyde] thiosemicarbazone and its first row transition metal complexes have remarkable anti-bacterial, anti-viral and SOD activities[4-6]. Antioxidant-, antimicrobial- and mutagenic activities and DNA interaction studies of Ni(II) complexes of 4-methoxy-3-benzyloxybenzaldehyde thiosemicarbazone were reported by Chetana *et al*[7]. The biological activities of Mn(II) and Co(II) complexes of benzyloxybenzaldehyde-4-phenyl-3-thiosemicarbazone were reported by Prathima *et al*[8]. The results showed that the complexes were more active than the free ligand. Elena Pahontu *et al*[9] reported the results of *in vitro* antibacterial activity of 1-phenyl-3-methyl-4-benzoyl-5-pyrazolone4-ethyl-thiosemicarbazone the complexes against *Escherichia coli, Salmonella abony, Staphylococcus aureus* and *Bacillus cereu*s and the antifungal activity against *Candida albicans* strains. They concluded that the metal complexes showed better activity when compared to the free ligand. The effect of the free ligand and their metal complexes on the proliferation of HL-60 cells

was also tested. The studies on biological activities of complexes of zinc(II), cadmium(II), mercury(II), palladium(II) and platinum(II) with 2-acetylpyridine-4-methyl-thiosemicarbazone were reported by Elena Bermejo *et al*[10]. Among the complexes, only that of zinc(II) showed appreciable activity. The studies on biological properties of copper(II) complex of 4[N-benzilidene)amino]antipyrinethiosemicarbazone and 4[N-(4'-methoxybenzilidene)amino]antipyrinethiosemicarbazone were reported by Agarwal *et al*[11]. The synthesis and antibacterial activities of twelve zinc(II) complexes of semi- and thiosemicarbazones were reported by Noriko Chikaraishi Kasuga *et al*[12]. It was revealed from the studies that the presence of bulky groups on the terminal nitrogen of the thiosemicarbazone moiety considerably enhanced their activity.

Hydrazones are another important class of related compounds with immense therapeutic-, industrial-, analytical- and biological applications. Transition metal complexes of hydrazones have gained great interest because of their versatile biological activities such as antitubercular-, antibacterial-, antifungal-, antitumor-, antiviral- and anti-inflammatory activities [13-16].

A number of studies are available on the biological activities of hydrazones. Surendra Prasad and Ram K. Agarwal reported the magneto-spectral, electrochemical-, thermal- and antimicrobial investigations of nickel(II) complexes of N-isonicotinamido-furfuraldimine[17]. They concluded that this complex showed moderate antibacterial- and antifungal activities. Moksharagni *et al*[18] reported that *in vitro* antibacterial activity of nicotinic- and isonicotinic

acid hydrazides of 2-formylpyridine, 2-acetylpyridine and 2-benzoylpyridine.They were screened for the activities against *Staphylococcus aureus, Bacillus subtilis, Escherichia coli* and *Salmonella typhi.* Isonicotinoylhydrazones showed more antibacterial activity than the corresponding nicotinoylhydrazones. Antibacterial study of series of complexes of Mn(II), Co(II), Ni(II), Cu(II) and Cd(II) with isonicotinoylhydrazone-4-diphenylaminobenzaldehyde (INHDAB) has been reported by Mitu *et al*[19]. These compounds were screened against *Staphylococcus aureus, Escherichia coli, Pseudomonas aeruginosa, Salmonella enteritidis and Shigella flexneri* bacterial strains. The metal complexes showed higher activity than the parent ligand.

In view of these observations, it has been decided to evaluate the antibacterial- and antifungal activities of the N(4)-disubstituted thiosemicarbazones of several carbonyl compounds, 4-[N,N-(dimethyl)amino]benzaldehyde isonicotinoylhydrazone and a few of their metal complexes that we have synthesized.

2. Antibacterial activity

The antibacterial activities of the following ligands,

- 2,4-Dihydroxybenzaldehyde N(4)-methyl(phenyl)thiosemicarbazone (DBMPTSC) (HL),
- 4-[N,N-(Dimethyl)amino]benzaldehyde N(4)-methyl(phenyl)thiosemicarbazone (PDBMPTSC) (HL),

- 4-Benzyloxybenzaldehyde N(4)-methyl(phenyl)thiosemicarbazone (BBMPTSC) (HL),
- 4-Hydroxy-3-methoxyacetophenone N(4)-methyl(phenyl)thiosemicarbazone (AMPTSC), (HL) and
- 4-[N,N-(Dimethyl)amino]benzaldehyde isonicotinoylhydrazone (PDBINH), (HL) and the Co(II), Ni(II) and Cu(II) complexes of the above ligands were evaluated.

2.1. Materials and methods

2.1.1. Culture medium

Mueller Hinton Agar M173 of HiMedia was used to prepare Petri plates for conducting antibacterial studies. Suspended 38 g of agar in 1000 ml of distilled water. The suspension was heated to boiling to dissolve it completely. Sterilized by autoclaving at 15 lbs pressure at 121°C for 15 minutes. Cooled to 45-50°C, mixed well and poured on sterile Petri plates.

2.1.2. Inoculums details

Inoculums were procured from The Microbial Type Culture Collection and Gene Bank (MTCC), Chandigarh**.**

Table 1. The inoculums details of test-bacteria

Bacteria	**MTCC No**	**Incubation condition**
Staphylococcus aureus	87	37^0C for 24 hours
Bacillus subtilis	2413	37^0C for 24 hours
Pseudomonas aeruginosa	424	37^0C for 24 hours
Escherichia coli	443	37^0C for 24 hours

2.1.3. Antibacterial activity by Agar well Diffusion method

Agar well diffusion method is widely used to evaluate the antimicrobial activity. The determination of antibacterial activities of the compounds was done by using Muller Hinton Agar medium (HIMEDIA- M173). Same amount (15-20 mL) of Mueller-Hinton agar was poured on glass Petri plates of same size and allowed to solidify. Wells with a diameter of 8 mm (20 mm apart from one another) were punched aseptically with a sterile cork borer on each plate. Standardized inoculums of the test organism were uniformly spread on the surface of these plates using sterile cotton swab. Sample solution (40 µL and 80 µL) at desired concentration from 10mg/mL stock solution was added to two wells. Gentamycin as positive-and the solvent (DMSO) used for sample preparation as negative controls were added to third and fourth well, respectively. Then the agar plates were incubated under suitable conditions depending upon the test microorganism. After incubation, clear zone was observed. Inhibition of the bacterial growth was measured in mm**.**

3. Results and discussion

3.1. 2,4-Dihydroxybenzaldehyde N(4)-methyl(phenyl) thiosemicarbazone (DBMPTSC), (HL)

Evaluation of antibacterial activities of 2,4-dihydroxybenzaldehyde N(4)-methyl(phenyl)thiosemicarbazone (HL) and its Co(II), Ni(II), and Cu(II) complexes were carried out using Agar well Diffusion method. The structure of the ligand, HL is given in Fig.1.

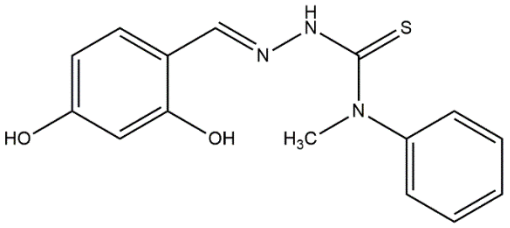

Fig.1. 2,4-Dihydroxybenzaldehyde N(4)-methyl(phenyl) thiosemicarbazone (HL)

Table 2. Antibacterial activity of 2,4-dihydroxybenzaldehyde N(4)-methyl(phenyl)thiosemicarbazone and its complexes

ANTIBACTERIAL ASSAY					
Organism name		**Zone of inhibition (mm)**			
Samples	**Concentration of samples**	***P. aeruginosa***	***E. coli***	***S. aureus***	***B. subtilis***
HL	Standard Gentamycin (80mcg)	25	21	22	29
	Negative control	-	-	-	-
	T1(400mcg)	12	-	-	18
	T2(800mcg	16	-	-	20
Co(II) complex	Standard Gentamycin (80mcg)	25	22	22	30
	Negative control	-	-	-	-
	T1(400mcg)	-	-	-	-
	T2(800mcg)	-	-	-	11
Ni(II) complex	Standard Gentamycin (80mcg)	25	22	23	28
	Negative control	-	-	-	-
	T1(400mcg)	-	10	-	17
	T2(800mcg)	-	12	12	20
Cu(II) complex	Standard Gentamycin (80mcg)	24	22	22	30
	Negative control	-	-	-	-
	T1(400mcg)	-	-	-	21
	T2(800mcg)	-	-	11	25

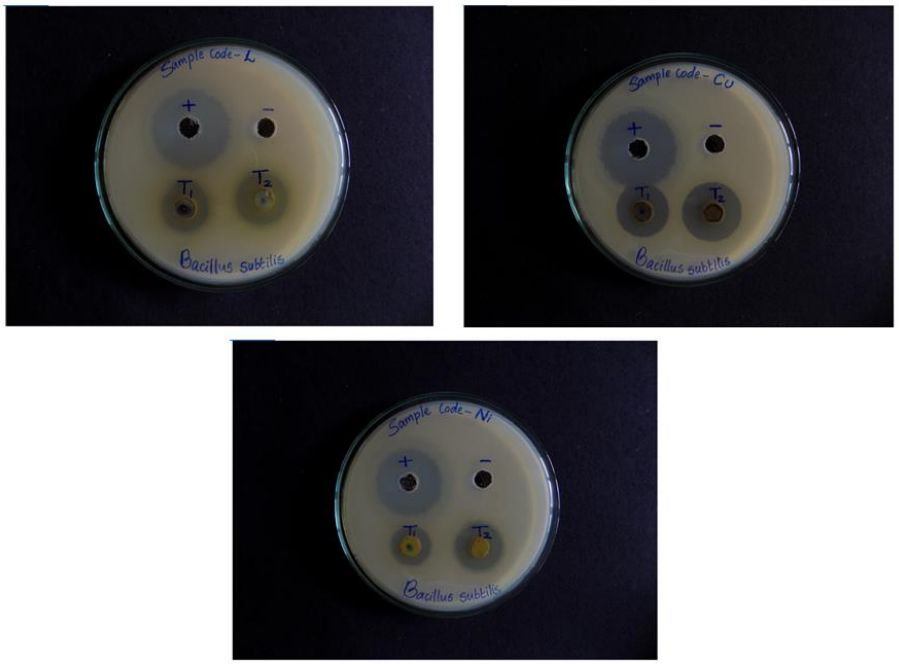

Fig.2. Antibacterial activity of Ligand (denoted as L), Cu(II) and Ni(II) complex on the *B. subtilis*

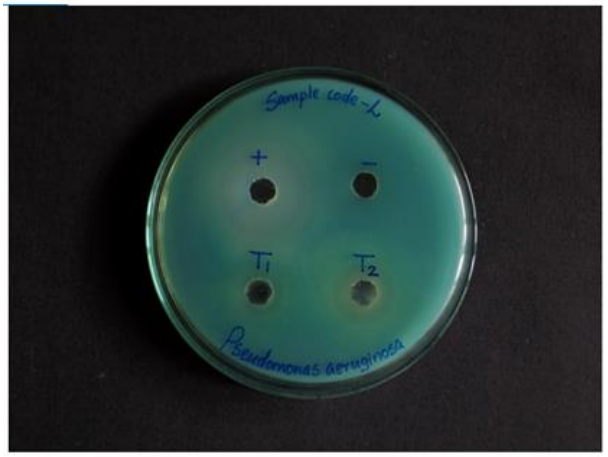

Fig.3. Antibacterial activity of ligand (denoted as L) on the *P. aeruginosa*

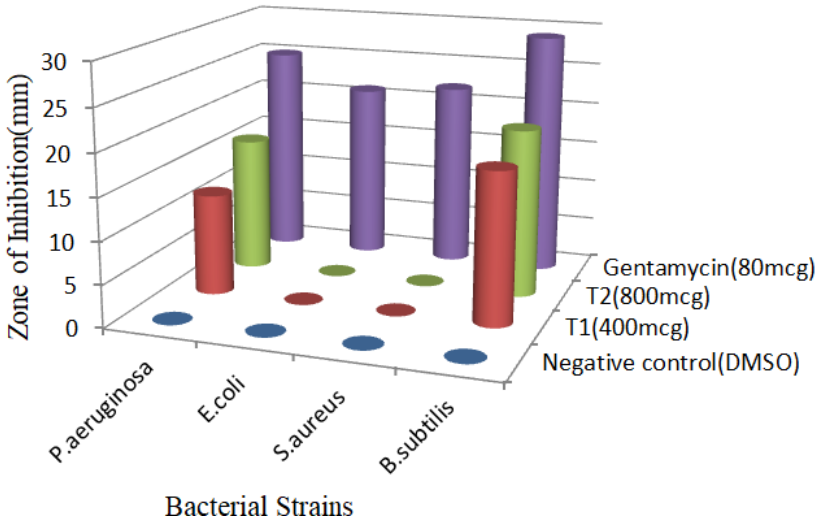

Fig.4. Graphical representation of antibacterial study of 2,4-dihydroxybenzaldehyde N(4)-methyl(phenyl)thiosemicarbazone

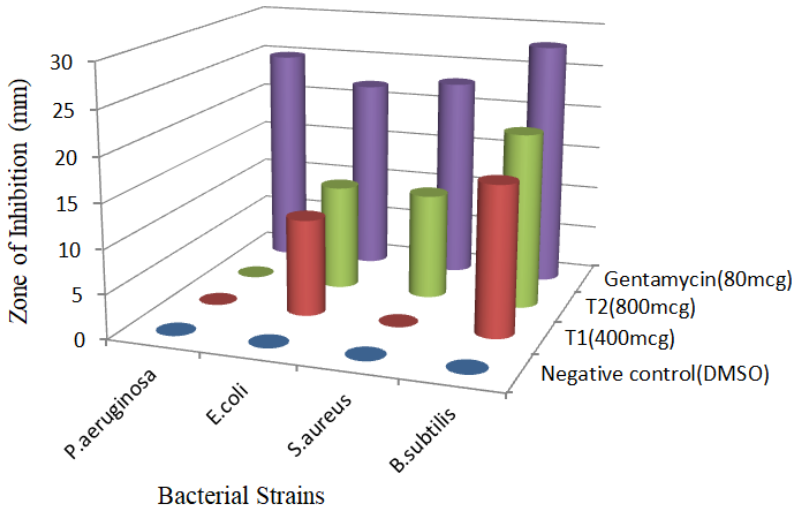

Fig.5. Graphical representation of antibacterial study of Ni(II) complex of 2,4-dihydroxybenzaldehyde N(4)-methyl(phenyl) thiosemicarbazone

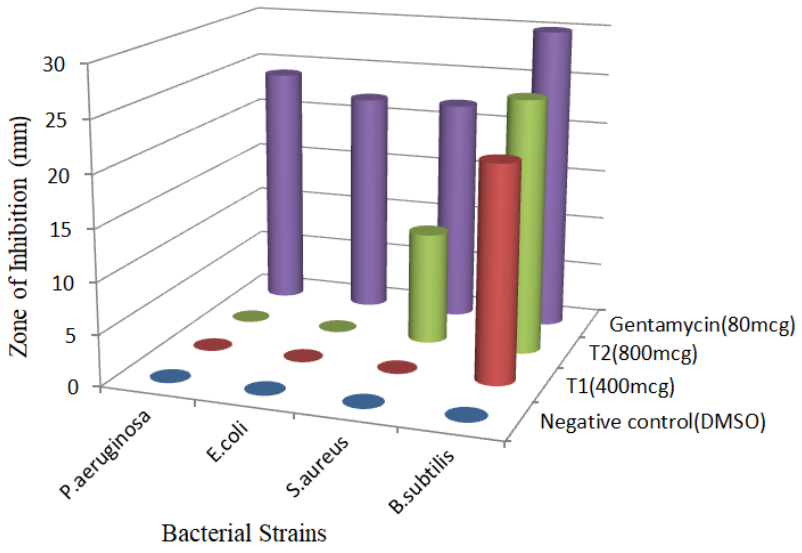

Fig.6. Graphical representation of antibacterial study of Cu(II) complex of 2,4-dihydroxybenzaldehyde N(4)-methyl(phenyl) thiosemicarbazone

It was found that the ligand, 2,4-dihydroxybenzaldehyde N(4)-methyl(phenyl)thiosemicarbazone exhibited activity against *P. aeruginosa* and *B. subtilis.* The Co(II) complex showed least activity among the samples. However, Ni(II) and Cu(II) complexes showed higher inhibition against *B. subtilis.*

3.2. 4-[N,N-(Dimethyl)amino]benzaldehyde N(4)-methyl(phenyl)thiosemicarbazone (PDBMPTSC), (HL)

Evaluation of antibacterial activities of the ligand and its Co(II), Ni(II) and Cu(II) complexes was carried out using Agar well Diffusion Method. The structure of the ligand, is given in Fig.7.

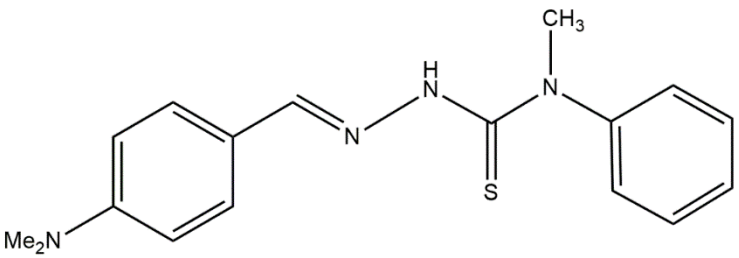

Fig.7. 4-[N,N-(Dimethyl)amino]benzaldehyde N(4)-methyl(phenyl) thiosemicarbazone (HL)

Fig.8. Antibacterial activity of Cu(II) complex of 4-[N,N-(dimethyl)amino]benzaldehyde N(4)-methyl(phenyl) thiosemicarbazone (denoted as CuL2) on the *B. subtilis*

Table 3. Antibacterial activity of 4-[N,N-(dimethyl) amino]benzaldehyde N(4)-methyl(phenyl)thiosemicarbazone and its complexes

ANTIBACTERIAL ASSAY					
Organism name		**Zone of inhibition (mm)**			
Samples	**Concentration of samples**	***P. aeurginosa***	***E. coli***	***S. aureus***	***B. subtilis***
HL	Standard Gentamycin (80mcg)	24	30	21	30
	Negative control	-	-	-	-
	T1(400mcg)	-	12	-	-
	T2(800mcg	-	13	11	- -
Co(II) complex	Standard Gentamycin (80mcg)	22	28	24	30
	Negative control	-	-	-	-
	T1(400mcg)	-	-	14	14
	T2(800mcg)	11	-	19	16
Ni(II) complex	Standard Gentamycin (80mcg)	22	28	25	30
	Negative control	-	-	-	-
	T1(400mcg)	11	11	-	11
	T2(800mcg)	12	15	-	14
Cu(II) complex	Standard Gentamycin (80mcg)	24	28	25	24
	Negative control	-	-	-	-
	T1(400mcg)	-	-	-	18
	T2(800mcg)	-	11	-	23

Fig.9. Antibacterial activity of 4-[N,N-(dimethyl)amino]benzaldehyde N(4)-methyl(phenyl)thiosemicarbazone (denoted as L2) on the *E. coli*

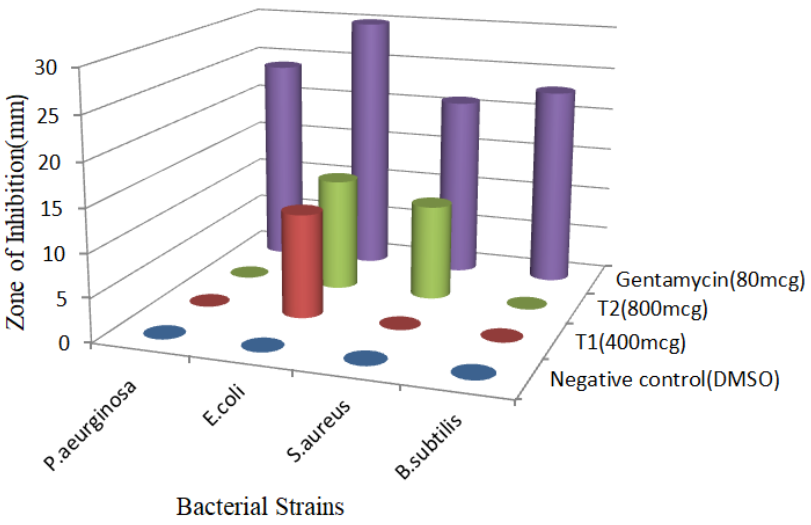

Fig.10. Graphical representation of antibacterial study of 4-[N,N-(dimethyl)amino]benzaldehyde N(4)-methyl(phenyl) thiosemicarbazone

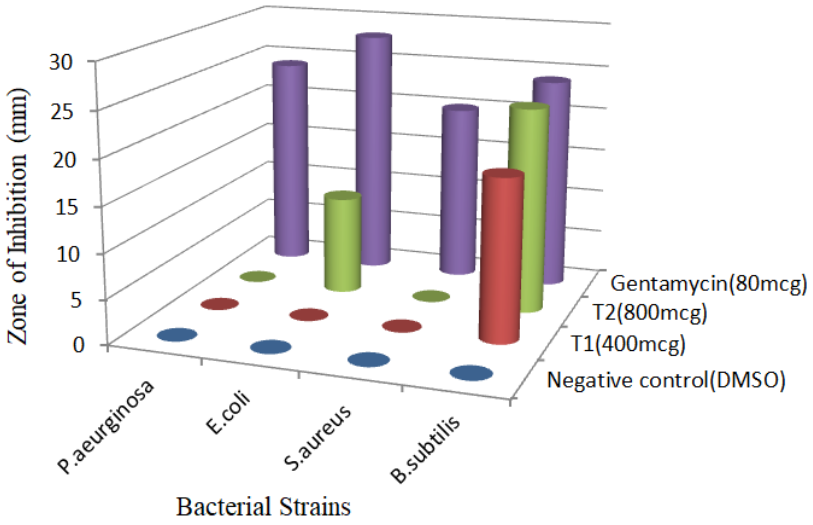

Fig.11. Graphical representation of antibacterial study of Cu(II) complex of 4-[N,N-(dimethyl)amino]benzaldehyde N(4)-methyl(phenyl)thiosemicarbazone

Preliminary studies showed that all the complexes were active towards all the four bacterial species. Further, a detailed study in this regard will be interesting. It was found that all the complexes showed higher activities than the ligand. The complexes showed variation in their activities against different bacteria. For example, Cu(II) complex exhibited higher activity against *Bacillus* species but lower activity towards the other three bacteria.

3.3. 4-Benzyloxybenzaldehyde N(4)-methyl(phenyl) thiosemicarbazone (BBMPTSC), (HL)

Evaluation of antibacterial activities of the ligand and its Co(II), Ni(II), and Cu(II) complexes was carried out using Agar well Diffusion Method. The structure of the ligand, HL is given in Fig.12.

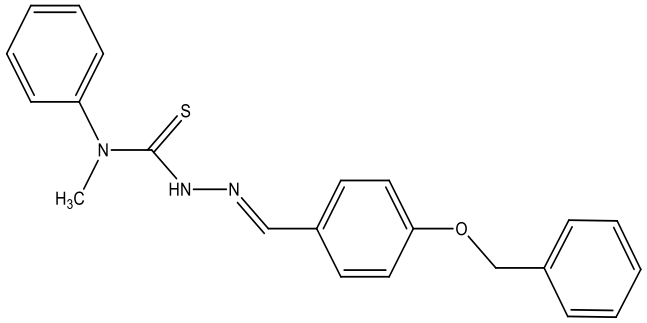

Fig.12. 4-Benzyloxybenzaldehyde N(4)-methyl(phenyl) thiosemicarbazone (HL)

Fig.13. Antibacterial activity of Ni(II) complex of 4-benzyloxybenzaldehyde N(4)-methyl(phenyl) thiosemicarbazone (denoted as NiL_3) on the *S. aureus*

Table 4. Antibacterial activity of 4-benzyloxybenzaldehyde N(4)-methyl(phenyl)thiosemicarbazone and its complexes

ANTIBACTERIAL ASSAY					
Organism name		**Zone of inhibition (mm)**			
Samples	**Concentration of samples**	***P. aeruginosa***	***E. coli***	***S. aureus***	***B. subtilis***
HL	Standard Gentamycin (80mcg)	27	23	26	29
	Negative control	-	-	-	-
	T1(400mcg)	-	-	-	-
	T2(800mcg	-	-	-	-
Co(II) complex	Standard Gentamycin (80mcg)	29	24	25	29
	Negative control	-	-	-	-
	T1(400mcg)	-	12	-	9
	2(800mcg)	-	-	-	12
Ni(II) complex	Standard Gentamycin (80mcg)	30	26	24	29
	Negative control	-	-	-	-
	T1(400mcg)	-	-	-	10
	T2(800mcg)	-	-	10	12
Cu(II) complex	Standard Gentamycin (80mcg)	30	28	24	28
	Negative control	-	-	-	-
	T1(400mcg)	-	-	-	10
	T2(800mcg)	-	-	11	14

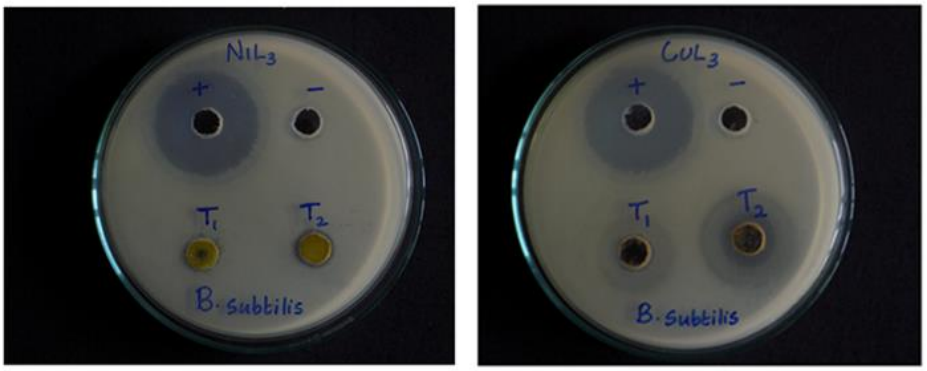

Fig.14. Antibacterial activity of Ni(II) (denoted as NiL_3) and Cu(II) (denoted as CuL_3) complexes on the *B. subtilis*

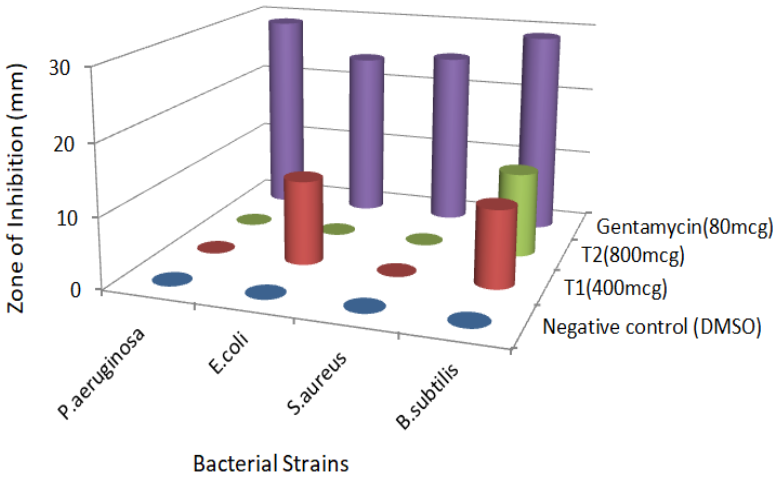

Fig.15. Graphical representation of antibacterial study of Co(II) complex of 4-benzyloxybenzaldehyde N(4)-methyl(phenyl) thiosemicarbazone

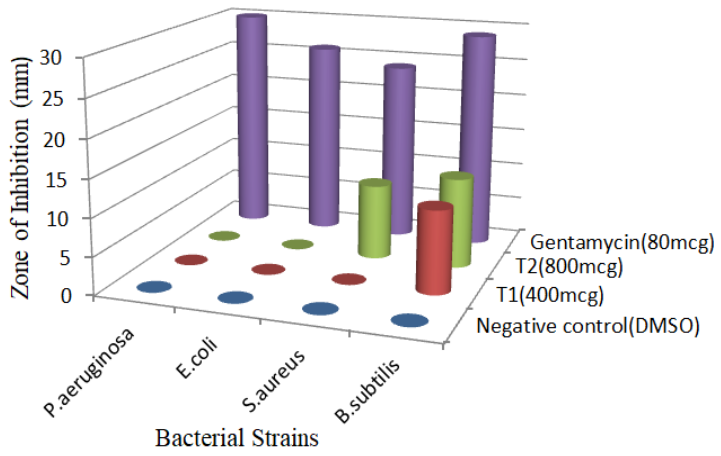

Fig.16. Graphical representation of antibacterial study of Ni(II) complex of 4-benzyloxybenzaldehyde N(4)-methyl(phenyl) thiosemicarbazone

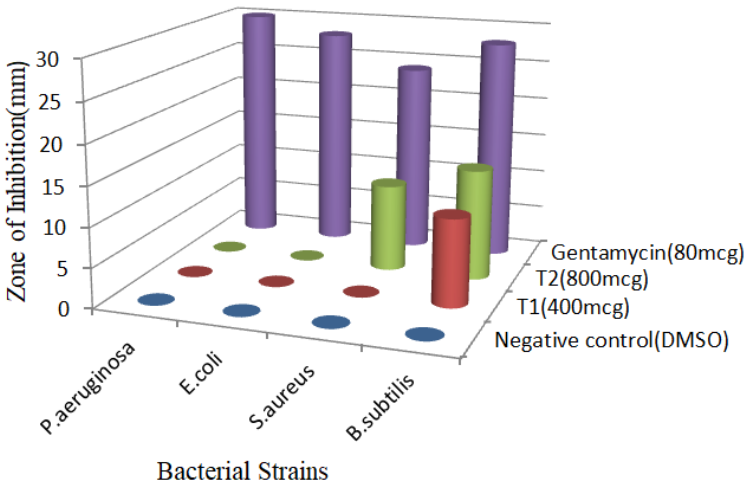

Fig.17. Graphical representation of antibacterial study of Cu(II) complex of 4-benzyloxybenzaldehyde N(4)-methyl(phenyl) thiosemicarbazone

The experimental results showed that the complexes of 4-benzyloxybenzaldehyde N(4)-methyl(phenyl)thiosemicarbazone showed activity against the tested bacterial strains in a concentration dependent manner. However, the free ligand was not found to possess any antibacterial activity. Of the complexes, that of Cu(II) showed higher activity than Co(II) and Ni(II) complexes against *B. subtilis*. However, for different strains of bacteria, the complexes showed difference in their activities. Based on the preliminary analysis, most of the complexes were active towards all the bacterial strains except *P. aeruginosa* and hence a detailed study in this regard will be interesting.

3.4. 4-Hydroxy-3-methoxyacetophenone N(4)-methyl(phenyl) thiosemicarbazone (AMPTSC), (HL)

Evaluation of antibacterial activities of the ligand and its Co(II), Ni(II) and Cu(II) complexes were carried out using Agar well Diffusion Method. The structure of the ligand is given in Fig.18.

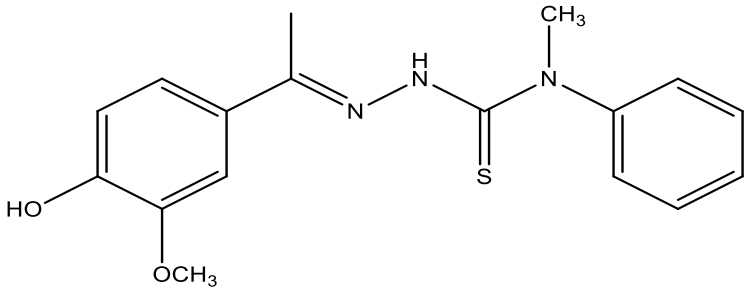

Fig.18. 4-Hydroxy-3-methoxyacetophenone N(4)-methyl(phenyl) thiosemicarbazone (AMPTSC), (HL)

Table 5. Antibacterial activity of 4-hydroxy-3-methoxyacetophenone N(4)-methyl(phenyl)thiosemicarbazone and its complexes

ANTIBACTERIAL ASSAY					
Organism name		**Zone of inhibition (mm)**			
Samples	**Concentration of samples**	***P. aeurginosa***	***E. coli***	***S. aureus***	***B. subtilis***
HL	Standard Gentamycin (80mcg)	23	23	20	22
	Negative control	-	-	-	-
	T1(400mcg)	-	-	-	-
	T2(800mcg	-	-	-	- -
Co(II) complex	Standard Gentamycin (80mcg)	27	23	19	26
	Negative control	-	-	-	-
	T1(400mcg)	-	-	-	-
	T2(800mcg)	-	12	-	12
Ni(II) complex	Standard Gentamycin (80mcg)	26	22	20	26
	Negative control	-	-	-	-
	T1(400mcg)	-	-	-	-
	T2(800mcg)	-	-	10	-
Cu(II) complex	Standard Gentamycin (80mcg)	24	28	18	24
	Negative control	-	-	-	-
	T1(400mcg)	-	-	-	10
	T2(800mcg)	-	12		17

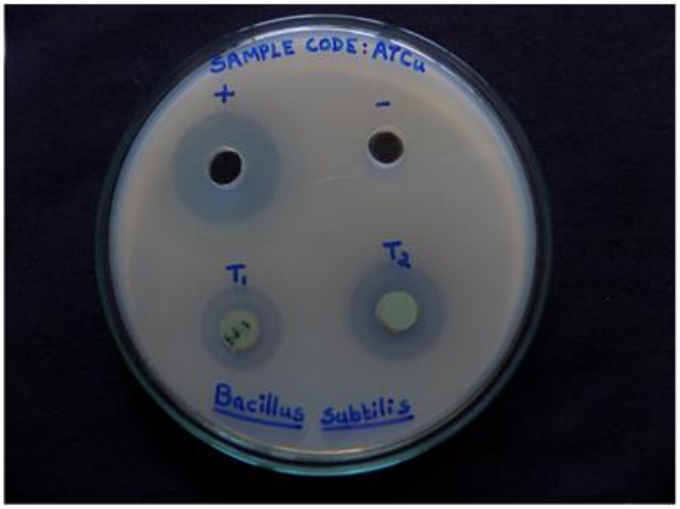

Fig.19. Antibacterial activity of Cu(II) complex of of 4-hydroxy-3-methoxyacetophenone N(4)-methyl(phenyl)thiosemicarbazone (denoted as ATCu) on the *B. subtilis*

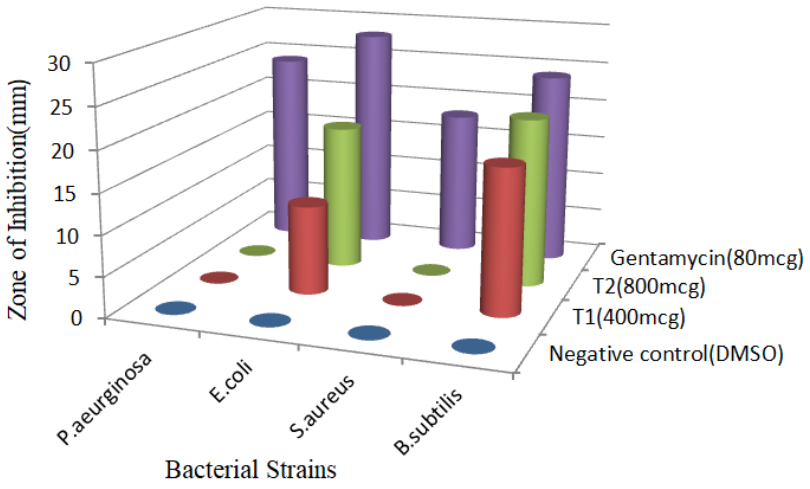

Fig.20. Graphical representation of antibacterial study of Cu(II) complex of 4-hydroxy-3-methoxyacetophenone N(4)-methyl(phenyl)thiosemicarbazone

Table 5 shows the results obtained in the antibacterial tests of the ligand, 4-hydroxy-3-methoxyacetophenone N(4)-methyl(phenyl) thiosemicarbazone and its Co(II), Ni(II) and Cu(II) complexes. The results are expressed as diameters of inhibition zones. The ligand didn't show any activity against the bacterial strains tested. However, the complexes showed mild activities.

3.5. 4-[N,N-(Dimethyl)amino]benzaldehyde isonicotinoylhydrazone (PDBINH), (HL)

Evaluation of antibacterial activities of the ligand and its Co(II), Ni(II) and Cu(II) complexes was carried out using Agar well Diffusion Method. The structure of the ligand, is given in Fig.21.

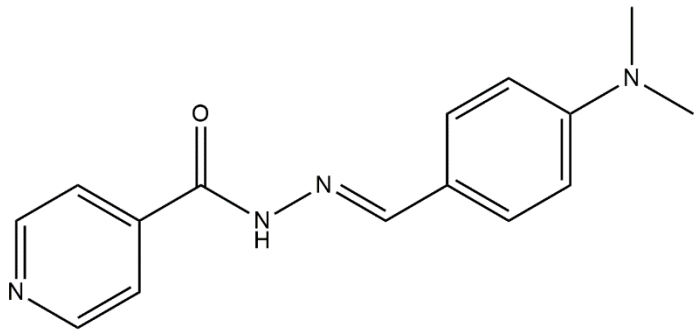

Fig.21. 4-[N,N-(dimethyl)amino]benzaldehyde isonicotinoylhydrazone (HL)

Table 6. Antibacterial activity of 4-[N,N-(dimethyl) amino]benzaldehyde isonicotinoylhydrazone and its complexes

ANTIBACTERIAL ASSAY					
Organism name		**Zone of inhibition (mm)**			
Samples	**Concentration of samples**	***P. aeurginosa***	***E. coli***	***S. aureus***	***B. subtilis***
HL	Standard Gentamycin (80mcg)	24	23	21	30
	Negative control	-	-	-	-
	T1(400mcg)	-	-	-	-
	T2(800mcg	-	10	11	10
Co(II) complex	Standard Gentamycin (80mcg)	22	28	24	30
	Negative control	-	-	-	-
	T1(400mcg)	-	-	-	-
	T2(800mcg)	11	-	12	11
Ni(II) complex	Standard Gentamycin (80mcg)	22	28	25	30
	Negative control	-	-	-	-
	T1(400mcg)	-	11	13	13
	T2(800mcg)	-	13	15	15
Cu(II) complex	Standard Gentamycin (80mcg)	22	28	25	30
	Negative control	-	-	-	-
	T1(400mcg)	-	-	-	15
	T2(800mcg)	-	11		16

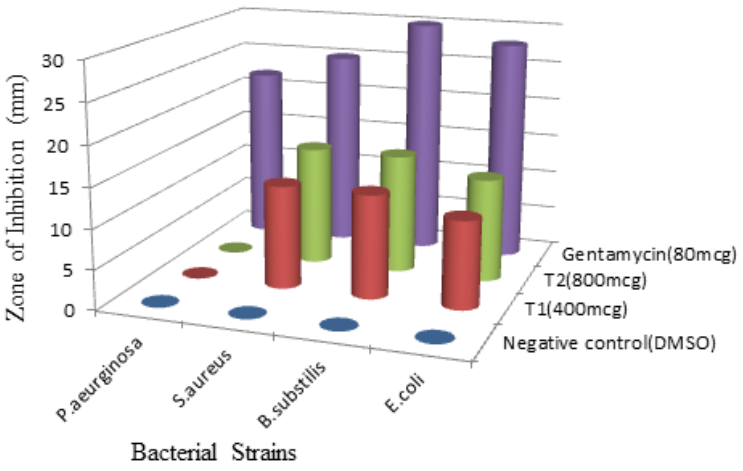

Fig.22. Graphical representation of antibacterial study of Ni(II) complex of 4-[N,N-(dimethyl)amino]benzaldehyde isonicotinoylhydrazone

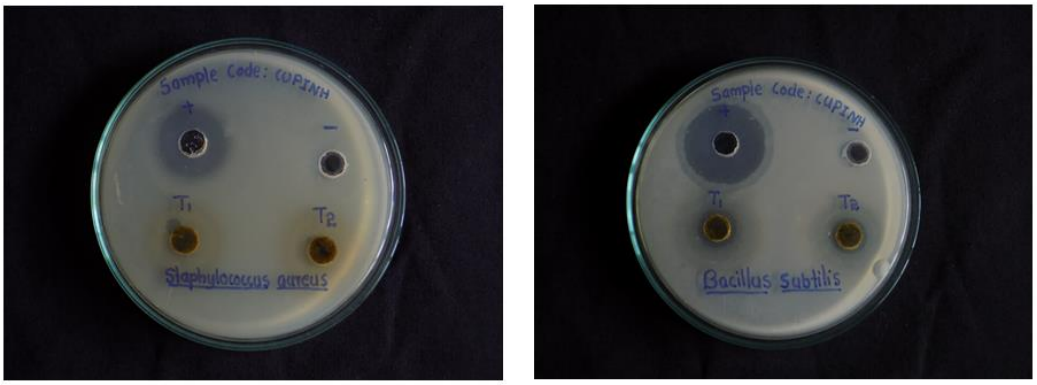

Fig.23. Antibacterial activity of Cu(II) complex of 4-[N,N-(dimethyl)amino] benzaldehyde isonicotinoylhydrazone (denoted as CUPINH) on the *S. aureus* and *B. subtilis*

Fig.24. Antibacterial activity of Ni(II) complex of 4-[N,N-(dimethyl)amino]benzaldehyde isonicotinoylhydrazone (denoted as NiPINH) on the *B. subtilis* and *E. coli*

The results of the tests of antibacterial activities are displayed in Table 6. Ni(II) and Cu(II) complexes showed good activities against three kinds of bacteria namely, *B. subtilis*, *S. aureus* and *E. coli*. In the case of the complexes, the inhibition area increased along with their concentrations. The ligand and the Co(II) complex were found to be less active. It was also noted that the activities of the compounds were concentration dependent.

4. Antifungal activity

The antifungal activities of the following ligands,

- 2,4-Dihydroxybenzaldehyde N(4)-methyl(phenyl)thiosemicarbazone (DBMPTSC) (HL),
- 4-[N,N-(Dimethyl)amino]benzaldehyde N(4)-methyl(phenyl)thiosemicarbazone (PDBMPTSC) (HL),

- 4-Benzyloxybenzaldehyde N(4)-methyl(phenyl)thiosemicarbazone (BBMPTSC) (HL),
- 4-Hydroxy-3-methoxyacetophenone N(4)-methyl(phenyl)thiosemicarbazone (AMPTSC) (HL) and
- 4-[N,N-(Dimethyl)amino]benzaldehyde isonicotinoylhydrazone (PDBINH) (HL) and the Co(II), Ni(II) and Cu(II) complexes of the above ligands were evaluated.

4.1. Materials and methods

4.1.1. Culture medium details

Rose Bengal agar M842 Himedia was used for the determination of susceptibility of fungal strains to antifungal agents. Suspended 31.55 grams of it in 1000 ml distilled water. Heated to boiling till the medium dissolved completely. It was sterilized by autoclaving at 15 lbs pressure at 121°C for 15 minutes, cooled to 45-50°C, mixed well and poured on sterile Petri plates.

4.1.2. Inoculums details

Inoculums were procured from The Microbial Type Culture Collection and Gene Bank (MTCC), Chandigarh.

Table 7. The inoculums details of test-fungi

Fungi	MTCC No	Incubation condition
Aspergillus niger	281	27^0C for 48 hours
Candida albicans	227	27^0C for 48 hours

4.1.3. Antifungal assay by Agar well Diffusion method

Agar well diffusion method is widely used to evaluate the antimicrobial activity of the plant extracts. Sterilized 15- 20 mL of Rose Bengal agar was poured on glass Petri plates of same size and allowed to solidify. After the solidification, wells (4 wells/plate) were made aseptically with a sterile cork borer of diameter 8 mm (20 mm apart from one another) were punched on each plate. Standardized inoculums of the test organism were uniformly spread on the surface of these solidified media using sterile cotton swab. The test volumes (40 µL & 80 µL) of the sample at desired concentrations were added to the first 2 wells. To the third well, 200mcg of Clotrimazole as positive control and to the fourth one with DMSO as negative control were added. Then the agar plates were incubated under suitable conditions depending upon the test microorganism. After incubation, clear zone was observed. Inhibition of the fungal growth was measured in mm.

5. Results and discussion

5.1. 2,4-Dihydroxybenzaldehyde N(4)-methyl(phenyl) thiosemicarbazone (DBMPTSC), (HL)

Evaluation of antifungal activities of 2,4-dihydroxybenzaldehyde N(4)-methyl(phenyl)thiosemicarbazone and its Co(II), Ni(II) and Cu(II) complexes was carried out using Agar well Diffusion Method.

Table 8. Antifungal assay of 2,4-dihydroxybenzaldehyde N(4)-methyl(phenyl)thiosemicarbazone and its complexes

ANTIFUNGAL ASSAY			
Organism name		**Zone of inhibition (mm)**	
Samples	**Concentration of samples**	***A. niger***	***C. albicans***
HL	Standard clotrimazole (200mcg)	21	17
	Negative control	-	-
	T1(400mcg)	14	-
	T2(800mcg	19	15
Co(II) complex	Standard clotrimazole (200mcg)	20	17
	Negative control	-	-
	T1(400mcg)	-	-
	T2(800mcg)	-	-
Ni(II) complex	Standard clotrimazole (200mcg)	20	18
	Negative control	-	-
	T1(400mcg)	-	-
	T2(800mcg)	-	11
Cu(II) complex	Standard clotrimazole (200mcg)	20	19
	Negative control	-	-
	T1(400mcg)	-	-
	T2(800mcg)	-	12

Fig.25. Antifungal assay of 2,4-dihydroxybenzaldehyde N(4)-methyl(phenyl)thiosemicarbazone (denoted as L) on the *A. niger*

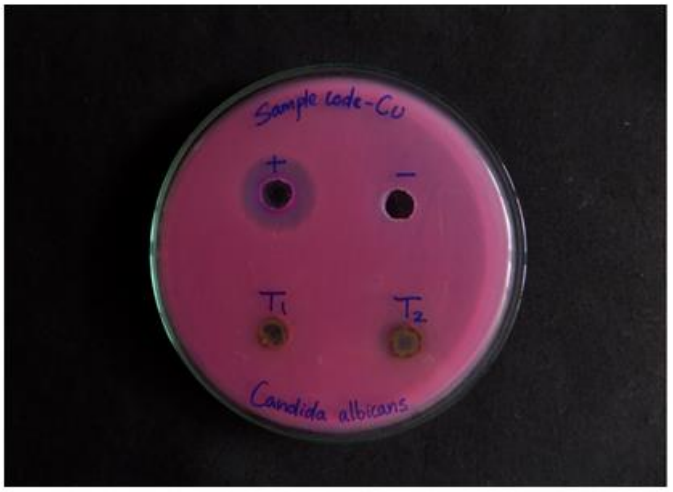

Fig.26. Antifungal assay of Cu(II) complex of 2,4-dihydroxybenzaldehydeN(4)-methyl(phenyl) thiosemicarbazone (denoted as Cu) on the *C. albicans*

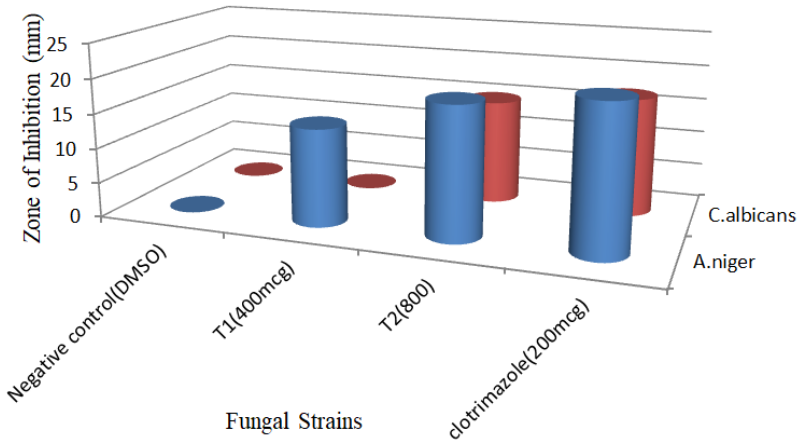

Fig.27. Graphical representation of antifungal assay of 2,4-dihydroxybenzaldehyde N(4)-methyl(phenyl) thiosemicarbazone

The ligand, 2,4-dihydroxybenzaldehyde N(4)-methyl(phenyl) thiosemicarbazone showed higher activity than its metal complexes towards both *A. niger* and *C. albicans*. Co(II) complex did not show any activity. Cu(II) and Ni(II) complexes exhibited moderate activities.

5.2. 4-[N,N(Dimethyl)amino]benzaldehyde N(4)-methyl(phenyl)thiosemicarbazone (PDBMPTSC), (HL)

Evaluation of antifungal activities of Co(II), Ni(II) and Cu(II) complexes and the ligand, 4-[N,N-(dimethyl)amino]benzaldehyde N(4)-methyl(phenyl)thiosemicarbazone was carried out using Agar well Diffusion Method.

Table 9. Antifungal assay of 4-[N,N(dimethyl)amino]benzaldehyde N(4)-methyl(phenyl)thiosemicarbazone and its complexes

ANTIFUNGAL ASSAY			
Organism name		**Zone of inhibition (mm)**	
Samples	**Concentration of samples**	***A. niger***	***C. albicans***
HL	Standard clotrimazole (200mcg)	20	22
	Negative control	-	-
	T1(400mcg)	12	13
	T2(800mcg	14	16
Co(II) complex	Standard clotrimazole (200mcg)	20	23
	Negative control	-	-
	T1(400mcg)	11	-
	T2(800mcg)	12	11
Ni(II) complex	Standard clotrimazole (200mcg)	20	23
	Negative control	-	-
	T1(400mcg)	11	-
	T2(800mcg)	13	11
Cu(II) complex	Standard clotrimazole (200mcg)	20	22
	Negative control	-	-
	T1(400mcg)	14	15
	T2(800mcg)	16	16

Fig.28. Antifungal assay of 4-[N,N-(dimethyl)amino]benzaldehyde N(4)-methyl(phenyl)thiosemicarbazone (denoted as L_2) and its Cu(II) complex (denoted as CuL_2) on the *C. albicans*

Fig.29. Antifungal assay of 4-[N,N-(dimethyl)amino]benzaldehyde N(4)-methyl(phenyl)thiosemicarbazone (denoted as L_2) and its Cu(II) complex (denoted as CuL_2) on the *A. niger*

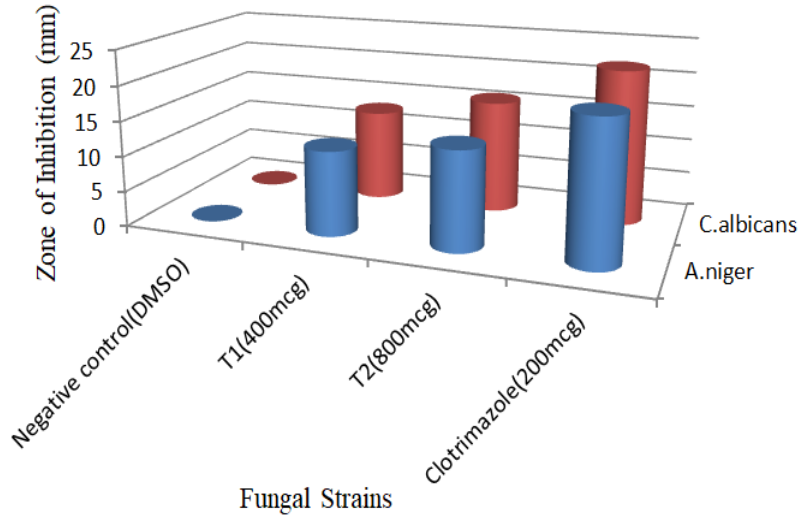

Fig.30. Graphical representation of antifungal assay of 4-[N,N-(dimethyl)amino]benzaldehyde N(4)-methyl(phenyl) thiosemicarbazone

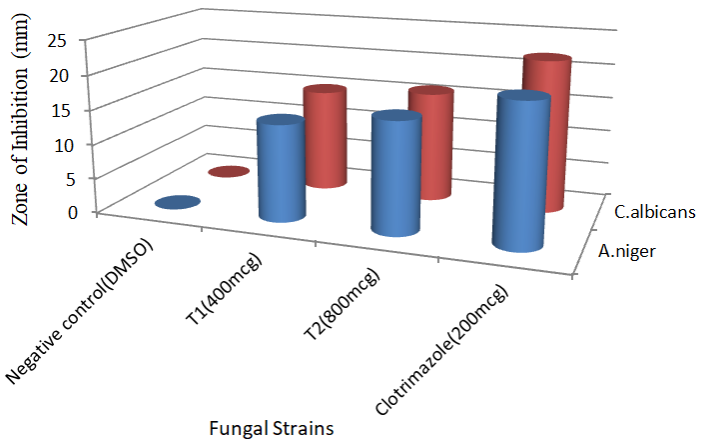

Fig.31. Graphical representation of antifungal assay of Cu(II) complex of 4-[N,N-(dimethyl)amino]benzaldehyde N(4)-methyl(phenyl)thiosemicarbazone

Table 9 displays the results obtained for antifungal studies. The ligand and the complexes showed activities in a concentration dependent manner against *A. niger* and *C. albicans*.

5.3. 4-Benzyloxybenzaldehyde N(4)-methyl(phenyl) thiosemicarbazone (BBMPTSC), (HL)

Antifungal activities of the ligand and its Co(II), Ni(II) and Cu(II) complexes were evaluated using Agar well Diffusion Method.

Table 10. Antifungal assay of 4-benzyloxybenzaldehyde N(4)-methyl(phenyl)thiosemicarbazone and its complexes

ANTIFUNGAL ASSAY			
Organism name		**Zone of inhibition (mm)**	
Samples	**Concentration of samples**	***A. niger***	***C. albicans***
HL	Standard clotrimazole (200mcg)	20	18
	Negative control	-	-
	T1(400mcg)	-	-
	T2(800mcg	-	-
Co(II) complex	Standard clotrimazole (200mcg)	19	18
	Negative control	-	-
	T1(400mcg)	-	-
	T2(800mcg)	11	-
Ni(II) complex	Standard clotrimazole (200mcg)	19	18
	Negative control	-	-
	T1(400mcg)	-	-
	T2(800mcg)	-	12
Cu(II) complex	Standard clotrimazole (200mcg)	20	18
	Negative control	-	-
	T1(400mcg)	11	13
	T2(800mcg)	-	12

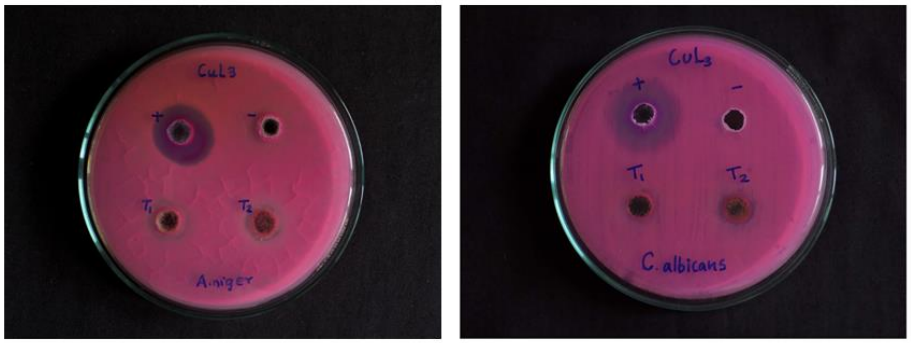

Fig.32. Antifungal assay of Cu(II) complex of 4-benzyloxybenzaldehyde N(4)-methyl(phenyl) thiosemicarbazone (denoted as CuL_3) on the *A. niger* and *C. albicans*

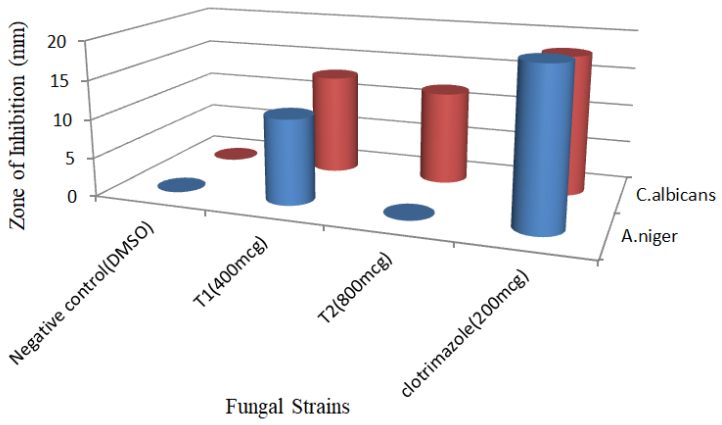

Fig.33. Graphical representation of antifungal assay of Cu(II) complex of 4-benzyloxybenzaldehyde N(4)-methyl(phenyl) thiosemicarbazone

It was found that 4-benzyloxybenzaldehyde N(4)-methyl(phenyl) thiosemicarbazone did not exhibit any antifungal activity. The Cu(II)

complex showed activity against *A. niger* and *C. albicans.* However, the Co(II) and Ni(II) complexes did show any appreciable activities.

5.4. 4-Hydroxy-3-methoxyacetophenone N(4)-methyl(phenyl) thiosemicarbazone (AMPTSC), (HL)

Evaluation of antifungal activities of 4-hydroxy-3-methoxyacetophenone N(4)-methyl(phenyl)thiosemicarbazone and its Co(II), Ni(II) and Cu(II) complexes was carried out using Agar well Diffusion Method.

Table 11. Antifungal assay of 4-hydroxy-3-methoxyacetophenone N(4)-methyl(phenyl)thiosemicarbazone and its complexes

ANTIFUNGAL ASSAY			
Organism name		**Zone of inhibition (mm)**	
Samples	**Concentration of samples**	***A. niger***	***C. albicans***
HL	Standard clotrimazole (200mcg)	20	23
	Negative control	-	-
	T1(400mcg)	12	19
	T2(800mcg	13	20
Co(II) complex	Standard clotrimazole (200mcg)	20	23
	Negative control	-	-
	T1(400mcg)	-	11
	T2(800mcg)	11	14
Ni(II) complex	Standard clotrimazole (200mcg)	21	23
	Negative control	-	-
	T1(400mcg)	-	-
	T2(800mcg)	11	12
Cu(II) complex	Standard clotrimazole (200mcg)	20	22
	Negative control	-	-
	T1(400mcg)	12	13
	T2(800mcg)	13	14

Fig.34. Antifungal assay of 4-hydroxy-3-methoxyacetophenone N(4)-methyl(phenyl)thiosemicarbazone (denoted as AT) and its Cu(II) complex (denoted as ATCu) on the *C. albicans*

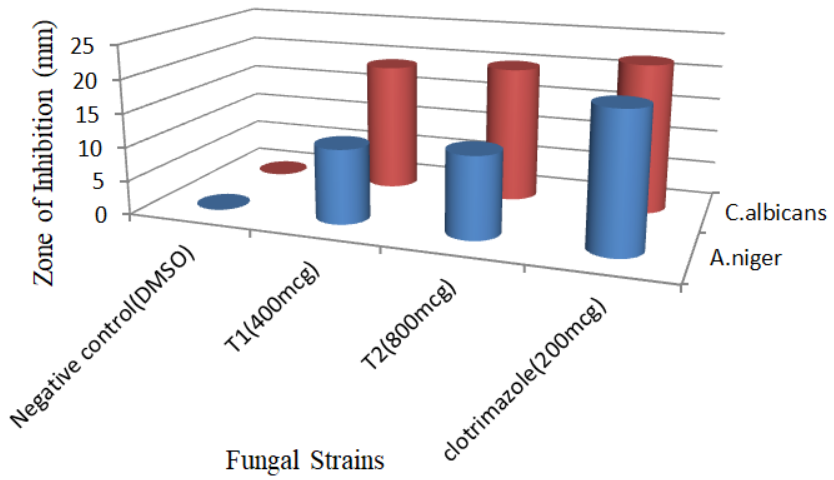

Fig.35. Graphical representation of antifungal assay of 4-hydroxy-3-methoxyacetophenone N(4)-methyl(phenyl)thiosemicarbazone

The results showed that the ligand has better antifungal activity against *C. albicans* and *A. niger* than the complexes.

5.5. 4-[N,N-(Dimethyl)amino]benzaldehyde isonicotinoylhydrazone (PDBINH), (HL)

Evaluation of antifungal activities of Co(II), Ni(II) and Cu(II) complexes and the ligand, 4-[N,N-(dimethyl)amino]benzaldehyde isonicotinoylhydrazone was carried out using Agar well Diffusion Method.

Table 12. Antifungal assay of 4-[N,N-(dimethyl)amino]benzaldehyde isonicotinoylhydrazone and its complexes

ANTIFUNGAL ASSAY			
Organism name		**Zone of inhibition (mm)**	
Samples	**Concentration of samples**	***A. niger***	***C. albicans***
HL	Standard clotrimazole (200mcg)	20	22
	Negative control	-	-
	T1(400mcg)	-	-
	T2(800mcg	10	11
Co(II) complex	Standard clotrimazole (200mcg)	20	23
	Negative control	-	-
	T1(400mcg)	-	-
	T2(800mcg)	11	11
Ni(II) complex	Standard clotrimazole (200mcg)	20	23
	Negative control	-	-
	T1(400mcg)	11	-
	T2(800mcg)	12	11
Cu(II) complex	Standard clotrimazole (200mcg)	20	23
	Negative control	-	-
	T1(400mcg)	12	-
	T2(800mcg)	13	-

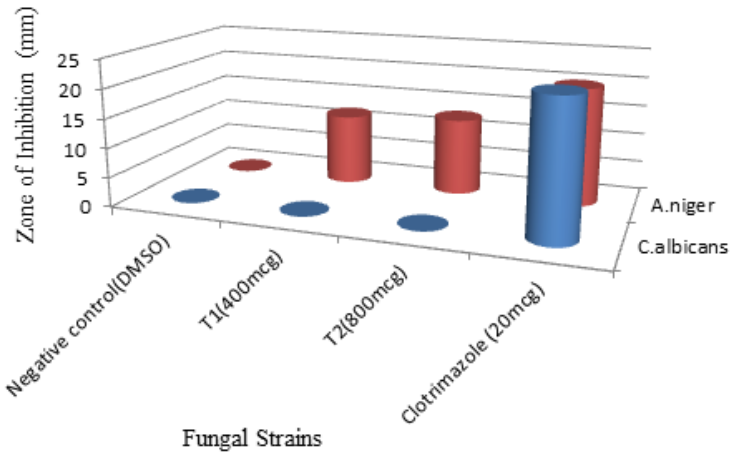

Fig.36. Graphical representation of antifungal assay of Cu(II) complex of 4-[N,N-(dimethyl)amino]benzaldehyde isonicotinoyl hydrazone

Fig.37 . Antifungal assay of Cu(II) complex of 4-[N,N-(dimethyl)amino]benzaldehyde isonicotinoylhydrazone (denoted as CUPINH) on the *A. niger* and *C. albicans*

It was found that complexes were more active than the free ligand. The complexes showed inhibitory activities towards the fungi in a concentration dependent manner.

6. Conclusions

The *in vitro* antimicrobial screening of the compounds were done against *S. aureus, B. subtilis, E. coli, P. aeruginosa, A. niger* and *C. albicans*. The zones of inhibition with different concentrations of the samples and the control were measured and discussed.

The higher activities of metal complexes compared to those of the free ligands can be explained on the basis of the Overtone's concept of cell permeability[20, 21]and Tweedy's chelation theory[22]. According to Overtone's concept of cell permeability, the lipid membrane around the cell favors the passage of lipid soluble materials alone. On chelation, the polarity will be turned down to a considerable extent due to the overlap of the ligand orbitals with the metal orbitals. Further, it leads to an increase of π-electrons delocalization over the entire chelate ring and enhances the lipophilicity. This plays a key role in the antimicrobial activity. The enhanced lipophilicity increases the penetration of the metal complexes into lipid membranes. Thus, it leads to the blocking of the metal binding sites of the microorganisms. This inhibits further growth of organism. The moderate activities of some of the compounds investigated here may be due to their low lipophilicity. This may restrict their penetration through the lipid membrane and hence, they could neither block nor resist the growth of the microorganisms effectively.

References

[1] D.L. Klayman, J.P. Scovill, J.F. Bartosevich, J. Bruce, 2-Acetylpyridine thiosemicarbazones. 5. 1-[1-(2-Pyridyl) ethyl]-3-thiosemicarbazides as potential antimalarial agents, Journal of medicinal chemistry 26(1) (1983) 35-39.

[2] U. Abram, K. Ortner, R. Gust, K. Sommer, Gold complexes with thiosemicarbazones: reactions of bi-and tridentate thiosemicarbazones with dichloro [2-(dimethylaminomethyl) phenyl-C 1, N] gold (III),[Au (damp-C 1, N) Cl 2], Journal of the Chemical Society, Dalton Transactions (5) (2000) 735-744.

[3] D. Rogolino, A. Gatti, M. Carcelli, G. Pelosi, F. Bisceglie, F.M. Restivo, F. Degola, A. Buschini, S. Montalbano, D. Feretti, C. Zani, Thiosemicarbazone scaffold for the design of antifungal and antiaflatoxigenic agents: evaluation of ligands and related copper complexes, Sci Rep 7(1) (2017) 11214-11214.

[4] X. Zhu, C. Wang, Z. Lu, Y. Dang, Synthesis, characterization and biological activity of the Schiff base derived from 3, 4-dihydroxybenzaldehyde and thiosemicarbazid, and its complexes with nickel (II) and iron (II), Transition Metal Chemistry 22(1) (1997) 9-13.

[5] Z. Xinde, Le Zhifeng and Wu Zhishen, J. Inorg. Chem.(Russ.) 36 (1991) 1748.

[6] X. Zhu, C. Wang, Z. Lu, Y. Dang, Synthesis, characterization and biological activity of the Schiff base derived from 3,4-dihydroxybenzaldehyde and thiosemicarbazid, and its complexes with nickel(II) and iron(II), Transition Metal Chemistry 22(1) (1997) 9-13.

[7] P. Chetana, M. Somashekar, B. Srinatha, R. Policegoudra, S. Aradhya, R. Rao, Synthesis, crystal structure, antioxidant, antimicrobial, and mutagenic activities and DNA interaction studies of Ni(II) Schiff base 4-methoxy-3-benzyloxybenzaldehyde thiosemicarbazide complexes, International Scholarly Research Notices 2013 (2013).

[8] B. Prathima, Y.S. Rao, G. Ramesh, M. Jagadeesh, Y. Reddy, P. Chalapathi, A.V. Reddy, Synthesis, spectral characterization and biological activities of Mn (II) and Co (II) complexes with benzyloxybenzaldehyde-4-phenyl-3-thiosemicarbazone, Spectrochimica

Acta Part A: Molecular and Biomolecular Spectroscopy 79(1) (2011) 39-44.

[9] E. Pahontu, F. Julea, T. Rosu, V. Purcarea, Y. Chumakov, P. Petrenco, A. Gulea, Antibacterial, antifungal and in vitro antileukaemia activity of metal complexes with thiosemicarbazones, J Cell Mol Med 19(4) (2015) 865-878.

[10] E. Bermejo, R. Carballo, A. Castiñeiras, R. Domínguez, A.E. Liberta, C. Maichle-Mössmer, M.M. Salberg, D.X. West, Synthesis, structural characteristics and biological activities of complexes of ZnII, CdII, HgII, PdII, and PtII with 2-acetylpyridine 4-methylthiosemicarbazone, European journal of inorganic chemistry (6) (1999) 965-973.

[11] R.K. Agarwal, L. Singh, D.K. Sharma, Synthesis, spectral, and biological properties of copper(II) complexes of thiosemicarbazones of Schiff bases derived from 4-aminoantipyrine and aromatic aldehydes, Bioinorganic Chemistry and Applications (2006) 59509.

[12] N.C. Kasuga, K. Sekino, M. Ishikawa, A. Honda, M. Yokoyama, S. Nakano, N. Shimada, C. Koumo, K. Nomiya, Synthesis, structural characterization and antimicrobial activities of 12 zinc (II) complexes with four thiosemicarbazone and two semicarbazone ligands, Journal of inorganic biochemistry 96(2-3) (2003) 298-310.

[13] L. Savini, L. Chiasserini, A. Gaeta, C. Pellerano, Synthesis and anti-tubercular evaluation of 4-quinolylhydrazones, Bioorganic & medicinal chemistry 10(7) (2002) 2193-2198.

[14] A. Walcourt, M. Loyevsky, D.B. Lovejoy, V.R. Gordeuk, D.R. Richardson, Novel aroylhydrazone and thiosemicarbazone iron chelators with anti-malarial activity against chloroquine-resistant and-sensitive parasites, The international journal of biochemistry & cell biology 36(3) (2004) 401-407.

[15] U. Salgın-Gökşen, N. Gökhan-Kelekçi, Ö. Göktaş, Y. Köysal, E. Kılıç, Ş. Işık, G. Aktay, M. Özalp, 1-Acylthiosemicarbazides, 1, 2, 4-triazole-5 (4H)-thiones, 1, 3, 4-thiadiazoles and hydrazones containing 5-methyl-2-benzoxazolinones: synthesis, analgesic-anti-inflammatory and antimicrobial activities, Bioorganic & medicinal chemistry 15(17) (2007) 5738-5751.

[16] G. Turan-Zitouni, Y. Blache, K. Güven, Synthesis and antimicrobial activity of some imidazo-[1, 2-a] pyridine-2-carboxylic acid

arylidenehydrazide derivatives, Bollettino chimico farmaceutico 140(6) (2001) 397-400.

[17] S. Prasad, R.K. Agarwal, Nickel (II) complexes of hydrazone of isoniazid and their magneto-spectral, electrochemical, thermal and antimicrobial investigations, International Journal of Inorganic Chemistry 2008 (2008).

[18] B. Moksharagni, S. Chandrasekhar, R.K. Hussain, K. Kumar, Synthesis, spectral characterization and evaluation of invitro antibacterial activity of isonicotinoyl hydrazones bearing pyridine moiety, International Journal of Pharma and Bio Sciences 6(3) (2015) 11-18.

[19] L. Mitu, M. Ilis, N. Raman, M. Imran, S. Ravichandran, Transition metal complexes of isonicotinoyl–hydrazone-4-diphenylaminobenzaldehyde: synthesis, characterization and antimicrobial studies, Journal of Chemistry 9(1) (2012) 365-372.

[20] Y. Anjaneyulu, R.P. Rao, Preparation, characterization and antimicrobial activity studies on some ternary complexes of Cu (II) with acetylacetone and various salicylic acids, Synthesis and Reactivity in Inorganic and Metal-Organic Chemistry 16(2) (1986) 257-272.

[21] N. Dharmaraj, P. Viswanathamurthi, K. Natarajan, Ruthenium (II) complexes containing bidentate Schiff bases and their antifungal activity, Transition Metal Chemistry 26(1-2) (2001) 105-109.

[22] B. Tweedy, Plant extracts with metal ions as potential antimicrobial agents, Phytopathology 55 (1964) 910-914.

CHAPTER XIII

ANTIOXIDANT STUDIES OF N(4)-DISUBSTITUTED THIOSEMICARBAZONES, ISONICOTINOYLHYDRAZONE AND THEIR METAL COMPLEXES

1. Introduction

In recent years, there has been a good deal of attention toward the field of free radical chemistry. Free radicals are reactive oxygen- and -nitrogen species generated in our body by different endogenous systems[1]. Free radicals are unstable and highly reactive species. They are either derived from normal essential metabolic processes in the human body, or ender the body from external sources such as exposure to X-rays, ozone, cigarette smoking, air pollutants, and industrial chemicals[2]. Adverse effects of free radicals have been postulated in many conditions, including inflammatory condition, atherosclerosis, certain cancers, and the process of aging of human body.

Antioxidants are substances that can prevent or slow damage to cells caused by free radicals. They are sometimes called "free-radical scavengers". The sources of antioxidants can be natural or artificial. Certain plant-based foods are thought to be rich in antioxidants. Plant-based antioxidants are a kind of phytonutrient, or plant-based nutrient. The body also produces some antioxidants, known as endogenous antioxidants.

A balance between free radicals and antioxidants is significant for proper physiological function. An oxidative stress, arising as a result of an imbalance between free radical production and antioxidant defences, is associated with damage to a wide range of molecular species including lipids, proteins, and nucleic acids, which is lead to the adverse changes in their structure and functions[3]. It expected to

produce progressive adverse changes that accumulate with age in the body. Thus, application of synthetic antioxidants are widely explored for their capacity to protect organism and cell from damage caused by free radicals. Researchers in many different disciplines become more interested in novel compounds that could provide active components to prevent or reduce the impact of oxidative stress on cell.

Thiosemicarbazones are significant category of ligands containing sulphur and nitrogen donor atoms. Structural simplicity, simple synthetic procedure, short span of reaction and versatile pharmacological profile make them a class of broadly studied and explored compounds. Thiosemicarbazones have versatile applications in medicinal-, pharmaceutical-and biological applications[4-7]. The biological activity of thiosemicarbazones are associated with the presence of the active pharmacophore. A thorough literature survey revealed that N(4)-substituted thiosemicarbazones have good antimicrobial- and antioxidant properties [8, 9]. Ahmed A Al-Amiery *et al*[10] reported that antioxidant-, antimicrobial- and theoretical studies of the thiosemicarbazone derivative of 2-(2-imino-1-methylimidazolidin-4-ylidene) hydrazinecarbothioamide (IMHC). Alka Choudhary *et al*[11] reported the antioxidant studies of complexes of Fe(III), Co(II) and Cu(II) with camphor semicarbazone (1,7,7-trimethylbicyclo[2,2,1]heptanesemicarbazone, (TBHSC) and camphor thiosemicarbazone (1,7,7-trimethylbicyclo[2,2,1]heptanethiosemicarbazone, (TBHTSC). The compounds and their metal complexes were screened for free radical

scavenging activity at a concentration range of 50-1000 µg/ml. All the compounds have shown encouraging antioxidant activities. Chetana *et al*[12] reported the antioxidant-, antimicrobial- and mutagenic activities and DNA interaction studies of Ni(II) Schiff base 4-methoxy-3-benzyloxybenzaldehyde thiosemicarbazide complexes. They showed potential antioxidant activities. Gujarathi[13] reported the antioxidant study of Ni(II) complexes derived from 5-chloro-2-hydroxyacetophenone N-methyl thiosemicarbazone. The free radical scavenging activity of compounds was screened. It was found that the complexes are more active than the free thiosemicarbazones.

Researchers are interested on isonicotinoylhydrazones because of their versatile applications in different fields such as anti-tubercular and antimicrobial agents, radical scavengers and corrosion inhibitors[14-16]. S.A. Aly and S.K. Fathalla[17] reported a new series of complexes of Pd(II), Cd(II) and Cu(II and I) with a polydentate Schiff base ligand (H_2L), namely ((Z)-2-(phenylamino)-N'-(thiophen-2-ylmethylene)acetohydrazide). The ligand and its metal complexes have been characterized based on various physico-chemical studies. The antibacterial studies of selected compounds against two pathogenic bacteria were carried out. The complexes and the ligand revealed excellent antioxidant properties and could be useful in fighting the free radicals which occur in close connection with cancerous cells. It was remarkable that the two complexes, Cu(II and I) demonstrated stronger antioxidant effects than their parent ligands. Senthil Raja *et al*[18] reported a novel water soluble ligand-bridged cobalt(II) coordination

polymer of a new ligand, 2-oxo-1,2-dihydroquinoline-3-carbaldehyde (isonicotinic)hydrazone (H_2L). Investigations on the antioxidant property showed that the polymeric Co(II) complex had a strong radical scavenging potency against hydroxyl-, DPPH-, nitric oxide- and superoxide radicals.

In view of these observations, it has been decided to evaluate the antioxidant activities of the following N(4)-methyl(phenyl) thiosemicarbazones, 4-hydroxy-3-methoxyaceto phenone isonicotinoylhydrazone and a few of their metal complexes that we have synthesized.

- 2,4-Dihydroxybenzaldehyde N(4)-methyl(phenyl)thiosemicarbazone (DBMPTSC) (HL),
- 4-Benzyloxybenzaldehyde N(4)-methyl(phenyl)thiosemicarbazone (BBMPTSC) (HL),
- 4-Hydroxy-3-methoxyacetophenone N(4)-methyl(phenyl)thiosemicarbazone (AMPTSC) (HL) and
- 4-Hydroxy-3-methoxyacetophenone isonicotinoylhydrazone (AINH) (HL)

2. Materials and methods

2.1. Evaluation of antioxidant property

Antioxidant assay was done using 2,2-Diphenyl-1-picryl-hydrazyl (DPPH) method. DPPH is a widely accepted stable free radical source

which is neutralized in the presence of molecules capable of donating H atoms or electrons. The DPPH radical scavenging method is considered as one of the best *in vitro* model to study the antioxidant activity of the compounds. It is simple-, reliable-, fast, cost-effective spectrophotometric method. The colour of DPPH is purple, which changes to yellow (2,2-diphenyl-1-picrylhydrazine, the non-radical, reduced form) by neutralizing with radical scavenger. Antioxidant activity of the ligands and metal complexes was determined by the method described by Brand-Williams *et al*[19]. The percentage of inhibition (%) of free radical was determined by the following equation:

$$\% \text{ Inhibition} = \frac{(\text{Absorbance of Control at 0 minute} - \text{Absorbance of Test})}{\text{Absorbance of Control at 15 minutes}} \times 100$$

that is:

$$\% \text{ Inhibition} = (C_0 - T) / C \times 100$$

(where, C_0 = absorbance of control sample (t=0 min), C = absorbance of control (t=15 min) and T=absorbance of test compound).

Low absorbance of the reaction mixture indicates high free radical scavenging activity of the test compound. IC_{50} (Half Maximal Inhibitory Concentration) value is a commonly used parameter to measure the antioxidant activity. It is the concentration of the sample that can scavenge 50% of DPPH free radical in DPPH radical scavenging method. The IC_{50} is determined from the slope of inhibition-concentration graph drawn using an equation, y=mx+c,

where y= concentration of antioxidant corresponding to 50% inhibition of free the radical, m= slope of the graph, c= intercept of the graph. The IC_{50} value is inversely proportional to the free radical scavenging activity/ antioxidant property of the sample. As the reaction between antioxidant compound and DPPH radical results in the scavenging of the radical by hydrogen- or electron donation, the absorbance at 517nm (due to DPPH radical) falls. This can be visually observed as the colour change is from purple to yellow[20].

It is observed that DPPH radical scavenging assay depends on two on the functional groups on the aromatic ring and their position on the ring. Radical scavengers donate hydrogen atoms to become stable free radicals. The degree of stability and antioxidant potential are in direct relationship with the range of electron delocalization. Generally, organic molecules containing an electron donating groups, such as amine, hydroxyl, or methoxy, are inquired as promising antioxidant molecules. Compounds with hydroxyl group at *ortho, meta* or *para* position of the benzene ring show good DPPH activity than the other. The antioxidant ability of a mono hydroxyl compound depends upon the position of the hydroxyl group. *Para* –substituted compounds could produce relatively stable radical resonance hybrid than *meta*-substituted ones. Lower activity of compound with hydroxyl group in *ortho*-position may be due to intramolecular hydrogen bonding [20].

In the present investigation, the antioxidant studies were completed in Athmic Biotech laboratory, Trivandrum.

2.2. Procedure of antioxidant activity by DPPH assay

Ascorbic acid was used as reference. It was dissolved in distilled water to make a stock solution of concentration,(1mg/1000µl). The fresh solution of DPPH in methanol, (60µM) was prepared daily before UV measurements. This solution (3.9ml) was mixed with various concentrations (25, 50, 100 & 200µL) of the test solutions. The samples were kept in the darkness for 15 minutes at room temperature and the decrease in absorbance was measured at 517 nm. The same volume of control (without the test solution) was prepared. Methanol (95%) was used as blank [21, 22].

3. Results and discussion

3.1. 2,4-Dihydroxybenzaldehyde N(4)-methyl(phenyl) thiosemicarbazone (DBMPTSC), (HL) and its complexes

Scavenging effects of 2,4-dihydroxybenzaldehyde N(4)-methyl(phenyl)thiosemicarbazone and its Co(II), Ni(II), Cu(II) complexes and ascorbic acid at various concentrations were established by DPPH method. The reduction of DPPH radical was assessed by the decrease of the absorbance at 517 nm. The optical densities of ascorbic acid, ligand and its complexes at 517 nm are presented in Table 1. The absorbance decreased as a result of colour change from purple to yellow as the radicals are scavenged by antioxidants. Lower absorbance of the reaction mixture indicates higher free radical scavenging activity of the compound.

Table 1. Percentage scavenging of DPPH by compounds

Sample	Concentration (µg)	OD at 517nm	% of Inhibition
Control at zero minute	-	1.053	-
Control at 15 minute	-	1.020	-
HL (Inhibition is not concentration dependent, so IC_{50} cannot be calculated)	25	0.427	60.03
	50	0.161	85.22
	100	0.072	93.65
	200	0.059	94.88
Co(II) complex (IC_{50}=32.16)	25	0.587	43.93
	50	0.410	61.64
	100	0.295	72.53
	200	0.250	76.79
Ni(II) complex (IC_{50}=71.82)	25	0.809	24.14
	50	0.549	48.71
	100	0.388	63.87
	200	0.041	96.71
Cu(II) complex (IC_{50}=117.65)	25	0.900	15.53
	50	0.746	30.06
	100	0.422	60.75
	200	0.359	66.66
Standard **Control at zero minute**	-	1.065	-
Control at 15 minute	-	1.059	-
Ascorbic acid (standard) (IC_{50}= 19.25)	3	0.985	7.55
	6.25	0.897	15.86
	12.5	0.747	30.02
	25	0.365	66.10

OD = Optical Density

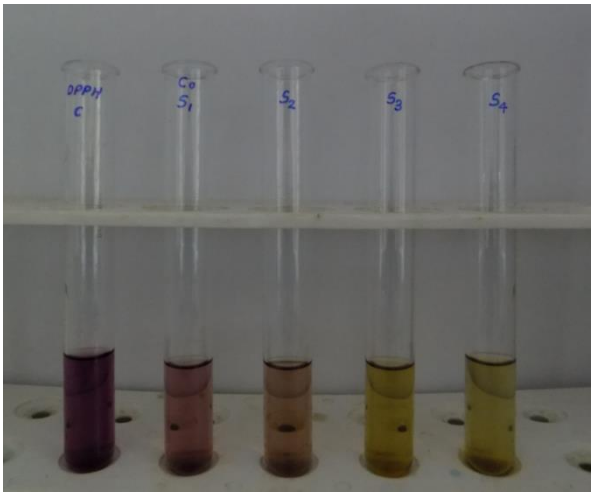

Fig.1. Scavenging of DPPH by Co(II) complex of 2,4-dihydroxybenzaldehyde N(4)-methyl(phenyl) thiosemicarbazone

The experimental results showed that the Co(II) complex of 2,4-dihydroxybenzaldehyde N(4)-methyl(phenyl)thiosemicarbazone showed good activity as a radical scavenger compared to the scavenging ability of ascorbic acid, which was used as a standard. The nickel and copper complexes showed average activity compared to ascorbic acid. The order of activity was Co(II)> Ni(II)> Cu(II) complexes compared to ascorbic acid.

3.2. 4-Benzyloxybenzaldehyde N(4)-methyl(phenyl) thiosemicarbazone (BBMPTSC), (HL) and its Co(II) complex

Evaluation of antioxidant activities of 4-benzyloxybenzaldehyde N(4)-methyl(phenyl)thiosemicarbazone and its Co(II) complex at various concentrations were carried out using DPPH assay.

Table 2. Percentage scavenging of DPPH by compounds

Sample	Concentration (µg)	OD at 517nm	% of Inhibition
Control at zero minute	-	1.053	-
Control at 15 minute	-	1.020	-
Co(II)complex (IC_{50}=153)	25	0.974	7.74
	50	0.940	11.07
	100	0.880	16.96
	200	0.772	27.54
HL(IC_{50}=46.67)	25	0.762	28.5
	50	0.468	57.35
	100	0.094	94.01
	200	0.052	98.13
Standard Control at zero minute	-	1.060	-
Control at 15 minute	-	1.046	-
Ascorbic acid (standard) (IC_{50}=19.24)	3	0.995	6.21
	6.25	0.887	16.53
	12.5	0.724	32.12
	25	0.119	89.77

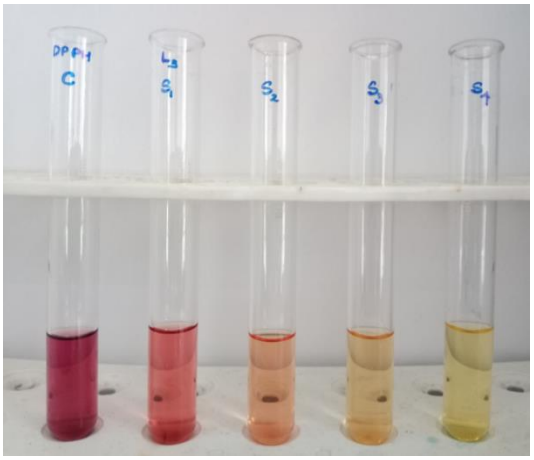

Fig.2. Scavenging of DPPH by 4-benzyloxybenzaldehyde N(4)-methyl(phenyl)thiosemicarbazone (denoted as L_3)

The experimental results indicated that the 4-benzyloxybenzaldehyde N(4)-methyl(phenyl)thiosemicarbazone showed better activity as a radical scavenger compared to the scavenging ability of ascorbic acid, which was used as a standard. The cobalt complex showed only medium activity when compared to that of ascorbic acid.

3.3. 4-Hydroxy-3-methoxyacetophenone N(4)-methyl(phenyl)thiosemicarbazone (AMPTSC), (HL) and its complexes

Evaluation of antioxidant activities of 4-hydroxy-3-methoxyacetophenone N(4)-methyl(phenyl)thiosemicarbazone and its Co(II), Ni(II) and Cu(II) complexes were carried out using DPPH assay. The optical densities and percentage of inhibition of ascorbic acid, ligand and its complexes at 517 nm are presented in Table 3.

Table 3. Percentage scavenging of DPPH by compounds

Sample	Concentration (µg)	OD at 517nm	% of Inhibition
Control at zero minute	-	1.063	-
Control at 15 minute	-	1.039	-
HL (IC_{50} =30.32)	25	0.622	41.83
	50	0.403	62.80
	100	0.178	84.32
	200	0.128	89.02
Co(II) complex (IC_{50}=137)	25	0.914	14.34
	50	0.876	17.99
	100	0.625	42.15
	200	0.345	69.10
Ni(II) complex (IC_{50}=31.62)	25	0.627	41.96
	50	0.417	62.17
	100	0.166	86.33
	200	0.096	93.07
Cu(II) complex (IC_{50}=132.01)	25	0.941	11.34
	50	0.851	19.99
	100	0.6191	42.15
	200	0.306	72.10
Standard Control at zero minute	-	1.060	-
Control at 15 minute	-	1.046	-
Ascorbic acid (standard) (IC_{50}=15.32)	3	0.995	6.21
	6.25	0.887	16.53
	12.5	0.724	32.12
	25	0.119	89.77

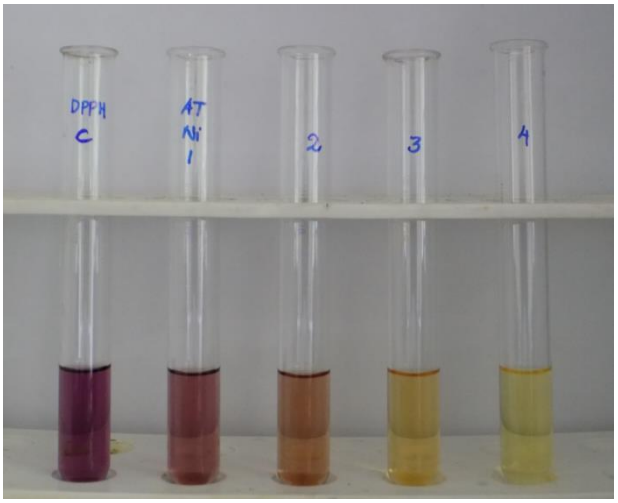

Fig.3. Scavenging of DPPH by Ni(II) complex of 4-hydroxy-3-methoxyacetophenone N(4)-methyl(phenyl)thiosemicarbazone (denoted as ATNi)

The experimental results showed that the ligand and its Ni(II) complex showed good activity as a radical scavenger compared to the scavenging ability of ascorbic acid, which was used as a standard. The Co(II) and Cu(II) complexes showed average activities compared to ascorbic acid. The order of activity was Ni(II) > Cu(II)> Co(II) complexes compared to ascorbic acid.

3.4. 4-Hydroxy-3-methoxyacetophenone isonicotinoylhydrazone (AINH), (HL) and its Cu(II) complex

Evaluation of antioxidant activities of 4-hydroxy-3-methoxyacetophenone isonicotinoylhydrazone and its Cu(II) complex and ascorbic acid at various concentrations were performed by DPPH method. The radical reduction capability of the compounds was determined by the decrease of the absorbance at 517 nm. The optical

densities and percentage of inhibition of ascorbic acid, ligand and its complex are presented in Table 4. The absorbance decreased as a result of colour change from purple to yellow as the radical was scavenged by antioxidants.

Table 4. Percentage scavenging of DPPH by compounds

Sample	Concentration (µg)	OD at 517nm	% of Inhibition
Control at zero minute	-	1.063	-
Control at 15 minute	-	1.017	-
HL (IC_{50}=55.91)	25	0.751	30.82
	50	0.452	60.29
	100	0.286	76.59
	200	0.152	89.77
Cu(II) complex (IC_{50}=145)	25	0.974	8.93
	50	0.896	16.60
	100	0.713	34.61
	200	0.671	38.68
Standard Control at zero minute	-	1.065	-
Control at 15 minute	-	1.017	-
Ascorbic acid (standard) (IC_{50}=14.79)	3	0.994	6.98
	6.25	0.886	17.60
	12.5	0.723	33.63
	25	0.118	93.12

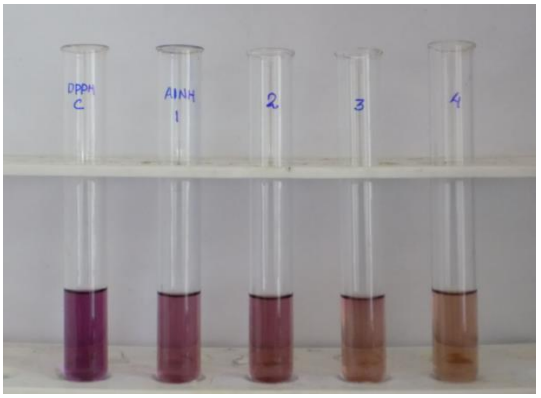

Fig.4. Scavenging of DPPH by 4-hydroxy-3-methoxyacetophenone isonicotinoylhydrazone (denoted as AINH)

It was evident from results that free radical scavenging activities of these compounds were concentration dependent. The ligand showed good antioxidant activity compared to ascorbic acid. The copper complex showed medium activity compared to standard. The tested compounds demonstrated better scavenging activities at higher concentrations.

4. Suggested mechanism for the antioxidant activity of thiosemicarbazone

The reaction mechanism of thiosemicarbazones (1-3) with DPPH radical is shown in the Scheme 1. The reaction of DPPH radical with tested compounds may be based on charge transfer between them [Eq.(I)] or combination of thiosemicarbazone radicals formed during scavenging assay with DPPH [Eq.(II)]. The reaction between DPPH molecules is not possible due to steric hindrance.

The scavenging activities of the compounds may be due to the presence of hydrogen atom of the secondary amine in the

thiosemicarbazone moiety. The DPPH radical can abstract a proton from the thiosemicarbazone. The radical stabilization is influenced by both the allylic double bond and inductive effect. The stabilized allyl double bond favours the release of hydrogen as a free radical (as proton). The inductive effect also favours the formation of free radical. The radical could delocalize the electrons on the aromatic ring to produce relatively stable resonance hybrid as shown in the Scheme [Eq.(I)]. When the concentration of DPPH radical was higher than that of the tested compound, the DPPH radical might combine with the thiosemicarbazone radical (R˙)[Eq.(II)]. The electronic conjugation in the compound facilitates radical stabilization, preventing it from destructive biochemical reaction.

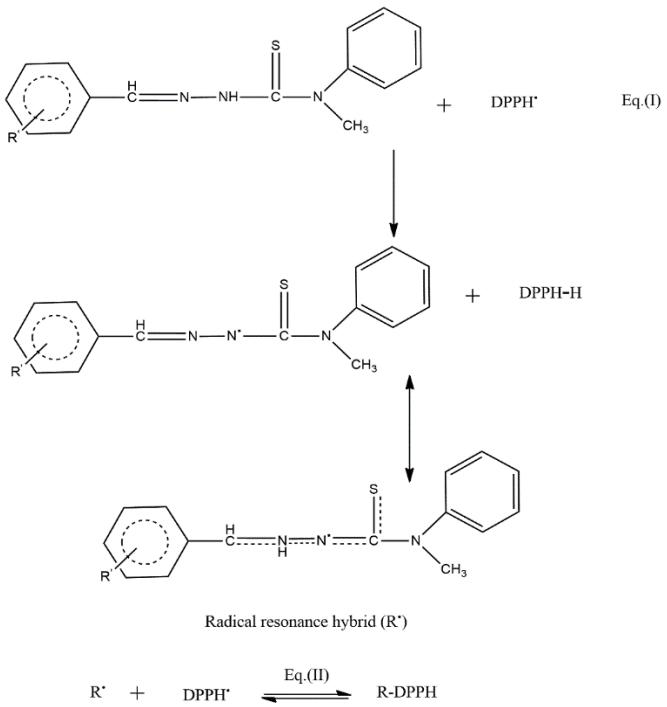

Scheme 1. Suggested mechanism of the antioxidant activity of thiosemicarbzones

5. Suggested mechanism of the antioxidant activity of isonicotinoylhydrazone

The reaction mechanism of isonicotinoylhydrazone with DPPH radical is shown in the Scheme 2. The mechanism depends on the hydrogen atom of the secondary amine in theisonicotinoylhydrazone moiety and hydroxyl group on aromatic ring. The compound with hydroxyl group at the *para*-position can produce relatively stable resonance hybrid. DPPH radical can abstract a proton from the isonicotinoylhydrazone. The radical formed could delocalize electron to aromatic ring to produce stable resonance hybrid. Radical stabilization is also influenced by the allylic type double bond and electron withdrawing carbonyl function. These effects push electron density toward the free radical.

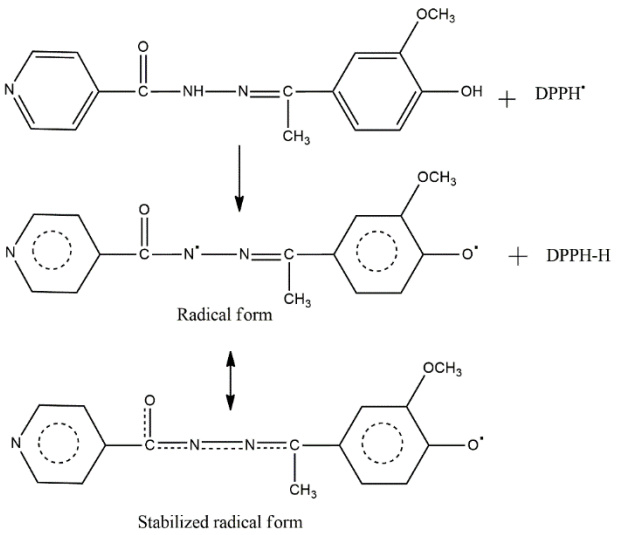

Scheme 2. Suggested mechanism of the antioxidant activity of 4-hydroxy-3-methoxyacetophenone isonicotinoylhydrazone

6. Conclusions

The antioxidant activities of the compounds were evaluated by DPPH method and compared with the standard (ascorbic acid). The IC_{50} values were determined by linear regression plot**,** where concentration of tested compound was represented on abscissa and percentage of antioxidant activity on ordinate**.** 4-Hydroxy-3-methoxyacetophenone N(4)-methyl(phenyl)thiosemicarbazone (IC_{50}=30.32) and its Ni(II) complex (IC_{50}=31.62) and Co(II) complex of 2,4-dihydroxybenzaldehyde N(4)-methyl(phenyl)thiosemicarbazone (IC_{50}=32.16) showed good antioxidant activities. These compounds may be used as antioxidants in future.

References

[1] V. Lobo, A. Patil, A. Phatak, N. Chandra, Free radicals, antioxidants and functional foods: Impact on human health, Pharmacognosy reviews 4(8) (2010) 118.

[2] K. Bagchi, S. Puri, Free radicals and antioxidants in health and disease: a review, 1998.

[3] J.M. McCord, The evolution of free radicals and oxidative stress, The American journal of medicine 108(8) (2000) 652-659.

[4] İ. Kizilcikli, Y. Kurt, B. Akkurt, A. Genel, S. Birteksöz, G. Ötük, B. Ülküseven, Antimicrobial activity of a series of thiosemicarbazones and their Zn II and Pd II complexes, Folia microbiologica 52(1) (2007) 15-25.

[5] A. Walcourt, M. Loyevsky, D.B. Lovejoy, V.R. Gordeuk, D.R. Richardson, Novel aroylhydrazone and thiosemicarbazone iron chelators with anti-malarial activity against chloroquine-resistant and-sensitive parasites, The international journal of biochemistry & cell biology 36(3) (2004) 401-407.

[6] T. Varadinova, D. Kovala-Demertzi, M. Rupelieva, M. Demertzis, P. Genova, Antiviral activity of platinum (II) and palladium (II) complexes of pyridine-2-carbaldehyde thiosemicarbazone, Acta virologica 45(2) (2001) 87-94.

[7] H. Yildirim, E. Guler, M. Yavuz, N. Ozturk, P.K. Yaman, E. Subasi, E. Sahin, S. Timur, Ruthenium (II) complexes of thiosemicarbazone: Synthesis, biosensor applications and evaluation as antimicrobial agents, Materials Science and Engineering: C 44 (2014) 1-8.

[8] H. Muğlu, Synthesis, characterization, and antioxidant activity of some new N4-arylsubstituted-5-methoxyisatin-β-thiosemicarbazone derivatives, Research on Chemical Intermediates 46(4) (2020) 2083-2098.

[9] T. Bakır, H.S. Sayiner, F. Kandemirli, Experimental and theoretical investigation of antioxidant activity and capacity of thiosemicarbazones based on isatin derivatives, Phosphorus, Sulfur, and Silicon and the Related Elements 193(8) (2018) 493-499.

[10] A.A. Al-Amiery, Y.K. Al-Majedy, H.H. Ibrahim, A.A. Al-Tamimi, Antioxidant, antimicrobial, and theoretical studies of the thiosemicarbazone derivative Schiff base 2-(2-imino-1-methylimidazolidin-4-ylidene) hydrazinecarbothioamide (IMHC), Organic and medicinal chemistry letters 2(1) (2012) 4.

[11] A. Choudhary, R. Sharma, M. Nagar, M. Mohsin, H.S. Meena, Synthesis, characterization and antioxidant activity of some transition metal complexes with terpenoid derivatives, Journal of the Chilean Chemical Society 56(4) (2011) 911-917.

[12] P.R. Chetana, M.N. Somashekar, B.S. Srinatha, R.S. Policegoudra, S.M. Aradhya, R. Rao, Synthesis, Crystal Structure, Antioxidant, Antimicrobial, and Mutagenic Activities and DNA Interaction Studies of Ni(II) Schiff Base 4-Methoxy-3-benzyloxybenzaldehyde Thiosemicarbazide Complexes, ISRN Inorganic Chemistry 2013 (2013) 250791.

[13] J. Gujarathi, N. Pawar, R. Bendrea, Synthesis, spectral and antioxidant assay of Nickel (II) adducts with heterocyclic bases derived from 5-chloro-2-hydroxy acetophenone N methyl thiosemicarbazone, Pharm Chem 5 (2013) 120-5.

[14] C. Sankar, K. Pandiarajan, Synthesis and anti-tubercular and antimicrobial activities of some 2r,4c-diaryl-3-azabicyclo[3.3.1]nonan-9-one N-isonicotinoylhydrazone derivatives, European journal of medicinal chemistry 45 (2010) 5480-5.

[15] E. Uddin, R. Islam, N.A. Bitu, S. Hossain, N. Uddin, M.M. Ali, A. Asraf, F. Hossen, M. Haque, Biological Applications of Isoniazid Derived Schiff Base Complexes: An Overview, Asian Journal of Research in Biochemistry (2020) 17-31.

[16] N. Kumar Hs, T. Parumasivam, F. Jumaat, P. Ibrahim, M. Abdullah, A. Sadikun, Synthesis and evaluation of isonicotinoyl hydrazone derivatives as antimycobacterial and anticancer agents, Medicinal Chemistry Research 23 (2014).

[17] S. Aly, S. Fathalla, Preparation, characterization of some transition metal complexes of hydrazone derivatives and their antibacterial and antioxidant activities, Arabian Journal of Chemistry 13(2) (2020) 3735-3750.

[18] D.S. Raja, N.S. Bhuvanesh, K. Natarajan, A novel water soluble ligand bridged cobalt (II) coordination polymer of 2-oxo-1, 2-dihydroquinoline-3-carbaldehyde (isonicotinic) hydrazone: evaluation of the DNA binding, protein interaction, radical scavenging and anticancer activity, Dalton Transactions 41(15) (2012) 4365-4377.

[19] W. Brand-Williams, M.-E. Cuvelier, C. Berset, Use of a free radical method to evaluate antioxidant activity, LWT-Food science and Technology 28(1) (1995) 25-30.

[20] G. Ceyhan, C. Celik, S. Uruş, İ. Demirtaş, M. Elmastaş, M. Tümer, Antioxidant, electrochemical, thermal, antimicrobial and alkane oxidation properties of tridentate Schiff base ligands and their metal complexes, Spectrochimica Acta Part A: Molecular and Biomolecular Spectroscopy 81(1) (2011) 184-198.

[21] T. Liu, L. Song, H. Wang, D. Huang, A high-throughput assay for quantification of starch hydrolase inhibition based on turbidity measurement, Journal of agricultural and food chemistry 59(18) (2011) 9756-9762.

[22] M. Buijnsters, D. Bicanic, M. Chirtoc, M.C. Nicoli, Y. Min-Kuo, Evaluation of Antioxidative Activity of Some Antioxidants by Means of a Combined Optothermal Window and a DPPH∗ Free Radical Colorimetry, Analytical Sciences/Supplements Proceedings of 11th International Conference of Photoacoustic and Photothermal Phenomena, The Japan Society for Analytical Chemistry (2002) 544-546.

PUBLICATIONS / PRESENTATIONS

- T. Nibila, T.S. Ahamed, P. Soufeena, K. Muraleedharan, P. Periyat, K. Aravindakshan, Synthesis, structural characterization, Hirshfeld surface and DFT based reactivity, UV filter and NLO studies of Schiff base analogue of 4-aminoantipyrine, Results in Chemistry 2 (2020) 100062.

- P.P. Soufeena, T.A. Nibila, K. Aravindakshan, Coumarin based yellow emissive AIEE active probe: A colorimetric sensor for Cu^{2+} and fluorescent sensor for picric acid, Spectrochimica Acta Part A: Molecular and Biomolecular Spectroscopy 223 (2019) 117201.

- T.A Nibila, P.P. Soufeena, Pradeepan Periyat, K. K. Aravindakshan, Synthesis, structural characterization and biological activities of transition metal complexes derived from 2,4-dihydroxybenzaldehyde N(4)-methyl(phenyl)thiosemi carbazone, under revision in Journal of Molecular Structure.

- An oral presentation on " Synthesis, characterization and biological activities of metal complexes of 4-benzyloxybenzaldehyde N(4)-methyl(phenyl) thiosemi carbazone" at 32^{nd} Kerala Science Congress held during the 25^{th}-27^{th} January, 2020 at Yuvakeshtra Institute of Management Studies, Mundur, Palakkad.

- A poster presentation on "Metal Complexes of 4-Hydroxy-3-methoxyacetophenone N(4)-methyl(phenyl)thiosemicarbazone: Synthesis, Characterization and Antimicrobial Activity" at International Conference on Emerging Frontiers in Chemical Science, Research & Post Graduate Department of Chemistry, Farook College (Autonomous), Calicut on 13-15 December 2019, Abstract No:17, Page No:53.

- An oral presentation on "Computational and biological studies of novel Schiff Base Analogue of 4-Aminoantipyrine" at MESMAC International Conference held in January 15-17, 2019 at D.G.M.M.E.S Mampad College, Malappuram.

Results in Chemistry 2 (2020) 100062

Contents lists available at ScienceDirect

Results in Chemistry

journal homepage: www.elsevier.com/locate/rechem

Synthesis, structural characterization, Hirshfeld surface and DFT based reactivity, UV filter and NLO studies of Schiff base analogue of 4-aminoantipyrine

T.A. Nibila, T.K. Shameera Ahamed, P.P. Soufeena, K. Muraleedharan, Pradeepan Periyat, K.K. Aravindakshan *

Department of Chemistry, University of Calicut, Malappuram 673635, India

ARTICLE INFO

Article history:
Received 19 April 2020
Accepted 26 June 2020
Available online xxxx

Keywords:
Pyrazolone
Schiff base
Single crystal
DFT
MEP
NLO

ABSTRACT

A pyrazolone based novel Schiff base, 4-(4-benzyloxybenzalidene) amino-2,3-dimethyl-1-phenyl-3-pyrazolo-5-one (L) was synthesized by appropriate synthetic route. It was characterized by elemental-, SCXRD-, FT-IR-, UV/Vis-, ESI-MS-, and Thermogravimetric analyses. Density Functional Theory (DFT) calculations were carried out to obtain the ground state optimized geometry of the molecule using the B3LYP method and the 6-311++G(d,p) Basis set. Calculated geometrical parameters and spectroscopic information agreed well with the single crystal X-ray data. Reactivity (Fukui functions), electronic properties (HOMO-LUMO) and surface properties (MEP and Hirshfeld) were also studied to establish the nature of the electrophilic- and nucleophilic sites and the interactions within the crystal structure of the compound. UV–Vis spectral- and molecular orbital distribution analyses ensured the UV filter activity of the compound. The computed hyperpolarizability showed that the compound might be used for non-linear optical (NLO) applications in the near future.

1. Introduction

Schiff bases are an important class of polydentate ligands that typically contain both nitrogen and oxygen donors. These are nitrogen analogues of aldehydes or ketones, having a growing interest due to their RC=N group, are known as azomethines. They are usually prepared by condensation of primary amine with carbonyl compounds under specific conditions. In general, aldehydes take part faster than ketones in condensation reactions because the reaction centre of an aldehyde is sterically less hindered than that of a ketone. Schiff bases of aliphatic aldehydes are relatively unstable and readily polymerize, while those of aromatic aldehydes, having an effective conjugation system, are more stable. Schiff bases are generally bi-or tri- dentate ligands capable of forming very stable complexes with transition metal ions. In organic synthesis, Schiff base formation reactions are useful in making carbon-nitrogen bonds. They have been extensively studied because of their exciting biological activities such as antitumor- [1], antimicrobial- [2] and antioxidant- [3] activities. These wide ranges of biological applications are due to the imine groups present in them [4].

Generally, pyrazolones comprise a group of organic compounds, which are heterocycles, and process a five- membered lactam ring with an additional keto group. Among pyrazolone analogues, synthetically important compounds derived from 4-aminoantipyrine have received much attention because they exhibit attractive multifunctional properties including antifungal-, antibacterial-, antimalarial-, antiviral-, anti-inflammatory- and antipyretic properties. Nowadays, 4-aminoantipyrine derivatives have been treated as important biomodel compounds in the biological- and medical fields [5]. Common Schiff bases are crystalline and feebly basic. They are characterized by the presence of an azomethine group, —RC=NR', where R and R' are alkyl-, cycloalkyl-, aryl- or heterocyclic groups. Schiff bases are widely designed by varying the chemical environment about the —C=N— group. The presence of a lone pair of an electron in the sp^2 hybridized orbital on the imino nitrogen atom makes the azomethine group more significant.

Recently, Density Functional Theory (DFT) has been recognized as a better auxiliary tool in the study of biological- and chemical properties of biologically active compounds than the *ab initio* methods used in the past. It has been endorsed as a well-known post-HF approach for the computational calculation of structural characteristics, vibrational frequencies and energies of compounds. It has been proved to be a reliable and potent tool with accuracy and cost effectiveness. We decided to explore the spectroscopic- and quantum chemical properties of the compound, which were calculated using the DFT-B3LYP method at 6-311++G(d,p) Basis set level [6]. These data were compared with experimental results.

A search through the literature revealed that no work has been done on the Schiff base formed by the condensation of 4-aminoantipyrine with 4-benzyloxybenzaldehyde and it prompted us to synthesis the

* Corresponding author.

https://doi.org/10.1016/j.rechem.2020.100062

Spectrochimica Acta Part A: Molecular and Biomolecular Spectroscopy 223 (2019) 117201

Contents lists available at ScienceDirect

Spectrochimica Acta Part A: Molecular and Biomolecular Spectroscopy

journal homepage: www.elsevier.com/locate/saa

Coumarin based yellow emissive AIEE active probe: A colorimetric sensor for Cu^{2+} and fluorescent sensor for picric acid

P.P. Soufeena, T.A. Nibila, K.K. Aravindakshan *

Department of Chemistry, University of Calicut, Malappuram, Kerala 673 635, India

ARTICLE INFO

Article history:
Received 18 January 2019
Received in revised form 20 April 2019
Accepted 26 May 2019
Available online 27 May 2019

Keywords:
Schiff base
Colourimetric and fluorescent sensor
Aggregation Induced Emission Enhancement
Picric acid

ABSTRACT

A hydrazine derived ESIPT active Schiff base, 1-(8-methanylylidene-7-hydroxy-4-methyl-2H-chromen-2-one)-2-(2, 4-dihydroxybenzylidene) hydrazine, L was synthesized and characterized by elemental analysis and by various spectroscopic techniques. L exhibited a colourimetric response towards Cu^{2+} ion by changing from colorless to yellow with relatively a little or no interference of other common metal ions. The probe also showed good response for the detection of Cu^{2+} in real water samples. The H-aggregated L displayed AIEE property in acetonitrile/water mixture. The restriction of molecular motions endued the luminogen with a yellow fluorescence through ESIPT emission at 562 nm having relatively large Stock's shift of 205 nm. The scanning electron microscopic study was carried out to investigate the morphology of the nanoaggregate. The aggregated luminogen displayed it yellow emission in the pH range of 4–7 without affecting the intensity. The applicability of the probe for the detection of picric acid was also checked.

1. Introduction

Monitoring of environmental pollutants and biological important metal ions is highly essential in present scenario. Among the transition metal ions, Cu^{2+}, an essential trace metal, is closely related to human life [1–4]. Because of the redox nature of Cu^{2+}, its enzymes involve in electron transfer, oxygen binding and oxidation catalysis [5–7]. It also has inevitable roles in bone and tissue formation, cellular respiration, immune and brain functions, and gene transcription [8–10]. Copper is also essential to the growth of plants and microorganisms [11]. Contrary to these active physiological roles of Cu^{2+}, its excessive intake adversely affect human health and leads to neurodegenerative diseases likes Menkes, Wilson's, Parkinson's, Alzheimer's and Prion disease [12–16]. The effluents from industries and the agricultural waste contribute copper contamination in water, air and soil. Therefore, on account of health and environmental issues, it is essential to monitor Cu^{2+} in a cost effective manner. For monitoring various metal ions, researchers are interested in methods based on chemical sensors. The simplicity in detection is the prime attraction of these methods. Their advantages are rapid response, high sensitivity and selectivity and inexpensive instrumental facility [17–19]. The changing photophysical properties of chemical sensors before and after the interaction with the metal ions can be monitored and quantified using UV–Visible- or fluorescence spectroscopic method. Among these optical sensing methods, colorimetric sensing is attractive because of the advantages of naked eye detection. A challenge of this chemical sensor based method for copper ion is the interference of other metal ions like Fe^{3+}, Zn^{2+}, Hg^{2+} and Pb^{2+} [20]. Even though, a number of chemical probes are available for monitoring Cu^{2+} [21–26], the development of new one with better capability is still challenging.

Solid state luminescent organic materials find promising applications in organic light emitting diodes (OLED), fluorescent sensors, bioimaging and so forth [27–32]. The major problem of fluorescent materials is that they become highly emissive in isolated molecular state and their emission either quenches or they will not be emissive in the solid or aggregated states which limit their applications. This effect, the quenching of fluorescence with concentration is commonly known as Aggregation Caused Quenching (ACQ) [33,34]. The intermolecular π-π stacking interactions of aromatic skeleton of organic molecules result in the formation of excimers and exciplexes which lead to quenching of fluorescence [35]. In 2001, Tang and co-workers [36,37] reported an interesting property in silole-based organic molecules, which was just reverse of the common ACQ effect. They observed that the non-emissive system in isolated state strongly emit bright green fluorescence upon aggregation and this unique phenomenon is termed as Aggregation Induced Emission (AIE) [38]. Another feature of aggregated luminogens, Aggregation Induced Emission Enhancement (AIEE), similar to the AIE was reported in 2002 by Park *et al* [32]. AIEE active luminogens are feebly emissive in the isolated state and their emission enhance in the aggregated state. The main mechanism proposed for AIE/AIEE activity is the restriction of intramolecular motion (RIM) in the aggregated- or solid state [39]. The other mechanisms reported are intramolecular charge transfer (ICT) [40], J-aggregation

* Corresponding author.
E-mail address: aravindkuttamath@yahoo.com (K.K. Aravindakshan).

https://doi.org/10.1016/j.saa.2019.117201
1386-1425/